OUKA
The University of Osaka
Institutional Knowledge Archive

Title	Development of a Data-Driven Approach to Road Asset Management in Cambodia Based on Pavement Condition Assessment
Author(s)	Sovanneth, Nut
Citation	大阪大学, 2026, 博士論文
Version Type	VoR
URL	https://doi.org/10.18910/105472
rights	
Note	

The University of Osaka Institutional Knowledge Archive : OUKA

https://ir.library.osaka-u.ac.jp/

The University of Osaka

Development of a Data-Driven Approach to Road Asset Management in Cambodia Based on Pavement Condition Assessment

カンボジアにおける舗装状態評価に基づくデータ駆動型道路資産管理手法の開発



A Dissertation Presented

by

NUT SOVANNETH

to

Division of Global Architecture,
Graduate School of Engineering,
The University of Osaka

In partial fulfillment of the requirements for the degree of

Doctor of Philosophy

December 2025

Acknowledgements

A Cambodian (Khmer) proverb states, “ផឹកទឹកឱ្យនឹកដល់ប្រភព ជ្រកម្លប់ឱ្យនឹកដល់អ្នកដាំ” , which means, “When drinking water, think of its sources; and when resting in the shade, think of the one who planted the tree” . This proverb emphasizes the gratitude and remembrance of the origins of what we received. Our Khmer ancestors advised the next generation to recognize, respect, and appreciate the efforts of others who support us.

In this spirit, I would like to express my deepest gratitude and appreciation to my advisor, Prof. Kiyoyuki Kaito (Kaito Sensei), whose continuous guidance has been the cornerstone of my academic and research journey during my three years of doctoral study in Japan. Being given the opportunity to join his laboratory was a priceless gift that allowed me to fulfill my dream of pursuing higher education. Thanks to his expertise, I have gained valuable knowledge and learned advanced models that I believe will significantly contribute to enhancing infrastructure management in Cambodia. Moreover, his dedicated supervision, insightful feedback, and careful refinement of my research have sharpened my work, making it more applicable to real-world engineering practice.

I would also like to extend my deepest gratitude and sincere appreciation to Prof. Toshiro Kamada and Prof. Kenji Doi of the University of Osaka’ s Graduate School of Engineering for their invaluable contributions as members of my dissertation review committee. Their meticulous review, insightful critique, and constructive guidance played a critical role in developing and refining this dissertation proposal, ensuring that its clarity, coherence, and scholarly rigor.

I am also sincerely grateful to Asst. Prof. Felix Obonguta, Asst. Prof. Kotaro Sasai, and Asst. Prof. Asnake Adraro Angelo for their valuable comments and constructive suggestions, as well as their thoughtful advice through research meetings and private communication. They have consistently paid close attention to my research progress and carefully monitored its development, ensuring that I remained on the right track. Their encouragement, critical feedback, and professional guidance not only facilitated the revision of my work but also enhanced its academic quality, paving the way for successful publication.

My heartfelt thanks also go to the Japan International Cooperation Agency (JICA) for generously providing a full scholarship, ensuring my safety and well-being, and offering continuous coordination and assistance before and throughout my stay in Japan. I especially appreciate the seminars arranged during vacation periods, which created opportunities for diverse knowledge

exchange with fellow scholarship candidates.

I would also like to acknowledge my colleagues at the Ministry of Public Works and Transport (MPWT) in Cambodia for encouraging me to pursue further studies and for their kind support in providing essential data for my analysis. In particular, I extend my sincere gratitude to Mr. Prak Vanna, Mr. Vasim Sotevind, and Mr. Eam Sovisoth for sharing valuable data on pavement condition surveys and traffic counts. I also thank Dr. Try Sophal for providing rainfall data. In addition, I am grateful to Prof. Yoshida Junji and Prof. Takeya Kouichi for making road-surface images from Yamanashi publicly available as open-source data. I also express my sincere appreciation to all individuals who shared data and resources during this study, even if not all of them were ultimately utilized in this dissertation. These contributions were essential to the success of my research and enhanced the quality of the research output, contributing to the development of practical engineering.

Finally, I owe my deepest gratitude to my parents (Nut Sovannath and Sarom Sothea), my sister (Nut Sovanneath), and especially my beloved wife (Lim Sreymom) and our adorable three-month-old daughter (Panhchapor, called Depi) for their unconditional love, encouragement, and motivation, which carried me through the most challenging moments of this journey.

December, 2025
Nut Sovanneth

Dedication

To my loving parents, sister, wife, and our adorable daughter.

Executive Summary

Developing countries such as Cambodia face significant challenges in implementing effective road asset management due to limited resources. Consequently, optimal maintenance planning across road networks is rarely achieved. Addressing this issue requires the design of an efficient, practical, and sustainable framework aligned with local policy. This framework shall integrate key components, including data acquisition, condition evaluation, performance modeling, and maintenance program design under budget constraints. This dissertation develops a scientific framework to support Cambodian road administrators in informed decision-making, optimizing outcomes, ensuring resource efficiency, and enhancing transparency in long-term infrastructure investment. The framework emphasizes AI-based pavement data collection, structural condition assessment, and maintenance and rehabilitation (M&R) optimization using a comprehensive probabilistic prediction model that accounts for the inherent uncertainties in infrastructure performance.

The thesis is structured into seven chapters. The core scientific contributions are presented in four key methodological chapters (Chapters 3 to 6), which together form a cohesive pavement management framework, as summarized below.

Chapter 1: Highlights the critical role of road networks in economic growth, connectivity, and regional resilience. It identifies a major challenge faced by governments worldwide: the persistent gap between limited public resources and the substantial investment required for transport infrastructure and maintenance. This underinvestment, particularly pronounced in developing countries, leads to progressive infrastructure deterioration, compromising safety and efficiency, and necessitating a paradigm shift in road administration.

Chapter 2: Presents an integrated modern pavement management framework built on three pillars: (i) data-driven condition assessment; (ii) advanced deterioration modeling employing deterministic, probabilistic and machine learning approaches to forecast future pavement conditions; and (iii) integration of these predictions into a Pavement Management System (PMS) to optimize maintenance decision-making and resource allocation.

Chapter 3: Introduces the use of the Segment Anything Model (SAM) for accurate segmentation from simple bounding box prompts, leveraging its zero-shot capability for generalization. To create an end-to-end solution, the framework integrates YOLOv8 for automated crack detection, eliminating manual annotation, and applies local refinement techniques to enhance mask precision. Moreover, Optical Character Recognition (OCR) is used to extract embedded GPS coordinates for geospatial mapping, improving data management and integrity.

Chapter 4: Defines structural thresholds derived from Falling Weight Deflectometer (FWD) data using a stochastic deterioration modeling approach. The Markov hazard model predicts surface roughness deterioration by incorporating structural indices such as maximum deflection, effective structural number, subgrade resilient modulus, and deflection bowl parameters. Data from asphalt concrete (AC) and double bituminous surface treatment (DBST) pavements are analyzed to establish thresholds at set failure probabilities: Sound (0–50%), Warning (50–75%), and Severe (75–100%). This approach allows road agencies to evaluate pavement conditions and optimize maintenance strategies without advanced mathematical modeling expertise.

Chapter 5: Focuses on defining FWD testing intervals based on failure risk and prioritizing critical road sections. The mixed Markov hazard (MMH) model captures deterioration progression, with a probability of reaching critical thresholds guiding testing intervals. A multi-criteria decision-making (MCDM) framework identifies critical sections by combining surface deterioration and other evaluation criteria, enhancing FWD application efficiency, reducing unnecessary testing, and directing resources to sections requiring immediate attention.

Chapter 6: Develops an integrated framework combining a deterioration prediction model with a genetic algorithm (GA) for cost-effective M&R planning of flexible pavements (AC and DBST). The GA schedules multi-year interventions considering deterioration rates and budget constraints to maximize pavement performance. The MMH model simulates condition transitions influenced by pavement capacity, traffic, and environmental factors, using Bayesian inference via Markov Chain Monte Carlo (MCMC) to estimate deterioration rates and lifespans. This framework enables data-driven, sustainable infrastructure management and optimal fund allocation.

Chapter 7: Concludes that a fully integrated, data-driven pavement management framework is achievable and effective even in low-resource environments. The research provides a foundation for future advancements in sustainable infrastructure management.

Abbreviations

AC – Asphalt Concrete
ADT – Average Daily Traffic
AHP – Analytic Hierarchy Process
AP – Average Precision
BLI – Base Layer Index
CB – Cost Benefit
CNN – Convolutional Neural Network
DBPs – Deflection Bowl Parameters
DBST – Double Bituminous Surface Treatment
DL – Deep Learning
DPWT – Provincial Department of Public Works and Transport
DRIMS – Dynamic Response Intelligent Monitoring System
ESALs – Equivalent Single Axle Loads
FAHP – Fuzzy Analytic Hierarchy Process
FN – False Negatives
FP – False Positives
FWA – Fuzzy Weighed Average
FWD – Falling Weight Deflectometer
GA – Genetic Algorithm
GrA – Greedy Algorithm
HDM-4 – Highway Development and Management Model Four
HIMS – Highways Information Management System
IoU – Intersection over Union
IRI – International Roughness Index
LCC – Life-Cycle Cost
LLI – Lower Layer Index
M&R – Maintenance and Rehabilitation
mAP – Mean Average Precision

MCDM – Multi-Criteria Decision-Making
MCI – Maintenance Control Index
MCMC – Markov Chain Monte Carlo
MGP – Maximum Graded Principle
M-H – Metropolis-Hastings
MHM – Markov Hazard Model
ML – Machine Learning
MLI – Middle Layer Index
MMH – Mixed Markov Hazard
MPD – Mean Profile Depth
MPWT – Ministry of Public Works and Transport
MUSTEM – Multi-Stage Exponential Markov
NDT – Non-Destructive Testing
OCR – Optical Character Recognition
PCI – Pavement Condition Index
PCR – Pavement Condition Rating
PDCA – Plan-Do-Check-Act
PMS – Pavement Management System
PQI – Pavement Quality Index
RDCMU – Road Data Collection and Management Unit
RGC – Royal Government of Cambodia
RMDS – Road Management Decision Support
RoC – Radius of Curvature
ROMDAS – ROad Measurement Data Acquisition System
RPNs – Region Proposal Networks
SAM – Segment Anything Model
SCI – Structural Condition Index
SDGs – Sustainable Development Goals
SN – Structural Number
TP – True Positives
TPM – Transition Probability Matrix
TSP – Traveling Salesman Problem
ViT – Vision Transformer
VOC – Vehicle Operating Cost
YOLO – You Only Look Once

Notation

H	Homography matrix
p_i	Source points in the original image
p'_i	Destination points on the target rectangular plane
N	Number of defect classes
$F1 - score$	Harmonic mean of precision and recall
Z	Inspection interval
τ_A, τ_B	Inspection at time A and B
i	Initial pavement condition states
j	Subsequent pavement condition states
J	Pavement with worst condition state
π_{ij}	Markov transition probability from condition state i to j
Π	Transition probability matrix
ζ_i	Life expectancy of a condition state i
f_i	Probability density function
F_i	Cumulative distribution function
$\tilde{F}_i$	Survival function
λ_i	Hazard function
x	Explanatory variables
β_i	Unknown parameters
m	Number of explanatory variables
θ_i	Hazard rate or deterioration rate
LE_{iJ}	Life expectancy from condition state i to J
D_0	Maximum deflection
E_p	Effective pavement modulus of all layers above the subgrade
SN_{eff}	Effective structural number
M_R	Resilient modulus of subgrade
θ_i^k	Hazard rate for group k
ε^k	Heterogeneity factor

X	Decision matrix
x_{ij}^T	Normalized value of beneficial and non-beneficial criteria
σ_j	Standard deviation
r_{jk}	Correlation coefficient between criteria j and k
C_j	Criterion information
w_j	Criteria weights
R'	Normalized fuzzy relation matrix
Y	Fuzzy evaluation vector
S_i	Benefit measure
R_i	Regret measure
Q_i	VIKOR index
$CB_{a,g,t}$	Cost benefit for road section in group g under action a at year t

Table of Contents

Acknowledgements **i**

Dedication **iii**

Executive Summary **iv**

Abbreviations **vi**

1 Introduction **1**

1.1 General introduction 1

1.2 Concept of sustainable road asset management 2

1.3 Problem statement in Cambodian road asset management 6

1.4 Objectives and significance of the study 15

1.5 Organization of dissertation 17

2 Literature Review **21**

2.1 Introduction 21

2.2 Pavement condition assessment 22

2.2.1 Functional evaluation 23

2.2.2 Structural evaluation 28

2.2.3 Artificial intelligence 30

2.3 Deterioration prediction . . . 34
2.3.1 Deterministic models . . . 34
2.3.2 Probabilistic models . . . 35
2.3.3 Intelligent models . . . 37
2.4 Decision-support for maintenance . . . 38
2.4.1 Operational research methods . . . 38
2.4.2 Metaheuristic algorithms . . . 38
2.4.3 Artificial intelligence methods . . . 39

3 An Integrated Framework with SAM and OCR for Pavement Crack Quantification and Geospatial Mapping 48

3.1 Introduction . . . 48
3.2 Methods . . . 52
3.2.1 Proposed framework . . . 52
3.2.2 Top-down perspective transformation based on homography . . . 54
3.2.3 YOLOv8 model for pavement distress detection . . . 56
3.2.4 Architecture of SAM for pavement distress segmentation . . . 57
3.3 Results . . . 58
3.3.1 Dataset preparation . . . 58
3.3.2 Model . . . 60
3.3.3 Training setup . . . 60
3.3.4 Evaluation metrics . . . 61
3.4 Discussion . . . 67
3.5 Conclusions . . . 69

4 Stochastic Approach to Defining Pavement Structural Thresholds from FWD measurements 76

4.1 Introduction . . . 76

4.2 Method . . . 79
4.2.1 Bayes' Rule for Markov hazard model . . . 84
4.2.2 MCMC by using M-H algorithm . . . 85
4.3 Empirical Study . . . 86
4.3.1 Back-calculated structural indices . . . 87
4.3.2 Data processing . . . 89
4.4 Results . . . 90
4.4.1 Estimation results based on BMH model . . . 90
4.4.2 Estimation results based on the BMH model incorporating structural indices . . . 92
4.5 Discussion and limitations . . . 95
4.6 Conclusions . . . 99

5 Strategic Application of FWD for Efficient Network-Level Pavement Assessment 104

5.1 Introduction . . . 104
5.2 Method . . . 106
5.2.1 Mixed Markov hazard (MMH) model . . . 107
5.2.2 Multi-criteria decision-making (MCDM) . . . 109
5.3 Empirical Study . . . 115
5.3.1 Data collection . . . 115
5.3.2 Data processing . . . 115
5.4 Results . . . 116
5.4.1 Estimation results based on MMH model . . . 116
5.5 Conclusions . . . 121

6 Optimization of Pavement Maintenance Planning in Cambodia Using a Probabilistic Model and Genetic Algorithm 124

6.1 Introduction 124
6.2 Pavement management system in Cambodia 126
6.3 Methodology 127
6.3.1 Decision process for repair action selection 127
6.3.2 Model framework 129
6.3.3 Deterioration prediction based on mixed Markov hazard (MMH) model . 132
6.3.4 GA optimization 135
6.4 Benefit optimization 136
6.5 Results 139
6.5.1 MMH model estimation result 139
6.5.2 GA optimization result 142
6.6 Discussion 146
6.7 Conclusions 148

7 Conclusions **154**

7.1 Summary of presented research 154
7.2 Conclusions and recommendations 155

List of Tables

2.1 Pavement condition rating systems. 24

2.2 Deflection bowl parameters and their significance. 30

3.1 Hyperparameter configuration for distress detection and segmentation. 61

3.2 Comparison of different segmentation models on the Crack500 dataset. 69

4.1 Benchmark structural indices. 78

4.2 Pavement performance rating. 90

4.3 Hazard Model Parameters for AC and DBST Pavements 91

4.4 Hazard Model Parameters via D_0 93

4.5 Hazard Model Parameters via SN_{eff} 94

4.6 Hazard Model Parameters via M_R 95

4.7 Hazard Model Parameters via BLI 96

4.8 Hazard Model Parameters via MLI 97

4.9 Hazard Model Parameters via LLI 98

4.10 Proposed structural thresholds for AC pavements. 99

4.11 Proposed structural thresholds for DBST pavements. 99

5.1 Pavement performance rating. 116

5.2 Estimation results for model' s parameters. 117

5.3 MTP matrix of AC and DBST pavement. 118

5.4 Proposed frequency of FWD testing. 118

5.5 Fuzzy relation and evaluation. 119

6.1 IRI condition rating, maintenance requirement, and IRI state updates. 129

6.2 Structural benchmark criteria. Adapted from [40], with permission from CRC Press, Talyor & Francis Group, 2025. 129

6.3 Structural classification, maintenance requirement, and structural state updates. 130

6.4 Repair details by maintenance type. 138

6.5 Maintenance unit cost. 139

6.6 Parameter estimation through Bayesian MMH model. 140

List of Figures

1.1 Infrastructure management cycle process. 3

1.2 Pavement performance with different maintenance policies. 4

1.3 Basic framework of pavement management. 5

1.4 The GMS transport sector strategy (Adapted from [26]) 7

1.5 Overview of road development master plan (Adapted from IRITWG [27]). . . . 8

1.6 Pavement maintenance practices in Cambodia. 9

1.7 Road data collection. 10

1.8 Stakeholder roles in force-account road maintenance project. 11

1.9 Typical content of a maintenance project proposal. 11

1.10 Road maintenance implementation using DRIMS. 12

1.11 HDM-4 system components (Adapted from [28]). 13

1.12 Maintenance selection proposed by RDCMU. 14

2.1 Distress survey vehicle. 25

2.2 Schematic diagram of FWD. 29

2.3 The DT process. 31

2.4 The RF process. 32

2.5 The SVM process. 32

2.6 CNN architecture for classification. 33

2.7 Basic architecture of CNN-based segmentation. 33
2.8 Mask R-CNN framework (Adapted from He et al.[50]). 34
2.9 Illustration of pavement condition through Markov process (no maintenance). . 36

3.1 ROMDAS survey vehicle. 49
3.2 Pavement image from ROMDAS survey vehicle. 49
3.3 Pipeline of the proposed framework. 53
3.4 Overview of the IPM transformation process. 55
3.5 Given camera perspective (**left**), transformed top-down perspective (**right**). . . 56
3.6 Overall architecture of YOLOv8. 57
3.7 Overview of modified SAM architecture. 59
3.8 YOLOv8 training process. 63
3.9 YOLOv8 Precision-Recall curve. 63
3.10 Confusion matrix normalized for crack detection. 64
3.11 SAM training process: (a) $Precision$, (b) $Recall$, (c) $F1-score$, and (d) IoU. . 65
3.12 Test results of combined YOLOv8 and SAM. 66
3.13 Effectiveness of local refinement on segmentation. 67
3.14 GIS-based visualization of detected pavement distress. 68

4.1 Pavement performance. 81
4.2 Deterioration paths between 1st and 2nd inspections. 82
4.3 Model of deterioration process. 82
4.4 1-digit and 2-digit roads surveyed for empirical study. 87
4.5 Condition state changes over time. 92
4.6 Failure probability due to D_0 within design life. 93
4.7 Failure probability due to SN_{eff} within design life. 94
4.8 Failure probability due to M_R within design life. 95

4.9 Failure probability due to BLI within design life. 96

4.10 Failure probability due to MLI within design life. 97

4.11 Failure probability due to LLI within design life. 98

5.1 Falling Weight Deflectometer (FWD) in operation. 105

5.2 Proposed framework for FWD application. 107

5.3 Membership functions of each criterion. 112

5.4 Condition state changes by elapsed year. 117

5.5 Prioritized road sections for FWD testing at network-level. 119

5.6 Minimal FWD testing route. 120

6.1 Road networks in Cambodia. 127

6.2 Flowchart of the model framework. 131

6.3 Illustration of pavement deterioration. 132

6.4 GA chromosome encoding. 136

6.5 Effectiveness of maintenance activities. 137

6.6 Pavement deterioration curves. 140

6.7 Deterioration curves through various structural groups (1–54). 141

6.8 Condition state evolution of the network with no repairs. 141

6.9 GA iteration process ($18M/Year Scenario). 142

6.10 Condition state evolution of network under various annual budget scenarios: (a) USD 12 M, (b) USD 15 M, (c) USD 18 M, (d) USD 21 M, (e) USD 24 M, and (f) USD 27 M. 143

6.11 Predicted IRI condition state over the year under various budget scenarios. . . . 144

6.12 Maintenance expenditure by repair action type ($18M/Year Scenario). 145

6.13 Performance of eight selected road segments ($18M/Year Scenario). 145

6.14 Cumulative cost–benefit: genetic vs. greedy algorithm. 146

6.15 Road maintenance selection: genetic vs. greedy algorithm. 146

6.16 Repair action selected for maintenance: genetic vs. greedy algorithm. 147

Chapter 1

Introduction

1.1 General introduction

Road networks serve as a fundamental component of transportation infrastructure and contribute significantly to sustained economic growth. They are instrumental in enhancing market accessibility and regional connectivity, improving firm productivity, and promoting regional convergence and equity [1–3]. Beyond mere physical connectivity, road infrastructure functions as a critical determinant of regional economic resilience, defined as a region' s capacity to withstand, recover from, and adapt to economic disruptions such as recessions. This resilience encompasses resistance to shocks, speed of recovery, and ability to learn and transform to ensure long-term stability [4]. By improving network efficiency, upgraded road pavements reduce transport and commuting costs, strengthen logistics performance, and facilitate industrial clustering, thereby enhancing regional competitiveness and supporting long-term economic growth [5].

Despite the essential economic role of roads, governments globally face increasing pressure to balance limited public resources with burgeoning infrastructure needs. Transportation infrastructure investment consistently accounts for a significant portion of national budgets. For context, in 2016, the average total transport infrastructure investment across OECD (Organization for Economic Co-operation and Development) countries was approximately 1% of GDP [1]. However, a significant global shortfall exists; World Bank data for 2010–2018 shows developing countries averaging less than 1% of GDP on public infrastructure spending, while estimates suggest that low- and middle-income countries (LMICs) need roughly 2.6% of GDP just for transport investment and operations/maintenance (O&M) to meet infrastructure-related Sustainable Development Goals (SDGs) [6]. This financial gap, coupled with the aging of existing systems, has driven a critical paradigm shift in road administration.

The consequence of underinvestment and accumulated maintenance backlogs is the progressive deterioration of infrastructure quality, which directly compromises safety and efficiency.

In most developed nations, the focus has moved from new construction to the preservation, maintenance, and expansion of existing road assets, as exemplified by highway agencies in the USA since the 1960s [7]. When roads fail to meet quality standards, average speeds decrease, and safety is compromised. Poor pavement condition, particularly increased roughness (quantified by the International Roughness Index, or IRI), leads to a rise in Vehicle Operating Cost (VOC) due to greater fuel consumption, maintenance, and tire wear [8]. Furthermore, several studies have consistently shown that pavement surface defects, including roughness, rut depth, and low skid resistance are shown to increase crash rates by promoting hydroplaning, reducing tire-road friction, and elevating accident risk [9–16].

The dual challenge of tighter budgets are increasingly public accountability necessitates the adoption of a structured, transparent, and efficient decision-making framework. This necessity for evidence-based action requires comprehensive evaluation methods to assess potential projects against defined policy objectives. For developing countries, establishing robust governance mechanisms is equally crucial for ensuring that road investment priorities align with national policies and that assets are constructed, maintained, and managed effectively [**van2024road**]. The U.S. Federal Highway Administration (FHWA) defines asset management as a systematic process that combines engineering principles with business practices and economic theory to maintain, upgrade, and operate physical assets cost-effectively [7]. This systematic approach has led to the development and implementation of road asset management system, providing the objective criteria and tools required to optimize resource allocation, extend service life, and ensure the safe use of road networks with minimal impact.

1.2 Concept of sustainable road asset management

The discipline of asset management provides a systematic framework for maximizing value delivery across public infrastructure system. The International Standards Organization (ISO) defines asset management as a set of coordinated activities that enable an entity to gain value from its assets [17]. These activities function as a continuous cycle that support the effective governance, maintenance, and optimization of public or governmental assets, as illustrated in Figure 1.1. This process is commonly conceptualized through the Plan-Do-Check-Act (PDCA) cycle, which entails: establishing target requirements and a maintenance timelines (Plan), executing scheduled maintenance tasks (Do), monitoring and evaluating asset performance (Check), and implementing improvements for subsequent cycles (Act) [18]. By integrating engineering principles with strategic financial planning and maintenance strategies, infrastructure asset management helps ensure that public assets continue to meet societal needs effectively and sustainably.

After pavement construction, road administrations must maintain ongoing surveillance of

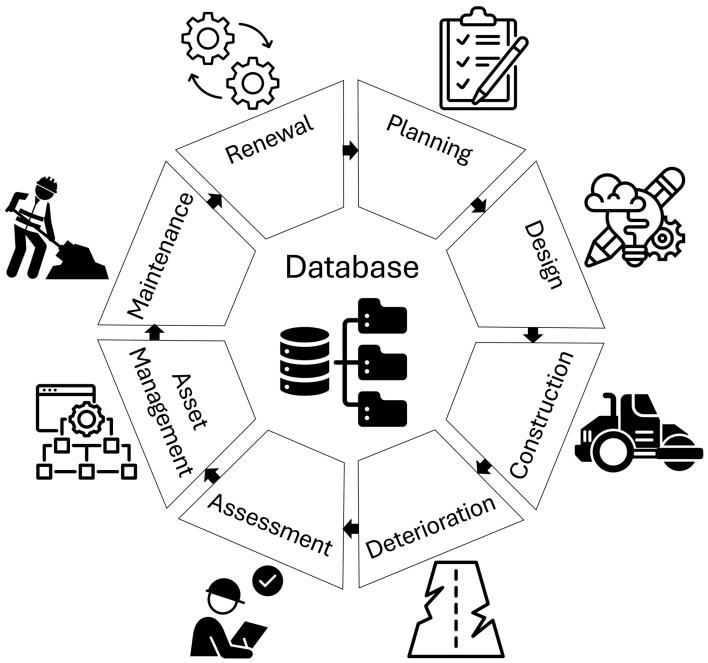


Figure 1.1: Infrastructure management cycle process.

pavement condition to detect defects and emerging problems that warrant prompt intervention. Regular inspections are essential for identifying and quantifying damage before functional performance deteriorates to unacceptable levels; they also help isolate the specific mechanisms driving decline. Historically, many practitioners adopted a "worst-first" approach, postponing treatment until pavements exhibited severe distress, a practice that often leads to costly, large-scale rehabilitation [19]. Consequently, agencies have increasingly adopted cost-effective preservation programs that emphasize preventive and proactive treatments to improve safety, maintain mobility, and extend service life [20].

Pavement preservation is inherently aligned with sustainability, as it seeks to prolong pavement life through cost-effective and environmentally responsible interventions. The current policy in road asset management typically aligns with this principle by emphasizing affordable diagnostic tools and preservation techniques to assist agencies, particularly those with limited resources, in managing pavement performance more effectively. As illustrated conceptually in Figure 1.2, preventive treatments can substantially delay major rehabilitation by altering the pavement performance curve. These treatments not only slow deterioration but also yield significant long-term savings due to their relatively low cost compared to full-scale rehabilitation. The selection of preventive maintenance is therefore a strategic decision, contingent upon its expected effectiveness in maximizing a pavement' s service life while minimizing its total Life-Cycle Cost (LCC).

Integrating sustainable maintenance planning into existing management frameworks requires agencies to reassess their data collection methods, performance modeling approaches, and maintenance programs. Effective alignment of pavement management systems with vari-

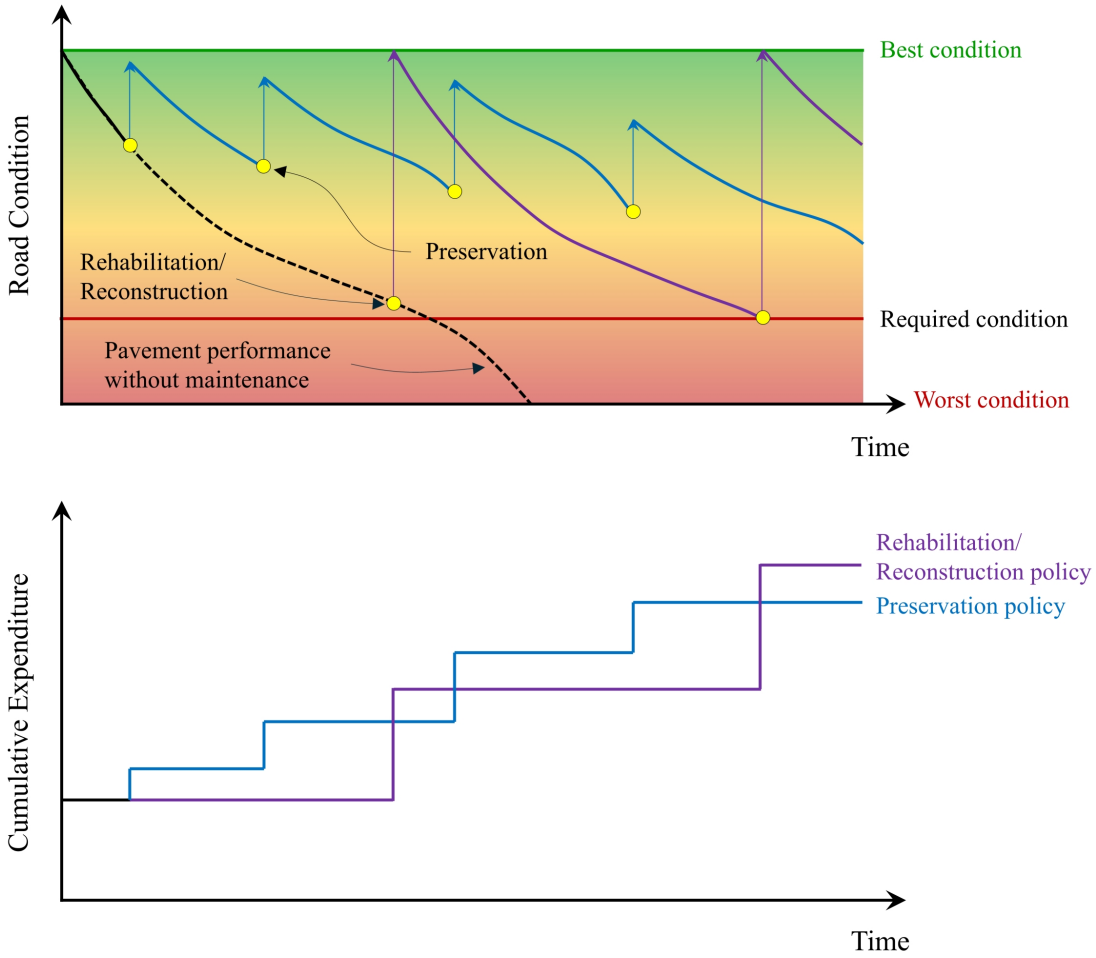


Figure 1.2: Pavement performance with different maintenance policies.

ous repair activities typically involves following components such as data collection, condition assessment, performance prediction, M&R programming, and budget planning and allocation [21]. Ultimately, treatment decisions must reflect project-specific constraints and objectives, but these decisions depend heavily on reliable data, comprehensive analysis, and accurate model for performance forecasting. Poor or incomplete data can lead to ineffective strategies that increase long-term costs and undermine sustainability.

In many developing countries, road agencies continue to operate under a facility-management model, addressing defects reactively within the limits of available budgets. However, the long-term goal for most agencies is to implement robust asset management systems that define service levels and identify the most cost-effective maintenance strategy in a transparent and informed manner [22]. Road segments deteriorate at different rates depending on the level and timing of maintenance; timely treatment can greatly extend road lifespan and reduce total LCC. In contrast, neglecting maintenance can increase costs by several multiples, underscoring the importance of regular, evidence-based decision-making to determine when and where maintenance is most needed.

Pavements exhibit structural and functional deterioration due to exposure to traffic load-

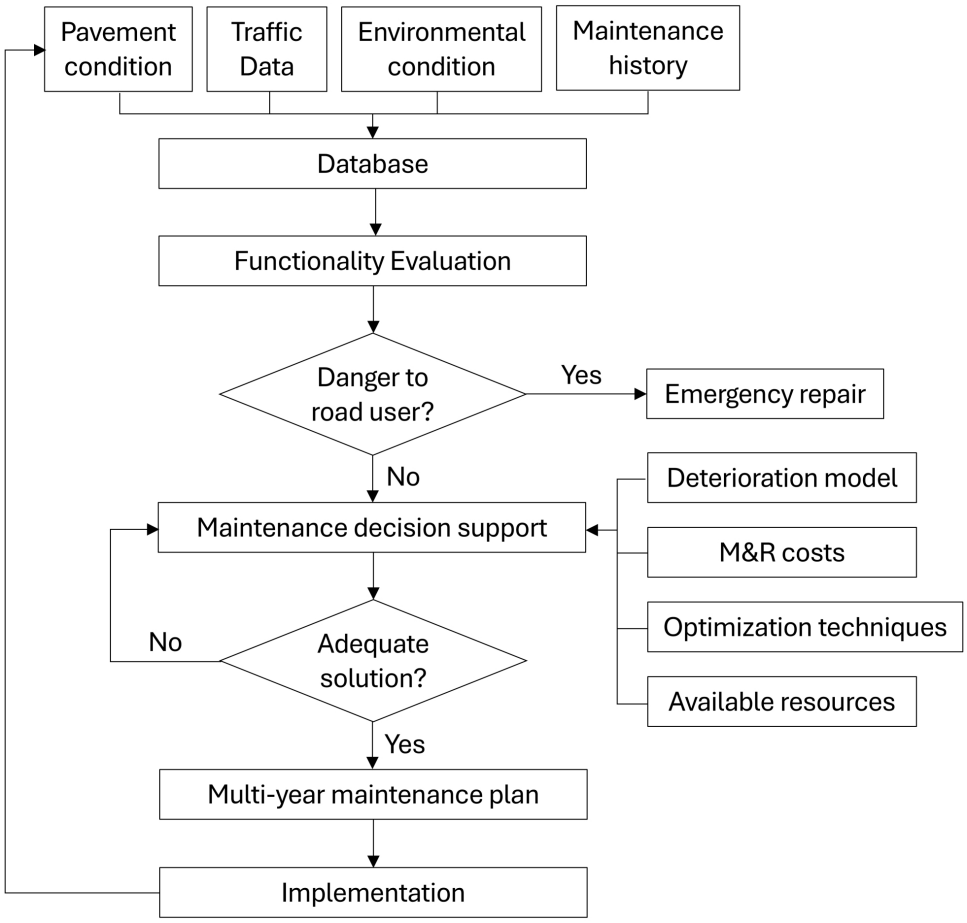


Figure 1.3: Basic framework of pavement management.

ing, material aging, and environmental conditions. Consequently, M&R interventions are mandated to sustain performance thresholds. Given the financial magnitude of M&R operations, road agencies are required to leverage analytical frameworks and strategies to ensure optimal, cost-effective treatment selection. Maintenance decision support tool, a specialized component of pavement management system (PMS), is utilized to inform those treatment decisions. The overview of PMS encompasses data acquisition, condition evaluation, performance modeling, M&R scheduling, and budget optimization. Effective PMS empowers agencies by providing precise understanding of pavement status, facilitating the comparison of strategic alternatives, enhancing prediction accuracy, determining appropriate funding levels, optimizing resource allocation, and supporting data-driven budgetary governance [23]. Basic framework of pavement management is illustrated in Figure 1.3.

The effectiveness of any PMS is built on high-quality data collection and reliable interpretation. Inputs, typically including existing pavement condition, traffic, and environment factors (e.g., rainfall), are critical for predicting future performance. To produce treatment recommendations, analytical decision-support tools combines this prediction with treatment-selection rules and treatment effects. An ideal maintenance strategy would preserve all road segments at a consistently high functional and structural levels [24]. However, rising traffic

volumes and budget limitations make timely repairs challenging. This creates the need for prioritization frameworks that rank road segments for maintenance, ensuring that constrained funds are allocated where they can achieve the greatest benefit [25]. Effective maintenance management therefore requires coordinated planning, timely execution, and adequate funding to maintain acceptable service levels.

1.3 Problem statement in Cambodian road asset management

Cambodia is situated in the Greater Mekong Subregion (GMS), a geopolitical and economic area encompassing the lower reaches of the Mekong River in Southeast Asia. This subregion is composed of six member nations: Cambodia, the People' s Republic of China (specifically the Yunnan Province and the Guangxi Zhuang Autonomous Region), the Lao People' s Democratic Republic (Lao PDR), Myanmar, Thailand, and Viet Nam [26]. The GMS transport sector strategy outlines a designated network of nine road corridors to serve as the sub-region's primary transportation links., as shown in Figure 1.4. These corridors are foundational to the creation of "economic corridors," which represent a comprehensive approach to regional development. This approach not only integrates infrastructure (such as transport links) with trade, investment, and economic opportunities but also incorporates measures to mitigate the potential social, environmental, and other effects arising from increased regional connectivity. Located in the southern part of the GMS, Cambodia, is a key component of the Southern Economic Corridor (SEC). The SEC encompasses interlinked routes that connect six provinces in eastern Thailand, four geographic clusters panning twenty-one provinces in Cambodia, four regions in Viet Nam, and six provinces in southern Lao PDR.

In response to the imperative of regional integration and simultaneous national development, Cambodia's Ministry of Public Works and Transport (MPWT) developed the road development master plan with support from the Japan International Cooperation Agency (JICA). High-quality road networks and infrastructure are fundamentally regarded as the "arteries" necessary to transform Cambodia into an integrated economy and are crucial for achieving distributed economic growth. These assets play a vital role in the national objective of poverty reduction, a top government priority, by facilitating the movement of goods and services, promoting trade and tourism, stimulating rural development, and fostering the integration of domestic markets. Furthermore, they are essential for enabling broader economic connection with the GMS region and the international community. To realize these multifaceted objectives, the Master Plan is executed through six distinct strategies (Strategy 1 through Strategy 6, as illustrated in Figure 1.5). These strategies reflect a commitment to:



Figure 1.4: The GMS transport sector strategy (Adapted from [26])

- Enhancing multi-growth pole development.
- Strengthening national integration.
- Developing international corridors.
- Boosting rural socio-economic development.
- Reinforcing economic growth corridor development.
- Promoting tourism development.

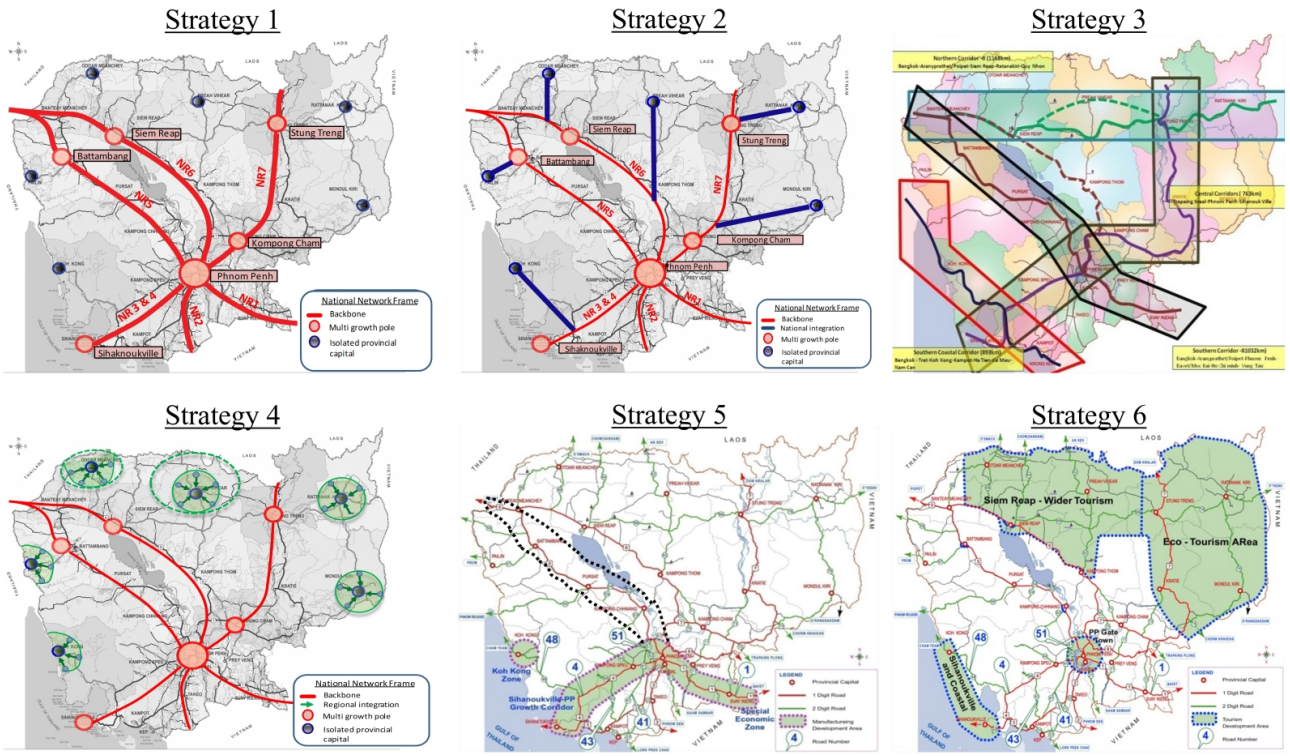


Figure 1.5: Overview of road development master plan (Adapted from IRITWG [27]).

As in many developing countries, flexible pavements in Cambodia often fail to achieve their intended design life, deteriorating more rapidly than those in developed countries. Several factors contribute to this accelerated decline. One contributing factor is the improper practices in the field, including inadequate construction quality control and the use of substandard materials that do not fully meet design specifications. The design guidelines issued by the MPWT explicitly stipulate the required structural capacity to withstand traffic loadings. For instance, under traffic loads ranging from 17 to 30 million ESALs (Equivalent Single Axle Loads), the prescribed design for a flexible pavement includes 15 cm asphalt surface layer, a 25 cm base course, and a 27.5 cm sub-base, all over a subgrade with a minimum soaked CBR of 5%. Furthermore, the sub-base and base courses must have minimum soaked CBR values of 30% and 80%, respectively, while the asphalt layer must achieve a Marshall stability of at least 7 kN. However, the aforementioned construction deficiencies prevent as-built pavement from achieving these specified characteristics. Consequently, the pavement structure cannot attain sufficient strength, resulting in premature deterioration.

Next, inadequate maintenance practices after roads are opened to traffic represent another significant factor contributing to rapid pavement deterioration. The pavement maintenance policies established by the MPWT classify maintenance into three categories: routine (preventive) maintenance, periodic (corrective) maintenance, and emergency maintenance. Routine maintenance aims to slow the progression of pavement distress and enhance surface friction, rather than waiting for distress to worsen. Typical activities include crack sealing, patching,



(a) Routine maintenance activity.



(b) Periodic maintenance activity.

Figure 1.6: Pavement maintenance practices in Cambodia.

and thin overlays (See Figure 1.6a). Periodic maintenance is carried out after significant damage has already manifested, such as severe cracking, deformation, or surface unevenness. This level of intervention, which includes thick overlays, rehabilitation, and reconstruction, seeks to restore structural integrity and extend the pavement's service life (See Figure 1.6b). Emergency maintenance, on the other hand, addresses conditions that pose immediate risks to traffic safety or cause network outages, often resulting from natural disasters such as severe flooding, and therefore requires urgent intervention. Effective maintenance, however, depends on a clear understanding of the underlying causes of pavement damages. Consequently, comprehensive and systematic monitoring, together with periodic assessment of pavement conditions, is essential to ensure acceptable performance throughout the service life of road assets.

Another contributing factor to pavement performance failure is the inability to identify functional and structural deficiencies during data collection, either due to technical limitations or practical constraints. In Cambodia, functional condition assessments are carried out at two levels: sub-national assessments by the offices of provincial Department of Public Works and Transport (DPWT) and national-level surveys by the MPWT. At the provincial level, DPWT engineers perform visual inspections using manual, paper-based methods to record surface distress such as cracks and potholes (See Figure 1.7a). This approach is labor-intensive and prone to inconsistencies. At the national level, the MPWT employs vehicle-based survey systems equipped with sensors and cameras to measure the roughness, rutting, skid resistance, and to capture pavement images (See Figure 3.1). This method accelerates data acquisition while improving data quality and reliability. While functional condition data can be obtained from surface-level observations, structural performance remains hidden and requires specialized testing. To address this, Falling Weight Deflectometer (FWD) surveys are used to evaluate the bearing capacity of subsurface layers, enabling agencies to determine appropriate maintenance intervention to restore pavement strength (See Figure 1.7c). Nevertheless, large volumes of images captured by survey vehicles requires extensive manual processing, underscoring the need



(a) Visual inspection.



(b) Vehicle-based functional data collection.



(c) FWD structural data collection.

Figure 1.7: Road data collection.

for automated analysis tools. Furthermore, FWD data interpretation lacks locally calibrated evaluation criteria, as current thresholds are adapted from other countries and may not reflect Cambodia' s construction practices, pavement designs, and material properties.

While survey data provide the primary for developing road maintenance plans, current maintenance decision-making practices remain traditional and reveal limitations. Maintenance works funded through the national budget are typically implemented through force-account projects. The project formulation involves multiple stakeholders, designated as Party A (the employer), Party B (the executor), Party C (the supervisor), and Party D (the inspector), as illustrated in Figure 1.8. Within this framework, the DPWTs are primarily responsible for compiling maintenance project lists for their respective regions. Engineers at the DPWTs estimate initial repair costs based on visual inspection reports and prioritize projects for short-term planning, formalized in a three-year rolling maintenance plan. Each project is documented using a standardized template that includes road inventory information, existing damage conditions, the scope of proposed repair works, and decisive criteria for intervention, as depicted in Figure 1.9. These criteria often encompass road class, strategic importance, and political

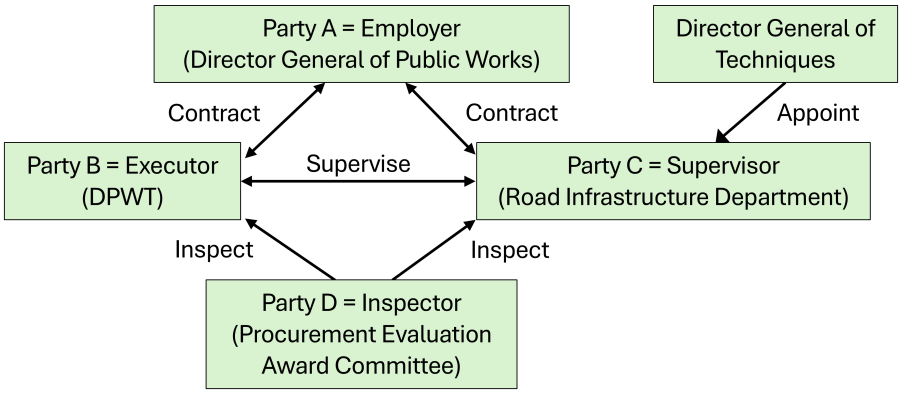


Figure 1.8: Stakeholder roles in force-account road maintenance project.

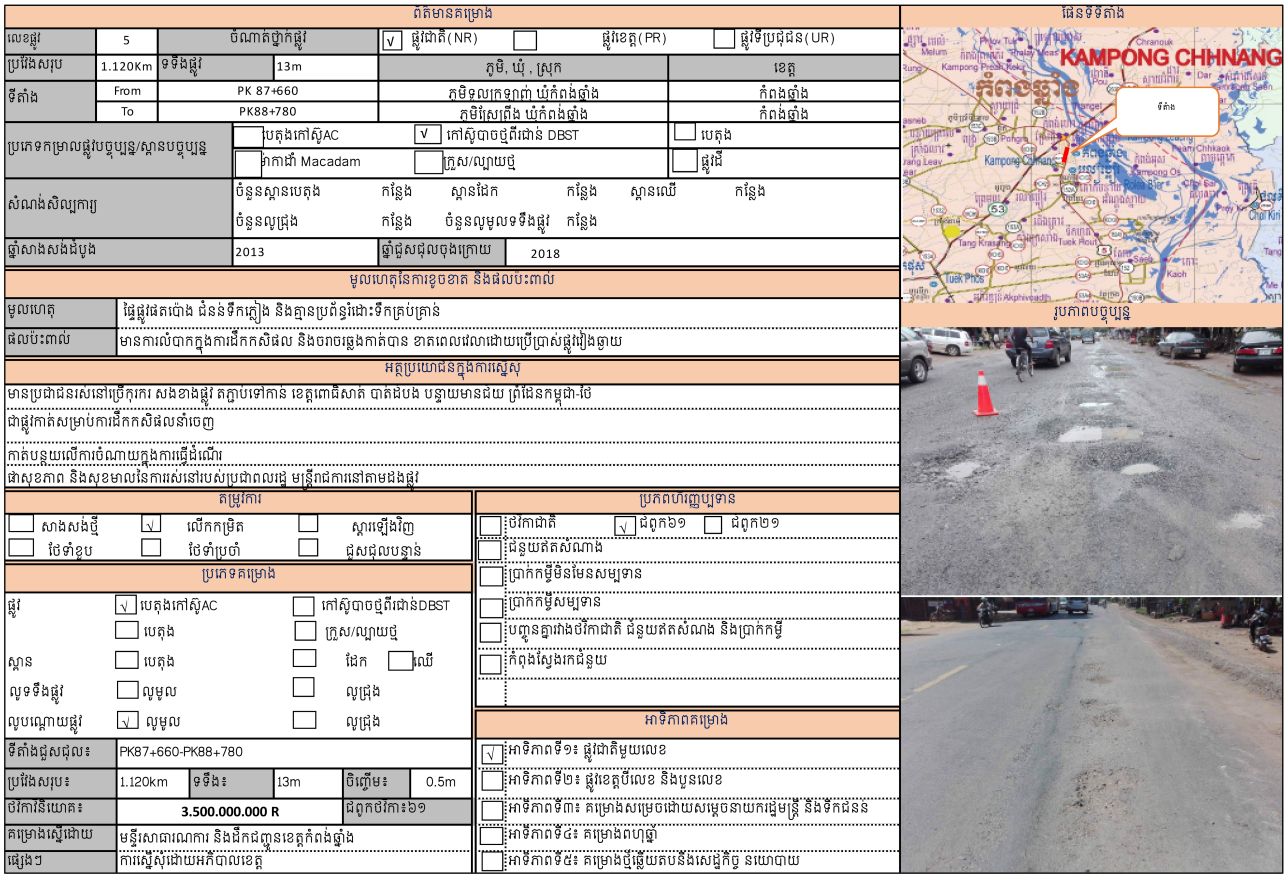


Figure 1.9: Typical content of a maintenance project proposal.

recommendations form the government, which can trigger immediate action.

Visual inspection is inherently subjective, as different inspectors may assess the same road segment differently. Moreover, several types of pavement irregularities that influence ride quality, such as subtle profile variations or localized swelling, are difficult to detect visually, and progress in pavement roughness often go unnoticed. To address these limitations, a new road maintenance system was introduced to the MPWT through the technical assistance project "The Project for Strengthening Capacity for Maintenance of Roads and Bridges (2015–2018)". A central feature of this system is the objective quantification of pavement condition using the

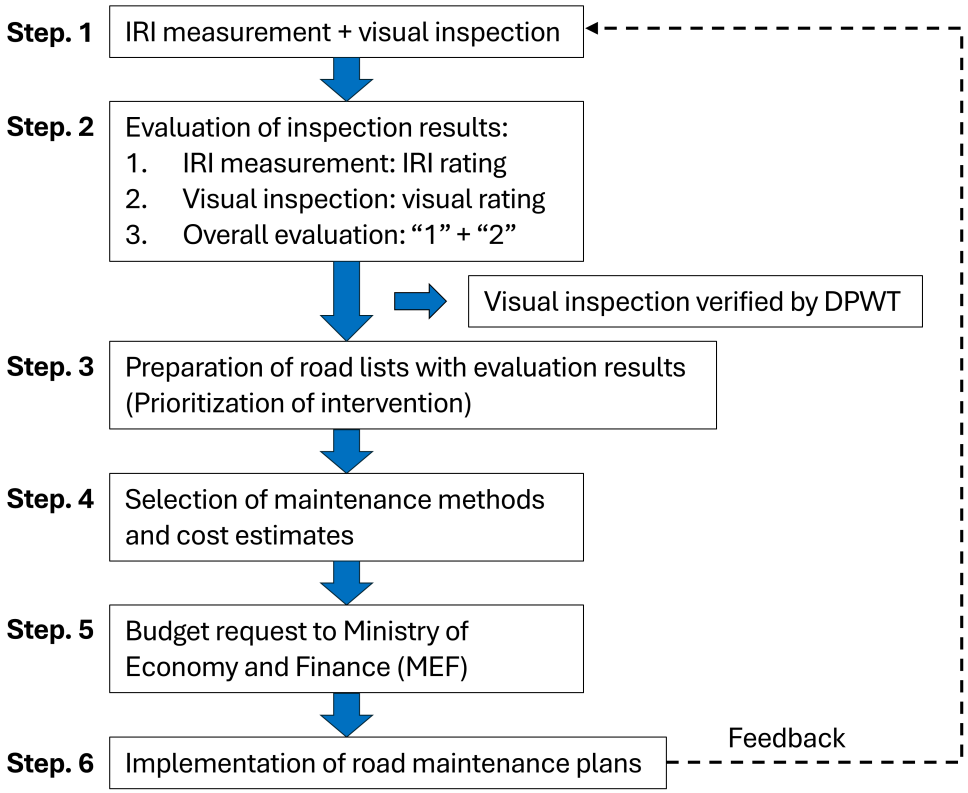


Figure 1.10: Road maintenance implementation using DRIMS.

IRI, measured by a vibration-based device under the Dynamic Response Intelligent Monitoring System (DRIMS). This system simultaneously captures road surface imagery via a dash camera, providing a preliminary visual record alongside the IRI data. The maintenance implementation process under this new framework follows a systematic six-step procedure, as illustrated in Figure 1.10: (1) IRI measurement with visual inspection, (2) evaluation of inspection results, (3) identification of critical sections, (4) selection of maintenance methods, (5) budget request, and (6) implementation of the maintenance plan.

Although the DRIMS framework offers a simplified and cost-effective approach for maintenance implementation, it lacks several essential modules necessary for multi-year maintenance planning. It limitations include an absence of long-term deterioration modeling and an advanced decision-support system for optimizing budget allocation over time. To address these gaps, the MPWT has enhanced the capacity of its Road Data Collection and Management Unit (RDCMU) by integrating two key systems: the Highways Information Management System (HIMS) and the Highway Development and Management Model (HDM-4), version 2.0. HIMS functions as the central database for storing and managing the raw pavement condition data collected by the ROMDAS (Road Measurement Data Acquisition System) survey vehicle. Subsequently, HDM-4 leverages this data, utilizing its integrated road deterioration models to provide a systemic, data-driven analysis. This analysis forecasts future pavement conditions, simulates the impact of various maintenance interventions, and supports investment decisions through cost-effectiveness evaluations. The system' s overall structure is shown in Figure 1.11.

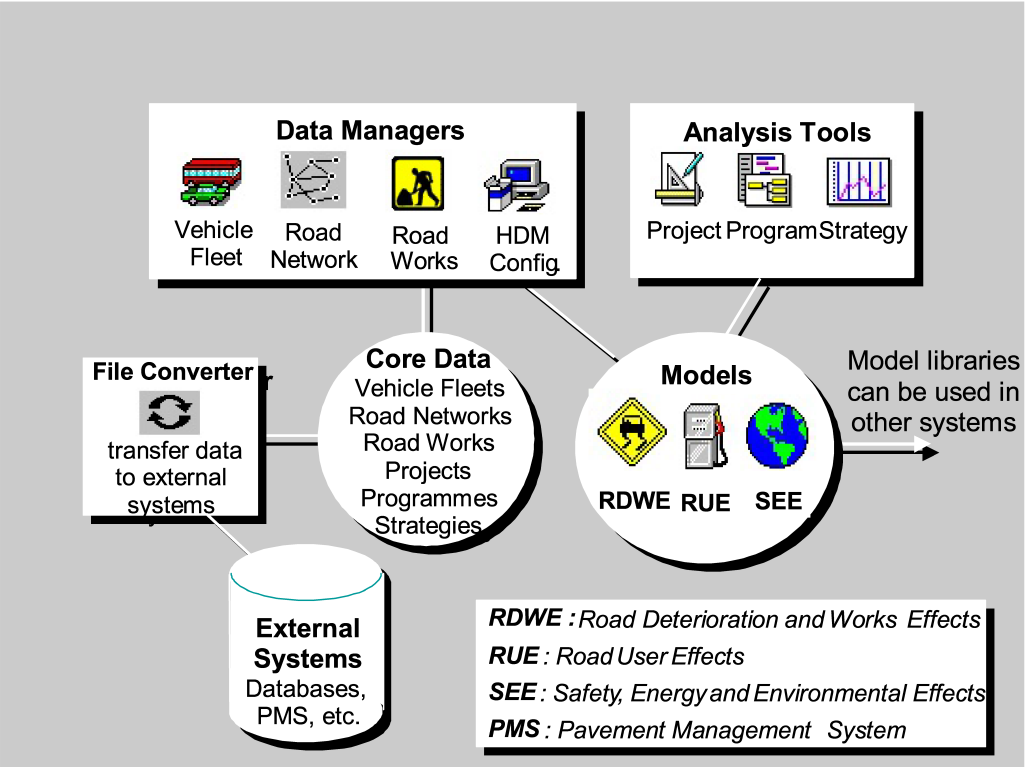
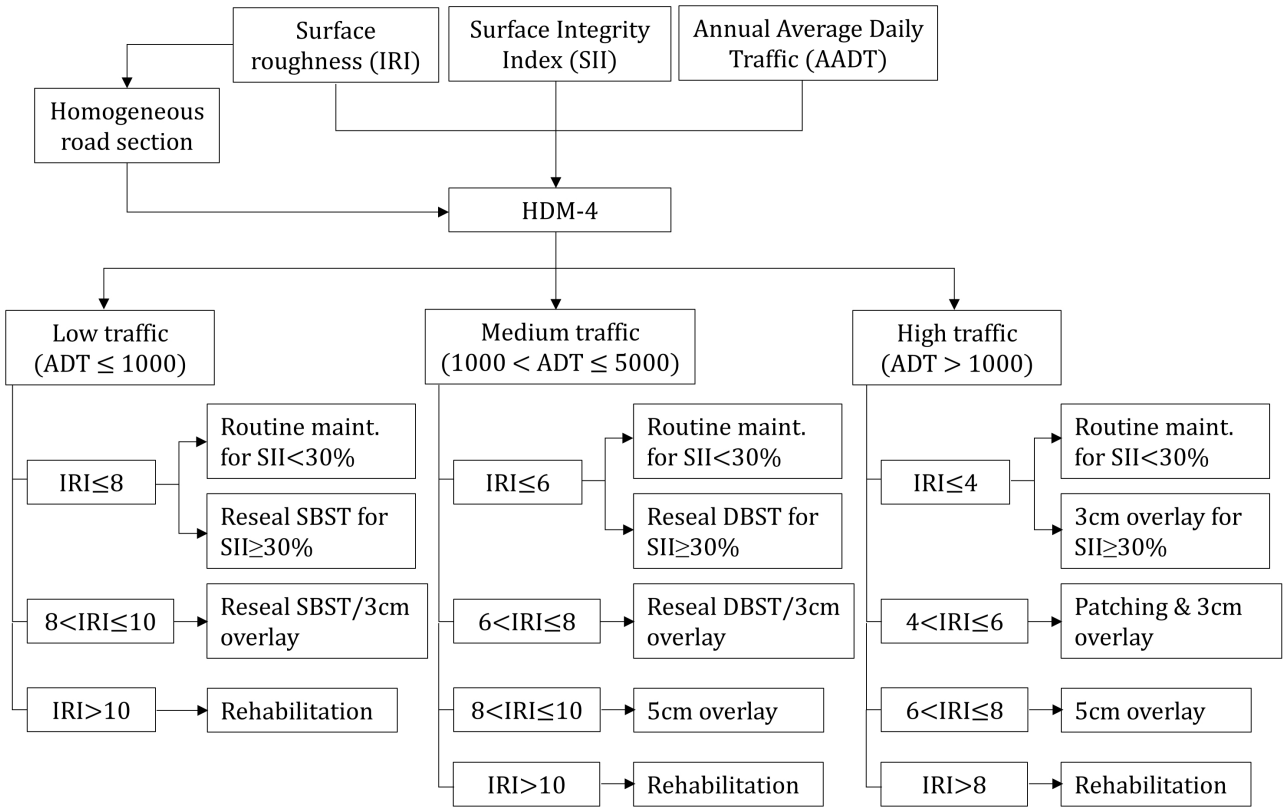


Figure 1.11: HDM-4 system components (Adapted from [28]).

HDM-4 assists decision-makers at three operational levels: strategic, network, and project. At the strategic level, senior officials establish long-term policies, performance targets, and investment priorities that align with institutional and stakeholder objectives. At the network level, agencies develop multi-year maintenance and improvement programs based on the needs of the entire road networks. Possible strategies may include worst-first prioritization or mixed approaches combining preventive maintenance, rehabilitation, and reconstruction. The project level involves the most detailed assessment, focusing on specific road sections. Decisions at this level require more detailed data, such as material testing and subsurface layer bearing capacities to ensure appropriate treatment selection.

To streamline the selection of maintenance treatments, the RDCMU introduced a decision framework based on two key performance indicators, the IRI and the Surface Integrity Index (SII), applied across three traffic categories (low, medium, and high). The overall procedure is illustrated in Figure 1.12. The process begins with the delineation of homogeneous sections using measured IRI values. A homogeneous section is defined as a road segment in which the roughness remains sufficiently consistent to justify treating the entire segment as a single characteristic value, thereby receiving the same maintenance treatment. While IRI reflects surface unevenness and overall ride quality, SII captures the severity of surface distress, including cracking, raveling, potholes, patching, and edge break. SII is expressed on a scale from 0 to 100, where higher values indicate more severe deterioration, similar to the IRI indicator. By integrating the prediction models available within the HDM-4, both the IRI and the defects



Remark: - IRI is expressed in m/km.
- maint. = maintenance

Figure 1.12: Maintenance selection proposed by RDCMU.

(which are parameters for calculating the SII) can be forecasted over time. The framework establishes specific IRI threshold limits categorized according to the level of traffic volume. Based on the defined criteria for both IRI and SII, the final maintenance decision is determined. This decision may range from routine maintenance to more extensive treatments such as resurfacing, overlay, or full rehabilitation. Although this approach provides a systematic methodology, its application is limited by the deterministic, uncalibrated HDM-4 models currently in use. Because these default models have not been calibrated to Cambodian conditions, their predictions may not fully reflect local pavement behavior and environmental factors.

Despite increasing the national maintenance allocation from USD 26 million (2004) to USD 60 million (2015), Cambodia faces a persistent routine and periodic maintenance financing gap [29]. The MPWT identifies that available funds primarily cover routine maintenance, leading to a growing backlog of periodic rehabilitation. This structural deficit is compounded by the technical requirements of the HDM-4 model. For reliable calibration, HDM-4 necessitates robust, multi-year time-series data on pavement characteristics such as roughness, cracking, rutting, structural strength, and traffic loading. A study in Macedonia, for instance, provides a useful preliminary calibration but highlights the intrinsic limitations of short-term data, underscoring the critical importance of long-term monitoring for accurate pavement performance modeling

[30]. To reliably calibrate the HDM-4 defect initiation and progression models, a commitment to multi-year time-series data, typically over at least 5 to 10 years, is often recommended. This duration is necessary to capture errors and model uncertainty. Given that the MPWT has only recently begun utilizing specialized equipment like the ROMDAS survey vehicle and FWD, the limited available historical data makes it nearly impossible to achieve an effective, locally-adapted HDM-4 calibration.

The HDM-4 is widely acknowledged as a critical tool for pavement maintenance and management. However, its implementation faces significant barriers, particularly in developing countries. While the requirement for extensive time-series datasets, as detailed above, is a fundamental technical obstacle that prevents the system from being operated as intended and undermines its core objective of rationalizing maintenance strategies [31]. This data insufficiency prevents the system from being operated as intended, thereby undermining its core objective of rationalizing maintenance strategies. Furthermore, the financial burden of software licensing for both HDM-4 and its complementary data conversion system, HIMS, presents a substantial operational cost. Consequently, the combined effect of inadequate data and high costs renders the standard HDM-4 application sub-optimal, unsustainable, and largely impractical for Cambodia.

1.4 Objectives and significance of the study

Road asset management in developing nations is frequently hindered by a set of challenges, including inadequate inspection policies, fragmented data management systems, unreliable deterioration forecasting, and suboptimal budget allocation. This dissertation addresses three primary gaps within this context: (1) the need for robust, automated data collection methodologies at the network level including pavement crack detection and structural testing; (2) the establishment of consistent, data-driven thresholds for interpreting structural condition; and (3) the development of integrated decision-support tools that leverage deterioration prediction and optimization for maintenance planning.

To bridge these gaps, this research adopts a data-driven approach, developing the methodologies and frameworks that are presented in detail across Chapters 3 through 6. This work makes the following significant contributions:

- **Automated Pavement Crack Quantification and Mapping:** This study develops a novel two-stage framework that integrates detection and segmentation models for the automated quantification of pavement cracks. Its primary contributions include a substantial reduction in manual annotation costs, high accuracy in a lightweight, end-to-end process, and the enabling of automatic geospatial mapping compatible with GIS. This

advancement supports more efficient maintenance management for road agencies. This work is detailed in Chapter 3 and is based on Sovanneth, N., Angelo A. A., Obonguta, F. and Kaito, K.: An Integrated Framework with SAM and OCR for Pavement Crack Quantification and Geospatial Mapping, Infrastructures, Vol.X, No.XX, XXXX.

- **Data-Driven Evaluation of Flexible Pavement Structural Condition:** An analytical framework based on deterioration is proposed to define critical thresholds for structural indices obtained from FWD surveys. This methodology classifies pavement structural condition into three distinct states: Sound, Warning, and Severe. A key impact of this research is its ability to establish structural benchmarks directly from observed surface deterioration, bypassing the need for detailed layer property, a significant advantage in data-scarce environments. Detailed discussion of this contribution is provided in Chapter 4, based on SOVANNETH, N., SASAI, K., OBUNGUTA, F. and KAITO, K.: Stochastic approach to defining pavement structural thresholds from FWD measurements, Intelligence, Informatics and Infrastructure, Vol.6, No.3, pp. 32–46, 2025. DOI:https://doi.org/10.11532/jsceiiai.6.3_32.

- **A Strategic Policy Framework for Network-Level FWD Testing:** This research formulates a policy framework that combines a probabilistic deterioration model with multi-criteria decision analysis. The framework provides road agencies with a systematic approach to determine optimal FWD testing timing intervals and to prioritize critical road sections for assessment. This leads to more efficient deployment of limited budgets, personnel, and equipment. The development of this framework is presented in Chapter 5, based on Sovanneth, N., Obunguta, F., Sasai, K. and Kaito, K.: Strategic application of FWD for efficient network-level pavement assessment, Life-Cycle Performance of Structures and Infrastructure Systems in Diverse Environments, pp. 694–704, 2025. DOI: https://doi.org/10.1201/9781003595120-84.

- **Integration of Deterioration Prediction with Optimization:** The study delivers a comprehensive methodology that integrates probabilistic deterioration prediction with a metaheuristic optimization algorithm. This integration offers substantial practical impact by enhancing maintenance decision-making, improving cost-effectiveness, and boosting overall network performance. The framework is designed to be scalable for large networks and supports dynamic, adaptive maintenance management, particularly in the context of developing countries. Chapter 6 provides detailed discussion, based on Sovanneth, N., Obunguta, F., Sasai, K. and Kaito, K.: Optimization of pavement maintenance planning in Cambodia using a probabilistic model and genetic algorithm, Infrastructures, Vol.10, No.10, 2025. DOI: https://doi.org/10.3390/infrastructures10100261.

Collectively, this dissertation underscores the pivotal role of data in modern road asset management. It contributes novel methodologies for collecting, analyzing, and interpreting

data to facilitate informed decision-making. The study advances the practice of road asset management and demonstrate the innovative application of modern technologies in Cambodia.

1.5 Organization of dissertation

This dissertation is structured into seven chapters to systematically address the identified challenges in road asset management. The research integrates state-of-the-art machine learning, comprehensive probabilistic deterioration modeling that accounts for uncertainty, multi-criteria decision-making, and efficient optimization techniques tailored to the Cambodian context. The organization is as follows:

- Chapter 1: Introduction.
- Chapter 2: Literature review.
- Chapter 3: An integrated framework with SAM and OCR for pavement crack quantification and geospatial mapping.
- Chapter 4: Stochastic approach to defining pavement structural thresholds from FWD measurements.
- Chapter 5: Strategic application of FWD for efficient network-level pavement assessment.
- Chapter 6: Optimization of Pavement Maintenance Planning in Cambodia Using a Probabilistic Model and Genetic Algorithm.
- Chapter 7: Conclusions.

References

[1] OECD. *Transport Bridging Divides*. Paris, 2020. DOI: https://doi.org/10.1787/55ae1fd8-en.

[2] Gibbons, S. et al. New Road Infrastructure: The Effects on Firms. *Journal of Urban Economics* 2019, **110**, pp. 35–50. DOI: https://doi.org/10.1016/j.jue.2019.01.002.

[3] Rosik, P.; Wójcik, J. Transport Infrastructure and Regional Development: A Survey of Literature on Wider Economic and Spatial Impacts. *Sustainability* 2022, **15**(1), p. 548. DOI: https://doi.org/10.3390/su15010548.

[4] Chacon-Hurtado, D. et al. The Role of Transportation Accessibility in Regional Economic Resilience. *Journal of Transport Geography* 2020, **84**, p. 102695. DOI: https://doi.org/10.1016/j.jtrang

[5] Xue, C. et al. Will Road Infrastructure Become the New Engine of Urban Growth? A Consideration of the Economic Externalities. *Sustainability* 2025, **17**(15). DOI: https://doi.org/10.3390/su

[6] Foster, V.; Rana, A.; Gorgulu, N. *Understanding Public Spending Trends for Infrastructure in Developing Countries*. Tech. rep. 9903. 2022. URL: `https://ideas.repec.org/p/wbk/wbrwps/9903.html`.

[7] Wu, Z. et al. Framework for Multiobjective Optimization of Physical Highway Assets Investments. *Journal of Transportation Engineering* 2012, **138**(12), pp. 1411–1421. DOI: https://doi.org/10.1061/(ASCE)TE.1943-5436.0000458.

[8] Zaabar, I.; Chatti, K. Estimating Vehicle Operating Costs Caused by Pavement Surface Conditions. *Transportation Research Record* 2014, **2455**(1), pp. 63–76. DOI: https://doi.org/10.3141/2
08.

[9] Deme, D. A Review on Effect of Pavement Surface Failure on Road Traffic Accident. *American international journal of sciences and engineering research* 2020, **3**(1), pp. 14–19. DOI: https://doi.org/10.46545/aijser.v3i1.137.

[10] Chan, C. Y. et al. Investigating Effects of Asphalt Pavement Conditions on Traffic Accidents in Tennessee Based on the Pavement Management System (PMS). *Journal of Advanced Transportation* 2010, **44**(3), pp. 150–161. DOI: https://doi.org/10.1002/atr.129.

[11] Cairney, P.; Bennett, P. *An Exploratory Study of Surface Characteristics and Crash Occurrence on Selected Roads in Australia*. ARR 382. 2013.

[12] Tehrani, S. S.; Falls, L. C. A Comparison of IRI and Collision Rates in the Province of Alberta. *GEN* 2012, **1024**, p. 1. DOI: https://doi.org/10.13140/RG.2.1.1599.1129.

[13] Mamlouk, M. et al. Effects of the International Roughness Index and Rut Depth on Crash Rates. *Transportation Research Record* 2018, **2672**(40), pp. 418–429. DOI: https://doi.org/10.1177/03

[14] Hall, J. et al. *Guide for Pavement Friction*. Tech. rep. 43. 2009, pp. 1372–76069. DOI: https://doi.org/10.17226/23038.

[15] Crisman, B.; Roberti, R. Tire Wet-Pavement Traction Management for Safer Roads. *Procedia-Social and Behavioral Sciences* 2012, **53**, pp. 1054–1067. DOI: https://doi.org/10.1016/j.sbsp

[16] Mayora, J. M. P.; Piña, R. J. An Assessment of the Skid Resistance Effect on Traffic Safety under Wet-Pavement Conditions. *Accident Analysis & Prevention* 2009, **41**(4), pp. 881–886. DOI: https://doi.org/10.1016/j.aap.2009.05.004.

[17] Standardization, I. O. for. *ISO 55000: Asset Management-Overview, Principles and Terminology*. International Organization for Standardization, 2024.

[18] Kaito, K. "Statistical Deterioration Forecasting Model". *Proceedings of the Road Infrastructure Asset Management Summer School 2013*. Kyoto University, University of Transport, and Communications. 2013.

[19] Van Dam, T. J. et al. *Towards Sustainable Pavement Systems: A Reference Document*. Tech. rep. United States. Federal Highway Administration, 2015. URL: `https://rosap.ntl.bts.gov/view/dot/38541`.

[20] Waidelich, W. Guidance on Highway Preservation and Maintenance. *Federal Highway Administration* 2016. URL: `https://www.fhwa.dot.gov/preservation/memos/160225.cfm`.

[21] Uddin, W.; Hudson, W.; Haas, R. *Public Infrastructure Asset Management, Second Edition*. McGraw Hill LLC, 2013. ISBN: 9780071820127. URL: `https://books.google.co.jp/books?id=ZQsKr5tKFGYC`.

[22] Geddes, R.; Gongera, K. "Economic Growth through Effective Road Asset Management". *International conference on transport and road research, 15th–17th March*. 2016.

[23] American Association of State Highway and Transportation Officials and AASHTO Joint Task Force on Pavements. *Pavement Management Guide*. Washington, DC: American Association of State Highway and Transportation Officials, 2001. URL: `http://app.knovel.com/hotlink/toc/id:kpPMGE0003/pavement-management-guide.`.

[24] Agarwal, P.; Das, A.; Chakroborty, P. "A Rational Approach for Prioritization of Highway Sections for Maintenance". *6th International Conference on Managing Pavements: The Lessons, The Challenges, The Way Ahead*. 2004.

[25] Fwa T, F.; Chan W, T. Priority Rating of Highway Maintenance Needs by Neural Networks. *Journal of Transportation Engineering* 1993, **119**(3), pp. 419–432. DOI: https://doi.org/10.1061/947X(1993)119:3(419).

[26] Bank, A. D. *Greater Mekong Subregion Economic Cooperation Program: Overview*. 2015.

[27] Infrastructure; (IRITWG), R. I. T. W. G. *Overview of the Transport Infrastructure Sector in the Kingdom of Cambodia*. 2023. URL: https://mpwt.gov.kh/index.php/en/documents/other/618.

[28] Kerali, H. G.; Odoki, J. B.; Stannard, E. E. Overview of HDM-4. Volume 1. *The highway development and management series* 2006.

[29] Group, W. B. *Cambodia - Second Road Asset Management Project*. English. Washington, D.C., 2015. URL: http://documents.worldbank.org/curated/en/804511467999119533.

[30] Ognjenovic, S.; Krakutovski, Z.; Vatin, N. Calibration of the Crack Initiation Model in HDM 4 on the Highways and Primary Urban Streets Network in Macedonia. *Procedia engineering* 2015, **117**, pp. 559–567. DOI: https://doi.org/10.1016/j.proeng.2015.08.214.

[31] Aoki, K. International De-Facto Standardization Strategy in Pavements: Kyoto Model. *Proceedings of Asset Management Summer School 2011* 2011, pp. 91–102.

Chapter 2

Literature Review

2.1 Introduction

Effective pavement infrastructure management relies on an integrated framework of condition assessment, deterioration modeling, and informed maintenance planning. Implementing this framework scientifically is crucial for optimizing outputs, ensuring the valid use of resources, and enhancing transparency in long-term infrastructure investment. This is particularly important as management decisions are typically made by road authorities, while funding is often determined through political and parliamentary processes.

The process begins with pavement condition assessment, which provides the foundational data on the existing state of the pavement through both functional and structural evaluations. A robust assessment ensures that network-level maintenance plans, developed by government agencies, align closely with the specific strategies implemented at the project level following detailed inspections. Advances in data collection, particularly the proliferation of automated imaging, have transformed this stage. To efficiently interpret the vast amount of visual data, advanced algorithms like deep learning techniques have been developed. These data-driven methods enable the rapid, high-accuracy detection and classification of pavement distress, significantly reducing reliance on labor-intensive traditional surveys.

The next critical component is deterioration modeling, which allows agencies to forecast future pavement conditions across the network. These predictions are influenced by factors such as traffic loads, environmental exposure, and material properties. While traditional deterministic models offer simplicity and have been widely used, the field has evolved towards more sophisticated probabilistic and machine learning-based approaches. These advanced models are better equipped to capture the inherent uncertainties and nonlinear dynamics of pavement performance.

Finally, reliable performance predictions feed into the maintenance decision-making process within a Pavement Management System (PMS). Decision-support tools within the PMS use

this data to identify cost-effective maintenance and rehabilitation (M&R) strategies. These tools estimate future maintenance needs and costs in response to projected demands, such as increasing traffic volumes and desired service levels. By prioritizing objectives related to network quality and performance, they enable authorities to develop optimized funding scenarios that ensure the timely maintenance and upgrading of road infrastructure.

Together, these interconnected elements form a comprehensive framework for sustaining highway networks, extending pavement service life, and minimizing long-term costs. This systematic process, grounded in engineering principles, provides a structured yet flexible approach for road administrators. It facilitates long-term, strategic planning that optimizes maintenance investments while also supporting broader political and economic objectives.

2.2 Pavement condition assessment

A reliable assessment of pavement condition is fundamental to evaluating performance and informing maintenance decisions. This process relies on condition indices derived from systematic surveys, which can be conducted through manual visual inspections or automated, vehicle-mounted systems. The inspection program begins with establishing standardized data collection rating protocols that specify exactly what pavement distress will be identified, how their severity will be classified, how measurements will be made, how often data will be recorded, and how overall condition values will be calculated. These protocols shall ensure consistency and help ensure that everyone involved understands what data is required and how it should be collected. Given the significant economic and social costs of pavement deterioration, regular inspection is a critical component of any PMS, providing the essential data for assessing current state and planning interventions.

Pavement condition is commonly evaluated from two primary perspectives: functional and structural performance. Functional condition relates to the road user' s experience, including ride quality and safety, whereas structural assessment reflects the pavement' s physical integrity and its ability to withstand traffic loading, typically expressed in terms of pavement response to applied loads [1]. Pavement monitoring generally begins at the early stage of service life (e.g., following construction completion and opening to traffic) and continues throughout the pavement' s life cycle. Although on-site visual inspection is effective for identifying defects that require immediate intervention, the extensive scale of modern road networks necessitates more efficient and automated approaches. Consequently, transportation agencies are increasingly adopting technologies such as image processing to enable broader coverage and more timely detection of pavement distress. While comprehensive indicators that capture both functional and structural performance are desirable, their computation often requires intensive data collecting using specialized and costly equipment, thereby necessitating a strategic selection of key

performance parameters.

Within a PMS framework, accurate evaluation of existing pavement condition is essential for implementing an effective management strategy [2]. Accordingly, collecting data that truly reflects the actual condition of the road networks helps agencies make better M&R decisions. When an agency implements an evaluation plan, it obtains more reliable and consistent data, which leads to improvements in planning, reporting, and budgeting. This also strengthens compliance with external requirements, enhances organizational credibility, and supports data integration across institutional systems. Pavement evaluation encompasses three primary components: (1) data collection, (2) condition rating, and (3) quality management [3]. Condition rating is the process of classifying the pavement condition based on a selected scale or index. These ratings, which can be qualitative or quantitative, serve multiple essential purposes: they facilitate maintenance scheduling, allow comparison among pavement sections, assist in estimating rehabilitation scope and cost, and support long-term budget planning [3–5].

Globally, transportation agencies use a variety of condition rating systems, which generally fall into two categories: estimated ratings and measured ratings, as shown in Table 2.1. Estimated ratings primarily rely on visual observations of pavement distress, whereas measured ratings incorporate physical data such as roughness, rutting, or deflection, supported by mathematical formulations. Some indices reflect only a single type of distress (e.g., IRI), while others integrate multiple distress types (e.g., PCI). Measured systems are commonly preferred because they provide more objective and consistent assessments. The choice of rating system depends on agency resources, the prevalent distress types in the region, and the desired level of precision. Comprehensive performance indices offer the most complete evaluation of pavement condition; however, collecting the extensive data required often involves costly equipment, such as high-speed multi-sensor survey vehicles or Falling Weight Deflectometer (FWD) devices. As a result, agencies frequently select indices that balance informational value with practical limitations. Overall, the use of condition rating systems encourages data-driven decision-making and reduces reliance on subjective judgment or political influence in pavement management.

2.2.1 Functional evaluation

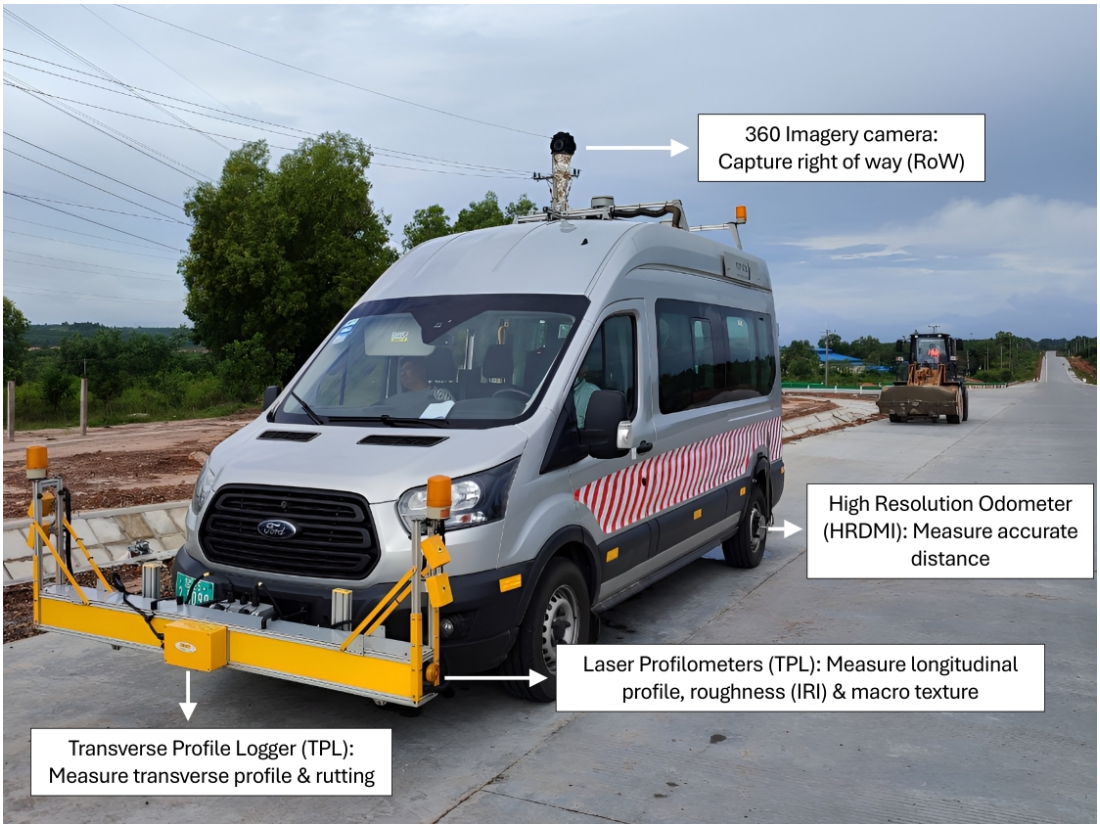
Pavements with strong functional performance contribute to safer travel while maintaining operational speed by enhancing the interaction between vehicle tires and the road surface. Functional evaluation assesses a pavement' s performance from the perspective of the road user, with emphasis on safety, ride smoothness and overall comfort [20]. To assess pavement functionality, several types of condition surveys may be conducted, including measurements of roughness, rutting, cracking, skid resistance, and surface texture. These surface distress significantly affect user's driving experience and can lead to secondary impacts such as increased

Table 2.1: Pavement condition rating systems.

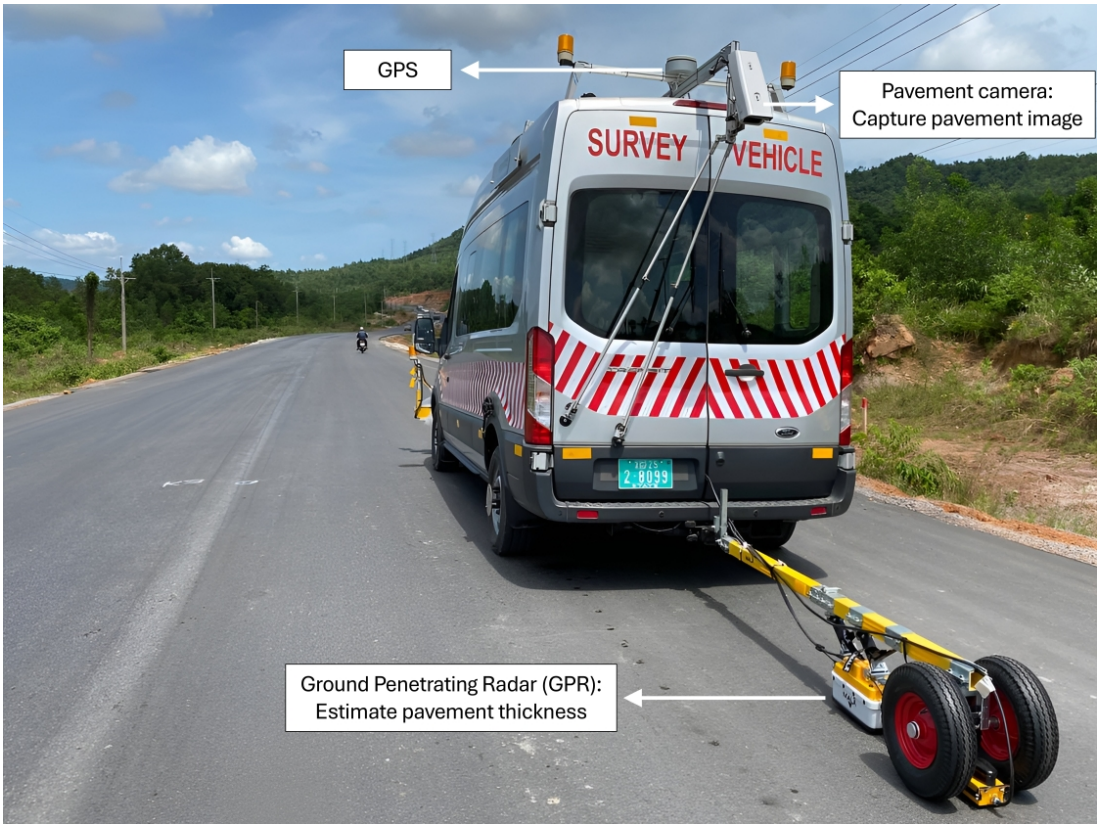
Estimated Condition Rating	Measured Condition Rating
• Present Serviceability Rating (PSR): Based on ride quality experienced by a panel of experts.[6] • Condition Rating Survey (CRS): Based expert estimates on visual distress.[7] • Pavement Surface Evaluation Rating (PASER): A direct rating based on visual distress.[8]	• Present Serviceability Index (PSI): Function of smoothness, rutting, cracking and patching.[9] • Pavement Condition Index (PCI): Function of 19 different distress such as rutting, cracks, bleeding and potholes.[10] • International Roughness Index (IRI): Function of ride quality.[9, 11, 12] • Maintenance Control Index (MCI): Function of cracks, rutting, and roughness.[13] • Pavement Quality Index (PQI): Function of ride quality index (RQI), IRI and surface rating (SR).[9] • Pavement Condition Rating (PCR): Function of 13 different distress such as rutting, cracks, bleeding and potholes.[14] • Surface Distress Index (SDI): Function of fatigue cracking, patching, transverse cracking, block cracking, rutting, and IRI.[15] • Overall Pavement Index (OPI): Based on the PSI which is derived from IRI.[16] • Structural Condition Index (SCI): Function of FWD data.[17] • Deflection Bowl Parameters (DBPs): Function of FWD data.[18, 19]

fuel consumption and higher greenhouse gas emissions. Data collection is commonly performed using specialized network survey vehicles, as illustrated in Figure 2.1. Accordingly, the use of reliable condition indicators is essential in a PMS to support accurate assessment and decision-making. Widely adopted performance indices include the Present Serviceability Rating (PSI), Pavement Condition Index (PCI), Pavement Condition Rating (PCR), Pavement Quality Index (PQI), Maintenance Control Index (MCI), and the International Roughness Index (IRI).

Among the most widely used composite indicators for functional evaluation is the Pavement Condition Index (PCI), a standardized system originally developed by the U.S. Army Corps of Engineers. The PCI assigns a numerical rating ranging from 0 to 100, where 0 represents a failed pavement and 100 indicates an excellent condition. PCI values are determined based



(a) Front view



(b) Back view

Figure 2.1: Distress survey vehicle.

on the type, density, and severity of distress observed on the pavement surface [10]. Distress density is defined as the proportion of the affected area or length of a particular distress type relative to the total area or length of the sample unit. The evaluation procedure, standardized under ASTM D6433-20, consists of either manual or automated survey covering up to 19 types of pavement distress. The method involves identifying and measuring each distress, assigning a deduct value, and applying correction procedures to derive the final PCI score, which represents the overall measure of pavement integrity and surface condition. The PCI can is calculated as follows:

$$PCI = 100 - maxCDV \tag{2.1}$$

where $maxCDV$ is the maximum corrected deduct value obtained from CDV-TDV adjustment curves.

Pavement Condition Rating (PCR) is another composite performance index that utilizes pavement surface distress information to provide a quantitative measure of maintenance requirements [20]. Similar to the PCI, the PCR is expressed on a scale ranging from 0 to 100, where higher values indicate better pavement condition. The rating reflects the overall surface condition of a pavement section based on the identification of 13 distress types, while accounting for both the extent and severity of each defect [21]. The PCR is calculated by first assigning a deduct value (DV) to each observed distress and then subtracting the total deductions from 100. The deduct value and PCR are defined as:

$$DV = DistressWeight \times Extent \times Severity \tag{2.2}$$

$$PCR = 100 - \sum DV \tag{2.3}$$

Although these distress measurements are traditionally used to compute the PCI, the formulation can be extended by incorporating pavement roughness through the Roughness Condition Index (RCI) [22]. The RCI is a dimensionless indicator scaled from 0 to 100, enabling compatibility with PCI values, and is estimated from the IRI [23]. The RCI and modified PCR are calculated as follows:

$$RCI = 253.67\, e^{-0.459\, IRI} \tag{2.4}$$

$$PCR_{modified} = 0.6\, PCI + 0.4\, RCI \tag{2.5}$$

Building upon the PCR, the Pavement Quality Index (PQI) integrates both ride quality and surface distress into a single performance indicator, as introduced by the Ohio Department of Transportation (ODOT) [24]. PQI provides a more comprehensive representation of pavement serviceability, particularly in the post-maintenance phase. Unlike the modified PCR, IRI is incorporated as a penalty term applied to the PCR. The PQI is calculated using the following equation:

$$PQI = PCR - a\,(IRI)^b \tag{2.6}$$

where a and b are regression coefficients according to roadway functional classification.

In Japan, the MCI is widely adopted as a practical indicator for evaluating the functional condition of pavement networks [13]. The MCI supports decision-making related to maintenance strategies by enabling comparisons among pavement sections and guiding actions that range from routine maintenance to full-scale rehabilitation, depending on the severity of observed deterioration. This index incorporates three primary pavement performance indicators: cracking ratio, rutting depth, and surface roughness. However, when complete datasets are unavailable, the MCI may also be estimated using only two or even one of these parameters. The MCI is determined using the following empirical relationship:

$$MCI = 10 - 1.48\,C^{0.3} - 0.29\,D^{0.7} - 0.47\,\sigma^{0.2} \tag{2.7}$$

where C represents the cracking ratio, D denotes the rutting depth, and σ indicates the roughness.

Roughness-based models play a key role in the functional evaluation of pavements, as they directly represent surface condition and user-perceived serviceability. The IRI, introduced by the World Bank in the 1980s, quantifies longitudinal surface irregularities and has become a standard measure in pavement performance assessment worldwide [20]. Lower IRI values indicate smoother pavement surfaces and correspond to higher user comfort and perceived quality. In the United States, pavement condition is commonly classified as good when the IRI is below 1.5 m/km and poor when it exceeds 2.7 m/km [25]. Although IRI-based models are effective for assessing ride quality, they do not explicitly account for subsurface deterioration. As a result, maintenance strategies based solely on roughness indicators may overlook structural deficiencies, potentially leading to premature failure of surface treatments and the need for more intensive rehabilitation measures in the long term [26].

From the users' perspective, pavement performance is primarily evaluated based on func-

tional attributes such as smoothness, safety, and ride comfort, with limited consideration of the underlying structural condition. Nevertheless, the emergence of surface distresses, including cracking, rutting, and increased roughness, often signals a degradation of structural capacity. Consequently, visible functional defects are not merely surface phenomena but symptomatic of deeper structural weaknesses that compromise the pavement' s long-term ability to withstand traffic loads.

2.2.2 Structural evaluation

The evaluation of pavement structural condition has traditionally relied on deflection-based testing, with the FWD being the most widely adopted device worldwide. The FWD implies an impulse load to the pavement surface while an array of sensors records the resulting deflection basin, as shown in Figure 2.2. These measurements may be used directly as indicators of structural performance or indirectly to estimate material properties, such as layer moduli, though backcalculation procedures. As noted by Haas et al. [27], understanding the structural capacity of pavement networks is essential for effective M&R planning. Although several types of deflection equipment exist, the FWD remains the preferred tool in many countries due to its reliability and operational efficiency. Structural condition is typically evaluated using inputs such as layer thickness, material properties, traffic loading, wheel load characteristics, and environmental factors. At the network level, FWD data also assist in identifying homogeneous management sections, grouping pavements with similar structural capacities for performance prediction, and selecting the candidate sections that require detailed project-level investigation [28].

One of the principal applications of FWD data is the determination of the Structural Condition Index (SCI), which serves as a screening tool for network-level M&R decision-making for asphalt concrete and thin surface-treated pavements [29, 30]. The SCI is defined as the ratio of the effective Structural Number (SN_{eff}), which represents the in situ structural capacity derived from FWD data, to the required Structural Number (SN_{req}), calculated using the AASHTO design procedure based on projected traffic loads in terms of equivalent single axle loads (ESALs). An SCI value greater than or equal to 1.0 indicates that the pavement structure is adequate to carry future traffic demands, whereas value below 1.0 suggest the need for structural strengthening. The formula is expressed as:

$$SCI = \frac{SN_{eff}}{SN_{req}} \tag{2.8}$$

While backcalculation of layer moduli is a common practice, it requires detailed layer thickness data that is often unavailable for network-level screening. In such cases, estimating the SN_{eff}

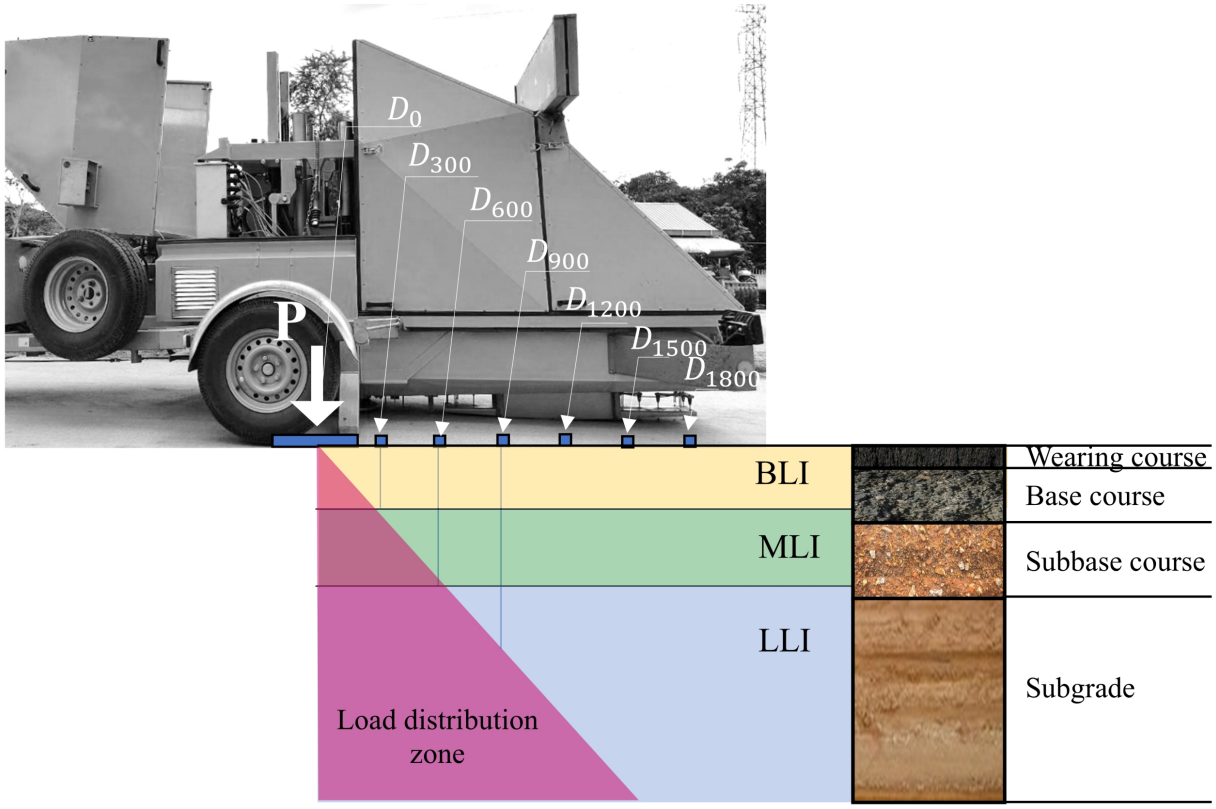


Figure 2.2: Schematic diagram of FWD.

directly from FWD deflection basins provides a robust and effective alternative for characterizing structural capacity across a network.

As an alternative to methods requiring SN calculation or full backcalculation, Deflection Bowl Parameters (DBPs) offer a semi-empirical technique for a rapid assessment of structural condition [18, 31]. This approach bypasses complex computational procedures by leveraging the strong correlation between the relative differences in FWD geophone readings and the strength of underlying layers. Key DBPs include the maximum deflection (D_0), which evaluates the entire pavement structure, as well as the Base Layer Index (BLI), Middle Layer Index (MLI), and Lower Layer Index (LLI), which are used to assess the surfacing and base course, the subbase, and subgrade, respectively [18].

Originally developed and validated in South Africa, DBP methodologies have since been adapted and applied in various regions worldwide [31, 32]. Pavement structural condition is typically classified using DBP thresholds corresponding to three levels such as “Sound”, “Warning”, and “Severe”. However, due to differences in pavement designs, material properties, and traffic loading, thresholds established in one region cannot be directly applied to others without local calibration. Consequently, numerous benchmarking and case studies have been conducted to adjust DBP limits for different contexts, including investigations of bituminous base pavements in the United States [33] and Colombia [34] which employed numerical modeling and probabilistic methods, respectively.

Table 2.2: Deflection bowl parameters and their significance.

Parameter	Formula	Remarks
Maximum deflection (D_0)	Directly measured at center of loading plate	Represents overall pavement bearing capacity
Radius of curvature (RoC)	$\text{RoC} = \dfrac{L^2}{2D_0\left(1 - \dfrac{D_{200}}{D_0}\right)}$	Highly correlated with wearing course bearing capacity
Base layer index (BLI)	$\text{BLI} = D_0 - D_{300}$	Highly correlated with combined wearing course and base course bearing capacity
Middle layer index (MLI)	$\text{MLI} = D_{300} - D_{600}$	Highly correlated with subbase course capacity
Lower layer index (LLI)	$\text{LLI} = D_{600} - D_{900}$	Highly correlated with subgrade bearing capacity

Note: $D_0, D_{200}, D_{300}, D_{600}$, and D_{900} are deflection measurements at distances of $0, 200, 300, 600$, and $900\,\text{mm}$ from the center of the loading plate, respectively, with units of micron.

2.2.3 Artificial intelligence

The advancement of pavement condition assessment has been profoundly transformed by the integration of computer vision-based systems, which facilitate the automated processes of distress detection and quantification. Although traditional visual inspection is considered as the simplified method, it is subjective, time-consuming, and sometimes inconsistent. Hence, extracting information from image pixels, specifically image captured from survey vehicles, using the domain of computer vision becomes popular. In recent years, the incorporation of image processing, machine learning (ML), and deep learning (DL) techniques has provided a nuanced and comprehensive approach to evaluating civil infrastructure [35–37]. These automated techniques leverage visual data captured through various modalities, including camera mounted on survey vehicle, drone-equipped cameras, thermal imaging, and ultrasonic scanning. The value of these image-based methods lies in their ability to address the limitations of conventional sensors, particularly by detecting subtle or highly localized damage that might otherwise be missed. Moreover, they provide essential visual context, enhancing the understanding of structural deformation and aiding in informed decision-making for maintenance and repair strategies [38–40].

In the context of image processing techniques, key methodologies include edge detection, texture analysis, and image registration [41]. Edge detection involves identifying boundaries and highlighting features or discontinuities within an image that may indicate potential damage or surface changes. By detecting abrupt changes in pixel intensity, edge detection provides a clear visualization of surface anomalies that may not be apparent through simple visual inspection.

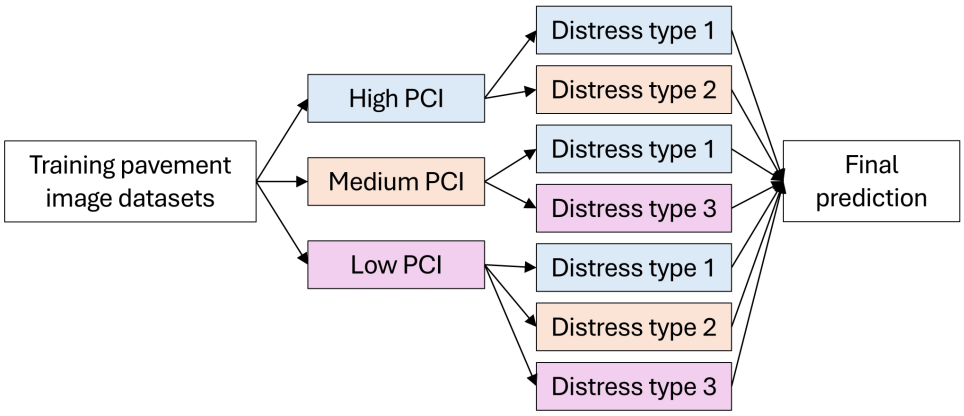


Figure 2.3: The DT process.

Texture analysis focuses on characterizing the spatial arrangement and relationship of pixels, enabling the identification of anomalous patterns on the pavement surface. By quantifying surface variations, texture analysis helps differentiate between damaged and undamaged regions. Image registration is used to align and overlay multiple images of the same perspective, allowing for precise comparison and the robust detection of temporal changes. This process can be achieved by identifying corresponding features or patterns, estimating a spatial transformation, and then interpolating pixel values to map onto the reference image in its new aligned position.

The subsequent incorporation of ML signifies a crucial step toward automated and efficient evolution, offering accurate identification of pavement surface status. The ML is an advanced system of algorithms, generally modeled as one of three tasks: object classification, detection problems, or pixel segmentation problems [42]. Traditional ML techniques are employed to classify pavement defects based on type and severity. Common supervised learning models developed for this task include Decision Trees (DT), Random Forest (RF), and Support Vector Machines (SVMs). The DT is suitable for developing prediction algorithms with large datasets, DTs utilize a hierarchical structure to classify input datasets into homogeneous classes [43]. The RF is an ensemble classification method that relies on aggregating the outcomes from multiple trained decision trees to produce highly accurate predictions in classification and detection tasks [44–46]. The SVM is primarily a binary classification model that employs principles of statistical learning to effectively distinguish between input variables, even with high-dimensional data, and is widely used to predict and classify pavement degradation [47]. The operational principles of DT, RF, and SVM are illustrated in Figure 3, 4, and 5, respectively. Nevertheless, traditional ML methods are often criticized for their limited generalization ability when faced with unseen, complex data from diverse environments [48]. This limitation prompted the shift toward deep learning.

The DL networks, particularly those incorporating convolutional operations, have demonstrated strong capabilities in addressing complex visual recognition and interpretation tasks. In general, DL frameworks are structured into two principal parts: the feature learning stage

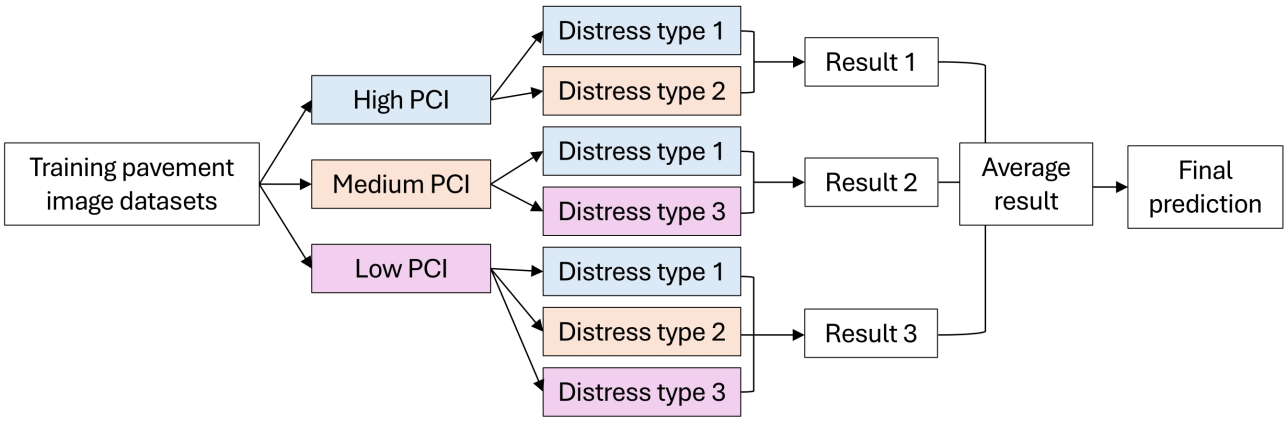


Figure 2.4: The RF process.

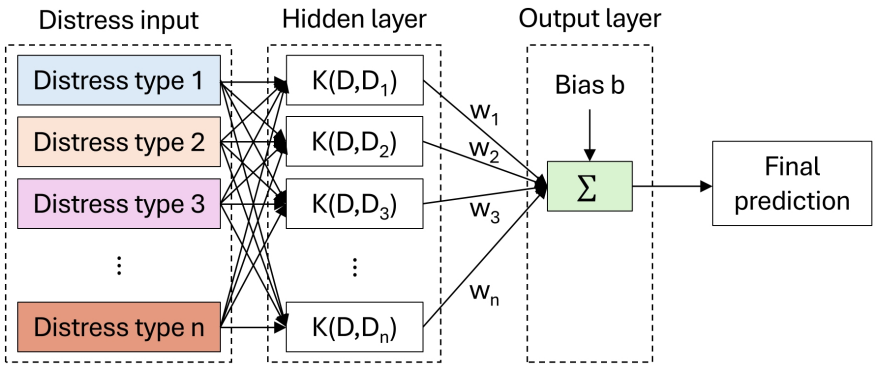


Figure 2.5: The SVM process.

and the inference stage for detection, classification, and segmentation phase. The arrangement of these interconnected layers is defined as the network architecture, while a trained instance of this architecture, including optimized weights and biases, is referred to as a model. In image analysis applications, the Convolutional Neural Network (CNN) constitutes a foundational architecture for the feature extraction phase [49]. For classification, the CNN extracts discriminative features which are subsequently processed by fully-connected (dense) layers to estimate a distress class, as depicted in Figure 2.6. In semantic segmentation, the CNN acts as an encoder, compressing the input into a feature representation. This is followed by a decoder network, often composed of transposed convolutional layers, which performs pixel-wise classification to precisely delineate distress boundaries, as shown in Figure 2.7. For object detection, the CNN-extracted features are fed into region proposal networks (RPNs) that generate bounding boxes to localize object of interest within the image. An advanced example is Mask R-CNN, an extension of Faster R-CNN, which is a unified framework for simultaneous object detection, classification, and instance segmentation; its architecture is illustrated in Figure 2.8 [50]. Consequently, distress identification using deep neural networks can be categorized into three methodological approaches: object detection, segmentation, and classification for pixel-level damage characterization.

A significant challenge in developing high-performance DL models is the requirement for a

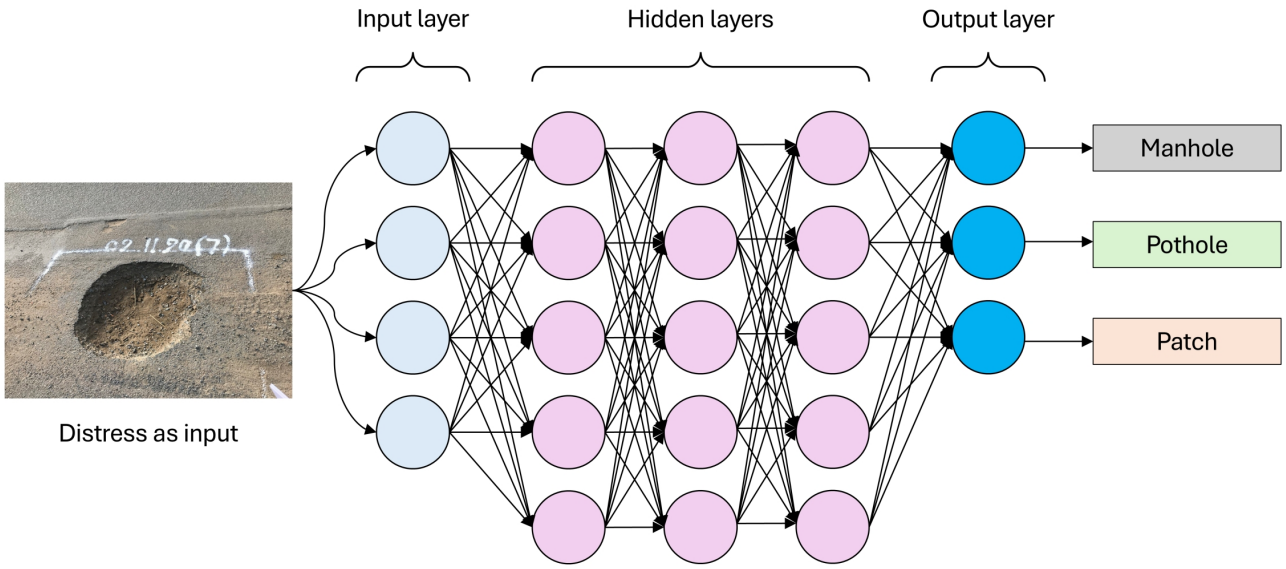


Figure 2.6: CNN architecture for classification.

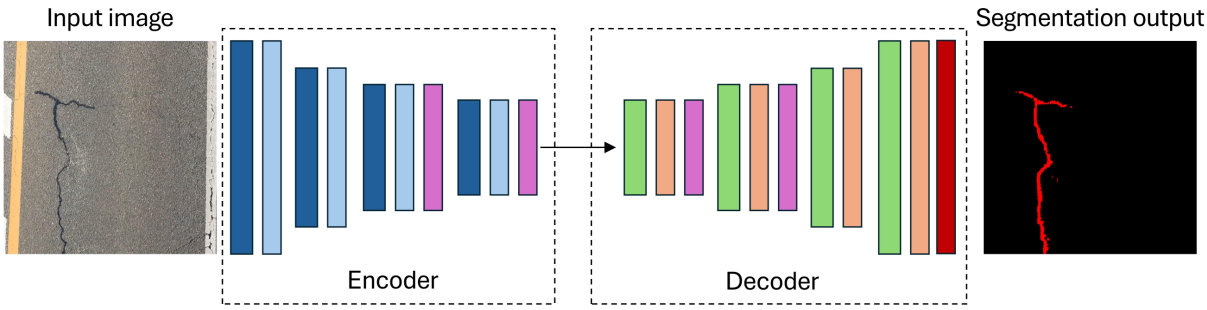


Figure 2.7: Basic architecture of CNN-based segmentation.

comprehensive and balanced training dataset that accurately represents the diversity, instance count, and severity of distress types encountered in real-world conditions [51]. Despite this constraint, notable progress has been achieved. For instance, Hsieh and Tsai [52] pioneered a CNN-based method for raveling detection by leveraging macro-texture features derived from 3D images captured by PaveVision3D. Their model reported accuracies of 90.8% for general raveling detection and 85% for severity classification. In a separate study, Dong et al. [53] enhanced Mask R-CNN by optimizing its RPNs, achieving a 95% accuracy in automated pavement crack detection.

Beside the transformative potential of the prescribed approaches, ML- and DL-based models still present several limitations. Foremost, these models rely heavily on large, diverse, and accurately labeled datasets; however, generating such datasets requires extensive manual annotation, which is both time-consuming and costly, particularly for pixel-level segmentation tasks. Moreover, models trained on data from one specific environment, such as a particular region's pavement characteristics, lighting conditions, or camera system, often experience significant performance degradation when applied to different settings. This challenge, commonly referred to as domain shift, restricts their generalizability and limits reliable deployment across diverse

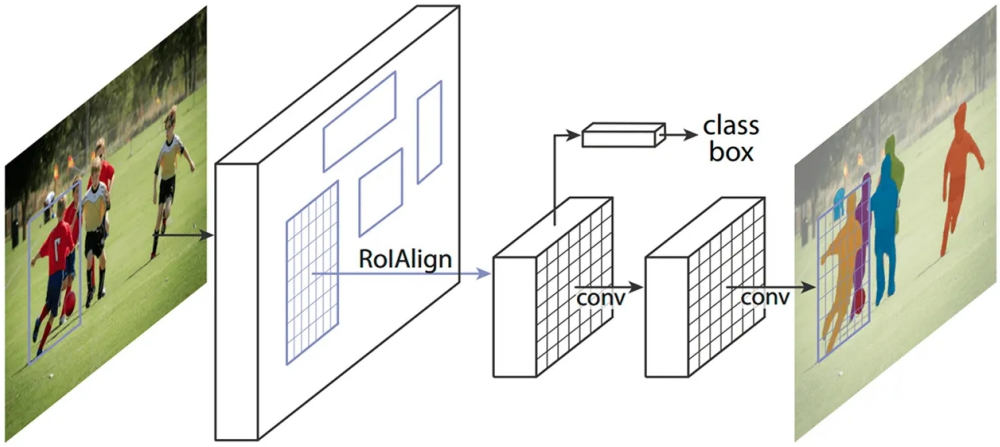


Figure 2.8: Mask R-CNN framework (Adapted from He et al.[50]).

real-world scenarios.

2.3 Deterioration prediction

An effective PMS requires reliable prediction models to accurately represent pavement deterioration under real-world conditions characterized by several influencing factors. Deterioration models are commonly classified into three categories: deterministic, probabilistic, and intelligent approaches. Each category provides distinct methodologies for forecasting pavement performance indicators, such as IRI. Such predictive capability enables road agencies to move from reactive maintenance practices to proactive, performance-based asset management. Over time, pavement performance modeling evolved from simplified empirical relationships to more advanced frameworks designed to capture non-linear deterioration behavior and inherent uncertainty. Although pavements are designed under the assumption of uniform material properties, consistent layer thicknesses, and homogeneous loading conditions, these idealized assumptions rarely hold in practice. In reality, pavement structures are subjected to highly variable traffic loading and environmental conditions. Traffic is not distributed uniformly across the pavement surface, and climatic factors such as temperature variation and rainfall patterns differ across regions and even along the same roadway. These spatial and temporal variations lead to non-uniform distress development, where pavement damage manifests irregularly rather than symmetrically.

2.3.1 Deterministic models

Deterministic models represent a foundation and enduring approach in pavement management, predicting future conditions through mathematical equations derived from long-term historical

data. These models operate on the principle of a direct cause-and-effect relationship, whereby a given set of inputs invariably produces the same output. For example, George et al. [54] developed an empirical-mechanistic deterioration model by classifying pavements and employing regression analysis to formulate prediction equations, which were subsequently validated against other established models. Their research highlighted pavement age as the most significant predictor of serviceability, with traffic volume and structural composition playing a secondary role. Similarly, Fuentes et al. [55] established deterministic serviceability models by correlating objective pavement indicators, specifically the IRI and PCI with user perception (PSI). The study provides a data-driven basis for prioritizing M&R projects by developing deterministic models based on linear regression analysis and exploring various equation forms to find the best fit between IRI/PCI and PSI. Using linear regression, they evaluated various equation forms to identify the optimal fit, thereby creating a data-driven foundation for prioritizing M&R projects.

The practical utility of this approach is demonstrated by the Arizona Department of Transportation (ADOT), which transitioned from a forecasting system to one that actively prescribes and prioritizes cost-effective treatments using a deterministic framework centered on marginal cost-effectiveness analysis [56]. This shift provided a more direct and actionable tool for engineers to manage infrastructure at both the network and project levels. The primary strengths of deterministic models lie in their simplicity, interpretability, and computational efficiency, making them well-suited for integration into PMS, especially in contexts with limited historical data. This is exemplified by a general Pavement Condition State (PCS) function, which can be formulated to model deterioration based on a fixed set of variables such as traffic, structural capacity, and environmental factors [57]. However, a significant limitation is their inherent inability to account for the stochastic variability in pavement performance. By treating uncertain factors like traffic and climate as deterministic inputs, they generate single-point estimates that can lack reliability [58, 59]. Furthermore, they often oversimplify complex, non-linear deterioration processes and lack the adaptability required for diverse regional conditions, which constrains their utility in large-scale, dynamic network analyses.

2.3.2 Probabilistic models

Probabilistic prediction models were developed to address the limitations of deterministic approaches by explicitly incorporating uncertainty into infrastructure performance forecasting. Rather than producing single-point estimates, these models generate probability distributions of pavement condition, thereby enabling risk-informed decision-making and improved asset management strategies. Among probabilistic approaches, Markov chain models are the most widely applied, representing pavement deterioration as transitions among discrete condition states governed by a Transition Probability Matrix (TPM) [60, 61].

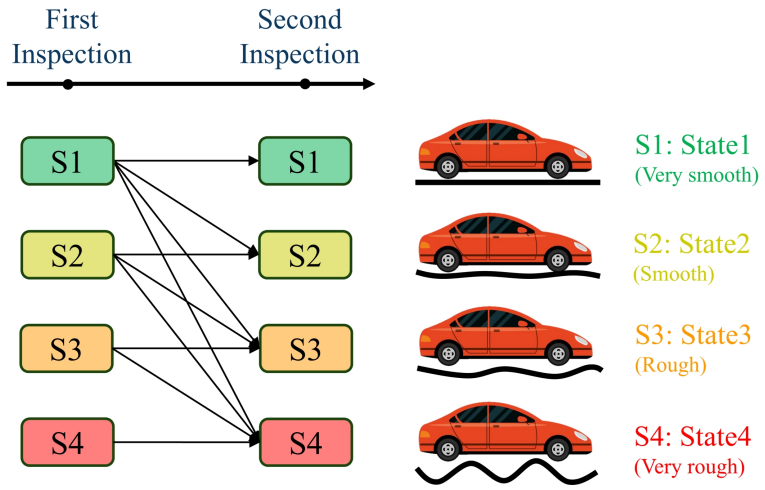


Figure 2.9: Illustration of pavement condition through Markov process (no maintenance).

A Markov chain is defined by the property that the probability of transitioning to a future state depends only on the current state and not on the sequence of preceding states, distinguishing it from deterministic models that rely primarily on long-term historical trends. The stochastic nature of the Markov process is illustrated in Figure 2.9. To enhance the theoretical foundation of standard Markov models, Tsuda et al. [62] integrated hazard-based reliability concepts into the Markov framework, developing the so-called Markov hazard model to estimate transition probabilities for bridge deterioration. This approach accounts for varying inspection intervals and incorporates explanatory variables influencing degradation. A key contribution of this work is the introduction of time-adjusted transition probabilities, allowing deterioration rates to be calculated across arbitrary time intervals and thereby improving compatibility with irregular inspection schedules commonly observed in practice. Furthermore, Obama et al. [63] extended the Markov hazard model by incorporating unobserved heterogeneity to reflect variation in deterioration rates across infrastructure groups with unknown material properties or design attributes. By introducing random effects at the class level, the model enables differentiation among infrastructure groups and supports classification of assets according to their relative deterioration severity. This enhancement allows decision-makers to identify rapidly deteriorating categories and prioritize them for early intervention. Beyond Markov-based approaches, Bayesian methods have gained prominence due to their capacity to combine prior knowledge with observed data and update predictions as new information becomes available. Hong and Prozzi demonstrated the utility of Bayesian inference in managing heterogeneous pavement datasets, while more recent advances, such as Bayesian Neural Networks (BNNs), further extend probabilistic prediction by providing uncertainty bounds alongside model outputs [64, 65]. Fuzzy regression techniques have also been adopted to address vagueness and qualitative uncertainty, particularly in data-limited environments where expert judgment plays an important role. For example, Wang and Li proposed a hybrid fuzzy-gray model to forecast pavement roughness under conditions of limited quantitative input data [66].

The principal advantage of probabilistic models lies in their explicit treatment of uncertainty, enabling transportation agencies to evaluate alternative future scenarios and incorporate risk into maintenance planning and investment decisions [67]. However, these models are not without limitations. Methodological assumptions, such as the Markov property's disregard for cumulative damage history and the impact of past maintenance actions, can sometimes oversimplify the deterioration process [68]. Furthermore, model calibration often requires substantial, high-quality datasets. Advanced frameworks like BNNs, while powerful, demand significant computational resources and specialized expertise, which can present barriers to their widespread implementation in practice.

2.3.3 Intelligent models

Intelligent models represent an advanced class of predictive modeling approaches. They employ ML and DL algorithms to extract nonlinear relationships from data without requiring explicit functional formulations. These techniques are particularly suitable for processing heterogeneous and high-dimensional datasets, including traffic loading, climatic variables, material characteristics, and maintenance records.

Several ML methods have demonstrated effectiveness in predicting pavement performance. Ensemble models, including Random Forest (RF), Gradient Boosting Decision Trees (GBDT), and XGBoost, have produced accurate results. Cheng et al. reported R^2 values above 0.97 for rutting prediction using these methods [69]. Similarly, Al-Samawi et al. showed that Gaussian Process Regression (GPR) can predict the IRI under varying climate conditions [70]. DL models have also been applied in this field. Two typical DL models combining CNNs and long short-term memory (LSTM) networks were employed by Deng et al. to capture rutting development over time using limited data, achieving an R^2 value of 0.936 [71]. In addition, pavement condition measured by the PCI has been predicted using feed-forward neural networks (FNNs) over a planning horizon based on inspection records and traffic and climate data [72]. Recent studies have introduced hybrid intelligent frameworks to enhance predictive accuracy and uncertainty quantification. Bayesian Neural Networks (BNNs) facilitate probabilistic inference by generating predictive distributions rather than point estimates, thereby addressing climate-related uncertainty in deterioration modeling, as demonstrated by Cui and Wang [65]. Similarly, Tao et al. proposed a differential evolution particle swarm optimization back-propagation (DEPSO-BP) neural network that integrates evolutionary optimization to improve the search efficiency of the BP neural network and enhance PCI prediction [73].

Overall, intelligent models exhibit strong predictive capability and scalability in capturing complex multi-variable interactions. However, their limited interpretability restricts engineering insight, and their implementation depends on the availability of high-quality data, adequate

computational resources, and proper model calibration. Furthermore, inadequate regularization may lead to overfitting and reduced generalization in real-world applications.

2.4 Decision-support for maintenance

The development of effective pavement maintenance plans is a critical yet complex task, requiring a balance between preserving a network's service level, structural integrity, and safety against the constraints of limited annual budgets. This process fundamentally involves determining the optimal timing and selecting the most cost-effective M&R strategies [74]. To systematize this decision-making, a progression of Decision Support Tools (DSTs) has been developed, evolving from operational research methods to metaheuristic algorithms and, most recently, intelligent techniques.

2.4.1 Operational research methods

Operational Research (OR) methods represent the foundational systematic approach to optimizing pavement maintenance decisions. These methods formulate the problem with explicit objectives, constraints, and decision variables, often solved through mathematical programming. A seminal contribution was made by Worm, who developed an OR-based model to minimize the net present value of maintenance costs [75]. A prevalent technique within OR involves modeling pavement deterioration as a Markov process. For instance, Kallen and Noortwijk created an optimal decision model to calculate the probabilities of needing preventive or corrective maintenance [76]. The critical aspect of timing was addressed by Selih et al. through a multiple-criteria system for prioritizing highway rehabilitation projects [77]. To enhance realism, Zhang and Gao employed linear programming based on a semi-Markov process to minimize life-cycle costs across a network [78]. The principal strengths of OR methods are their clear optimization objectives, transparent decision-making processes, and the provision of mathematically optimal solutions, with parameters that often have direct physical interpretations. Their primary limitation, however, is the necessary simplification of complex real-world conditions, which can result in models that fail to fully capture the intricacies of pavement behavior due to the consideration of a relatively narrow set of factors.

2.4.2 Metaheuristic algorithms

To overcome the computational intractability of large-scale, complex pavement networks, metaheuristic algorithms were introduced. These methods provide efficient, near-optimal solutions for problems where exact OR methods are infeasible. A diverse range of these algorithms

has been successfully applied, including genetic algorithms, ant colony optimization, particle swarm optimization, and the Water Cycle Algorithm [79–85]. The key advantage of meta-heuristic approaches lies in their flexibility and ability to accommodate complex constraints and nonlinear relationships that more closely reflect real-world conditions. As a result, they generally outperform conventional optimization techniques in large and combinatorial problem settings. Nevertheless, these methods may encounter limitations when applied to very large or high-dimensional datasets, and the stochastic nature of their search processes can lead to convergence toward locally optimal rather than globally optimal solutions. Moreover, the solutions generated may lack interpretability and often require further refinement through expert judgment before practical implementation.

2.4.3 Artificial intelligence methods

With advances in computational power, Artificial Intelligence (AI), particularly Artificial Neural Networks (ANNs), has become increasingly prominent for road maintenance management [86]. ANN-based models learn the complex, non-linear relationship between a road's state and an appropriate maintenance strategy directly from historical data, representing a high degree of refinement and possessing a strong capability to handle big data from practical scenarios [87–89]. A common practice is to incorporate the road's service time as an input parameter to account for life-cycle influences. However, as a supervised learning method, ANN requires pre-labeled training samples and approximates actual maintenance situations by learning from incorporated parameters. Significant drawbacks persist with AI methods. Their decision-making process is often implicit, functioning as a "black box" that reduces interpretability and trust. Furthermore, the generalization ability of the model can be poor, and a fundamental issue is that a model trained purely on historical data may not fully or optimally consider the complete life-cycle implications of maintenance decisions, limiting its flexibility for general application.

References

[1] AASHTO. *AASHTO Guide for Design of Pavement Structures*. Washington, DC: American Association of State Highway and Transportation Officials, 1993.

[2] Elhadidy, A. A.; El-Badawy, S. M.; Elbeltagi, E. E. A Simplified Pavement Condition Index Regression Model for Pavement Evaluation. *International Journal of Pavement Engineering* 2021, **22**(5), pp. 643–652. DOI: https://doi.org/10.1080/10298436.2019.1633579.

[3] Attoh-Okine, N.; Adarkwa, O. *Pavement Condition Surveys – Overview of Current Practices*. Tech. rep. Newark, DE, USA: Delaware Center for Transportation, University of Delaware, 2013.

[4] Hastings, N. *Physical Asset Management: With an Introduction to ISO55000*. Springer International Publishing, 2015. ISBN: 9783319147772. URL: `https://books.google.co.jp/books?id=wxnGBgAAQBAJ`.

[5] Marcelino, P.; Antunes Maria, d. L.; Fortunato, E. Comprehensive Performance Indicators for Road Pavement Condition Assessment. *Structure and Infrastructure Engineering* 2018, **14**(11), pp. 1433–1445. DOI: https://doi.org/10.1080/15732479.2018.1446179.

[6] Cary, W. N. The Pavement Serviceability-Performance Concept. *HRB Bulletin* 1960, **250**. URL: `https://api.semanticscholar.org/CorpusID:59456635`.

[7] Wolters, A. et al. *Implementing Pavement Management Systems for Local Agencies —State-of-the-Art/State-of-the-Practice Synthesis*. Technical Report FHWA-ICT-11-094. Federal Highway Administration, 2011. DOI: https://doi.org/10.13140/RG.2.2.31043.30246.

[8] Walker, D.; Entine, L.; Kumer, S. *PASER-Manual Asphalt Roads*. Wisconsin Transportation Information Center, College of Engineering, University of Wisconsin. Madison, WI, 2002.

[9] Hafez, M.; Ksaibati, K.; Atadero, R. Best Practices to Support and Improve Pavement Management Systems for Low-Volume Paved Roads. *International Journal of Pavement Engineering* 2019, **20**(5), pp. 592–599. DOI: https://doi.org/10.1080/10298436.2017.1316648.

[10] ASTM D6433-24. *Standard Practice for Roads and Parking Lots Pavement Condition Index Surveys*. Tech. rep. D6433-24. West Conshohocken, PA, USA: ASTM International, 2024. DOI: https://doi.org/10.1520/D6433-24.

[11] ASTM E1926-08(2021). *Standard Practice for Computing International Roughness Index of Roads from Longitudinal Profile Measurements*. Tech. rep. 2021. DOI: https://doi.org/10.1520/E1926-08R21.

[12] Smith, K. L.; Titus-Glover, L.; Evans, L. *Pavement Smoothness Index Relationships, Final Report*. Technical Report. United States. Federal Highway Administration. Office of Pavement Technology, 2002.

[13] Yoshida, T. Composite Indicators for Assessing Maintenance Needs for Road Pavements from the View Point of Road Functions. *Journal of Japan Society of Civil Engineers, Ser. E1 (Pavement Engineering)* 2016, **72**(1), pp. 12–20. ISSN: 2185-6559. DOI: https://doi.org/10.2208/jsc

[14] Ohio Department of Transportation (ODOT). *Pavement Condition Rating System*. pp. 1–3. Ohio Department of Transportation. 2004.

[15] Papagiannakis, A. et al. *Pavement Scores Synthesis*. Technical Report FHWA/TX-09/0-6386-1. Corporate Contributors: Texas Department of Transportation, Research and Technology Implementation Office; United States Federal Highway Administration. Texas Transportation Institute, Feb. 2009. URL: `https://rosap.ntl.bts.gov/view/dot/16766`.

[16] Rafiah, R. "Advanced Pavement Management System Implementation for the Nigerian Federal Road Network". *7th International Conference on Managing Pavement Assets, June 23–28, 2008, Calgary, Alberta, Canada: "Preserving What We Have, Investing in the Future, and Finding the Balance"*. Calgary, Alberta, Canada, 2008, pp. 1–8.

[17] Nam, B. H. et al. Improvements to the Structural Condition Index (SCI) for Pavement Structural Evaluation at Network Level. *International Journal of Pavement Engineering* 2016, **17**(8), pp. 680–697. DOI: https://doi.org/10.1080/10298436.2015.1014369.

[18] Horak, E. Benchmarking the Structural Condition of Flexible Pavements with Deflection Bowl Parameters. *Journal of the South African Institution of Civil Engineering* 2008, **50**, pp. 2–9.

[19] Nguyen, T.; Tan, J. Y.; Ho, N. Y. Deflection Bowl Parameters for Falling Weight Deflectometer Testing: Data Collection and Threshold Benchmarking. *International Journal of Pavement Engineering* 2023, **24**(2), p. 2034815. DOI: https://doi.org/10.1080/10298436.2022.2034815

[20] Sayers, M. W.; Gillespie, T. D.; Paterson, W. D. *Guidelines for Conducting and Calibrating Road Roughness Measurements*. Technical Report. Ann Arbor, MI: University of Michigan, Transportation Research Institute, 1986.

[21] Ibrahim, E. et al. A Modified Pavement Condition Rating Index for Flexible Pavement Evaluation in Egypt. *Innovative Infrastructure Solutions* 2020, **5**(2), p. 55. DOI: https://doi.org/10.1007/s41062-020-00304-z.

[22] Pantuso, A. et al. Analysis of Pavement Condition Survey Data for Effective Implementation of a Network Level Pavement Management Program for Kazakhstan. *Sustainability* 2019, **11**(3), p. 901. DOI: https://doi.org/10.3390/su11030901.

[23] ASTM E1926-08. Standard Practice for Computing International Roughness Index of Roads from Longitudinal Profile Measurements. *West Conshohocken, PA: ASTM International* 2015.

[24] Reza, F.; Boriboonsomsin, K.; Bazlamit, S. Development of a Pavement Quality Index for the State of Ohio. 2006. URL: https://escholarship.org/uc/item/3w68q7z6.

[25] Arhin, S. A.; Noel, E. C.; Ribbiso, A. Acceptable International Roughness Index Thresholds Based on Present Serviceability Rating. *Journal of Civil Engineering Research* 2015, **5**(4), pp. 90–96. DOI: https://doi.org/10.5923/j.jce.20150504.03.

[26] Arhin, S. A. et al. Predicting Pavement Condition Index Using International Roughness Index in a Dense Urban Area. *Journal of Civil Engineering Research* 2015, **5**(1), pp. 10–17. DOI: https://doi.org/10.5923/j.jce.20150501.02.

[27] Haas, R.; Hudson, W.; Zaniewski, J. *Modern Pavement Management*. Bibliyografya Ve Indeks. Krieger Publishing Company, 1994. ISBN: 9780894645884. URL: https://books.google.co.jp/books?id=-swSrwGItT4C.

[28] Shahin, M. *Pavement Management for Airports, Roads, and Parking Lots*. Chapman & Hall, 1994. ISBN: 9780412992018. URL: https://books.google.co.jp/books?id=dK8XVI9qMIEC.

[29] Zhang, Z. et al. Development of Structural Condition Index to Support Pavement Maintenance and Rehabilitation Decisions at Network Level. *Transportation Research Record* 2003, **1827**(1), pp. 10–17. DOI: https://doi.org/10.3141/1827-02.

[30] Peddibhotla, S. S. S.; Murphy, M.; Zhang, Z. *Validation and Implementation of the Structural Condition Index (SCI) for Network-Level Pavement Evaluation*. Tech. rep. FHWA/TX-11/5-4322-01-1. Austin, TX and Washington, DC, United States: Center for Transportation Research, University of Texas at Austin; Texas Department of Transportation; Federal Highway Administration, 2011.

[31] Pereira, P.; Pais, J. Main Flexible Pavement and Mix Design Methods in Europe and Challenges for the Development of an European Method. *Journal of Traffic and Transportation Engineering (English Edition)* 2017, **4**(4). Special Issue on Maintenance and Rehabilitation of Pavements, pp. 316–346. ISSN: 2095-7564. DOI: https://doi.org/https://doi.org/10.1016/j.jtte.2
URL: https://www.sciencedirect.com/science/article/pii/S2095756416303002.

[32] South African National Roads Agency Limited (SANRAL). *South African Pavement Engineering Manual*. South African National Roads Agency Limited. 2014.

[33] Rabbi, M. F.; Mishra, D. Using FWD Deflection Basin Parameters for Network-Level Assessment of Flexible Pavements. *International Journal of Pavement Engineering* 2021, **22**(2), pp. 147–161. DOI: https://doi.org/10.1080/10298436.2019.1580366.

[34] Fuentes, L. et al. A Probabilistic Approach to Detect Structural Problems in Flexible Pavement Sections at Network Level Assessment. *International Journal of Pavement Engineering* 2022, **23**(6), pp. 1867–1880. DOI: https://doi.org/10.1080/10298436.2020.1828586.

[35] Pham, G. N.; Nguyen, P. H. Drone Detection Experiment Based on Image Processing and Machine Learning. 2020. URL: https://urn.fi/URN:NBN:fi-fe2020062245143.

[36] Chrysafi, A.; Athanasopoulos, N.; Siakavellas, N. Damage Detection on Composite Materials with Active Thermography and Digital Image Processing. *International journal of thermal sciences* 2017, **116**, pp. 242–253. DOI: https://doi.org/10.1016/j.ijthermalsci.2017.02.017.

[37] Ciampa, F. et al. Nonlinear Imaging of Damage in Composite Structures Using Sparse Ultrasonic Sensor Arrays. *Structural Control and Health Monitoring* 2017, **24**(5), e1911. DOI: https://doi.org/10.1002/stc.1911.

[38] Shrivakshan, G.; Chandrasekar, C. A Comparison of Various Edge Detection Techniques Used in Image Processing. *International Journal of Computer Science Issues (IJCSI)* 2012, **9**(5), p. 269. DOI: https://doi.org/https://www.proquest.com/scholarly-journals/comparison-various-edge-detection-techniques-used/docview/1270312987/se-2.

[39] Öztürk, Ş.; Akdemir, B. Comparison of Edge Detection Algorithms for Texture Analysis on Glass Production. *Procedia-Social and Behavioral Sciences* 2015, **195**, pp. 2675–2682. DOI: https://doi.org/10.1016/j.sbspro.2015.06.477.

[40] Kong, X.; Li, J. Image Registration-Based Bolt Loosening Detection of Steel Joints. *Sensors* 2018, **18**(4), p. 1000. DOI: https://doi.org/10.3390/s18041000.

[41] Kim, J.-W. et al. Review of Image-Processing-Based Technology for Structural Health Monitoring of Civil Infrastructures. *Journal of Imaging* 2024, **10**(4), p. 93. DOI: https://doi.org/10.339

[42] Hechun, W.; Xiaohong, Z. "Survey of Deep Learning Based Object Detection". *Proceedings of the 2nd international conference on big data technologies*. 2019, pp. 149–153. DOI: https://doi.org/10.1145/3358528.3358574.

[43] Tehrany, M. S.; Pradhan, B.; Jebur, M. N. Spatial Prediction of Flood Susceptible Areas Using Rule Based Decision Tree (DT) and a Novel Ensemble Bivariate and Multivariate Statistical Models in GIS. *Journal of hydrology* 2013, **504**, pp. 69–79. DOI: https://doi.org/10.1016/j.jhydrol.2013.09.034.

[44] Ho, C.-H.; Snyder, M.; Zhang, D. Application of Vehicle-Based Sensing Technology in Monitoring Vibration Response of Pavement Conditions. *Journal of Transportation Engineering, Part B: Pavements* 2020, **146**(3), p. 04020053. DOI: https://doi.org/10.1061/JPEODX.00002

[45] Wu, C. et al. An Automated Machine-Learning Approach for Road Pothole Detection Using Smartphone Sensor Data. *Sensors* 2020, **20**(19), p. 5564. DOI: https://doi.org/10.3390/s20195564.

[46] Mednis, A. et al. "Real Time Pothole Detection Using Android Smartphones with Accelerometers". *2011 International conference on distributed computing in sensor systems and workshops (DCOSS)*. IEEE. 2011, pp. 1–6. DOI: https://doi.org/10.1109/DCOSS.2011.5982206.

[47] Ziari, H. et al. Prediction of Pavement Performance: Application of Support Vector Regression with Different Kernels. *Transportation Research Record* 2016, **2589**(1), pp. 135–145. DOI: https://doi.org/10.3141/2589-15.

[48] Fan, Z. et al. Automatic Pavement Crack Detection Based on Structured Prediction with the Convolutional Neural Network. 2018. DOI: https://doi.org/10.48550/arXiv.1802.02208.

[49] Girshick, R. et al. "Rich Feature Hierarchies for Accurate Object Detection and Semantic Segmentation". *Proceedings of the IEEE conference on computer vision and pattern recognition*. 2014, pp. 580–587.

[50] He, K. et al. "Mask R-CNN". *Proceedings of the IEEE international conference on computer vision*. 2017, pp. 2961–2969.

[51] Maeda, H. et al. Generative Adversarial Network for Road Damage Detection. *Computer-Aided Civil and Infrastructure Engineering* 2021, **36**(1), pp. 47–60. DOI: https://doi.org/10.1111/mice.

[52] Hsieh, Y.-A.; Tsai, Y. Automated Asphalt Pavement Raveling Detection and Classification Using Convolutional Neural Network and Macrotexture Analysis. *Transportation Research Record* 2021, **2675**(9), pp. 984–994. DOI: https://doi.org/10.1177/03611981211005450.

[53] Dong, J. et al. Intelligent Segmentation and Measurement Model for Asphalt Road Cracks Based on Modified Mask R-CNN Algorithm. *Computer Modeling in Engineering & Sciences* 2021, **128**(2), pp. 541–564. DOI: https://doi.org/10.32604/cmes.2021.015875.

[54] George, K.; Rajagopal, A.; Lim, L. Models for Predicting Pavement Deterioration. *Transportation Research Record* 1989, (1215). URL: `http://worldcat.org/isbn/0309048192`.

[55] Fuentes, L. et al. Modelling Pavement Serviceability of Urban Roads Using Deterministic and Probabilistic Approaches. *International Journal of Pavement Engineering* 2021, **22**(1), pp. 77–86. DOI: https://doi.org/10298436.2019.1577422.

[56] Bekheet, W. et al. "Comparison between Probabilistic and Deterministic Pavement Management Analysis: A Case Study for Arizona DOT". *Seventh International Conference on Managing Pavement AssetsTransportation Research BoardAlberta Infrastructure and Transportation, CanadaFederal Highway Administration*. 2008.

[57] Amin, M. S. R. "The Pavement Performance Modeling: Deterministic vs. Stochastic Approaches". *Numerical Methods for Reliability and Safety Assessment: Multiscale and Multiphysics Systems*. Springer, 2014, pp. 179–196. DOI: https://doi.org/10.1007/978-3-319-07167-1_5.

[58] Saha, P.; Ksaibati, K.; Atadero, R. Developing Pavement Distress Deterioration Models for Pavement Management System Using Markovian Probabilistic Process. *Advances in Civil Engineering* 2017, **2017**(1), p. 8292056. DOI: https://doi.org/10.1155/2017/8292056.

[59] Fani, A. et al. Analysis of the Pavement Deterioration Uncertainty Scenarios on Pavement Maintenance and Rehabilitation Planning Optimization. *Structure and Infrastructure Engineering* 2025, **21**(3), pp. 507–524. DOI: https://doi.org/10.1080/15732479.2023.2218359.

[60] Wasiq, S.; Golroo, A. Probabilistic Pavement Performance Modeling Using Hybrid Markov Chain: A Case Study in Afghanistan. *Case Studies in Construction Materials* 2024, **20**, e03023. DOI: https://doi.org/10.1016/j.cscm.2024.e03023.

[61] Thomas, O.; Sobanjo, J. Comparison of Markov Chain and Semi-Markov Models for Crack Deterioration on Flexible Pavements. *Journal of Infrastructure Systems* 2013, **19**(2), pp. 186–195. DOI: https://doi.org/10.1061/(ASCE)IS.1943-555X.0000112.

[62] Tsuda, Y. et al. Estimating Markovian Transition Probabilities for Bridge Deterioration Forecasting. *Structural Engineering/Earthquake Engineering* 2006, **23**(2), 241s–256s. DOI: https://doi.org/10.2208/jsceseee.23.241s.

[63] Obama, K. et al. Disaggregated Hazard Rates Evaluation and Bench-marking. *J. Jpn. Soc. Civ. Eng* 2008, **64**, pp. 857–874.

[64] Hong, F.; Prozzi, J. A. Estimation of Pavement Performance Deterioration Using Bayesian Approach. *Journal of infrastructure systems* 2006, **12**(2), pp. 77–86. DOI: https://doi.org/10.1061/(AS 0342(2006)12:2(77).

[65] Cui, B.; Wang, H. Predicting Asphalt Pavement Deterioration Under Climate Change Uncertainty Using Bayesian Neural Network. *IEEE Transactions on Intelligent Transportation Systems* 2024. DOI: https://doi.org/10.1109/TITS.2024.3505237.

[66] Wang, K. C.; Li, Q. Pavement Smoothness Prediction Based on Fuzzy and Gray Theories. *Computer-Aided Civil and Infrastructure Engineering* 2011, **26**(1), pp. 69–76. DOI: https://doi.org/10.1111/j.1467-8667.2009.00639.x.

[67] Yamany, M. S.; Abraham, D. M. Hybrid Approach to Incorporate Preventive Maintenance Effectiveness into Probabilistic Pavement Performance Models. *Journal of Transportation Engineering, Part B: Pavements* 2021, **147**(1), p. 04020077. DOI: https://doi.org/10.1061/JPEODX.0

[68] Mishalani, R. G.; Madanat, S. M. Computation of Infrastructure Transition Probabilities Using Stochastic Duration Models. *Journal of Infrastructure systems* 2002, **8**(4), pp. 139–148. DOI: https://doi.org/10.1061/(ASCE)1076-0342(2002)8:4(139).

[69] Cheng, C. et al. Predicting Rutting Development Using Machine Learning Methods Based on RIOCHTrack Data. *Applied Sciences* 2024, **14**(8), p. 3177. DOI: https://doi.org/10.3390/app14083

[70] Al-Samahi, S. et al. A Comparative Study of Pavement Roughness Prediction Models under Different Climatic Conditions. *Infrastructures* 2024, **9**(10). DOI: https://doi.org/10.3390/infrastru

[71] Deng, Y.; Shi, X. Short-Term Predictions of Asphalt Pavement Rutting Using Deep-Learning Models. *Journal of Transportation Engineering, Part B: Pavements* 2024, **150**(2), p. 04024004. DOI: https://doi.org/10.1061/JPEODX.PVENG-1409.

[72] Molinero-Perez, N. et al. “Artificial Intelligent Techniques to Improve Pavement Maintenance Management”. *Construction Research Congress 2024*. 2024, pp. 1097–1106. DOI: https://doi.org/10.1061/9780784485262.112.

[73] Tao, R. et al. Prediction of Asphalt Pavement Performance Based on DEPSO-BP Neural Network. *Canadian Journal of Civil Engineering* 2023, **50**(8), pp. 709–720. DOI: https://doi.org/10.1139/cjce-2022-0198.

[74] Kilić Pamuković, J. et al. A Sustainable Approach for the Maintenance of Asphalt Pavement Construction. *Sustainability* 2020, **13**(1), p. 109. DOI: https://doi.org/10.3390/su13010109.

[75] Worm, J.; Van Harten, A. Model Based Decision Support for Planning of Road Maintenance. *Reliability Engineering & System Safety* 1996, **51**(3), pp. 305–316. DOI: https://doi.org/10.1016/0951-8320(95)00100-X.

[76] Kallen, M.; Van Noortwijk, J. Optimal Periodic Inspection of a Deterioration Process with Sequential Condition States. *International Journal of Pressure Vessels and Piping* 2006, **83**(4), pp. 249–255. DOI: https://doi.org/10.1016/j.ijpvp.2006.02.007.

[77] Šelih, J. et al. Multiple-Criteria Decision Support System in Highway Infrastructure Management. *Transport* 2008, **23**(4), pp. 299–305. DOI: https://doi.org/10.3846/1648-4142.2008.23.299-305.

[78] Zhang, X.; Gao, H. Road Maintenance Optimization through a Discrete-Time Semi-Markov Decision Process. *Reliability Engineering & System Safety* 2012, **103**, pp. 110–119. DOI: https://doi.org/10.1016/j.ress.2012.03.011.

[79] Morcous, G.; Lounis, Z. Maintenance Optimization of Infrastructure Networks Using Genetic Algorithms. *Automation in construction* 2005, **14**(1), pp. 129–142. DOI: https://doi.org/10.1016/

[80] Mathew, B. S.; Isaac, K. P. Optimisation of Maintenance Strategy for Rural Road Network Using Genetic Algorithm. *International Journal of Pavement Engineering* 2014, **15**(4), pp. 352–360. DOI: https://doi.org/10.1080/10298436.2013.806807.

[81] Xiong, Z. et al. “An Algorithmic Framework for the Scheduling of Construction Projects Based on Ant Colony Optimization and Expert Knowledge”. *17th international IEEE conference on intelligent transportation systems (ITSC)*. IEEE. 2014, pp. 2446–2452. DOI: https://doi.org/10.1109/ITSC.2014.6958082.

[82] Mahmood, M.; Mathavan, S.; Rahman, M. A Parameter-Free Discrete Particle Swarm Algorithm and Its Application to Multi-Objective Pavement Maintenance Schemes. *Swarm and evolutionary computation* 2018, **43**, pp. 69–87. DOI: https://doi.org/10.1016/j.swevo.2018.03.013.

[83] Han, C. et al. Intelligent Decision Model of Road Maintenance Based on Improved Weight Random Forest Algorithm. *International Journal of Pavement Engineering* 2022, **23**(4), pp. 985–997. DOI: https://doi.org/10.1080/10298436.2020.1784418.

[84] Han, C. et al. An Intelligent Decision-Making Framework for Asphalt Pavement Maintenance Using the Clustering-PageRank Algorithm. *Engineering Optimization* 2020, **52**(11), pp. 1829–1847. DOI: https://doi.org/10.1080/0305215X.2019.1677636.

[85] Naseri, H.; Fani, A.; Golroo, A. Toward Equity in Large-Scale Network-Level Pavement Maintenance and Rehabilitation Scheduling Using Water Cycle and Genetic Algorithms. *International Journal of Pavement Engineering* 2022, **23**(4), pp. 1095–1107. DOI: https://doi.org/10.1080/10298436.2020.1790558.

[86] Sundin, S.; Braban-Ledoux, C. Artificial Intelligence–Based Decision Support Technologies in Pavement Management. *Computer-Aided Civil and Infrastructure Engineering* 2001, **16**(2), pp. 143–157. DOI: https://doi.org/10.1111/0885-9507.00220.

[87] Alsugair, A. M.; Al-Qudrah, A. A. Artificial Neural Network Approach for Pavement Maintenance. *Journal of computing in civil engineering* 1998, **12**(4), pp. 249–255. DOI: https://doi.org/10.1061/(ASCE)0887-3801(1998)12:4(249).

[88] Brovarnyi, D. Road Maintenance Planning Model Based on Neural Networks. *Automation and Remote Control* 2011, **72**(6), pp. 1333–1337. DOI: https://doi.org/10.1134/S000511791106021X.

[89] Bosurgi, G.; Pellegrino, O.; Sollazzo, G. Optimizing Artificial Neural Networks for the Evaluation of Asphalt Pavement Structural Performance. *The Baltic Journal of Road and Bridge Engineering* 2019, **14**(1), pp. 58–79. DOI: https://doi.org/10.7250/bjrbe.2019-14.433.

Chapter 3

An Integrated Framework with SAM and OCR for Pavement Crack Quantification and Geospatial Mapping

3.1 Introduction

Efficient pavement distress assessment plays a vital role in modern road asset management, enabling informed infrastructure preservation, enhanced traffic safety, and cost-effective maintenance planning. Traditionally, pavement condition evaluation has relied on manual visual inspections, where trained personnel identify surface defects such as cracks, potholes, rut depths, and patches directly on-site. While this method provides detailed observations, it suffers from several limitations: it is labor-intensive, time-consuming, subjective, and inconsistent, especially when applied to large-scale road networks [1, 2]. Moreover, manual surveys expose inspectors to hazardous traffic conditions, making frequent, network-wide assessments impractical under limited resources [3, 4].

To overcome these challenges, automated pavement condition survey systems have been introduced, integrating high-resolution imaging sensors, onboard computing, distance measurement tools, and Global Positioning System (GPS) modules to improve efficiency, accuracy, and consistency in pavement data collection [5, 6]. Automated pavement inspection generally involves multiple stages, including pavement surface classification, distress detection and quantification, and condition rating based on the type and severity of detected distress [2]. In Cambodia, for example, the Road Measurement Data Acquisition System (ROMDAS) is employed by the Ministry of Public Works and Transport (MPWT) for pavement monitoring, as shown in Figure 3.1. ROMDAS utilizes downward-facing high-resolution cameras mounted on survey vehicles to continuously capture pavement images at driving speeds, as illustrated in Figure 3.2. The collected imagery is synchronized with GPS and distance measurements, allowing accurate georeferencing of pavement distress such as cracks, potholes, and patches.



Figure 3.1: ROMDAS survey vehicle.



Figure 3.2: Pavement image from ROMDAS survey vehicle.

This approach has significantly enhanced Cambodia' s capability to maintain comprehensive and up-to-date pavement condition records, facilitating data-driven maintenance planning.

Although data acquisition technologies have advanced, the automated interpretation of captured images into pavement condition assessment remains crucial for effective maintenance planning and optimal repair strategies. Instead of relying on labor-intensive measurements, image processing methods enable the automated quantification of pavement distress severity. These quantified features can then be systematically converted into standardized evaluation indices such as the Pavement Condition Index (PCI) or the Maintenance Control Index(MCI), thereby supporting data-driven maintenance intervention [7, 8]. In Japan, the MCI is widely adopted by road administrators to guide maintenance interventions based on its severity. This index is primarily derived from distress density, such as crack ratios, which require careful measurement to ensure accuracy. The definition and calculation of the MCI can be found in

relevant references [9–13]. In recent years, advances in image processing have further improved this process by reducing subjectivity and enhancing consistency. However, early approaches that depended on handcrafted features and heuristic algorithms (e.g., thresholding, region-based segmentation) often failed to generalize across diverse pavement surface conditions and struggled with detecting low-contrast features like fine cracks against complex backgrounds [14–17].

Latest advances in deep learning have revolutionized and overcome the limitations of conventional methods in pavement distress detection by enabling models to learn discriminative features automatically from large-annotated datasets [18–21]. Among deep learning-based detectors, two major approaches dominate the literature: region-based convolutional neural network (CNN) detectors and one-stage detectors such as You Only Look Once (YOLO). Convolutional architectures, such as Faster R-CNN, have been widely applied to pavement distress detection, often incorporating ResNet and Feature Pyramid Network (FPN) backbones to improve feature extraction and enhance detection accuracy [22]. However, this approach still requires intensive feature computation when handling numerous proposals [23]. On the other hand, the YOLO model has gained popularity for its high inference speed, real-time processing capability, and robust performance in complex environments [3, 24, 25]. Additional improvements have been proposed by integrating sub-networks and advanced IoU-based loss functions to enhance detection precision [19, 26]. Despite these advancements, such detection models typically yield bounding boxes rather than precise distress quantification, as they cannot provide pixel-level measurements of critical metrics such as crack width, length, or area, which are essential for severity assessment and maintenance decision-making [27, 28].

To overcome this shortcoming, segmentation-based methods have been introduced to provide pixel-level contours of pavement distress. A key advantage over detection methods is their capability to obtain the actual area of distress, achieving a result with pixel-level precision [29]. This is attributed to the higher model complexity and richer parameterization of segmentation networks [30]. By distinguishing between distressed and non-distressed pixels, these methods enable a fine-grained analysis, allowing for a prediction label to be assigned to individual pixels.

Among the most widely used deep learning architectures for pavement distress segmentation are convolutional neural network (CNN) based models such as U-Net, DeepLabV3+, Mask R-CNN, SegNet, and domain-specific frameworks like CrackNet. U-Net, a classic U-shaped encoder–decoder architecture, efficiently localizes features using skip connections that fuse feature maps between the downsampling (encoder) and up-sampling (decoder) paths, enabling faster processing and refined segmentation, as utilized by Li et al. [31] and adapted by Lau et al. [32] with a pre-trained ResNet-34 encoder to better distinguish distress regions from intact pavement. Another state-of-the-art approach is DeepLabV3+, an encoder–decoder model for pavement crack segmentation that commonly incorporates a pre-trained CNN encoder and an

Atrous Spatial Pyramid Pooling (ASPP) module to capture multi-scale context, often enhanced with an attention mechanism to handle diverse environmental conditions, as demonstrated by Li et al. [33] and Sun et al. [34]. For instance segmentation, Mask R-CNN, an improved R-CNN variant, integrates image data with pixel-segmented annotations to precisely identify and position cracks, a method applied by Wang et al. [35] and modified by Dong et al. [36] to extract detailed crack properties. Alternatively, SegNet provides an efficient encoder–decoder structure for scene understanding tasks and crack segmentation in concrete and asphalt pavement, with Chen et al. [37] presenting a modified version capable of end-to-end, pixel-by-pixel training for arbitrary image sizes. Finally, models like CrackNet developed by Kyem et al. [38] integrate specialized modules and refinement operations to address the challenge of accurately segmenting tiny and subtle cracks across varying scales in high-resolution images.

Despite their documented success, a critical limitation shared by these traditional supervised models is their reliance on large volumes of meticulously annotated ground-truth data. Their generalization to real-world conditions is directly dependent on the quality and diversity of the training datasets. The necessity for extensive labeling introduces a significant bottleneck in practical deep learning applications for remote sensing image segmentation. Xu et al. [39] proposed an end-to-end framework for the automatic detection and segmentation of tunnel cracks, which balances annotation cost with performance by enhancing YOLOv8. Although the model effectively detects and segments thin cracks and ignores complex backgrounds, the annotation process remains labor-intensive. Specifically, the pixel-level labeling required for segmentation, which involves drawing precise polygons, can still take several minutes per image. Moreover, the inherent variability, resolution differences, and environmental complexity of remote sensing data make the labeling process even more demanding [40]. Consequently, developing segmentation models that can operate effectively with minimal labeled data offers the potential for reductions in annotation costs and time.

Recent breakthroughs in foundation models introduce a paradigm shift that minimizes the need for extensive manual labeling while ensuring better generalization to unseen images. The Segment Anything Model (SAM), a foundational model from Meta AI Research, significantly advances image segmentation by leveraging generalized learning across diverse, massive datasets. This training allows SAM to establish a robust pre-training objective, covering a wide array of applications and often outperforming other models in complex or noisy environments [41, 42]. SAM offers powerful zero-shot segmentation capabilities, generating high-fidelity masks from simple input prompts (e.g., points, bounding boxes) without task-specific training [43]. Nonetheless, SAM is not a complete solution for pavement distress analysis; its performance is contingent on receiving accurate prompts, and it can underperform on slender, low-contrast features like cracks without further refinement [44].

Furthermore, if the image includes relevant details, such as coordinates as shown in the

ROMDAS image, it is crucial to extract this information in addition to any identified distress. Optical Character Recognition (OCR) technology plays a crucial role in retrieving text from different types of documents, including handwritten content, and converting it into digital text [45]. As an OCR engine, Tesseract, becomes an efficient and reliable tool for recognizing and extracting text from images [46]. For instance, Tesseract OCR has found extensive use in applications such as reading letters and numbers on vehicle license plates when paired with deep learning detection systems [47].

This study bridges this critical gap by proposing a lightweight framework that synergizes the strengths of object detection, foundation models, and metadata parsing to create an end-to-end solution for pavement distress analysis. Our methodology leverages a YOLOv8 model to automatically generate high-quality bounding box prompts for distress regions. These prompts are then fed into SAM to produce initial pixel-level segmentation masks. To address SAM' s limitations with thin cracks, we introduced a local refinement module to enhance mask accuracy. Finally, to enable geospatial localization, the Tesseract OCR engine is employed to extract embedded GPS coordinates directly from the survey imagery, linking each quantified distress to a precise geographical location. The proposed framework is validated using an open-source pavement image dataset from Yamanashi, Japan. The results demonstrate robust performance in automated detection, precise segmentation, accurate quantification of distress dimensions, and seamless geospatial mapping. By integrating advanced deep learning and foundation segmentation models, this work provides a scalable, efficient, and comprehensive tool for automated pavement condition assessment, contributing to data-driven infrastructure management practices.

3.2 Methods

3.2.1 Proposed framework

The objective of this research is to develop and implement an end-to-end framework for automated pavement distress detection and quantification. In addition to quantitative assessment, this process also aims to localize the distress on a map for improved visualization and informed decision-making by road agencies. Figure 3.3 illustrates the process in this study, which begins with data preparation, where images from a vehicle-mounted camera are transformed from a horizontal perspective to a top-down view. This transformation, known as Inverse Perspective Mapping (IPM), uses a homography to map pixels from the camera' s perspective onto a different 2D coordinate frame, creating a bird' s-eye view of the scene [48, 49]. After this transformation, the images are cropped to a 1:1 aspect ratio to prepare them for input to the subsequent detection and segmentation model.

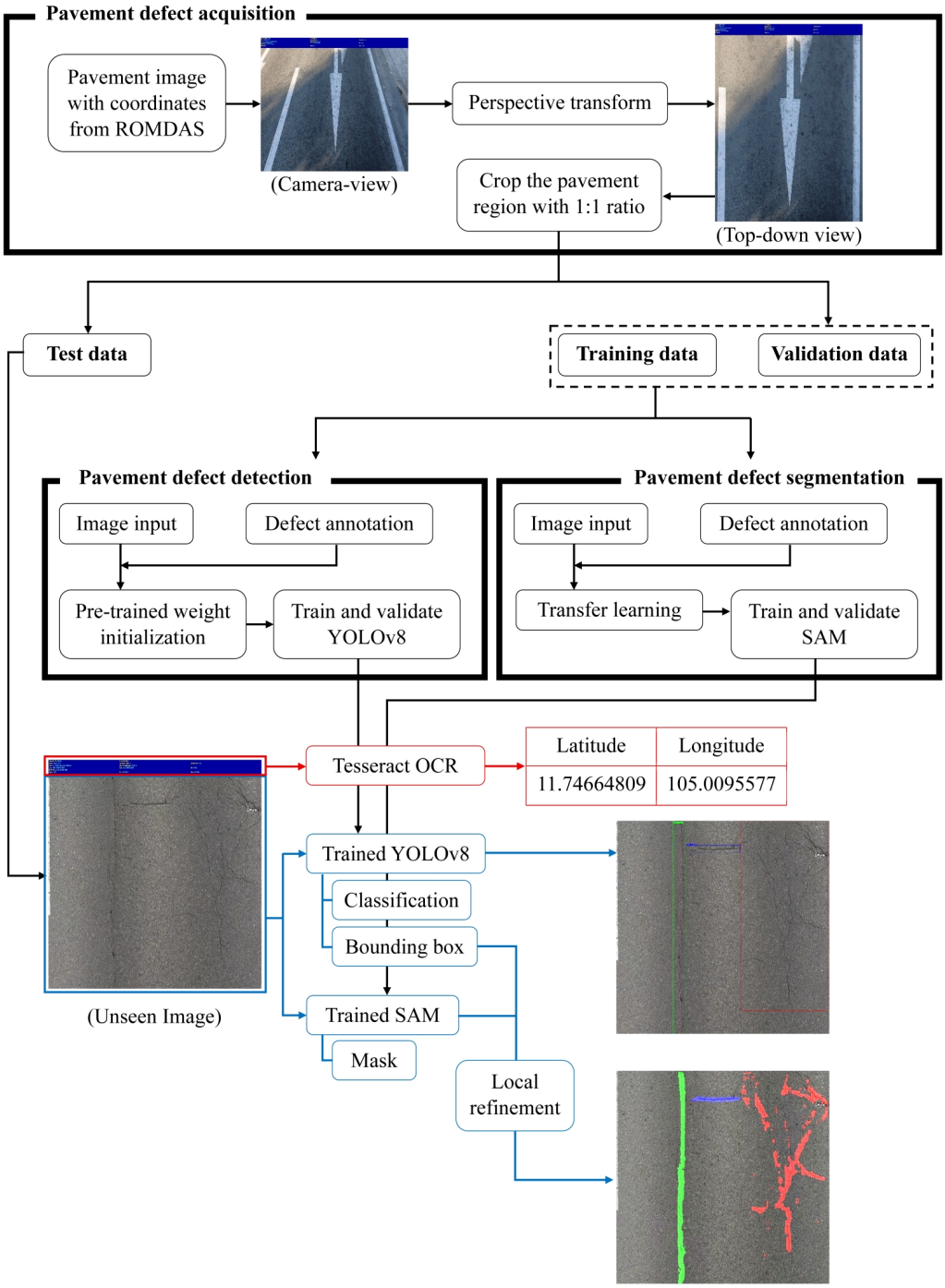


Figure 3.3: Pipeline of the proposed framework.

A two-step process based on a modified YOLOv8 and the SAM was proposed to handle distress detection and segmentation. The dataset of pavement cracks was divided into training and validation sets, and each image was manually annotated to create ground truth data for both detection and segmentation. The first step involves using YOLOv8 for pavement crack detection, which classifies and localizes cracks by generating bounding boxes around them. These bounding boxes serve as prompts for the second step, which utilizes the SAM for crack segmentation. By using the bounding boxes from the first step as prompts and local refinement,

the proposed method can segment the detected pavement cracks with greater purpose and accuracy, isolating the exact pixels that constitute the distress.

Simultaneously, a region containing pixel-based coordinates digits, typically in a blue header, is extracted using Tesseract OCR. This enables the system to save the latitude and longitude alongside the identified cracks. Since these coordinate digits are standardized and associated with the ROMDAS, the pre-trained Tesseract OCR model can be used directly without retraining, unlike scenarios involving distorted or irregular text (e.g., license plate or traffic signs). Once the entire process is complete, pavement cracks are automatically detected, their severity quantified, and their location mapped onto a geospatial platform. This integrated approach allows road agencies to efficiently manage and implement timely maintenance planning.

3.2.2 Top-down perspective transformation based on homography

IPM is fundamentally a geometrical transformation that re-projects pixel coordinates from the 2D image plan, often described within the camera coordinate system (X_c, Y_c, Z_c), onto a corresponding 2D plane in the real-world object coordinate system (X_w, Y_w, Z_w), as illustrated in Figure 3.4. This technique effectively converts the perspective view of a scene into a rectified image where objects, particularly those on a planar surface like the ground or pavement, appear with a uniform scale and corrected geometry. A common application involves taking quadrilateral points defining a surface in the tilted image (e.g., pavement surface) and mapping them to a true rectangular shape in the bird' s-eye view. This is especially useful for analyzing features paralleled in the real world, such as road markings, which appear converged in the perspective view but are rendered and horizontal after the IPM transformation.

The transformation from a camera's perspective view to a metrically accurate top-down view is fundamentally governed by homography, a projective transformation matrix. This process corrects for perspective distortion and yields a rectified image with a uniform scale, making it suitable for subsequent metric analysis, such as measuring actual object sizes or distances. The core of this transformation is the homography matrix, which maps points from one plane to another.

As illustrated in Figure 3.5, four reference points were manually selected on the pavement region. These points form a trapezoidal region due to perspective distortion caused by the oblique camera angle. Under an ideal bird' s eye view, however, these same points would form a perfect rectangle, demonstrating the geometric deformation present in the raw images. The homography matrix mathematically maps the pixel coordinates from the original image plane to their corresponding positions on a rectified, top-down plane. The homography matrix H encapsulates this transformation and is defined as:

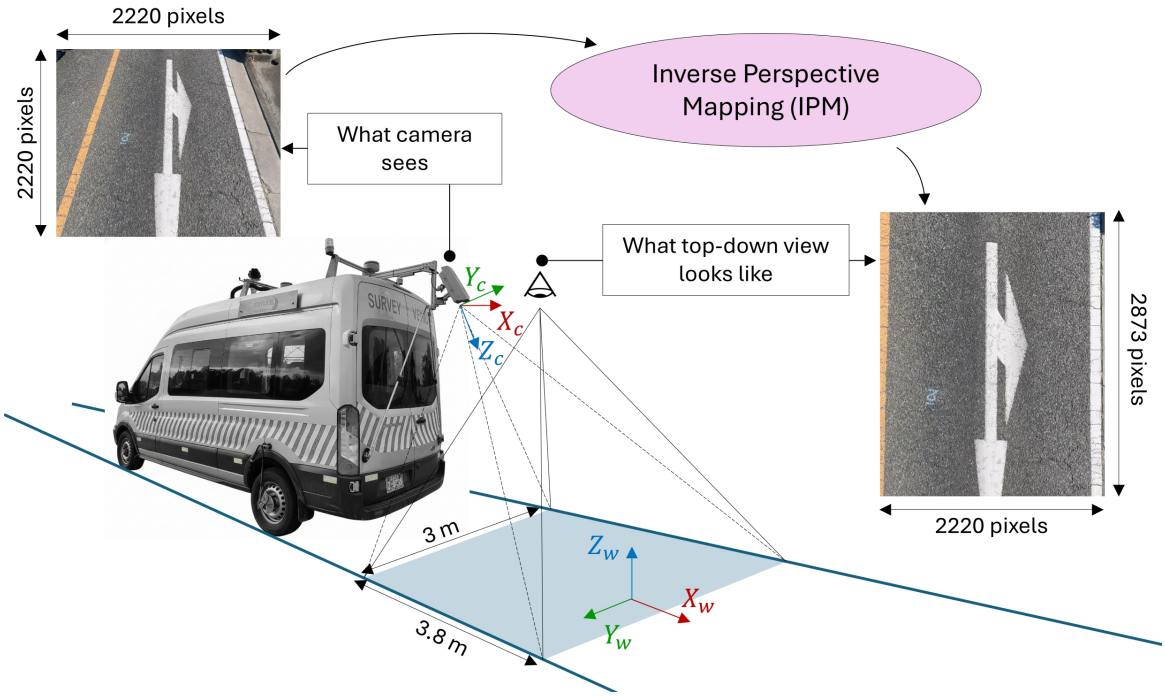


Figure 3.4: Overview of the IPM transformation process.

$$\begin{bmatrix} x' \\ y' \\ 1 \end{bmatrix} = H \cdot \begin{bmatrix} x \\ y \\ 1 \end{bmatrix} \tag{3.1}$$

Where H is the 3×3 homography matrix:

$$H = \begin{bmatrix} h_{11} & h_{12} & h_{13} \\ h_{21} & h_{22} & h_{23} \\ h_{31} & h_{32} & h_{33} \end{bmatrix} \tag{3.2}$$

Where H is estimated using the four pairs of the corresponding points:

$$p_i = (x_i, y_i) \longrightarrow p'_i = (x'_i, y'_i) \quad \text{for } i = 1, 2, 3, 4 \tag{3.3}$$

In this study:

p_i = manually selected source points in the original pavement image.

p'_i = destination points on the target rectangular plane.

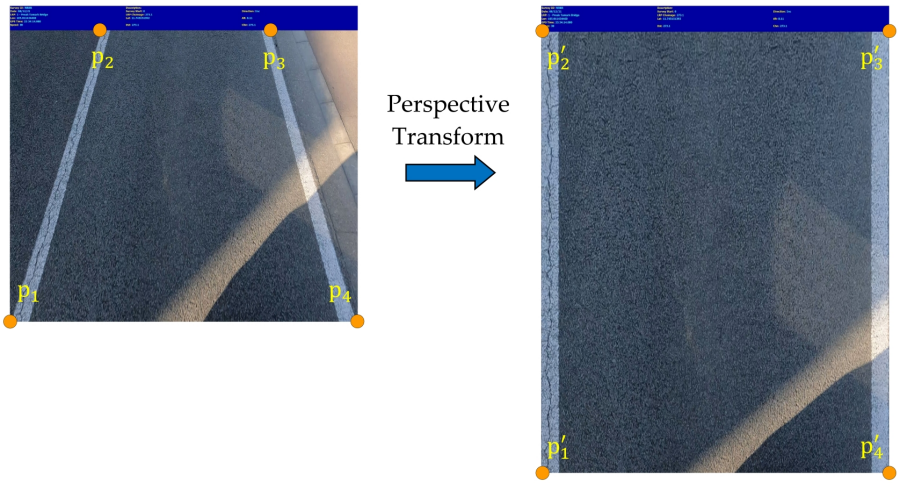


Figure 3.5: Given camera perspective (**left**), transformed top-down perspective (**right**).

For implementation, the homography matrix H was computed in a Python script utilizing cv2.getPerspectiveTransform from the OpenCV library [50]. The four corner points of the trapezoidal pavement region were manually defined. Their corresponding destination points were calculated based on a known physical scale (pixels per meter) to create a rectangular output image of specified real-world dimensions (e.g., 3.0m $\times$ 3.8m). The perspective warping was then performed using cv2.warpPerspective, generating a rectified pavement image with a uniform scale. This rectified view eliminates perspective distortion, providing a metrically accurate representation of the pavement for further analysis. All the images used in this study, including those for training, validation, and testing, underwent this transformation process prior to being input into the crack detection and segmentation framework.

3.2.3 YOLOv8 model for pavement distress detection

YOLOv8 represents a state-of-the-art advancement in single-stage object detection. While retaining the backbone-neck-head design paradigm established in earlier YOLO models, it introduces several architectural refinements that improve both accuracy and computational efficiency. The model processes an input image in a single forward pass, simultaneously predicting bounding boxes, object classes, and confidence scores.

The backbone is responsible for hierarchical feature extraction. It employs convolutional layers with cross-stage partial (CSP) connections and bottleneck structures, which progressively reduce spatial resolution while expanding channel depth. This design produces a multi-scale feature hierarchy that captures both fine-grained details and high-level semantic information. The neck aggregates these multi-scale features through an enhanced feature fusion strategy. Building upon the FPN, YOLOv8 incorporates a Path Aggregation Network (PAN), which adds a

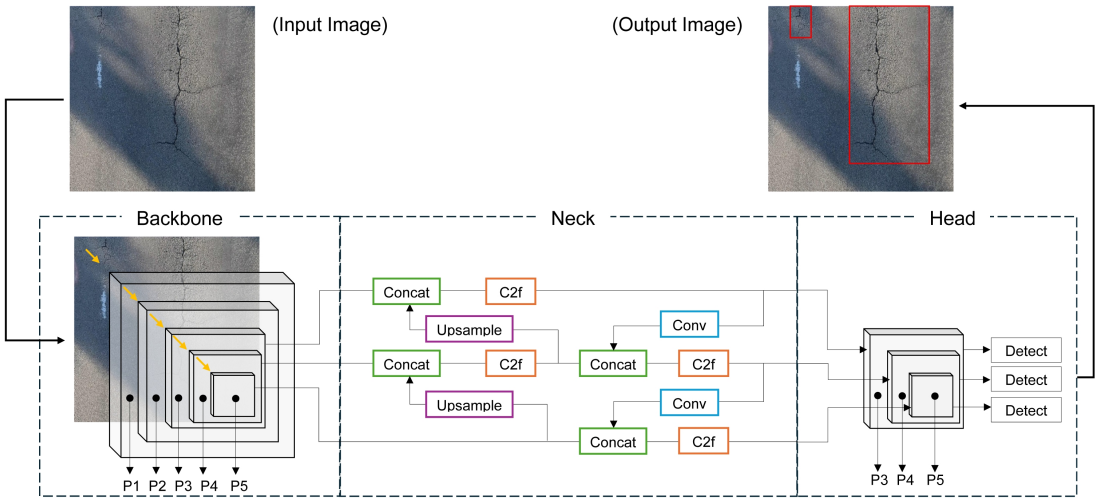


Figure 3.6: Overall architecture of YOLOv8.

complementary bottom-up pathway to the FPN's top-down flow [51, 52]. This bi-directional information exchange enriches the feature maps with both semantic and localization cues, thereby improving detection robustness across objects of different sizes. The head executes the final detection tasks. Unlike earlier coupled designs, YOLOv8 adopts a decoupled head structure that separates classification (object categories) from regression (bounding box coordinates). This reduces inference between two objectives, stabilizes training, and yields more accurate predictions. The output includes the bounding boxes' coordinates, class, and confidence scores.

Compared to two-stage detectors such as Faster R-CNN, which rely on a Region Proposal Network (RPN) followed by classification, YOLOv8 performs detection in a single stage [53]. This streamlined design significantly reduces computational overhead and enables real-time inference without sacrificing detection quality. The complete architecture of YOLOv8 is depicted in Figure 3.6.

3.2.4 Architecture of SAM for pavement distress segmentation

Traditional segmentation models typically require training for specific tasks and are limited in their applicability across different domains. SAM by Meta AI has gained attention for its impressive zero-shot performance and capability to produce high-quality object masks from diverse input prompts. The primary advantage of SAM compared to other state-of-the-art segmentation models lies in its ability to generalize across a wide range of tasks without task-specific fine-tuning. This adaptability makes SAM a versatile tool, especially when high accuracy is needed across diverse datasets. However, the specific visual examples in the figure might not fully convey this strength, and we will consider adding more representative images to better illustrate SAM's capabilities. SAM functions as a class-agnostic segmentation model, utilizing a Vision Transformer (ViT) for image encoding and a sophisticated two-layer mask decoder.

SAM' s architecture features an image encoder with ViT to extract detailed embeddings, a prompt encoder to interpret various user inputs, and a lightweight mask decoder for precise pixel-level segmentation decisions. This design enables SAM to effectively adapt to new segmentation tasks with minimal additional training, ensuring high accuracy.

The architecture of SAM, as shown in Figure 3.7, primarily consists of three components: the image encoder (Vision Transformer (ViT)), the prompt encoder, and the mask decoder. The SAM utilizes the ViT as the image encoder, serving as the backbone network for image feature extraction. The choice of ViT architecture stems from its ability to capture long-range dependencies and intricate visual information. The prompt encoder processes user inputs (e.g., boxes) to guide the segmentation process. Specifically, it is based on box encoding, where user-drawn bounding boxes were encoded to provide spatial constraints for segmentation. The mask decoder integrates features from both the ViT backbone and the prompt encoder to generate segmentation masks. The decoder comprises: feature fusion, upsampling layers, and mask generation.

The pre-training process of SAM occurs on a large-scale and diverse dataset (SA-1B dataset), which comprises over a billion finely annotated images and segmentation masks covering various image types and segmentation tasks. The pretraining process adopts a multitask learning strategy, combining Cross-Entropy loss and Dice loss to optimize segmentation accuracy. The objective of pretraining was to enable SAM to learn rich feature representations, allowing it to generalize to different segmentation tasks and application scenarios without the need for retraining. However, the conventional SAM does not perform well on pavement distress because pavement distress is thin and irregular, unlike the natural images that the SAM was trained on. Therefore, SAM is finetuned with the bounding box prompt to create a pavement distress-specific segmentation model, called modified SAM. To reduce the computational cost, the image encoder is frozen, while only the prompt encoder and the mask decoder are fine-tuned for pavement distress segmentation. Masks are generated for top-down pavement images using polygon-based annotations on LabelMe. The model was trained for 200 epochs. The loss was the summation of the dice loss and the cross-entropy loss, which together provide a robust loss for segmentation tasks. Adam optimizer was used with different learning rates.

3.3 Results

3.3.1 Dataset preparation

MPWT has recently introduced the ROMDAS for road network assessment. However, due to limited server capacity and the lack of dedicated software tools for image-based analysis, high-

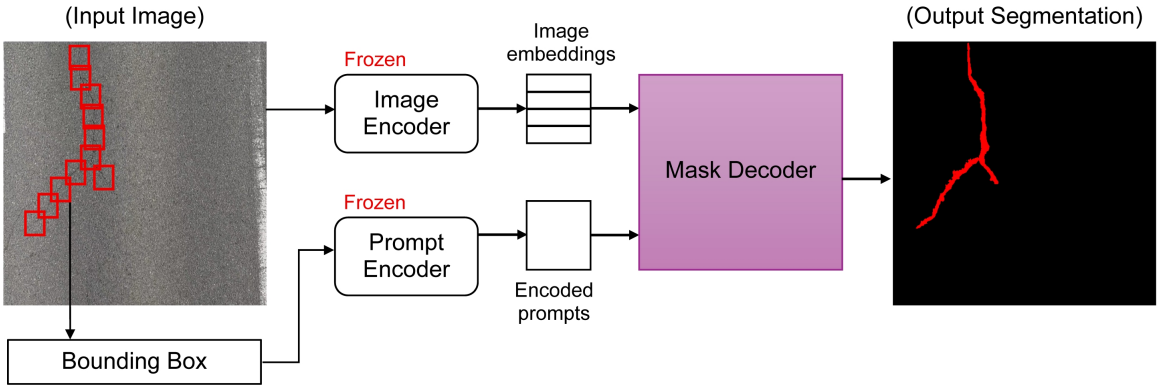


Figure 3.7: Overview of modified SAM architecture.

resolution pavement images captured by ROMDAS are generally retained only for a short period before being deleted. In contrast, conventional outputs such as the International Roughness Index (IRI), Rut Depth, and Mean Profile Depth (MPD), which require far less storage space, are systematically preserved. Moreover, the ROMDAS pavement image available from a small number of survey routes in Cambodia does not provide sufficient coverage of surface distress for comprehensive analysis.

To address these limitations, a synthetic dataset was created that emulates the characteristics of ROMDAS imagery. Specifically, pavement surface regions were cropped from Cambodian ROMDAS survey images while retaining the blue header that contains embedded coordinate information. These cropped regions were then replaced with pavement surface images captured in Yamanashi, Japan, using an action camera [54]. This strategy ensured that the resulting dataset maintained the perspective and visual style of ROMDAS data while expanding the availability of distress cases required for training and validation. Nonetheless, as this synthesis primarily demonstrates the feasibility of the proposed framework, variations in pavement texture, illumination, and imaging conditions between two sources may influence the model' s generalization to purely local datasets. Therefore, retraining or fine-tuning with larger, fully local datasets is recommended for practical deployment.

In total, 1260 images were prepared for model development and randomly divided into two subsets: 80% for training and 20% for validation. Additionally, a separate set of 700 unseen images was used for independent testing to assess model generalization performance. The dataset was annotated into three primary categories of cracks (transverse, longitudinal, and pattern cracks), using the LabelMe tool. Polygonal annotations were subsequently converted into binary ground truth masks to facilitate segmentation tasks.

3.3.2 Model

The proposed framework integrates two models: YOLOv8 for crack detection and SAM for segmentation. YOLOv8 was chosen for its simplified training and deployment through the Ultralytics library and for its anchor-free detection mechanisms, which allow faster inference without compromising accuracy. The YOLOv8n variant, in particular, was selected due to its lightweight architecture, making it suitable for deployment on limited hardware. As reported by Li and Gu [55], comparative experiments were conducted using multiple YOLOv8 versions (YOLOv8n, YOLOv8s, YOLOv8m, YOLOv8l, and YOLOv8x) for road crack detection. Their results showed that YOLOv8n achieved competitive accuracy with significantly lower inference time and reduced hardware requirements compared with the larger models; therefore, it was selected as the baseline in their study and further modified to improve accuracy and efficiency. Despite its compact design, YOLOv8n achieves higher accuracy than comparable lightweight models such as MobileNet-SSD, which rely on older CNN backbones. Furthermore, YOLOv8 supports deployment formats like TensorRT, enabling performance optimization on embedded NVIDIA Jetson platforms and ensuring stable operation in continuous field environments.

For segmentation, SAM was incorporated to generate fine-grained crack masks from bounding box prompts. SAM is a transformer-based vision model designed for general purpose segmentation, and in this study, its ViT-H backbone was fine-tuned using a transfer learning strategy. The image encoder and prompt encoder were frozen to preserve SAM' s feature extraction capability, while the mask decoder was optimized for pavement crack imagery. To improve the accuracy of segmenting thin and irregular crack structures, a hybrid loss function combining Binary Cross-Entropy (BCE) loss and Dice loss was employed. In addition, to refine segmentation quality when bounding box prompts were overly broad, a simpler local refinement, crop-and-refine, was adopted in the test dataset to work on image patches [56, 57]. This refinement module crops local regions in the bounding boxes, performs localized corrections based on error maps, and then reinserts the refined patches into the global region.

3.3.3 Training setup

All experiments were conducted on a Windows 11 operating system with PyCharm as the development environment. To ensure reproducibility, the code and experimental configurations used for both training and testing are publicly accessible on GitHub at https://github.com/Nut-Sovanneth/YOLOv8-SAM-OCR.git. Model training and validation were performed on a NVIDIA GeForce RTX 4070 Ti GPU. The optimizer was set to automatic selection, enabling adaptive tuning of optimization parameters during training. Parameters quantify the learnable elements within a model, reflecting the complexity and capacity of the model. The detailed configurations pertaining to the hyperparameters for network training are outlined in Table 3.1.

Table 3.1: Hyperparameter configuration for distress detection and segmentation.

Parameter	**YOLOv8**	**SAM**
Pretrained Model	YOLOv8n.pt	sam_vit_h_4b8939.pth
Epochs	200	200
Batch size	8	1
Input size	640×640	1024×1024
Learning rate	0.01	0.001, 0.0001, 0.00001
Classes	T_Crack, L_Crack, P_Crack[1]	T_Crack, L_Crack, P_Crack[1]

[1] T_Crack = Transverse Crack, L_Crack = Longitudinal Crack, P_Crack = Pattern Crack.

YOLOv8 was trained for 200 epochs with an input size of 640×640 pixels and a batch size of eight, using pretrained weights (YOLOv8n.pt). SAM was fine-tuned for 200 epochs with a batch size of one image, an input size of 1024×1024 pixels, and pretrained weights (sam_vit_h_4b8939.pth). For YOLOv8, the initial learning rate was set to 0.01 and gradually decreased to near zero following a cosine schedule, where an initial warm-up phase enables stable early training and the non-linear decay shows the reduction toward the end of the process. For SAM, learning rates of 0.001, 0.0001, and 0.00001 were evaluated based on sensitivity analyses to balance training stability, convergence speed, and computational efficiency, ensuring optimal mask segmentation performance while maintaining feasible resource usage. Both models were trained on the same three classes of cracks: trans-verse, longitudinal, and pattern cracks.

Hyperparameters such as image size, batch size, and learning rate were carefully selected based on sensitivity analyses to balance training stability, convergence speed, and computational efficiency.

3.3.4 Evaluation metrics

The performance of the YOLOv8 detection model was evaluated using precision, recall, and mean average precision (mAP). Precision measures the proportion of correctly identified cracks among all positive predictions, while recall reflects the proportion of actual cracks successfully detected by the model. Average Precision (AP) corresponds to the area under the precision-recall curve for each crack type. The mAP at IoU = 0.5 (mAP50) quantifies performance when a 50% overlap is required between predicted and ground truth bounding boxes, whereas mAP50–95 average AP across thresholds from 0.5 to 0.95 in increments of 0.05, providing a more comprehensive measure of detection accuracy. YOLOv8 was optimized using a composite loss function consisting of box regression loss (box_loss), classification loss (cls_loss), and distribution focal loss (dfl_loss), which together improved bounding box localization, crack classification, and boundary refinement. These evaluation metrics can be calculated as follows:

$$Precision = \frac{TP}{TP + FP} \tag{3.4}$$

$$Recall = \frac{TP}{TP + FN} \tag{3.5}$$

$$AP = \int_0^1 P(R)\, dR \tag{3.6}$$

$$mAP = \frac{1}{N} \sum_{i=1}^{N} AP_i \tag{3.7}$$

$$mAP_{50} = \frac{1}{m} \sum_{i=1}^{m} AP_i \quad (\text{with } IoU = 0.5) \tag{3.8}$$

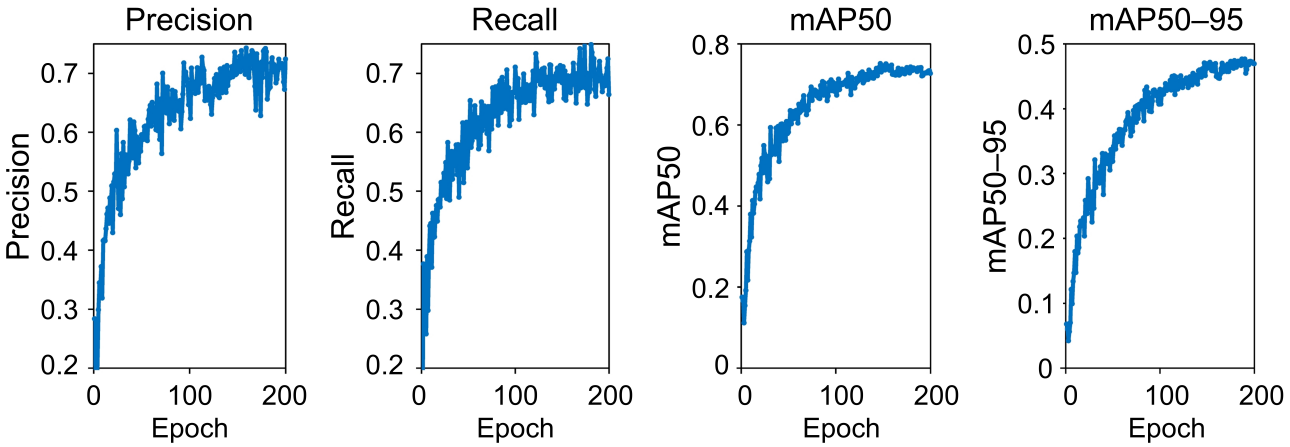
$$mAP_{50\text{-}95} = \frac{1}{N} \sum_{t \in \{0.5, 0.55, \ldots, 0.95\}} AP_t \quad (\text{with } IoU = t) \tag{3.9}$$

Here, TP (true positives) refers to correctly detected cracks, FP (false positives) represents background regions incorrectly identified as cracks, and FN (false negatives) denotes missed cracks. N represents the number of crack classes (e.g., transverse, longitudinal, and pattern cracks).

During the YOLOv8 training, key evaluation metrics, including *Precision*, *Recall*, $mAP50$, and $mAP50$–95, were monitored at each epoch, as shown in Figure 3.8. All metrics exhibited a gradual improvement with increasing iterations. By the end of training, *Precision*, *Recall*, $mAP50$, and $mAP50$–95 reached 0.704, 0.694, 0.733, and 0.468, respectively, indicating that YOLOv8 achieves strong performance in detecting pavement cracks.

Figure 3.9 illustrates the Precision-Recall curves for YOLOv8. The horizontal axis represents *Recall*, and the vertical axis corresponds to *Precision*. Figure 3.9 also reports the AP values for each crack class as well as the mAP across all classes. Specifically, the areas under the curves for transverse crack, longitudinal crack, and pattern crack are 0.75, 0.763, and 0.712, respectively, demonstrating that YOLOv8 effectively identifies different types of pavement cracks.

The performance of YOLOv8 was evaluated on a validation set containing all crack categories: T_Crack, L_Crack, and P_Crack, as illustrated in Figure 3.10. Overall, the model shows solid capability in classifying crack types. It correctly identifies Transverse, Longitudinal, and Pattern cracks with normalized accuracies of 0.76, 0.78, and 0.82, respectively, with



(a) Precision (b) Recall (c) mAP50 (d) mAP50–95

Figure 3.8: YOLOv8 training process.

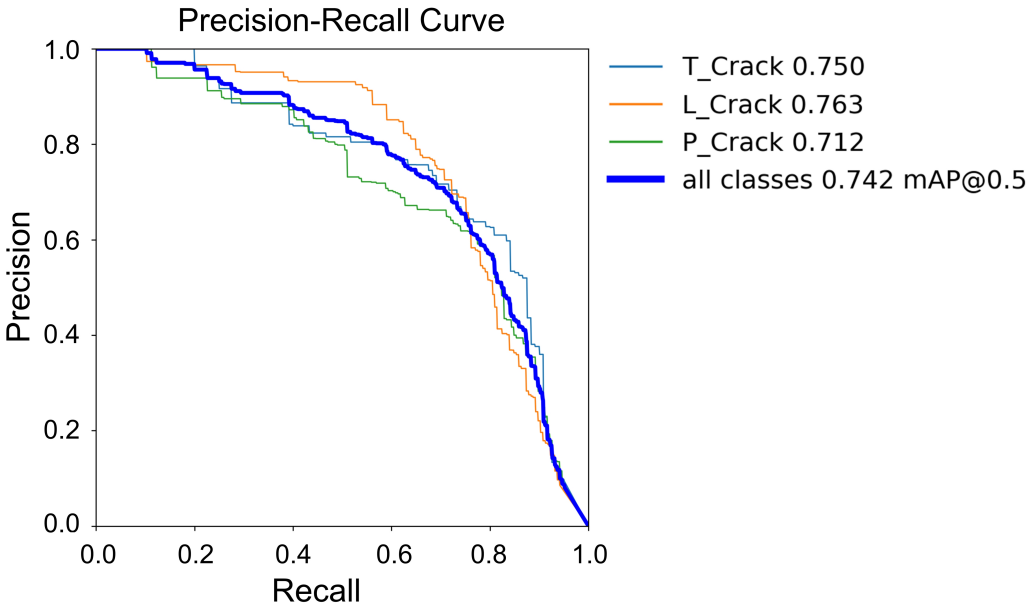


Figure 3.9: YOLOv8 Precision-Recall curve.

little confusion between the crack classes. The main limitation arises in distinguishing cracks from background regions. These results suggest that the model may re-quire enhancements in feature differentiation to reduce false positives.

The performance of SAM was evaluated using $Precision$, $Recall$, $F1-score$, and Intersection over Union (IoU). The $F1-score$, defined as the harmonic mean of $Precision$ and $Recall$, offers a balanced indicator of segmentation accuracy and robustness, especially in the case of imbalanced datasets. IoU quantifies the geometric overlap between predicted (A_p) and ground truth labels (A_r), thereby evaluating the fidelity of predicted crack boundaries.

$$F1\text{-score} = 2 \times \frac{\text{Precision} \times \text{Recall}}{\text{Precision} + \text{Recall}} \tag{3.10}$$

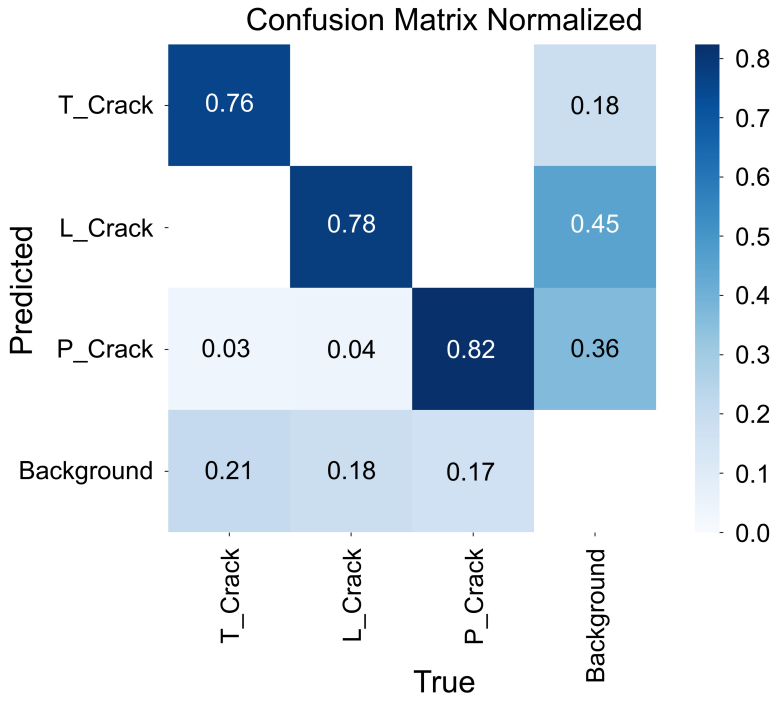


Figure 3.10: Confusion matrix normalized for crack detection.

$$IoU = \frac{\text{area}(A_p \cap A_r)}{\text{area}(A_p \cup A_r)} \tag{3.11}$$

For the SAM training process, metrics such as $Precision$, $Recall$, $F1-\text{score}$, and IoU were tracked over the same 200 epochs using three distinct learning rates: 0.001, 0.0001, and 0.00001. As depicted in Figure 3.11, all metrics improved progressively as the number of iterations increased. Among the test-ed learning rates, 0.0001 yielded the best performance, with $Precision$, $Recall$, $F1-\text{score}$, and IoU values of 0.938, 0.947, 0.942, and 0.891, respectively, suggesting that this configuration allowed the model to capture crack features more accurately than the other learning rates. Although full convergence was not reached within the 200 epochs, the attained $F1-score$ of 0.942 demonstrates robust segmentation performance, as values above 0.9 are widely regarded as indicative of highly accurate prediction, whereas scores below 0.5 typically reflect substantial misclassifications [44]. The implication is that while marginal gains might be realized with extended training, the current performance is operationally sufficient and robust for the application domain.

To assess practical deployment feasibility, we measured model size, computational complexity, and inference performance. The YOLOv8-based detector contains 3.01 million parameters and requires 8.2 GFLOPs per 640×640 input image, achieving an average inference time of 3.65 ms per image, corresponding to 274 FPS. On the other hand, the fine-tuned SAM model with ViT-H backbone contains 631.6 million parameters and requires 2733.6 GFLOPs for 1024×1024

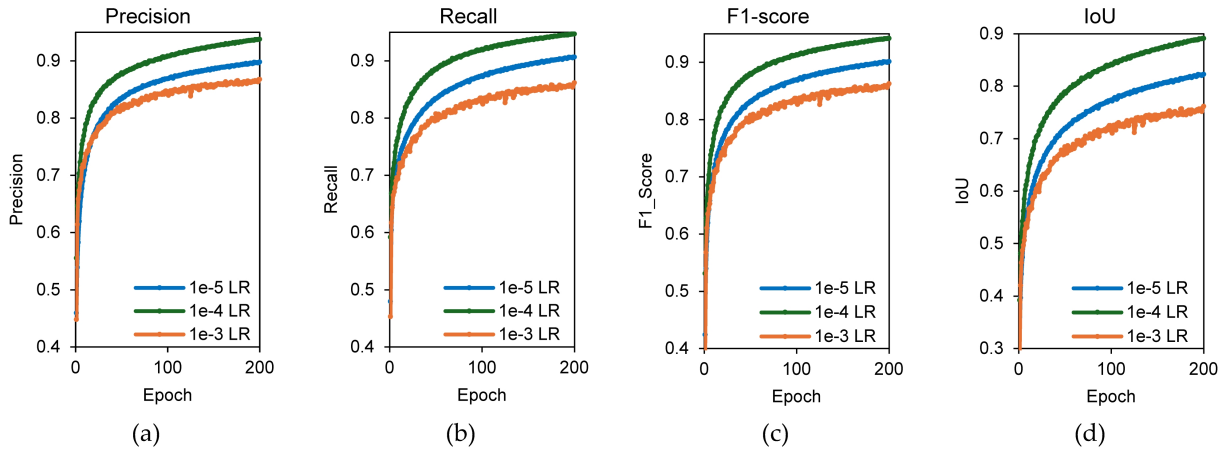


Figure 3.11: SAM training process: (a) *Precision*, (b) *Recall*, (c) $F1-score$, and (d) *IoU*.

inputs, with an inference time of 431.7 ms per image, corresponding to 2.32 FPS.

For each connected component within the coarse segmented mask, an expanded region of interest (ROI) was extracted from the original input image using direct array slicing. This hard-crop operation supplies the refinement process with a high-resolution con-textual pixel centered on the target component, without any interpolation artifacts. The SAM is then applied to the isolated patch, using a translated bounding-box prompt, to produce a high-fidelity local segmentation. The refined-level masks are subsequently mapped back into global coordinates and composited into the final output mask. This local refinement procedure improves boundary precision and detail while maintaining consistency across the entire image domain. The inference results on unseen images from the combined YOLOv8 and SAM framework are visualized in Figure 3.12, where transverse, longitudinal, and pattern cracks are indicated by blue, green, and red bounding boxes and masks, respectively.

Figure 3.13 confirms that the local refinement procedure effectively reduces coarse-level artifacts and produces masks that more closely approximate ground-truth crack structures. Without refinement, the initial coarse masks often appear blocky or exhibit jagged edges, failing to conform to the subtle curvatures and irregular widths of the actual cracks. In contrast, the locally refined masks display a markedly improved ability to follow true crack boundaries with high fidelity, capturing fine-scale details and variations in crack geometry. The localized application of the SAM model on the isolated, high-resolution ROI further resolves ambiguities that arise in the coarse segmentation, yielding cleaner, more intricate, and ultimately more accurate representations of the underlying crack ex-tent. These results highlight the advantage of combining global detection with localized high-resolution segmentation, enabling the system to preserve contextual consistency while achieving fine-scale precision across heterogeneous pavement surfaces.

Upon completion of the two-stage process, the segmented mask can be quantified by counting the pixels, allowing computation of distress density, as described in [58]. Simultaneously, a

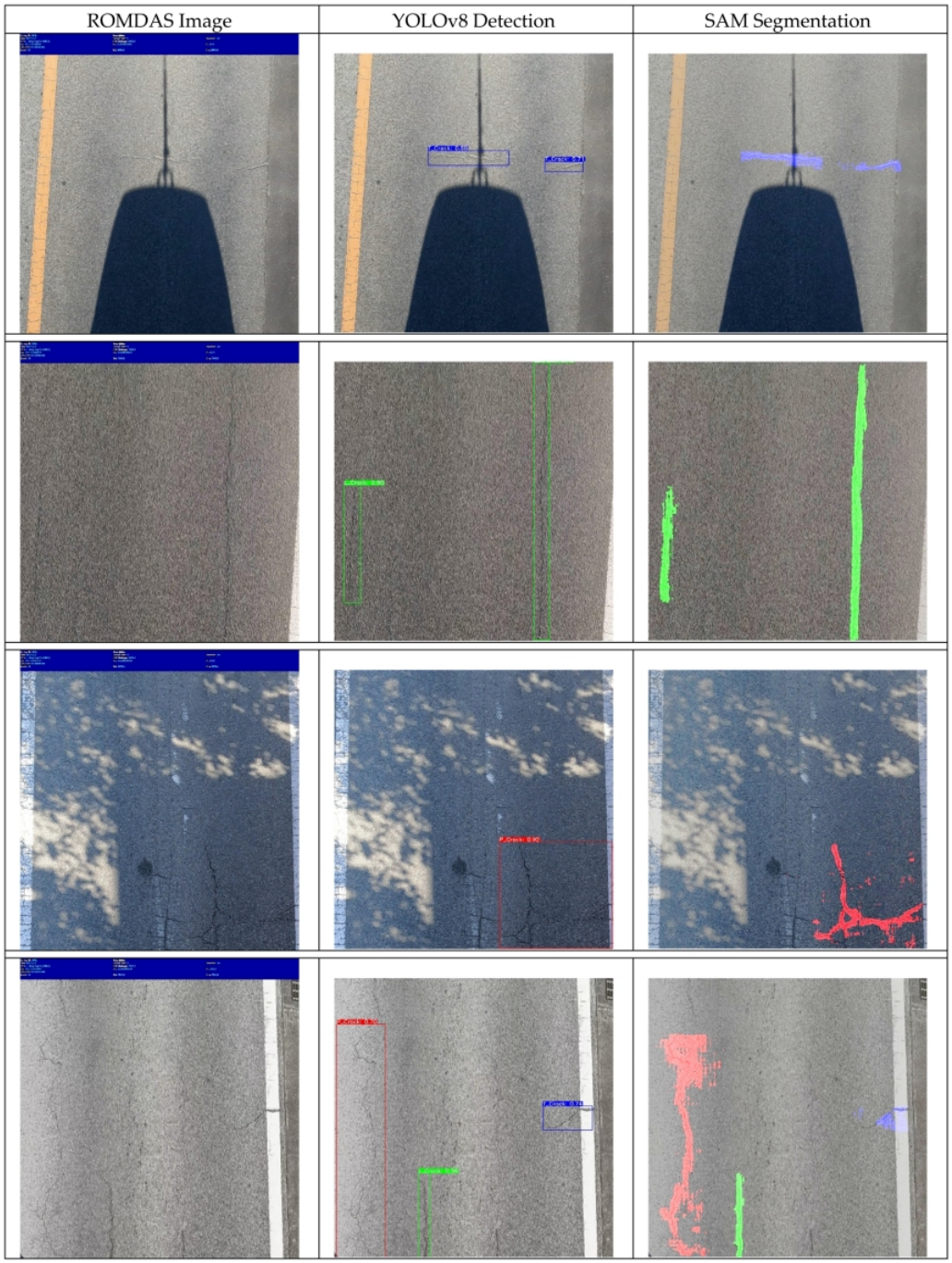


Figure 3.12: Test results of combined YOLOv8 and SAM.

region containing pixel-level coordinates is extracted using Tesseract OCR to enable geospatial mapping of the detected and segmented distress, as illustrated in Figure 3.14. The OCR reliably recognizes the coordinate digits at the pixel level, producing digital values that accurately correspond to the road alignment when imported into a GIS.

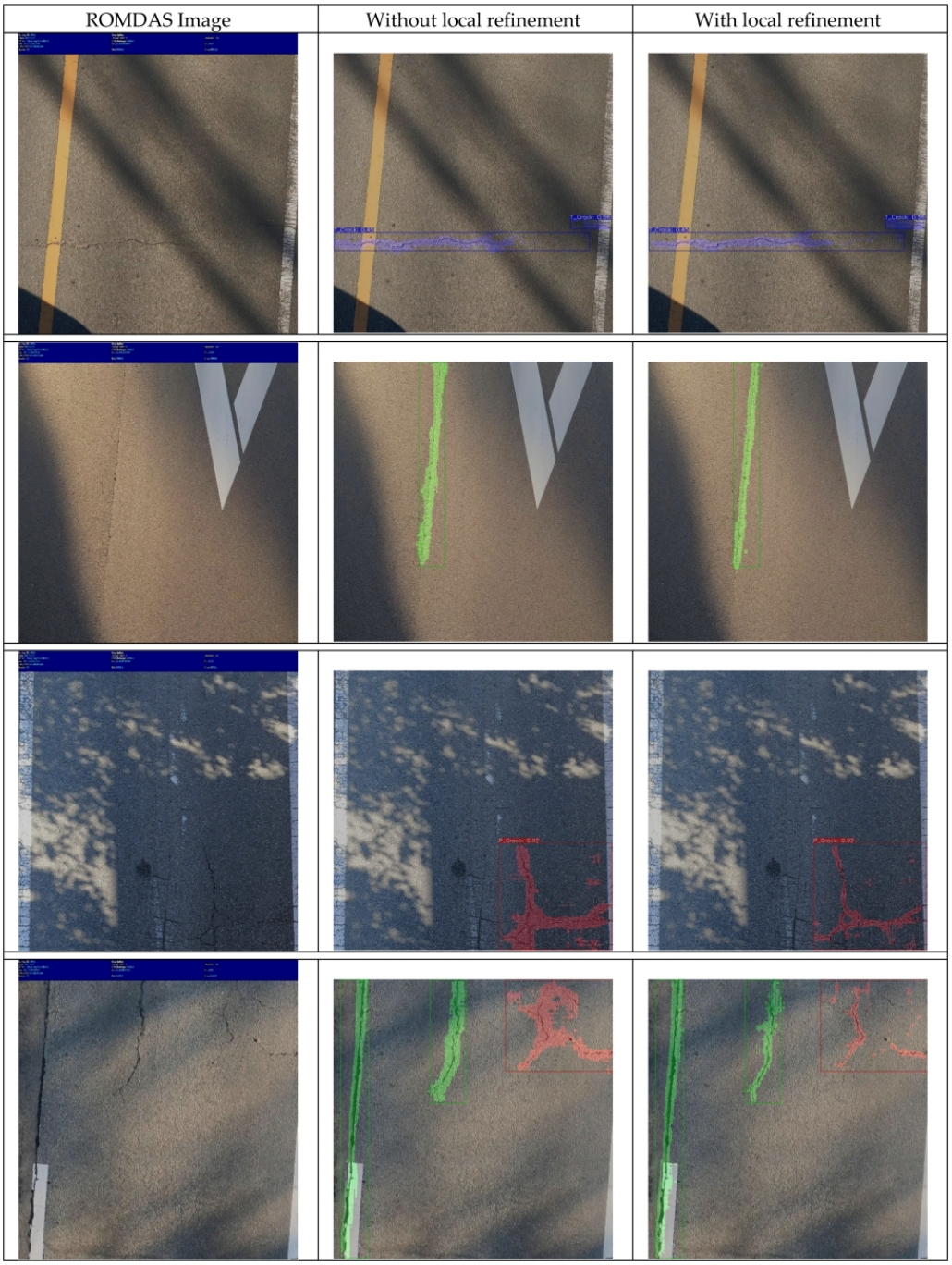


Figure 3.13: Effectiveness of local refinement on segmentation.

3.4 Discussion

The cornerstone of the proposed framework lies in the integration of efficient pavement crack detection using YOLOv8n and high-fidelity segmentation using SAM. The choice of the lightweight YOLOv8n model as the baseline detector was deliberate, prioritizing an optimal balance between computational efficiency and detection efficacy. The results presented in the previous section demonstrate that YOLOv8n achieves satisfactory performance given its compact size and high inference speed. This efficiency is particularly critical for large-scale deployment by

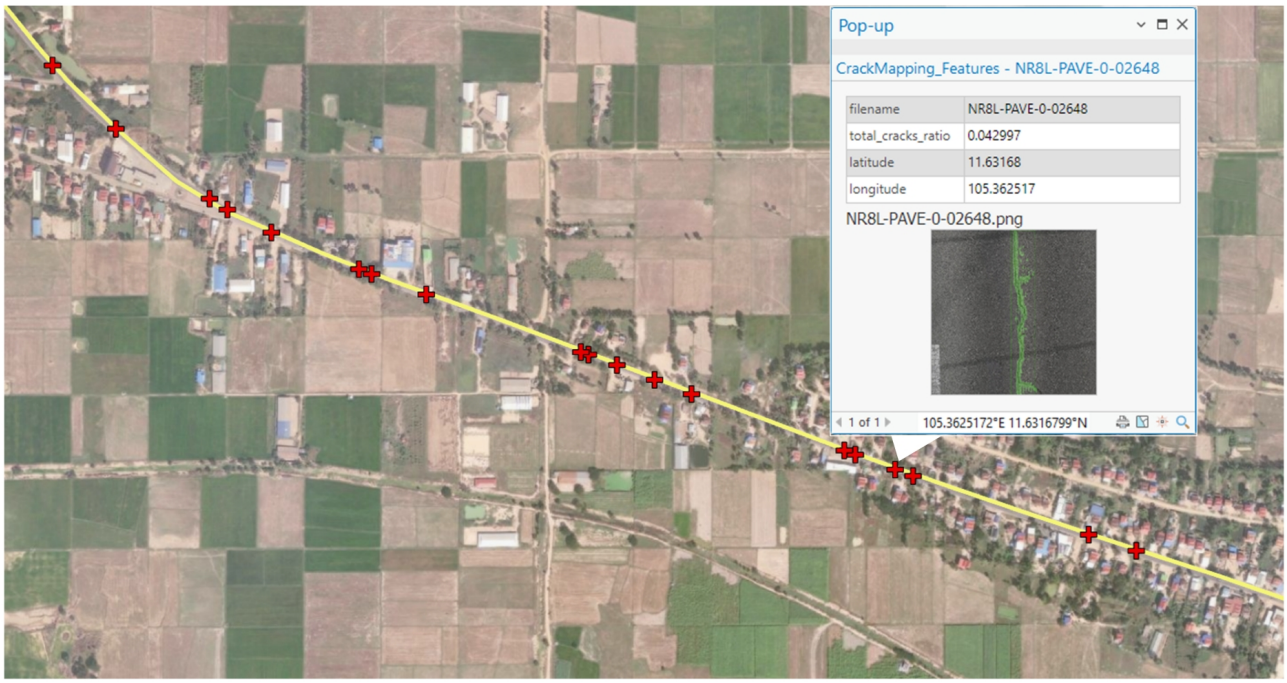


Figure 3.14: GIS-based visualization of detected pavement distress.

road agencies.

However, pavement distress datasets inherently pose challenges such as thin cracks or complex pavement textures, which can lead to false positives, missed detections, and reduced accuracy in the baseline YOLOv8n. To address these limitations, potential improvements could involve modifications to the backbone and neck structures to strengthen feature extraction and multi-scale representation. Such architectural refinements would enable the model to better capture fine-grained crack details more effectively, minimize redundant computation, and enhance localization accuracy across varying spatial scales.

For the segmentation task, the SAM component delivered exceptional results following fine-tuning. This high fidelity in mask generation is essential for accurate quantification of crack severity, which underpins efficient maintenance planning. Two complementary loss functions, including BCE and Dice loss, were employed during training. BCE promotes precise pixel-level classification, while Dice loss enhances overlap quality between predicted and ground-truth masks. This hybrid objective facilitates robust boundary delineation and improves the model' s ability to generalize across diverse crack morphologies. The fine-tuned SAM' s mask decoder, optimized under this combined loss, effectively captured both global structure and local boundary details.

As summarized in Table 3.2, a comparative evaluation on the Crack500 dataset demonstrated that the proposed SAM notably outperformed several state-of-the-art segmentation frameworks. In particular, the SAM attains the highest IoU of 76.69%, demonstrating its strong capability in accurately delineating crack regions. Although its $Precision$ (79.07%) and

Table 3.2: Comparison of different segmentation models on the Crack500 dataset.

Model	Precision	Recall	F1-score	IoU
DeepCrack [59]	0.3607	0.8982	0.4911	0.3425
U-Net [60]	0.6998	0.6876	0.6693	0.5279
TransUNet [61]	0.7014	0.6587	0.6520	0.5053
Swin-Unet [62]	0.6915	0.6519	0.6426	0.4971
CrackNet [63]	0.6474	0.7595	0.6744	0.5293
W-segnet [20]	0.7986	0.8156	0.8070	0.7326
Modified DeepLabv3+ [34]	0.6950	0.8000	0.7440	0.5590
Our SAM	0.7907	0.8053	0.7962	0.7669

$F1-$score (79.62%) are marginally lower than those of W-segnet, which achieved 79.86% and 80.70%, respectively, the SAM maintains highly competitive results across these metrics. Furthermore, its *Recall* (80.53%) is comparable to that of W-segnet (81.56%) and the modified DeepLabv3+ (80.00%), and remains close to the top-performing DeepCrack (89.82%). These findings confirm that fine-tuning SAM with appropriate loss functions and learning configurations significantly enhances segmentation accuracy for pavement crack analysis.

3.5 Conclusions

This study introduces a novel, integrated framework for end-to-end pavement crack detection and segmentation. The proposed methodology leverages the YOLOv8 model for efficient crack detection and a modified SAM for high-precision, pixel-level segmentation. This two-step approach addresses the significant challenge of high labeling costs by utilizing bounding box prompts from the detection phase to guide the segmentation process.

The framework' s effectiveness was validated using a real-world, open-source dataset from Yamanashi, Japan. The YOLOv8-based detection model demonstrated robust performance with a *Precision* of 0.704, a *Recall* of 0.694, and mAP scores of 0.733 (at an IoU of 0.5) and 0.468 (averaged from 0.5 to 0.95). These metrics confirm the model' s capacity for crack detection on smart road-measuring devices with minimal computational requirements.

A key contribution of this research is the integration of SAM, which offers significant advantages in reducing annotation burdens. Unlike traditional segmentation models that are limited to pre-trained classes and require extensive annotated datasets, our modified SAM approach enables zero-shot segmentation. This allows the model to accurately delineate crack boundaries on new, unseen images without the need for additional training, a capability that no current

segmentation model offers for this application. The segmentation results, with a *Precision* of 0.938, a *Recall* of 0.947, an $F1-$score of 0.942, and an IoU of 0.891, underscore the model' s precision in identifying the exact pixels that constitute a crack.

To further illustrate the performance of the proposed framework, a comparative evaluation was conducted on the Crack500 dataset. The SAM-based approach achieved the highest IoU of 76.69%, indicating superior ability in delineating crack regions. While its *Precision* (79.07%) and $F1-score$ (79.62%) are slightly lower than W-segnet, the SAM remains highly competitive. Its *Recall* (80.53%) is comparable to other leading methods, such as W-segnet and DeepLabv3+, and approaches the performance of DeepCrack.

Furthermore, the framework integrates OCR to automatically extract geospatial coordinates, enabling the automated mapping of detected distress onto real-world road networks. This end-to-end solution provides a quantitative assessment of distress, including its type, severity, and extent, which is essential for calculating the MCI and facilitating efficient maintenance planning for road agencies.

Despite the demonstrated effectiveness of the proposed framework, several challenges remain. For instance, some cracks obscured by shadows exhibit reduced identifiability, as illustrated in Figure 3.12 Environmental factors, including uneven lighting and motion blur caused by vehicle movement, can adversely affect model accuracy. Moreover, the complexity of real-world road scenes, such as the presence of debris or irregular pavement textures, may result in missed detections or incomplete segmentation, even when detection is successful. Future work will aim to enhance the model' s robustness by refining the YOLO and SAM architecture with advanced attention mechanisms to better handle complex and noisy environments, as well as by improving the local refinement strategy, for example, through the incorporation of techniques such as RoIAlign.

References

[1] Hu, G. X. et al. Pavement Crack Detection Method Based on Deep Learning Models. *Wireless Communications and Mobile Computing* 2021, **2021**(1), p. 5573590. DOI: https://doi.org/10.1155/2021/5573590.

[2] Qureshi, W. S. et al. An Exploration of Recent Intelligent Image Analysis Techniques for Visual Pavement Surface Condition Assessment. *Sensors* 2022, **22**(22), p. 9019. DOI: https://doi.org/10.3390/s22229019.

[3] Zhang, Z.; Zhang, H.; Zhang, T. Enhanced YOLOv8-Based Pavement Crack Detection: A High-Precision Approach. *PLoS One* 2025, **20**(5), e0324512. DOI: https://doi.org/10.1371/journal.pon

[4] Zakeri, H.; Nejad, F. M.; Fahimifar, A. Image Based Techniques for Crack Detection, Classification and Quantification in Asphalt Pavement: A Review. *Archives of Computational Methods in Engineering* 2017, **24**(4), pp. 935–977. DOI: https://doi.org/10.1007/s11831-016-9194-z.

[5] Mathavan, S.; Kamal, K.; Rahman, M. A Review of Three-Dimensional Imaging Technologies for Pavement Distress Detection and Measurements. *IEEE Transactions on Intelligent Transportation Systems* 2015, **16**(5), pp. 2353–2362. DOI: https://doi.org/10.1109/TITS.2015.2428655

[6] Fei, Y. et al. Pixel-Level Cracking Detection on 3D Asphalt Pavement Images Through Deep-Learning-Based CrackNet-V. *IEEE Transactions on Intelligent Transportation Systems* 2019, **21**(1), pp. 273–284. DOI: https://doi.org/10.1109/TITS.2019.2891167.

[7] Ibragimov, E. et al. Automated Pavement Condition Index Assessment with Deep Learning and Image Analysis: An End-to-End Approach. *Sensors* 2024, **24**(7), p. 2333. DOI: https://doi.org/10.3390/s24072333.

[8] Chun, P.-j.; Yamane, T.; Tsuzuki, Y. Automatic Detection of Cracks in Asphalt Pavement Using Deep Learning to Overcome Weaknesses in Images and GIS Visualization. *Applied Sciences* 2021, **11**(3), p. 892. DOI: https://doi.org/10.3390/app11030892.

[9] Minami, M.; Suzuki, T. Pavement Maintenance Level and Annual Budget over the Regional Road Network. *Journal of Construction Management, JSCE* 2008, **15**, pp. 71–79. DOI: https://doi.org/10.2208/procm.15.71.

[10] Miyamoto, A.; Yoshitake, T. "Development of a Remote Condition Assessment System for Road Infrastructures". *International ECCE Conference, EUROINFRA 2009, Current State and Challenges for Sustainable Development of Infrastructure*. 2009, pp. 21–22.

[11] Japan Road Association. *Maintenance Guidebook for Road Pavement : 2013 Edition*. Japan Road Association and sold by Maruzen, 2017. URL: `https://cir.nii.ac.jp/crid/1970304959868170016`.

[12] Yoshida, T. Composite Indicators for Assessing Maintenance Needs for Road Pavements from the View Point of Road Functions. *Journal of Japan Society of Civil Engineers, Ser. E1 (Pavement Engineering)* 2016, **72**(1), pp. 12–20. ISSN: 2185-6559. DOI: https://doi.org/10.2208/jsc

[13] Kubo, K. "Pavement Maintenance in Japan". *Road Conference 2017 International Symposium.* 2017.

[14] Ali, L. et al. Rs-Net: Residual Sharp U-Net Architecture for Pavement Crack Segmentation and Severity Assessment. *Journal of Big Data* 2024, **11**(1), p. 116. DOI: https://doi.org/10.1186/s 024-00981-y.

[15] Li, Q. et al. A Novel YOLO Algorithm Integrating Attention Mechanisms and Fuzzy Information for Pavement Crack Detection. *International Journal of Computational Intelligence Systems* 2025, **18**(1), p. 158. DOI: https://doi.org/10.1007/s44196-025-00894-5.

[16] Peraka, N. S. P.; Biligiri, K. P. Pavement Asset Management Systems and Technologies: A Review. *Automation in Construction* 2020, **119**, p. 103336. DOI: https://doi.org/10.1016/j.autcon.202

[17] Zhou, W. et al. Road Defect Detection from On-Board Cameras with Scarce and Cross-Domain Data. *Automation in Construction* 2022, **144**, p. 104628. DOI: https://doi.org/10.1016/j.autc

[18] Chong, D.; Liao, P.; Fu, W. Multi-Objective Optimization for Sustainable Pavement Maintenance Decision Making by Integrating Pavement Image Segmentation and TOPSIS Methods. *Sustainability* 2024, **16**(3), p. 1257. DOI: https://doi.org/10.3390/su16031257.

[19] Han, Z. et al. MS-YOLOv8-Based Object Detection Method for Pavement Diseases. *Sensors (Basel, Switzerland)* 2024, **24**(14), p. 4569. DOI: https://doi.org/10.3390/s24144569.

[20] Zhong, J. et al. Multi-Scale Feature Fusion Network for Pixel-Level Pavement Distress Detection. *Automation in Construction* 2022, **141**, p. 104436. DOI: https://doi.org/10.1016/j.autcon.202

[21] Koch, C. et al. A Review on Computer Vision Based Defect Detection and Condition Assessment of Concrete and Asphalt Civil Infrastructure. *Advanced engineering informatics* 2015, **29**(2), pp. 196–210. DOI: https://doi.org/10.1016/j.aei.2015.01.008.

[22] He, Y. et al. Pavement Surface Defect Detection Using Mask Region-Based Convolutional Neural Networks and Transfer Learning. *Applied Sciences* 2022, **12**(15), p. 7364. DOI: https://doi.org/10.3390/app12157364.

[23] Ren, J. et al. Deep Learning and Machine Learning–Object Detection and Semantic Segmentation: From Theory to Applications. 2024. DOI: https://doi.org/10.48550/arXiv.2410.15584.

[24] Ghosh, R.; Smadi, O. Automated Detection and Classification of Pavement Distresses Using 3D Pavement Surface Images and Deep Learning. *Transportation Research Record* 2021, **2675**(9), pp. 1359–1374. DOI: https://doi.org/10.1177/03611981211007481.

[25] Zhang, A. A. et al. Intelligent Pavement Condition Survey: Overview of Current Researches and Practices. *Journal of Road Engineering* 2024, **4**(3), pp. 257–281. DOI: https://doi.org/10.

[26] Zeng, K.; Fan, R.; Tang, X. Efficient and Accurate Road Crack Detection Technology Based on YOLOv8-ES. *Autonomous Intelligent Systems* 2025, **5**(1), p. 4. DOI: https://doi.org/10.1007 025-00091-3.

[27] Oliveira, H.; Correia, P. L. Automatic Road Crack Detection and Characterization. *IEEE Transactions on Intelligent Transportation Systems* 2012, **14**(1), pp. 155–168. DOI: https://doi.org/10.

[28] Elsharkawy, Z. F.; Kasban, H.; Abbass, M. Y. Efficient Surface Crack Segmentation for Industrial and Civil Applications Based on an Enhanced YOLOv8 Model. *Journal of Big Data* 2025, **12**(1), p. 16. DOI: https://doi.org/10.1186/s40537-025-01065-1.

[29] Wen, T. et al. Automated Pavement Distress Segmentation on Asphalt Surfaces Using a Deep Learning Network. *International Journal of Pavement Engineering* 2023, **24**(2), p. 2027414. DOI: https://doi.org/10.1080/10298436.2022.2027414.

[30] Alshawabkeh, S. et al. A Hybrid Approach for Pavement Crack Detection Using Mask R-CNN and Vision Transformer Model. *Computers, Materials & Continua* 2025, **82**(1). DOI: https://doi.org/10.32604/cmc.2024.057213.

[31] Li, D. et al. Pixel-Level Recognition of Pavement Distresses Based on U-Net. *Advances in Materials Science and Engineering* 2021, **2021**(1), p. 5586615. DOI: https://doi.org/10.1155/2021/558

[32] Lau, S. L. et al. Automated Pavement Crack Segmentation Using U-Net-Based Convolutional Neural Network. *Ieee Access* 2020, **8**, pp. 114892–114899. DOI: https://doi.org/10.1109/ACCES

[33] Li, F. et al. A Novel Model for the Pavement Distress Segmentation Based on Multi-Level Attention DeepLabV3+. *Engineering Applications of Artificial Intelligence* 2024, **137**, p. 109175. DOI: https://doi.org/10.1016/j.engappai.2024.109175.

[34] Sun, X. et al. DMA-Net: DeepLab with Multi-Scale Attention for Pavement Crack Segmentation. *IEEE Transactions on Intelligent Transportation Systems* 2022, **23**(10), pp. 18392–18403. DOI: https://doi.org/10.1109/TITS.2022.3158670.

[35] Wang, P. et al. *Research on Automatic Pavement Crack Recognition Based on the Mask R-CNN Model*. 2023. DOI: https://doi.org/10.3390/coatings13020430.

[36] Dong, J. et al. Intelligent Segmentation and Measurement Model for Asphalt Road Cracks Based on Modified Mask R-CNN Algorithm. *Computer Modeling in Engineering & Sciences* 2021, **128**(2), pp. 541–564. DOI: https://doi.org/10.32604/cmes.2021.015875.

[37] Chen, T. et al. Pavement Crack Detection and Recognition Using the Architecture of SegNet. *Journal of Industrial Information Integration* 2020, **18**, p. 100144. DOI: https://doi.org/10.1016/j

[38] Kyem, B. A.; Asamoah, J. K.; Aboah, A. Context-Cracknet: A Context-Aware Framework for Precise Segmentation of Tiny Cracks in Pavement Images. *Construction and Building Materials* 2025, **484**, p. 141583. DOI: https://doi.org/10.1016/j.conbuildmat.2025.141583.

[39] Xu, H. et al. Automatic Detection of Tunnel Lining Crack Based on Mobile Image Acquisition System and Deep Learning Ensemble Model. *Tunnelling and Underground Space Technology* 2024, **154**, p. 106124. DOI: https://doi.org/10.1016/j.tust.2024.106124.

[40] Amani, M. et al. Google Earth Engine Cloud Computing Platform for Remote Sensing Big Data Applications: A Comprehensive Review. *IEEE Journal of Selected Topics in Applied Earth Observations and Remote Sensing* 2020, **13**, pp. 5326–5350. DOI: https://doi.org/10.1109/JSTARS.2020.3021052.

[41] Rakshitha, R. et al. Crack SAM: Enhancing Crack Detection Utilizing Foundation Models and Detectron2 Architecture. *Journal of Infrastructure Preservation and Resilience* 2024, **5**(1), p. 11. DOI: https://doi.org/10.1186/s43065-024-00103-1.

[42] Ahmadi, M. et al. Application of Segment Anything Model for Civil Infrastructure Defect Assessment. *Innovative Infrastructure Solutions* 2025, **10**(7), p. 269. DOI: https://doi.org/10.1007/s41
025-02073-z.

[43] Li, J. et al. Semi-Supervised Crack Detection Using Segment Anything Model and Deep Transfer Learning. *Automation in Construction* 2025, **170**, p. 105899. DOI: https://doi.org/10.1016/j.a

[44] Owor, N. J. et al. PaveSAM –Segment Anything for Pavement Distress. *Road Materials and Pavement Design* 2025, **26**(3), pp. 593–617. DOI: https://doi.org/10.1080/14680629.2024.2374863

[45] Mursari, L. R.; Wibowo, A. The Effectiveness of Image Preprocessing on Digital Handwritten Scripts Recognition with the Implementation of OCR Tesseract. *Computer Engineering and Applications Journal* 2021, **10**(3), pp. 177–186.

[46] Saoji, S.; Eqbal, A.; Vidyapeeth, B. Text Recognition and Detection from Images Using Pytesseract. *Journal of Interdisciplinary Cycle Research* 2021, **13**, pp. 1674–1679.

[47] Güler, A. K.; Musa, A. An End-to-End Automatic Number Plate Recognition System Based on YOLOv12 and Tesseract OCR. *International Journal of New Horizons in the Sciences* 2025, **3**(1), pp. 42–52. URL: `https://jihsci.com/index.php/jihsci/article/view/37`.

[48] Hartley, R.; Zisserman, A. *Multiple View Geometry in Computer Vision*. 2nd. Cambridge, UK: Cambridge University Press, 2006.

[49] Bruls, T. et al. *The Right (Angled) Perspective: Improving the Understanding of Road Scenes Using Boosted Inverse Perspective Mapping*. IEEE, 2019, pp. 302–309. DOI: https://doi.org/10.

[50] Bradski, G. The OpenCV Library. *Dr. Dobb's Journal: Software Tools for the Professional Programmer* 2000, **25**(11), pp. 120–123.

[51] Terven, J.; Córdova-Esparza, D.-M.; Romero-González, J.-A. A Comprehensive Review of YOLO Architectures in Computer Vision: From YOLOv1 to YOLOv8 and YOLO-NAS. *Machine Learning and Knowledge Extraction* 2023, **5**(4), pp. 1680–1716. DOI: https://doi.org/10.3390/

[52] Ju, R.-Y.; Cai, W. Fracture Detection in Pediatric Wrist Trauma X-ray Images Using YOLOv8 Algorithm. *Scientific Reports* 2023, **13**(1), p. 20077. DOI: https://doi.org/10.1038/s41598-023-47460-7.

[53] Choi, Y. et al. Application of Mask R-CNN and YOLOv8 Algorithms for Concrete Crack Detection. *IEEE Access* 2024. DOI: https://doi.org/10.1109/ACCESS.2024.3469951.

[54] Junji, Y.; Kouichi, T. Image Files of Road Surface in Yamanashi by an Action Camera. 2023. URL: `https://jstagedata.jst.go.jp/articles/dataset/Image_files_of_road_surface_by_an_action_camera/23507232`.

[55] Li, R.; Gu, M. Road Crack Detection Method Based on Lightweight YOLOv8-LUAPD and UAV Images. *Measurement Science and Technology* 2025, **36**(4), p. 045411. DOI: https://doi.org/10.1088/1361-6501/adc3b5.

[56] Chen, X. et al. FocalClick: Towards Practical Interactive Image Segmentation. *Proceedings of the IEEE/CVF Conference on Computer Vision and Pattern Recognition (CVPR)* 2022, pp. 1300–1309.

[57] Sofiiuk, K.; Petrov, I. A.; Konushin, A. Reviving Iterative Training with Mask Guidance for Interactive Segmentation. 2022, pp. 3141–3145. DOI: https://doi.org/10.1109/ICIP46576.2022.989

[58] Obunguta, F.; Matsushima, K.; Susaki, J. Probabilistic Management of Pavement Defects with Image Processing Techniques. *Journal of Civil Engineering and Management* 2024, **30**(2), pp. 114–132. DOI: https://doi.org/10.3846/jcem.2024.20401.

[59] Liu, Y. et al. DeepCrack: A Deep Hierarchical Feature Learning Architecture for Crack Segmentation. *Neurocomputing* 2019, **338**, pp. 139–153. DOI: https://doi.org/10.1016/j.neucom.2019.

[60] Ronneberger, O.; Fischer, P.; Brox, T. "U-Net: Convolutional Networks for Biomedical Image Segmentation". *International Conference on Medical Image Computing and Computer-Assisted Intervention*. Springer. 2015, pp. 234–241. DOI: https://doi.org/10.1007/978-3-319-24574-4_28.

[61] Chen, J. et al. Transunet: Transformers Make Strong Encoders for Medical Image Segmentation. 2021. DOI: https://doi.org/10.48550/arXiv.2102.04306.

[62] Cao, H. et al. "Swin-Unet: Unet-Like Pure Transformer for Medical Image Segmentation". *European Conference on Computer Vision*. Springer. 2022, pp. 205–218. DOI: https://doi.org/10.1007/978-3-031-25066-8_9.

[63] Fan, Y. et al. CrackNet: A Hybrid Model for Crack Segmentation with Dynamic Loss Function. *Sensors* 2024, **24**(22), p. 7134. DOI: https://doi.org/10.3390/s24227134.

Chapter 4

Stochastic Approach to Defining Pavement Structural Thresholds from FWD measurements

4.1 Introduction

Maintaining aging road infrastructure within limited budgets poses a significant challenge for civil engineers worldwide. Effective road asset management is essential to address this challenge, ensuring the longevity and safety of road networks [1]. In Cambodia, the goal of road asset management is to implement a system that provides optimal maintenance strategies and ensures acceptable pavement performance for users. The core components of this system include an inventory of road assets, regular condition evaluations, performance prediction models, and decision support tools. These tools help prioritize maintenance activities and allocate resources efficiently [2]. Pavement evaluation involves assessing both functional and structural conditions, determining current performance, and identifying the progress of deterioration.

In Cambodia, flexible pavements are commonly used and can be categorized into two types of surfacing: asphalt concrete (AC) and double bituminous surface treatment (DBST). AC, which is composed of asphalt binder and aggregates, provides a smooth and durable riding surface. It is typically applied to 1-digit national roads, also referred to as primary roads. DBST, on the other hand, consists of a bituminous binder sprayed over a prepared base course and covered with aggregates (19 mm and 12 mm). It is more economical and quicker to construct compared to AC and is normally applied to 2-digit national roads, also referred to as secondary roads. Both 1-digit and 2-digit national roads are regularly evaluated through functional and structural assessments.

Functional evaluation focuses on assessing ride quality, which impacts user comfort and safety, typically measured using indices such as the International Roughness Index (IRI) [3, 4].

Structural evaluation, on the other hand, focuses on assessing the bearing capacity of the underlying layers or the overall pavement to withstand traffic loading [5]. Structural evaluation can be conducted through non-destructive testing methods, such as Falling Weight Deflectometer (FWD) measurements. FWD helps identify weak spots or locations with potential structural issues, which may result from insufficient layer thickness, poor compaction, low material quality, or deterioration due to aging or environmental factors. By back-calculating the moduli for each layer (surface, base, sub-base, and subgrade), the pavement stiffness or structural strength can be quantified [6, 7].

Although the moduli of each layer can be back-calculated, the process typically faces some challenges and limitations. These include variability caused by different software algorithms, the need for accurate input variables, potential errors from local optima convergence due to initial modulus value guesses, and limitations in handling complex pavement structures [8–11]. Moreover, some degree of unreliability arises when various inputs relating to the existing pavement structure, such as temperature, layer thickness, initial estimated elastic modulus, Poisson' s ratio, loading setup, humidity, and moisture condition, are required [8].

To address this issue, Horak et al. introduced a simplified method of benchmarking effective structural number (SN_{eff}), and deflection bowl parameters to avoid the need for complex back-analysis techniques such as linear elastic layered software or finite element method [12, 13]. Deflection bowl parameters correspond to the deflection basin zones and include the maximum deflection (D_0), the base layer index (BLI) (primarily correlated with surface and base layer), the middle layer index (MLI) (primarily correlated with subbase layer), and the lower layer index (LLI) (primarily correlated with selected and subgrade layers). By correlating these indices with levels of surface distress such as cracking, rutting, and potholes, the authors developed a pavement diagnostic framework for identifying structural issues.

Since thresholds for these parameters may vary depending on existing pavement conditions, Ramanath et al. similarly determined benchmark values for Indian conditions using the pavement condition index (PCI) [14]. PCI is a metric for evaluating pavement surface conditions based on surface distress. The authors categorized PCI limits based on cracking and rutting severity (Crack $\leq 10\%$, 10–20%, and $> 20\%$; Rut ≤ 10 mm, 10–20 mm, and > 20 mm, respectively), which align with the failure limits specified by IRC 37 [15].

Fuentes et al. proposed a statistical approach to determine deflection bowl parameter thresholds at the network level based on the probability of structural failure or damage [16]. The authors employed PITRA PAVE software, which uses elastic multi-layer analysis, to simulate the mechanical response of a three-layer pavement structure with various thicknesses and moduli values. The thresholds at the failure point were determined by identifying responses where the moduli of each layer fell below the minimum required values.

Table 4.1: Benchmark structural indices.

Indices	**Rating**	**Horak et al. [9]**	**Ramanath et al. [14]**	**Fuentes et al. [16]**
D_0 (μm)	Sound	<500	–	–
	Warning	500–750		
	Severe	>750		
BLI (μm)	Sound	<200	≤400	<306
	Warning	200–400	400–600	306–365
	Severe	>400	≥600	>365
MLI (μm)	Sound	<100	≤50	<134
	Warning	100–200	150–250	134–245
	Severe	>200	>250	>245
LLI (μm)	Sound	<50	≤75	<96
	Warning	50–100	75–125	96–180
	Severe	>100	≥125	>180
SN_{eff}	Sound	>6	–	–
	Warning	4–6		
	Severe	<4		

Table 4.1 summarizes the benchmark criteria, categorized as Sound, Warning, and Severe, to represent the structural condition rating of hot-mix asphalt pavement layers at 20°C.

While pavement condition can be assessed by the level of defects, it can also be evaluated through the rate of deterioration [17]. In recent years, significant progress has been made in developing deterioration prediction models using stochastic approaches. The Markov chain model has emerged as a popular option for estimating pavement deterioration. The Markov process has enabled users to forecast hazard or deterioration rates, life expectancies, Markov transition probability (MTP) matrix, and deterioration curves for infrastructure systems such as bridges and highways. These predictions are derived from condition states, historically obtained through inspection survey data.

To incorporate the multifaceted factors influencing deterioration, such as traffic patterns, pavement structures, and environmental conditions, the Multi-Stage Exponential Markov (MUSTEM) model was developed [18–20]. The estimation method for the Markov model was improved using the Bayesian approach, which replaced the traditional Maximum Likelihood Estimator (MLE) [21]. This approach employs the Markov Chain Monte Carlo (MCMC) algorithm, a non-parametric approach, including methods such as Gibbs sampling or Metropolis-Hastings (M-H). This adjustment has been pivotal in addressing persistent challenges in deterioration modeling, including limited sample sizes, issues with MLE overflow, and the occurrence of local maxima with increasing dimensions. By utilizing MCMC, the Bayesian approach offers enhanced flexibility and robustness, enabling more accurate and reliable predictions in pavement management and infrastructure planning.

Pavement deterioration is a complex process influenced by various factors. To accurately model this phenomenon, it is crucial to select critical explanatory parameters that can capture

deterioration uncertainty. Salpisoth et al. conducted an insightful analysis examining various factors that influence the deterioration of pavement roughness for a national road in Cambodia [22]. Their study employed multiple deterioration prediction models, including a Markov hazard model that integrated traffic loads and maximum deflection obtained from FWD surveys to forecast changes in IRI. The investigation revealed that while the pavement' s structural condition, as represented by deflection, is crucial for withstanding traffic loading, its impact on the deterioration process was relatively minor. Additionally, the prolonged life expectancy projected by the models was attributed to the limitations stemming from insufficient sample size, highlighting the need for comprehensive data collection for more accurate predictions. Furthermore, the study did not establish deflection thresholds for developing a structural evaluation.

Moreover, many other developing countries face similar challenges due to limited technical capacity for hindering the development of accurate mathematical models for estimating pavement deterioration processes [23, 24]. This highlights the need to determine structural thresholds for cost-effective pavement assessment, particularly in contexts where data and technical expertise are scarce.

The primary objective of this paper is to define and benchmark structural indices derived from FWD data, establishing standardized criteria for flexible pavement structural evaluation based on a stochastic deterioration prediction model. The FWD-derived structural indices, such as maximum deflection (D_0), effective structural number (SN_{eff}), subgrade resilient modulus (M_R), and deflection bowl parameters, including the base layer index (BLI), middle layer index (MLI), and lower layer index (LLI), are incorporated into surface roughness deterioration processes. These processes are modeled using a Markov hazard model (MHM) with a Bayesian estimator, employing the M-H algorithm. The transition probability of reaching the worst condition state, also referred to as failure probability, corresponding to various levels of structural indices, is used to determine structural thresholds for both AC and DBST pavements in Cambodia. Furthermore, this study also aims to address a gap in previous research by considering the influence of pavement layer structures through these indices, enabling more comprehensive predictions. By classifying the structural condition, the road agencies can identify when and where maintenance is most needed before severe damage occurs.

4.2 Method

The Markov hazard model, developed by Tsuda et al., offers greater flexibility for modeling time-dependent transitions while addressing inherent unobserved variability [25]. This model focuses particularly on the formulation of the MTP matrix, which highlights various deterioration patterns of infrastructure conditions. The MTP matrix concept is implemented through a MUSTEM hazard function, which aligns with the use of the MLE.

However, the MLE estimation method has been increasingly replaced by the Bayesian estimation method, as the latter offers enhanced flexibility and robustness, facilitating more accurate and reliable predictions [26]. Bayesian inference for parameter estimation also effectively addresses the challenge of insufficient monitoring data, a common issue faced by road agencies. Bayesian estimation relies on deriving the posterior distribution based on the likelihood function, given inspection data and an assumed prior distribution. However, there is the complexity of analytically deriving the posterior distribution when the likelihood function involves multiple integration forms [21]. To overcome these difficulties, the MCMC method is applied. The M-H algorithm, an MCMC method, allows for parameter estimation by generating a sequence of samples from the target posterior distribution [18].

The Markov hazard model, which utilizes the principles of Markov chains, represents pavement performance (e.g., IRI) with continuous values through discrete condition states, denoted as i (where $i = 1, \ldots, J$). In this context, the condition state $i = 1$ corresponds to newly constructed or best-condition pavement, while $i = J$ represents the worst-condition pavement, requiring intervention. The model considers deterioration with no maintenance or repair activities occurring between the first and second inspections. Accordingly, pavement sections that show an improvement in condition, where the IRI value at the second is lower than at the first, are excluded from the analysis. At a specific calendar time, denoted as τ_i, the condition state transitions from i to $i+1$ (See Figure 4.1). Figure 4.2 illustrates the possible deterioration paths of pavement condition through the Markov chain concept. Here, τ_A represents the calendar time of the first inspection, and τ_B represents the calendar time of the second inspection.

The deterioration process, as illustrated in Figure 4.3, assumes that information about the condition state i at the beginning of the calendar time τ_{i-1} is not observed during periodic inspections, except during two inspections at times τ_A and τ_B. The probability of a condition state changing from one state to another can be expressed using the MTP matrix between two inspection points, τ_A and τ_B, where the interval is defined as $Z = \tau_B - \tau_A$.

For the model to be valid, the transition probabilities must be non-negative, and the sum of probabilities for transitions from state i to all other states j must equal one. By assuming pavement' s health at the first and second inspection as $h(\tau_A)$ and $h(\tau_B)$, respectively, the deterioration process without maintenance intervention can be formulated as follows:

$$\text{Prob}[h(\tau_B) = j \mid h(\tau_A) = i] = \pi_{ij} \tag{4.1}$$

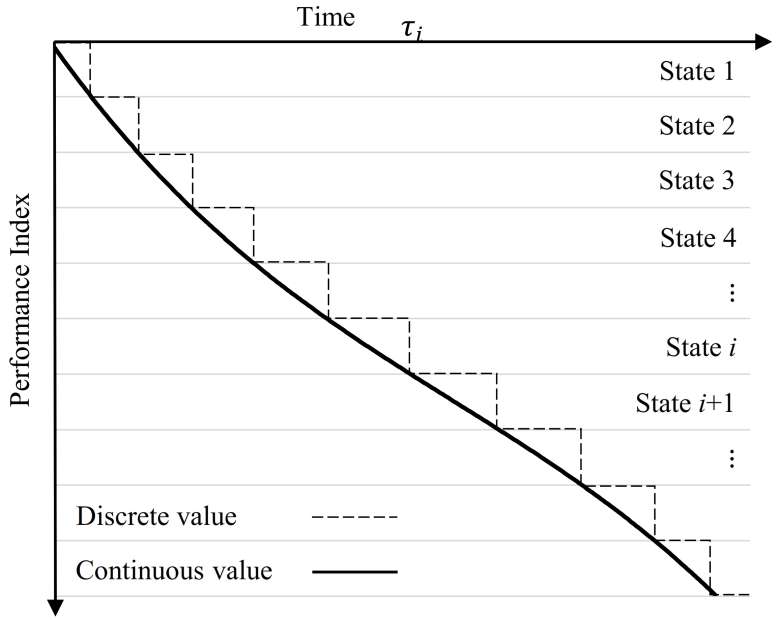


Figure 4.1: Pavement performance.

$$\Pi = \begin{bmatrix} \pi_{11} & \cdots & \pi_{1J} \\ \vdots & \ddots & \vdots \\ 0 & \cdots & \pi_{JJ} \end{bmatrix} \tag{4.2}$$

Where the property of the Markov transition probability incorporates the following condition:

$$\begin{cases} \pi_{ij} \geq 0, \\ \pi_{ij} = 0, & \text{when } i > j, \\ \sum_{j=1}^{J} \pi_{ij} = 1. \end{cases} \tag{4.3}$$

The duration for which the pavement remains in the condition state i before transitioning, denoted as $\zeta_i = \tau_i - \tau_{i-1} = y_c$, is referred to as the life expectancy of a condition state i. This life expectancy is a stochastic variable characterized by a probability density function $f_i(\zeta_i)$. Consequently, the cumulative distribution function $F_i(\zeta_i)$ and the survival function $\tilde{F}_i(\zeta_i)$ are defined as follows:

$$F_i(y_i) = \int_0^{y_i} f_i(\zeta_i)\, d\zeta_i \tag{4.4}$$

$$\tilde{F}_i(\zeta_i) = \Pr[\zeta_i \geq y_i] = 1 - F_i(y_i) \tag{4.5}$$

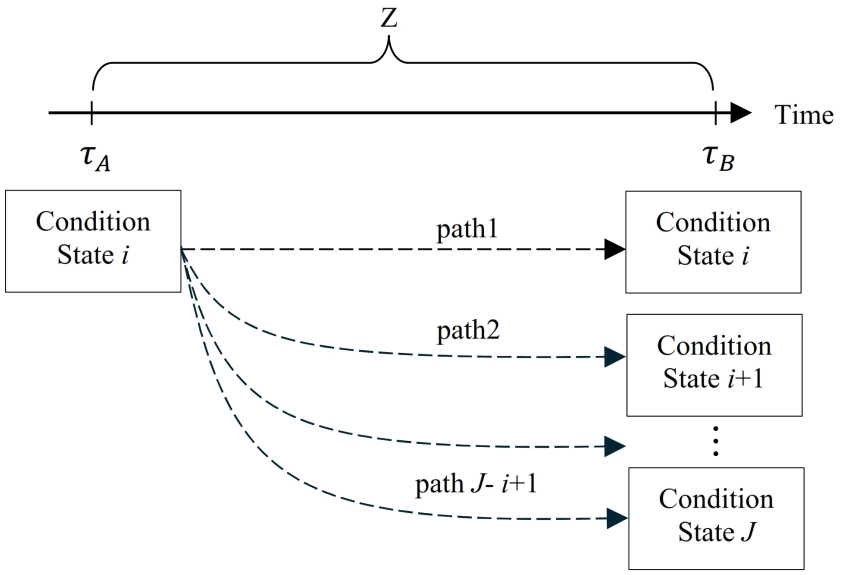


Figure 4.2: Deterioration paths between 1st and 2nd inspections.

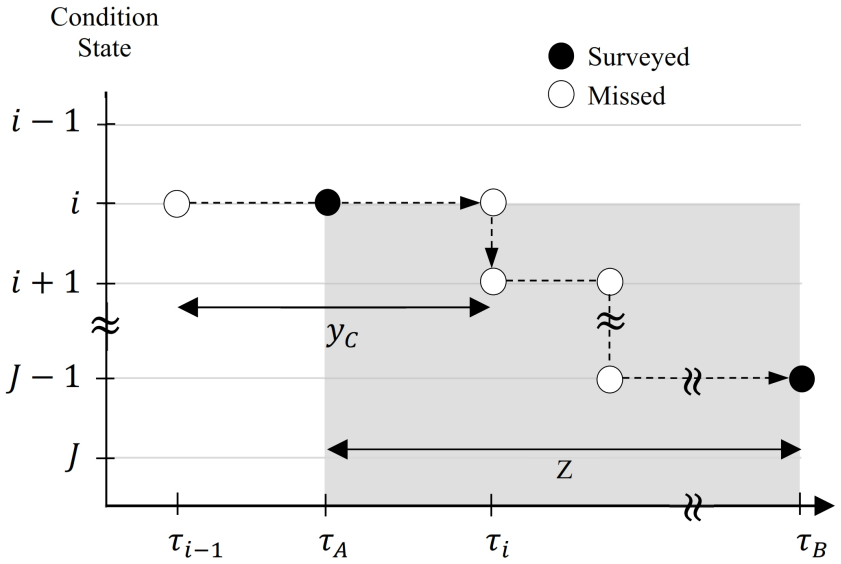


Figure 4.3: Model of deterioration process.

To illustrate the deterioration process, the hazard function $\lambda_i(y_i)$ is employed and can be defined as follows:

$$\lambda_i(y_i) = \frac{f_i(y_i)}{\tilde{F}_i(y_i)} = \frac{\dfrac{dF_i(y_i)}{dy_i}}{\tilde{F}_i(y_i)} = -\frac{\dfrac{d\,\tilde{F}_i(y_i)}{dy_i}}{\tilde{F}_i(y_i)} \tag{4.6}$$

Assuming $\lambda_i(y_i) = \theta_i$, integrating both sides of the above equation yields:

$$\int_0^{y_i} \theta_i \, dy_i = -\int_0^{y_i} \frac{\dfrac{d}{dy_i}\tilde{F}_i(y_i)}{\tilde{F}_i(y_i)} \, dy_i$$

$$\theta_i y_i = -\ln\left(\tilde{F}_i(y_i)\right)$$
$$\tilde{F}_i(y_i) = e^{-\theta_i y_i} \tag{4.7}$$

As depicted in Figure 4.2, paths of condition state transitions such as π_{ii}, π_{ii+1}, π_{ij}, and π_{iJ} can exist. Thus, the transition matrix can be described as follows:

$$\pi_{ii} = e^{-\theta_i Z} \tag{4.8}$$

$$\pi_{i(i+1)} = \frac{\theta_i}{\theta_i - \theta_{i+1}}\left(-e^{-\theta_i Z} + e^{-\theta_{i+1} Z}\right) \tag{4.9}$$

$$\pi_{ij} = \sum_{k=i}^{j}\left[\left(\prod_{m=i}^{k-1}\frac{\theta_m}{\theta_m - \theta_k}\right)\left(\prod_{m=k}^{j-1}\frac{\theta_m}{\theta_{m+1} - \theta_k}\right)e^{-\theta_k Z}\right] \tag{4.10}$$

$$\text{Where, } \begin{cases} \prod_{m=i}^{k-1}\frac{\theta_m}{\theta_m - \theta_k} = 1, & \text{for } k = i, \\ \prod_{m=k}^{j-1}\frac{\theta_m}{\theta_{m+1} - \theta_k} = 1, & \text{for } k = j. \end{cases}$$

$$\pi_{iJ} = 1 - \sum_{j=i}^{J-1}\pi_{ij} \tag{4.11}$$

However, the MTP matrix, formulated as a function of θ_i $(i = 1, \ldots, J-1)$ using Equation 4.8–Equation 4.11, does not incorporate explanatory variables. These variables are crucial for explaining uncertainty in the deterioration process. Therefore, it is essential to consider independent explanatory variables x^k when calculating θ_i. By doing so, the deterioration characteristics can be better understood by accounting for the contribution of these influencing factors. The unknown parameters are estimated as $\boldsymbol{\beta}_i = (\beta_{i,0}, \beta_{i,1}, \ldots, \beta_{i,M})$, where $m = 1, \ldots, M$ represents the number of explanatory variables and $k = 1, \ldots, K$ represents individual road sections from the inspection data. The hazard rate of overall road infrastructure and a specific road section can be calculated using Equation 4.12 and Equation 4.13, respectively.

$$\theta_i = f(\bar{x}^k; \boldsymbol{\beta}_i) = \exp\left(\beta_{i,0} + \beta_{i,1}\bar{x}_1^k + \cdots + \beta_{i,M}\bar{x}_M^k\right) \tag{4.12}$$

$$\theta_i^k = f(x^k; \boldsymbol{\beta}_i) = \exp\left(\beta_{i,0} + \beta_{i,1}x_1^k + \cdots + \beta_{i,M}x_M^k\right) \tag{4.13}$$

The bar "$^-$" represents the average values. The unknown parameters β_i can be estimated using the Bayesian method. Once the hazard rate is determined, the expected life expectancy of each condition state i can be obtained as the inverse of the hazard rate. The benchmark life expectancy from i to j results from the summation of the life expectancies across the condition state.

$$\mathrm{LE}_i = \int_0^\infty \tilde{F}_i(y_i)\, dy_i = \int_0^\infty e^{-\theta_i y_i}\, dy_i = \frac{1}{\theta_i} \tag{4.14}$$

$$\mathrm{LE}_{iJ} = \sum_{i=1}^{J-1} \mathrm{LE}_i \tag{4.15}$$

For life expectancy of each condition state for a specific road section, the θ_i in Equation 4.14 can be replaced with θ_i^k, and the life expectancy from i to j can be determined using the same Equation 4.15. Furthermore, the failure probability, or the probability of reaching absorbing state for a road section over a certain time, can be determined using Equation 4.8–Equation 4.11 with θ_i^k.

This study employs Bayesian inference for parameter estimation which integrates prior knowledge, such as the expertise of professional engineers, with limited field data. It allows for continual updating of estimation results as additional data accumulates.

4.2.1 Bayes' Rule for Markov hazard model

This section demonstrates the application of Bayesian principles to parameter estimation in the Markov hazard model. The field survey data, denoted as $\bar{\xi} = (\bar{\delta}_{ij}^k, \bar{z}^k, \bar{x}^k)$, includes a dummy variable $\bar{\delta}_{ij}^k$, which takes the value 1 if $h(\tau_A^k) = i$ and $h(\tau_B^k) = j$, and 0 otherwise.

In Bayesian inference, the posterior distribution reflects the updated belief about a parameter after incorporating new data. It is computed by multiplying the prior distribution by the likelihood function, divided by a normalizing constant to ensure the posterior distribution aligns with the form of the prior.

In this study, the prior probability density function is assumed to follow a multidimensional normal distribution, expressed as $\boldsymbol{\beta}_i \sim \mathcal{N}_M(\boldsymbol{\mu}_i, \boldsymbol{\Sigma}_i)$, where $\boldsymbol{\mu}_i$ represents the prior expectation vector of $\mathcal{N}_M(\boldsymbol{\mu}_i, \boldsymbol{\Sigma}_i)$, and $\boldsymbol{\Sigma}_i$ is the prior variance-covariance matrix. Thus, the posterior distribution can be expressed as follows:

$$\pi(\boldsymbol{\beta} \mid \bar{\xi}) = \frac{L(\boldsymbol{\beta} \mid \bar{\xi})\, \pi(\boldsymbol{\beta})}{\int L(\boldsymbol{\beta} \mid \bar{\xi})\, \pi(\boldsymbol{\beta})\, d\boldsymbol{\beta}} \tag{4.16}$$

$$\pi(\boldsymbol{\beta} \mid \bar{\boldsymbol{\xi}}) \propto \prod_{i=1}^{J-1} \prod_{j=i}^{J} \prod_{k=1}^{K} \left\{ \prod_{l=1}^{j-1} \theta_l^k \sum_{h=i}^{j} \left[\prod_{l=i}^{h-1} \frac{1}{(\theta_l^k - \theta_h^k)} \prod_{l=h}^{j-1} \frac{1}{(\theta_{l+1}^k - \theta_h^k)} e^{-\theta_h^k \bar{z}^k} \right] \right\}^{\delta_{ij}^k} \cdot \prod_{i=1}^{J-1} \exp\left[-\tfrac{1}{2} (\boldsymbol{\beta}_i - \boldsymbol{\mu}_i)' \boldsymbol{\Sigma}_i^{-1} (\boldsymbol{\beta}_i - \boldsymbol{\mu}_i) \right] \tag{4.17}$$

This study employs the MCMC method, specifically the M-H algorithm, to estimate unknown parameters iteratively.

4.2.2 MCMC by using M-H algorithm

The H-M algorithm is employed when the target distribution is too complex to solve mathematically [27]. The M-H algorithm is particularly advantageous for non-symmetric proposal distributions, as it efficiently explores parameter space by adjusting acceptance probabilities.

The steps of H-M algorithm are outlined as follows:

1. Define an initial value for the parameter vector, $\boldsymbol{\beta}(0)$.

2. Draw a candidate value

$$\tilde{\boldsymbol{\beta}}(n) = \boldsymbol{\beta}(n-1) + \boldsymbol{\varepsilon}(n) \sim \mathcal{N}(0, \sigma^2),$$

   where $\boldsymbol{\varepsilon}(n)$ is a normally distributed random vector that determines the step size in the random walk.

3. Calculate the proposal density using $\tilde{\boldsymbol{\beta}}(n)$ as the candidate parameter, $\pi(\tilde{\boldsymbol{\beta}}(n))$, and compare it with $\pi(\boldsymbol{\beta}(n-1))$ under the following conditions:

$$\boldsymbol{\beta}(n) = \begin{cases} \tilde{\boldsymbol{\beta}}(n), & \text{if } \pi(\tilde{\boldsymbol{\beta}}(n)) > \pi(\boldsymbol{\beta}(n-1)), \\ \tilde{\boldsymbol{\beta}}(n), & \text{if } R \leq r, \\ \boldsymbol{\beta}(n-1), & \text{otherwise.} \end{cases} \tag{4.18}$$

   where

$$r = \frac{\pi(\tilde{\boldsymbol{\beta}}(n))}{\pi(\boldsymbol{\beta}(n-1))}, \qquad R \sim \mathcal{U}(0,1).$$

4. Iterate steps 2 and 3 until the sequence $\boldsymbol{\beta}(n)$ achieves stationarity.

5. Discard burn-in samples and compute the average of the remaining sampled parameters $(\underline{n+1}, \ldots, \overline{n})$.

To confirm the attainment of a stationary distribution in the MCMC process, Geweke's test is adopted [28]. This test examines the equality of means between initial and final segments of a single Markov chain; equality suggests stationarity. A modified z-test is utilized to verify this equality, providing a statistical result in the form of Geweke's z-score, Z_{β_i}.

4.3 Empirical Study

The performance of Cambodian 1-digit and 2-digit national roads through surface unevenness was evaluated using the IRI. The IRI, a metric that quantifies accumulated vertical deviations in a road's longitudinal profile, was measured using a road distress survey vehicle equipped with laser profilometers.

In this empirical study, IRI data were collected from road sections along four 1-digit National Roads (AC), highlighted in bold red, and nine 2-digit National Roads (DBST), highlighted in bold blue shown in Figure 4.4. The 1-digit national roads represent primary highways with higher design classifications and thicker pavement layers, intended to accommodate heavier traffic volumes. In contrast, 2-digit National Roads are secondary routes that branch off from the 1-digit roads and are designed to handle lighter traffic. The dataset comprised 2,757 pairs of IRI inspections for AC pavements and 2,915 pairs for DBST pavements. The data were gathered from 100-meter segments, with some sections covering the period from 2021-2022 and others from 2022-2023. The dataset used for model calibration included the following variables:

- IRI measurements from the first inspection, denoted as $h(\tau_A)$,
- IRI measurements from the second inspection, denoted as $h(\tau_B)$,
- The time interval between inspections, calculated as $z = \tau_B - \tau_A$,
- The explanatory variables x^k, representing the influences on the deterioration process.

These influences are represented by pavement bearing capacities in terms of structural indices derived from FWD. In addition to the deflections measured directly by the FWD, the structural indices are indicated by various metrics corresponding to pavement design or evaluation guidelines. According to AASHTO 1993 standards, indicators such as the effective structural number (SN_{eff}) and resilient modulus of subgrade (M_R) reflect pavement bearing capacities [29, 30]. Furthermore, parameters from the deflection bowl approach (DBPs), including base layer index (BLI), middle layer index (MLI), and lower layer index (LLI), are utilized to evaluate the structural condition of the existing pavements [12].

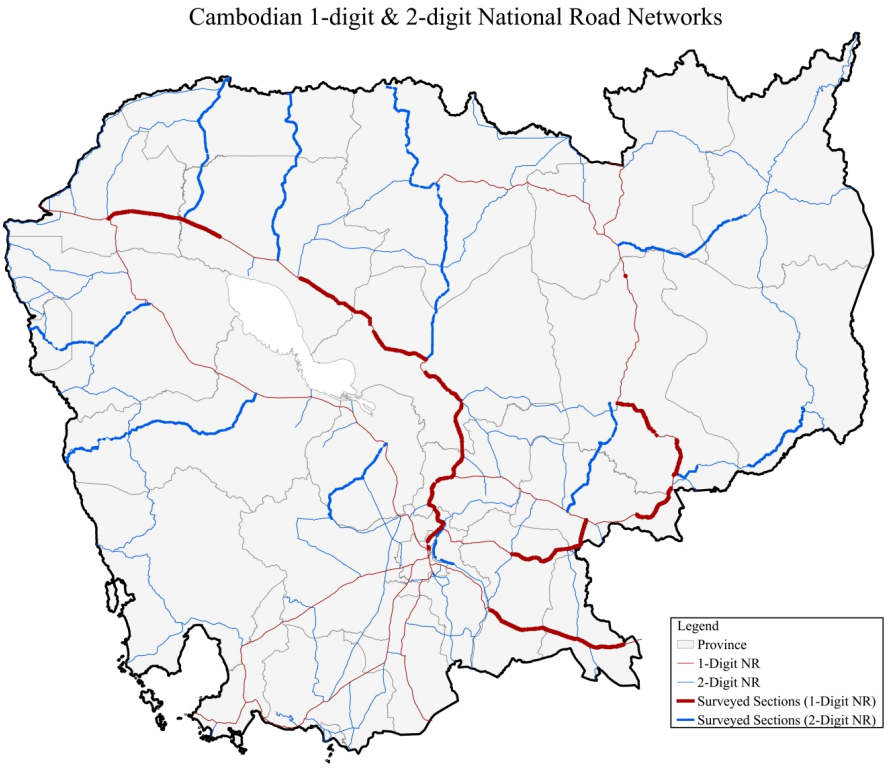


Figure 4.4: 1-digit and 2-digit roads surveyed for empirical study.

4.3.1 Back-calculated structural indices

Flexible pavements with an asphalt binder surface are typically sensitive to temperature variations. Temperature gradients caused by diurnal cycles lead to changes in the stiffness of the asphalt layer [31]. Consequently, the measured deflection at a specific location varies depending on the time of day the measurement is taken. To ensure consistency in evaluating pavement bearing capacity, temperature corrections must be applied to deflection measurements [32].

The FWD devices used in this study were equipped with thermometers to record road surface temperatures at the same locations where deflection measurements were taken. Each FWD device included nine deflection sensors positioned at various distances: 0, 20, 30, 45, 60, 90, 120, 150, and 180 cm from the load plate. The applied load was 50 kN, and the plate diameter is 300 mm. The road surface temperatures recorded during the FWD survey ranged from 21°C to 65°C.

In this study, a temperature correction of 20°C, consistent with the AASHTO pavement design guide, was applied before calculating structural indices. For simplicity and practicality, the empirical correction model proposed by Březina et al. [32] was adopted, as it aligns with the same impulse load in this study. The uncertainty associated with such temperature correction is acknowledged, but comprehensive validation is beyond the scope of this study. Notably, temperature corrections were applied only to AC pavements. For DBST pavements, which

consist of thin bituminous layers (seal coats) over granular bases, temperature sensitivity is significantly lower compared to AC pavements. This is because the FWD response of DBST pavement is primarily governed by the underlying granular layers and subgrade.

According to the AASHTO 1993, SN_{eff} represents the bearing capacity of pavement design layers, accounting for the contributions of the surface, base, and subbase layers, while M_R describes the bearing capacity of the subgrade [30]. Alternatively, the structural condition of the pavement can also be evaluated using deflection bowl parameters [12]. Four key deflection bowl parameters are: (1) maximum deflection (D_0), (2) base layer index (BLI), (3) middle layer index (MLI), and (4) lower layer index (LLI). D_0 represents the overall bearing capacity of pavement. The BLI, sometimes referred to as the surface curvature index (SCI), indicates the bearing capacity of the combined surface and base layers. The MLI, sometimes referred to as the base curvature index (BCI), reflects the bearing capacity of the subbase layer. The LLI, sometimes referred to as the base damage index (BDI), represents the bearing capacity of the combined selected and subgrade layers.

Besides D_0, which is directly measured from FWD, the other structural indices can be calculated as follows:

$$M_R = \frac{0.24P}{D_r\, r} \tag{4.19}$$

Where M_R = resilient modulus of subgrade (psi) which will later be converted to MPa for use in Cambodia, P = applied load (lb), and r = distance from load center (in), and D_r = deflection at a distance r from the load center.

In our study, the deflection measured at 60 cm from the load center is used to represent subgrade response. Next, the effective pavement modulus of the layers above the subgrade (E_p) is determined by solving Equation 4.20 iteratively using an estimation method. This calculated modulus is then used in Equation 4.21 to determine the effective structural number (SN_{eff}).

$$D_0 = 1.5\, p\, a \left[\frac{1}{M_R \sqrt{1 + \left(\frac{\frac{H}{a}}{\sqrt[3]{\frac{E_p}{M_R}}} \right)^2}} + \frac{1 - \frac{1}{\sqrt{1 + \left(\frac{H}{a} \right)^2}}}{E_p} \right] \tag{4.20}$$

Where D_0 = maximum deflection at the load plate (in), p = contact pressure (psi), a =

radius of load plate (in), H = total pavement layer thickness above the subgrade (in), E_p = effective pavement modulus of all layers above the subgrade (psi), and M_R = resilient modulus of subgrade (psi).

$$SN_{\text{eff}} = 0.0045\, H \sqrt[3]{E_p} \tag{4.21}$$

Where SN_{eff} = effective structural number, H = total pavement layer thickness above the subgrade (in), and E_p = effective pavement modulus of all layers above the subgrade.

The deflection bowl parameters can be further defined as:

$$BLI = D_0 - D_{300} \tag{4.22}$$

$$MLI = D_{300} - D_{600} \tag{4.23}$$

$$LLI = D_{600} - D_{900} \tag{4.24}$$

Where BLI = base layer index (µm), MLI = middle layer index (µm), LLI = lower layer index (µm), and D_0, D_{300}, D_{600}, D_{900} = the deflections measured at 0, 30, 60, 90 cm from the load center (µm), respectively.

4.3.2 Data processing

The application of Markov transition probabilities requires the use of discrete condition states. This study converted continuous IRI values into condition rating criteria ranging from the original state to a terminal condition that requires rehabilitation or reconstruction. The IRI values surveyed in the field are classified from 1 to 5, as shown in Table 4.2.

To analyze the deterioration behavior of AC and DBST pavements, the Markov hazard model was applied to each pavement type independently, without incorporating any explanatory variables. This approach allows for the determination of the benchmark life expectancy of each pavement type and the illustration of basic transition probabilities over time. Subsequently, the structural indices mentioned earlier were considered in the model individually to assess their contributions to deterioration. The estimated parameters from each case were used to calculate the hazard rates for each road section. Based on varying levels of structural indices, the probability of a pavement transitioning to the worst condition within a specified timeframe

Table 4.2: Pavement performance rating.

Condition State	**IRI (m/km)**	**Rating Remark**
1	≤ 2	Excellent
2	$2-3$	Good
3	$3-4$	Fair
4	$4-5$	Poor
5	>5	Very Poor

can be computed. Structural index values corresponding to a 50% probability of reaching this state are then considered as critical thresholds.

4.4 Results

4.4.1 Estimation results based on BMH model

This section presents the results of the model' s estimated parameters. The MCMC sampling process involved a total of 40,000 iterations per parameter. The initial 20,000 iterations were treated as burn-in samples to ensure convergence, and the subsequent 20,000 iterations were used for parameter estimation. The final model parameters were calculated as the mean of these post-burn-in samples. Geweke' s Z-score, used to assess the convergence of β_i, was close to 0, indicating optimal convergence within the tolerance interval [-1.96,1.96]. The life expectancy of each condition state was calculated based on the hazard rate, and the total life expectancy was obtained by summing the life expectancies across all states.

Table 4.3 presents the estimated parameters for the Markov deterioration processes without considering structural conditions. The result indicates that AC pavement deteriorates at a slower rate compared to DBST pavements, as evidenced by the hazard rates and life expectancies for each condition state. The unknown parameters $_i$, along with their 90% confidence intervals, correspond to the constant term. The absolute values of Geweke Z-score, all below 1.96, confirm the convergence of the parameter estimates at a 5% significance level, consistent with Geweke's criteria [28]. The benchmark hazard rate (θ_i) was computed using Equation 4.12 based on the posterior mean values of the estimated parameters. The life expectancy of each state (LE_i) was calculated as the reciprocal of the corresponding hazard rate. Consequently, the total life expectancies, or benchmark life expectancies, for AC and DBST pavements are found to be 16.6 and 7.4 years, respectively. The results are in close agreement with the typical design life of AC pavements, which is 15 years according to the MPWT' s standard design.

Table 4.3: Hazard Model Parameters for AC and DBST Pavements

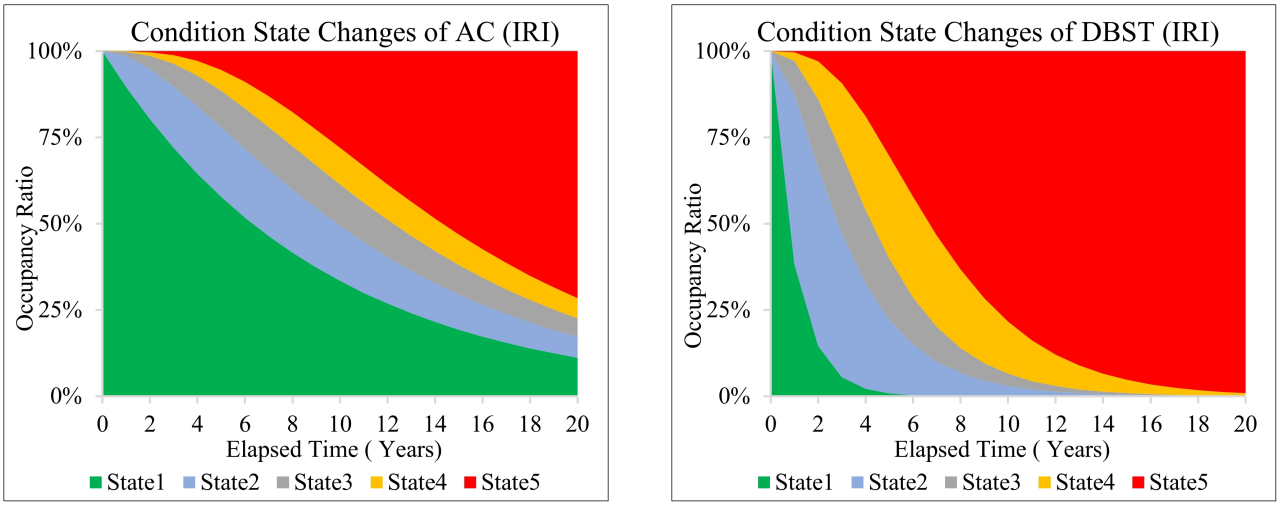
IRI Rating	AC pavement				DBST pavement			
	Constant	Geweke Z-score	Hazard Rate (θ_i)	LE_i	**Constant**	Geweke Z-score	Hazard Rate (θ_i)	LE_i
$1 \rightarrow 2$	-2.21 (-2.34, -2.08)	0.26	0.110	9.11	-0.04 (-0.23, 0.16)	0.60	0.964	1.04
$2 \rightarrow 3$	-1.18 (-1.32, -1.04)	-0.82	0.307	3.26	-0.90 (-1.03, -0.78)	-0.92	0.405	2.47
$3 \rightarrow 4$	-0.80 (-1.01, -0.60)	0.40	0.450	2.22	-0.33 (-0.40, -0.25)	-0.70	0.721	1.39
$4 \rightarrow 5$	-0.69 (-1.00, -0.40)	-0.56	0.501	1.99	-0.92 (-1.03, -0.81)	-1.19	0.399	2.50

Note: Lower and upper 90% confidence intervals are in parentheses.

This standard is largely based on the Overseas Road Note (ORN) 31, a widely adopted guideline for the structural design of bitumen-surfaced roads in tropical regions. In practice, DBST pavements commonly exhibit service lives of 7 to 8 years. Therefore, the use of a 15-year benchmark for AC pavements and a 7.5-year benchmark for DBST pavements is both realistic and consistent with Cambodian design standards. These values are thus selected as reference years for calculating the probability of reaching a failure condition and for defining structural threshold levels in the next section.

The state transition properties are derived from the hazard rates, which are the deterioration patterns across the road sections, as illustrated in Figure 4.2 in section 2. The Markov model adheres to the time adjustment condition, expressed as $\Pi(nZ) = \{\Pi(Z)\}^n$ [20]. By applying the estimated hazard rates within the MUSTEM hazard function using Equation 4.8–Equation 4.11, the progress of condition states over time for newly constructed pavements can be visualized, as demonstrated in Figure 4.5. This figure shows how the proportion of road networks for both AC and DBST pavements shifts across different condition states over time in the absence of any maintenance intervention.

In this study, "failure" is defined as the pavement reaching condition state 5, which indicates the worst level of surface roughness based on IRI. This threshold reflects a functional performance failure requiring maintenance interventions. From Figure 4.5, it can be observed that DBST pavements transition into state 5 at a much faster rate compared to the AC pavements. Accordingly, the proportion of pavement sections that reach state 5 at year 15 for AC pavements and at 7.5 years for DBST pavements is used to define the failure probability.



(a) AC pavement (b) DBST pavement

Figure 4.5: Condition state changes over time.

4.4.2 Estimation results based on the BMH model incorporating structural indices

In case 1, maximum deflection (D_0) serves as a structural parameter that incorporates pavement surface deterioration, which leads to varying degradation patterns. Table 4.4 presents the estimated parameters for the condition transition of AC and DBST pavements. The table includes the constant terms ($\beta_{i,0}$) and D_0 coefficient ($\beta_{i,1}$) for each transition state. Geweke' s Z-scores for all parameters are included in parentheses. These Z-scores fall within the range of $[-1.96, +1.96]$, indicating the convergence of the parameter estimates at a 5% significance level. The hazard rate (θ_i^k) for specific road section is calculated based on the corresponding individual D_0 values for that road section using Equation 4.13. Then, the probability of each road section transitioning to failure at the design life can be estimated using $\Pi(nZ) = \{\Pi(Z)\}^n$ where the Z is represented by the design life.

Figure 4.6 indicates that pavements with high values of D_0, which signify weak bearing capacities, tend to have a higher probability of failure at design life (at a 15-year lifespan for AC pavement and 7.5-year lifespan for DBST). The critical thresholds of D_0 for AC and DBST pavement are assumed to correspond to a 50% failure probability and are found to be 380 μm and 620 μm, respectively. The benchmark thresholds are then determined on three scales: Sound, Warning, and Severe conditions, corresponding to 0-50%, 50-75%, and 75-100% failure probability, respectively.

Finally, $D_0 < 380$ μm and $D_0 < 640$ μm are marked as Sound conditions for AC and DBST pavement, respectively. The ranges 380 μm $< D_0 <$ 590 μm and 640 μm $< D_0 <$ 880 μm are considered as Warning conditions for AC and DBST pavement, respectively, requiring attention. Meanwhile, $D_0 > 590$ μm and $D_0 > 880$ μm are determined as Severe conditions for AC and

Table 4.4: Hazard Model Parameters via D_0

IRI Rating	AC Pavement		DBST Pavement	
	Constant ($\beta_{i,0}$)	D_0 ($\beta_{i,1}$)	Constant ($\beta_{i,0}$)	D_0 ($\beta_{i,1}$)
$1 \rightarrow 2$	-2.62 (0.27)	1.80 (-0.11)	-1.92 (-1.23)	6.79 (1.15)
$2 \rightarrow 3$	-1.69 (-0.12)	2.06 (0.05)	-0.98 (0.54)	0.24 (-0.55)
$3 \rightarrow 4$	-1.75 (-0.26)	3.03 (-0.25)	-1.38 (0.51)	4.03 (-0.27)
$4 \rightarrow 5$	-1.45 (1.77)	1.87 (-1.66)	-1.53 (0.88)	1.97 (-1.14)

Note: Geweke's z-score in parentheses.

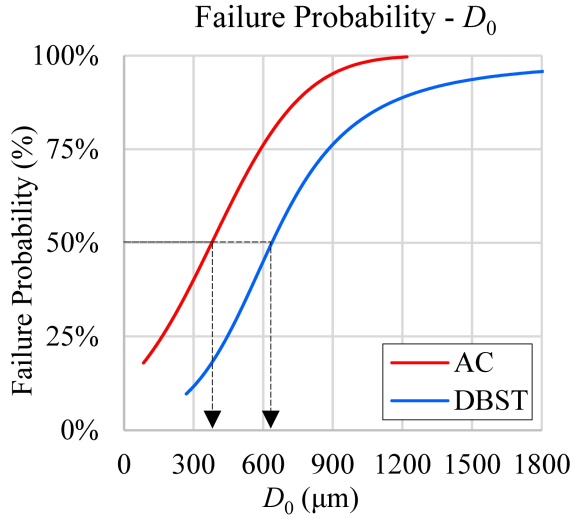


Figure 4.6: Failure probability due to D_0 within design life.

DBST pavements, respectively, necessitating immediate intervention.

Cases 2 through 6 involve repeating the model processing with other structural indices: SN_{eff}, M_R, BLI, MLI, and LLI. Table 4.5 to Table 4.9 present the estimated parameters, along with Geweke's Z-scores for both AC and DBST pavements. From Fig. 7 to Fig. 11, the critical threshold values of other structural indices derived from FWD at a 50% failure probability are presented. The critical threshold for SN_{eff} is 3.9 for AC pavement and 3.0 for DBST pavement. For MR, the critical threshold is 190 MPa for AC pavement and 180 MPa for DBST pavement. In the case of BLI, the critical threshold is 140 μm for AC pavement and 320 μm for DBST pavement. Similarly, the critical threshold for MLI is 105 μm for AC pavement and 150 μm for DBST pavement. Finally, the critical threshold for LLI is 45 μm for AC pavement and 50 μm for DBST pavement.

Table 4.5: Hazard Model Parameters via SN_{eff}

IRI Rating	AC Pavement		DBST Pavement	
	Constant ($\beta_{i,0}$)	SN_{eff} ($\beta_{i,1}$)	Constant ($\beta_{i,0}$)	SN_{eff} ($\beta_{i,1}$)
$1 \rightarrow 2$	-1.44 (0.61)	-1.29 (-0.31)	2.39 (-0.18)	-7.42 (0.26)
$2 \rightarrow 3$	-0.55 (1.67)	-1.13 (-1.71)	-1.09 (1.24)	–
$3 \rightarrow 4$	0.63 (-1.53)	-3.12 (1.37)	0.88 (-0.93)	-3.50 (0.80)
$4 \rightarrow 5$	0.11 (-0.67)	-2.15 (0.76)	-0.19 (-1.73)	-2.29 (1.77)

Note:

- The [–] indicates insignificant variables due to inverted relationship.
- Geweke' s Z-score in parentheses.

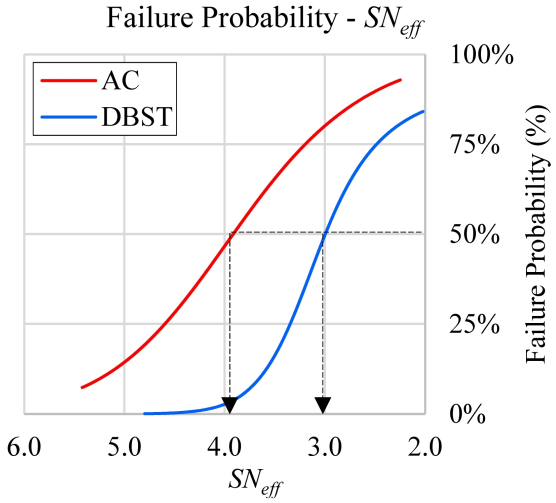


Figure 4.7: Failure probability due to SN_{eff} within design life.

The proposed benchmark thresholds for structural indices of AC and DBST pavements, classified to Sound (0-50% failure probability), Warning (50-75%), and Severe (75-100%), are summarized in Table 4.10 and Table 4.11, respectively. This approach, based on inspection data and deterioration estimation, offers a faster and more straightforward method for structural evaluation, avoiding the need for complex back-calculation algorithms with assumed inputs or extensive laboratory testing to determine layer moduli.

Moreover, this study establishes distinct evaluation criteria for two different types of flexible pavements, recognizing their unique structural characteristics, material compositions, and response behaviors. By accounting for their different deterioration mechanisms, this method

Table 4.6: Hazard Model Parameters via M_R

IRI Rating	AC Pavement		DBST Pavement	
	Constant ($\beta_{i,0}$)	M_R ($\beta_{i,1}$)	Constant ($\beta_{i,0}$)	M_R ($\beta_{i,1}$)
$1 \rightarrow 2$	-1.56	-2.01	0.47	-2.21
	(-1.17)	(1.38)	(0.92)	(-0.66)
$2 \rightarrow 3$	-0.49	-2.43	-0.81	-0.35
	(1.50)	(-1.54)	(1.29)	(-1.19)
$3 \rightarrow 4$	0.08	-3.81	0.31	-2.54
	(-1.39)	(1.30)	(-0.68)	(0.48)
$4 \rightarrow 5$	-0.31	-2.04	-0.52	-1.85
	(-0.06)	(0.41)	(-1.00)	(0.90)

Note: Geweke's z-score in parentheses.

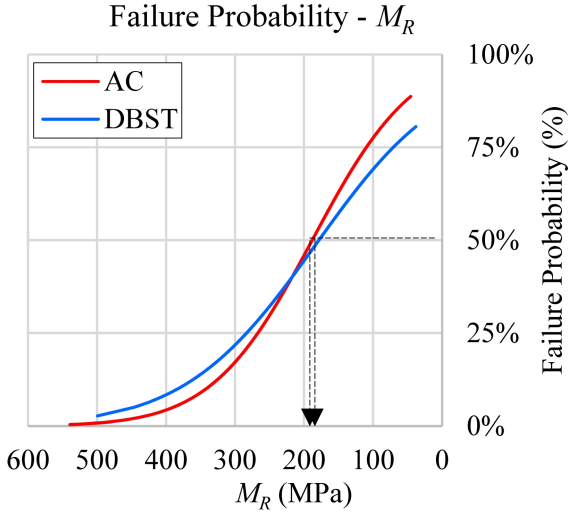


Figure 4.8: Failure probability due to M_R within design life.

enables road agencies to make a more comprehensive and context-sensitive assessment of pavement structural conditions.

4.5 Discussion and limitations

This study presents a stochastic framework that models the progression of surface roughness using inspection data, focusing on IRI as the sole performance indicator. The results demonstrate that structural indices derived from FWD measurements adequately show the effect of pavement subsurface layer's structural conditions on surface deterioration, as evidenced by the estimated Markov model parameters. However, direct comparisons with thresholds from

Table 4.7: Hazard Model Parameters via BLI

IRI Rating	AC Pavement		DBST Pavement	
	Constant ($\beta_{i,0}$)	BLI ($\beta_{i,1}$)	Constant ($\beta_{i,0}$)	BLI ($\beta_{i,1}$)
$1 \rightarrow 2$	-2.49 (0.94)	1.82 (-0.44)	-2.69 (-1.83)	8.28 (1.89)
$2 \rightarrow 3$	-1.51 (1.79)	1.93 (-1.80)	-0.89 (-1.49)	–
$3 \rightarrow 4$	-1.58 (-1.31)	3.75 (1.19)	-1.35 (-0.77)	3.42 (0.66)
$4 \rightarrow 5$	-1.39 (-0.22)	2.58 (0.20)	-1.48 (-0.79)	1.75 (0.72)

Note:

- The [–] indicates insignificant variables due to inverted relationship.
- Geweke' s Z-score in parentheses.

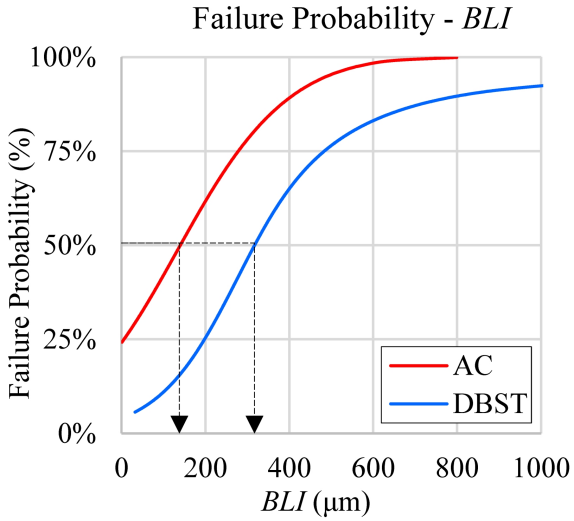


Figure 4.9: Failure probability due to BLI within design life.

previous studies were not feasible due to differences in impulse loads during FWD data collection (50 kN in this study versus 40 kN in prior research). Because deflection magnitudes and the resulting structural indices are dependent on the applied load, establishing a consistent comparison would require adjustment across different loading configurations, which was beyond the scope of this study.

A key outcome is the pronounced impact of pavement subsurface condition using structural indices related to upper pavement layers, such as SN_{eff}, BLI, and MLI, on pavement surface roughness progression. These indices exhibited a more significant association with surface dete-

Table 4.8: Hazard Model Parameters via MLI

IRI Rating	AC Pavement		DBST Pavement	
	Constant ($\beta_{i,0}$)	MLI ($\beta_{i,1}$)	Constant ($\beta_{i,0}$)	MLI ($\beta_{i,1}$)
$1 \rightarrow 2$	-2.65 (-0.02)	1.82 (0.40)	-1.78 (-0.43)	6.83 (0.38)
$2 \rightarrow 3$	-1.65 (0.32)	1.86 (-0.28)	-1.05 (-0.24)	0.57 (0.30)
$3 \rightarrow 4$	-1.67 (-1.47)	2.73 (1.00)	-1.37 (1.45)	3.81 (-1.35)
$4 \rightarrow 5$	-1.31 (-0.11)	1.53 (0.29)	-1.49 (0.27)	1.78 (-0.53)

Note: Geweke' s z-score in parentheses.

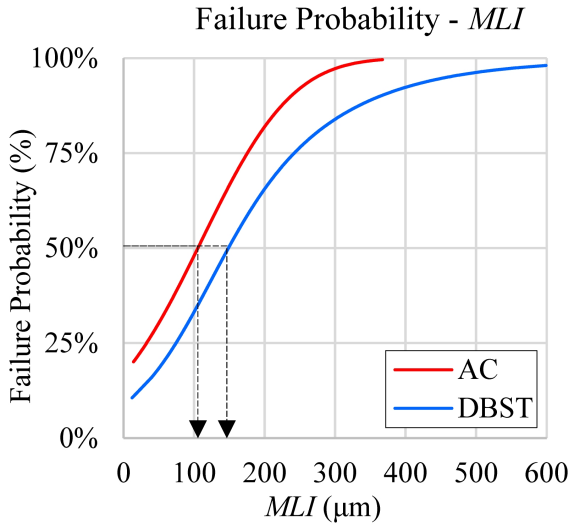


Figure 4.10: Failure probability due to MLI within design life.

rioration compared to subgrade-related indices such as M_R and LLI. This result is consistent with the mechanistic behavior of layered systems: upper layers absorb high stresses from direct traffic loading and tire pressure, leading to accelerated deformation [33]. Conversely, subgrade layers, located deeper in the pavement structure, experience attenuated load impacts, resulting in a less immediate influence on surface deterioration.

The analysis further reveals that the structural indices-failure probability curves for AC pavements generally lie above those for DBST pavements, except for MR and LLI, where the curves partially overlap. This divergence can be attributed to the superior design standards of AC pavements, which typically feature thicker subbase and base layers, as well as stiffer surfacing materials. Notably, AC pavements exhibit prolonged retention in state 1 but accelerate in deterioration at subsequent states. This behavior may stem from aging-induced brittleness

Table 4.9: Hazard Model Parameters via *LLI*

IRI Rating	**AC Pavement**		**DBST Pavement**	
	Constant ($\beta_{i,0}$)	*LLI* ($\beta_{i,1}$)	Constant ($\beta_{i,0}$)	*LLI* ($\beta_{i,1}$)
$1 \rightarrow 2$	-2.61	1.78	-0.96	3.81
	(0.03)	(0.40)	(0.73)	(-0.68)
$2 \rightarrow 3$	-1.69	2.20	-1.16	1.12
	(1.50)	(-1.30)	(0.66)	(-0.91)
$3 \rightarrow 4$	-1.52	2.42	-1.08	2.96
	(-1.36)	(1.14)	(-0.89)	(0.97)
$4 \rightarrow 5$	-1.23	1.47	-1.29	1.23
	(-1.54)	(1.549)	(1.64)	(-1.95)

Note: Geweke's z-score in parentheses.

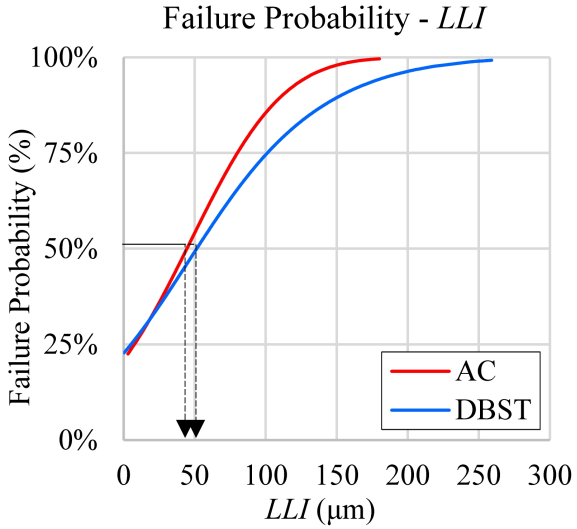


Figure 4.11: Failure probability due to *LLI* within design life.

in asphalt layers, which exacerbates distress mechanisms like cracking and accelerates surface unevenness.

Despite its contributions, this study has several limitations that warrant consideration. First, the reliance on IRI alone overlooks other critical distress types (e.g., rutting, cracking) that may be more directly linked to specific structural deficiencies. Incorporating multiple performance indicators could provide a more comprehensive benchmarking framework.

Second, while the model effectively captures the probabilistic relationship between structural condition and surface deterioration, it does not incorporate the effects of traffic loading, climate variables (e.g., rainfall), or maintenance history. These factors are known to significantly influence the deterioration process and could lead to mismatches between observed func-

Table 4.10: Proposed structural thresholds for AC pavements.

Structural Condition	D_0 (μm)	SN_{eff}	M_R (MPa)	BLI (μm)	MLI (μm)	LLI (μm)
Sound	< 380	> 3.9	> 190	< 140	< 105	< 45
Warning	380 – 590	3.2 – 3.9	110 – 190	140 – 280	105 – 175	45 – 80
Severe	> 590	< 3.2	< 110	> 280	> 175	> 80

Table 4.11: Proposed structural thresholds for DBST pavements.

Structural Condition	D_0 (μm)	SN_{eff}	M_R (MPa)	BLI (μm)	MLI (μm)	LLI (μm)
Sound	< 640	> 3.0	> 180	< 320	< 150	< 50
Warning	640 – 880	2.5 – 3.0	70 – 180	320 – 480	150 – 240	50 – 100
Severe	> 880	< 2.5	< 70	> 480	> 240	> 100

tional and underlying structural states. For instance, a pavement may display a low IRI due to recent maintenance activities while still suffering from deep structural damage, or vice versa. Ignoring these factors limits the generalizability of the model for forecasting under variable environmental and loading conditions.

Third, the deterioration process was modeled using only two inspection points, which may not fully capture characteristics of deterioration over time. While the Markov model accommodates uncertainty, its predictive accuracy can be improved based on the availability and updates of rich time-series data. Incorporating longer time-series IRI inspections, along with records of maintenance interventions, would enhance model calibration and improve transition probability estimation.

4.6 Conclusions

This research establishes benchmarks for structural indices derived from FWD measurements for evaluating flexible pavement condition. While these thresholds may vary across countries due to differences in materials, construction technologies, and environmental conditions, the developed deterioration-based framework provides a robust tool for assessing structural condition for both AC and DBST pavements, particularly within the context of Cambodian roads. Moreover, such a condition assessment tool is cost-effective and enables countries with limited resource; e.g., technical knowledge for mathematical model development to have a decision support tool for better pavement management.

Without requiring detailed information about pavement layer properties, the study analyzed six cases using various structural parameters as inputs to derive deterioration rates and condi-

tion state transition probabilities using the Markov hazard model with a Bayesian estimation approach. The Bayesian procedure enables robust statistical analysis with limited data and simplifies parameter estimation. Key findings include:

- Critical thresholds for maximum deflection (D_0), effective structural number (SN_{eff}), subgrade resilient modulus (M_R), and deflection bowl parameters (BLI, MLI, LLI) were identified for AC and DBST pavements. Pavements exceeding deflection thresholds or falling below SN_{eff} and M_R thresholds exhibit higher failure probability within their design life.
- Structural indices categorize pavements into three levels: Sound, Warning, and Severe. For AC and DBST pavements, thresholds for each index (D_0, SN_{eff}, M_R, BLI, MLI, LLI) align with these categories, providing clear guidance for condition assessments.

The proposed models and thresholds serve as valuable tools for dynamic decision-making at network and project levels, enabling the identification of pavements requiring rehabilitation and facilitating the selection of appropriate intervention strategies. Additionally, these thresholds can be used as benchmarks for quality control during construction and project handover stages.

In practical applications, road agencies may use a hierarchical procedure to evaluate structural condition based on multiple indices. For instance, global indices such as D_0 and SN_{eff} may be used as primary indicators to determine whether minor surface repairs are appropriate. If these indices indicate inadequate structural capacity, more intensive interventions such as overlays may be considered. In cases where localized structural failure is suspected, indices such as BLI, MLI, LLI, and M_R can help identify which pavement layers require targeted excavation and replacement with new materials.

Future research directions should include expanding the framework to incorporate multiple performance indicators and additional influencing factors, such as traffic loading and environmental conditions, to enhance deterioration prediction accuracy. Furthermore, the integration of in-situ field tests such as dynamic cone penetration (DCP) or laboratory analysis of core samples would provide empirical validation for the proposed structural benchmarks, thereby increasing the model' s applicability and reliability.

References

[1] AASHTO. *Pavement Management Guide*. 2nd. Washington, DC: American Association of State Highway and Transportation Officials, 2012.

[2] Salpisoth, H. Simple Evaluation Methods for Road Pavement Management in Developing Country. 2014. URL: http://hdl.handle.net/2433/188562.

[3] Abudinen, D.; Fuentes, L. G.; Carvajal Muñoz, J. S. Travel Quality Assessment of Urban Roads Based on International Roughness Index: Case Study in Colombia. *Transportation Research Record* 2017, **2612**(1), pp. 1–10. DOI: https://doi.org/10.3141/2612-01.

[4] Fuentes, L. et al. Modelling Pavement Serviceability of Urban Roads Using Deterministic and Probabilistic Approaches. *International Journal of Pavement Engineering* 2021, **22**(1), pp. 77–86. DOI: https://doi.org/10298436.2019.1577422.

[5] Rusmanto, U.; Handayani, D. "Structural and Functional Prediction of Pavement Condition (A Case Study on South Arterial Road, Yogyakarta)". *AIP Conference Proceedings*. Vol. 1977. 1. AIP Publishing LLC. 2018, p. 040014. DOI: https://doi.org/10.1063/1.5042984.

[6] Solanki, U.; Gundalia, P. J.; Barasara, M. D. A Review on Structural Evaluation of Flexible Pavements Using Falling Weight Deflectometer. *STM J* 2014, **2**(Jan), pp. 1–10.

[7] Walubita, L. F. et al. *Texas Flexible Pavements and Overlays: Year 1 Report, Test Sections, Data Collection, Analyses, and Data Storage System*. Tech. rep. Texas Transportation Institute, 2012. URL: https://rosap.ntl.bts.gov/view/dot/24645.

[8] Alkasawneh, W. M. "Backcalculation of Pavement Moduli Using Genetic Algorithms". PhD thesis. University of Akron, 2007.

[9] Horak, E.; Emery, S.; Maina, J. "Review of Falling Weight Deflectometer Deflection Benchmark Analysis on Roads and Airfields". *Proceedings of the Conference on Asphalt Pavements in Southern Africa (CAPSA), Sun City, South Africa*. 2015, pp. 16–19.

[10] Terzi, S. et al. Backcalculation of Pavement Layer Thickness Using Data Mining. *Neural Computing and Applications* 2013, **23**(5), pp. 1369–1379. DOI: https://doi.org/10.1007/s00521-012-1083-2.

[11] Walubita, L. F.; Liu, W.; Scullion, T., et al. *Texas Perpetual Pavements: Experience Overview and the Way Forward*. Tech. rep. Texas Transportation Institute, 2010. DOI: https://doi.org/https://rosap.ntl.bts.gov/view/dot/18312.

[12] Horak, E. Benchmarking the Structural Condition of Flexible Pavements with Deflection Bowl Parameters. *Journal of the South African Institution of Civil Engineering* 2008, **50**, pp. 2–9.

[13] Horak, E.; Hefer, A.; Maina, J. Modified Structural Number Determined from Falling Weight Deflectometer Deflection Bowl Parameters and Its Proposed Use in a Benchmark Methodology. *Journal of Traffic and Transportation Engineering* 2015, **3**, pp. 215–226. DOI: https://doi.org/10.17265/2328-2142/2015.04.003.

[14] Mosale Ramanath, A. et al. Benchmarking Falling Weight Deflectometer Deflection Bowl Parameters: Case Study for Indian Conditions and the Applications to Rehabilitation Design. *Journal of Transportation Engineering, Part B: Pavements* 2020, **146**(3), p. 05020003. DOI: https://doi.org/10.1061/JPEODX.0000204.

[15] Congress, I. R. IRC 37: Guidelines for the Design of Flexible Pavements. *July. New Delhi, India* 2012, pp. 1–104.

[16] Fuentes, L. et al. A Probabilistic Approach to Detect Structural Problems in Flexible Pavement Sections at Network Level Assessment. *International Journal of Pavement Engineering* 2022, **23**(6), pp. 1867–1880. DOI: https://doi.org/10.1080/10298436.2020.1828586.

[17] Angelo, A. A.; Sasai, K.; Kaito, K. Assessing Critical Road Sections: A Decision Matrix Approach Considering Safety and Pavement Condition. *Sustainability* 2023, **15**(9), p. 7244. DOI: https://doi.org/10.3390/su15097244.

[18] Han, D.; Kaito, K.; Kobayashi, K. Application of Bayesian Estimation Method with Markov Hazard Model to Improve Deterioration Forecasts for Infrastructure Asset Management. *KSCE Journal of Civil Engineering* 2014, **18**(7), pp. 2107–2119. DOI: https://doi.org/10.1007/s12205-012-0070-6.

[19] Kobayashi, K.; Do, M.; Han, D. Estimation of Markovian Transition Probabilities for Pavement Deterioration Forecasting. *KSCE Journal of Civil Engineering* 2010, **14**(3), pp. 343–351. DOI: https://doi.org/10.1007/s12205-010-0343-x.

[20] Tsuda, Y. et al. Estimating Markovian Transition Probabilities for Bridge Deterioration Forecasting. *Structural Engineering/Earthquake Engineering* 2006, **23**(2), 241s–256s. DOI: https://doi.org/10.2208/jsceseee.23.241s.

[21] Kobayashi, K.; Kaito, K.; Lethanh, N. A Bayesian Estimation Method to Improve Deterioration Prediction for Infrastructure System with Markov Chain Model. *International Journal of Architecture, Engineering and Construction* 2012, **1**(1), pp. 1–13. DOI: https://doi.org/10.7492/IJAEC.2012.001.

[22] HENG, S.; Oshima, Y.; Kawano, H. A Study on Evaluation of IRI Prediction Model For Cambodian National Road Pavement Roughness. *Journal of Japan Society of Civil Engineers, Ser. E1 (Pavement Engineering)* 2012, **68**(3). DOI: https://doi.org/10.2208/jscejpe.68.I_139.

[23] Khahro, S. H. et al. Low-Cost Pavement Management System for Developing Countries. *Sustainability* 2021, **13**(11), p. 5941. DOI: https://doi.org/10.3390/su13115941.

[24] Obunguta, F.; Matsushima, K. Optimal Pavement Management Strategy Development with a Stochastic Model and Its Practical Application to Ugandan National Roads. *International Journal of Pavement Engineering* 2022, **23**(7), pp. 2405–2419. DOI: https://doi.org/10.1080/1

[25] Obama, K. et al. Disaggregated Hazard Rates Evaluation and Bench-marking. *J. Jpn. Soc. Civ. Eng* 2008, **64**, pp. 857–874.

[26] Kaito, K. et al. Hierarchical Bayesian Estimation of Mixed Hazard Models. *J. Jpn. Soc. Civ. Eng* 2012, **68**, pp. 255–271. DOI: https://doi.org/10.2208/jscejipm.68.255.

[27] Train, K. E. *Discrete Choice Methods with Simulation*. Cambridge University Press, 2009.

[28] Geweke, J. *Evaluating the Accuracy of Sampling-Based Approaches to the Calculation of Posterior Moments*. Tech. rep. Federal Reserve Bank of Minneapolis, 1991. URL: `https://ideas.repec.org/p/fip/fedmsr/148.html`.

[29] AASHTO. *AASHTO Guide for Design of Pavement Structures*. Washington, DC: American Association of State Highway and Transportation Officials, 1993.

[30] Galal, K. A.; Diefenderfer, B. K.; Alam, J., et al. *Determination by the Falling Weight Deflectometer of the In-Situ Subgrade Resilient Modulus and Effective Structural Number for I-77 in Virginia*. Tech. rep. Virginia Transportation Research Council (VTRC), 2007. URL: `https://rosap.ntl.bts.gov/view/dot/19850`.

[31] Piala, J. K.-.-M. K.-.-J. Relation of Temperature Changes in Asphalt Pavements to Pavement Bearing Capacity Evaluation. *A VEHICLE–BRIDGE INTERACTION*, p. 33.

[32] Březina, I.; Machel, O.; Zavřel, T. Temperature Correction of Deflections and Backcalculated Elasticity Moduli Determined from Falling Weight Deflectometer Measurements on Asphalt Pavements. *Communications-Scientific letters of the University of Zilina* 2022, **24**(1), pp. D1–D8. DOI: https://doi.org/10.26552/com.C.2022.1.D1-D8.

[33] Huang, Y. H. et al. *Pavement Analysis and Design*. Vol. 2. Pearson/Prentice Hall Upper Saddle River, NJ, 2004.

Chapter 5

Strategic Application of FWD for Efficient Network-Level Pavement Assessment

5.1 Introduction

The Falling Weight Deflectometer (FWD) is a widely used nondestructive testing (NDT) device for evaluating the structural condition of pavements at both project and network levels. The deflection measurements from the FWD are crucial for calculating structural parameters that are essential for pavement research, design, and management [1]. As mechanistic-empirical (M-E) pavement design approaches become more prevalent, the application of FWD in pavement engineering is expected to expand significantly. For instance, the AASHTO 1993 design guide incorporates FWD-derived deflections to back-calculate layer moduli, particularly the subgrade resilient modulus, which is a critical input for M-E design [2]. The use of FWD testing is also advantageous because it can offer a feasible alternative to the complex and costly laboratory testing required to determine subgrade moduli. In Cambodia, the Ministry of Public Works and Transport (MPWT) employs vehicle-mounted FWD systems, as depicted in Figure 5.1.

Network-level monitoring involves assessing and managing the performance and condition of an entire road network rather than individual roads. This process is essential for effective budgeting, planning, and evaluation, ensuring that transportation infrastructure meets current and future needs [3]. The use of FWD for network-level studies is particularly valuable due to its ability to provide precise measurements of pavement structural capacity. By leveraging FWD data, road authorities can gain critical insights into pavement performance, enabling them to make informed, strategic decisions about the timing and location of maintenance interventions. However, despite its advantages, the FWD faces challenges in network-level assessments. Its stop-and-go operation is time-consuming, leading to increased costs, especially when traffic control is necessary on high-speed roads [4, 5].



(a) KUAB FWD. (b) TBTFWD-NJ-M.

Figure 5.1: Falling Weight Deflectometer (FWD) in operation.

FWD surveys on road networks have been widely conducted by various agencies to enhance pavement infrastructure management through integrated structural analysis. For instance, the Virginia DOT developed a cost-effective FWD data collection protocol by minimizing the number of testing points and load level per mile [6, 7]. The study found that network-level FWD surveys could be effectively conducted using three points per mile with one load level and two repetitions. However, it recommended five points per mile with three load levels and two repetitions to ensure data reliability. Similarly, the Texas DOT introduced a risk-based method using the structural condition index (SCI) to determine the optimal frequency and interval for network-level FWD testing [8]. The study concluded that conducting two FWD tests per 800 meters maintains a failure probability of less than 30% in the mean SCI at the network level.

In Kansas, project-level FWD testing at five to ten tests per mile is feasible but impractical for the entire network annually. To address this, Kansas DOT used statistical analysis to recommend three tests per mile every three years [9]. Similarly, Indiana DOT proposed integrating FWD testing into its pavement management system with a protocol of three tests per mile for efficient data collection [10]. To minimize traffic disruption and enhance safety during FWD testing, Iran implemented a policy for network-level FWD applications that maximizes the interval between testing points [5]. Structural analysis indicated that the interval between FWD testing points could be extended from 0.2 km to 0.6 km.

Prioritizing road sections for monitoring and maintenance is essential for managing and improving transportation infrastructure efficiently, enhancing safety, quality, and cost-effective [11, 12]. This involves evaluating and scoring alternatives based on multiple criteria, a process known as multi-criteria decision-making (MCDM). Most MCDM approaches follow a two-phase framework: (1) determining the relative weight or importance of each criterion, and (2) evaluating and ranking alternatives based on these weighted criteria.

Analytic Hierarchy Process (AHP) is a MCDM method widely used for its ability to calculate individual weights of evaluation criteria and convert qualitative assessments into quantitative measures [13, 14]. AHP breaks down complex decisions into manageable pairwise comparisons, creating a logical and consistent decision-making framework [15]. An extension of the AHP, the Fuzzy Analytic Hierarchy Process (FAHP), incorporates fuzzy logic to address uncertainties and subjective judgment more effectively [16]. An enhanced AHP method was developed for prioritizing pavement maintenance sections, using pairwise comparisons of distresses such as alligator cracking, patching, potholes, raveling, and rutting [17]. Likewise, condition criteria like the pavement condition index (PCI), traffic congestion, pavement width, maintenance costs, and project duration under budget constraint are evaluated using FAHP, while VIKOR (VlseKriterijumska Optimizacija I Kompromisno Resenje) approach ranked alternatives [18]. FAHP and Fuzzy Weighed Average (FWA) were integrated to assess road condition using IRI, surface modulus, rut depth, and friction coefficient [19].

However, these studies often neglect long-term considerations like deterioration rates, which significantly affect road infrastructure over time. The aim of this study is to develop a protocol for the effective use of FWD testing at the network level. The first objective is to determine the optimal time interval or frequency for FWD data collection for specific pavement types using a stochastic approach. The second objective is to evaluate and prioritize critical road sections for FWD testing across the road network by integrating a MCDM approach. This framework will minimize the need for extensive network-level FWD data collection by focusing preliminary efforts on the most critical road sections.

5.2 Method

As previously mentioned, the primary goal focuses on determining the optimal frequency and priority for conducting these tests. The proposed framework is illustrated in Figure 5.2. The frequency of FWD testing refers to the planned time intervals. However, more frequent testing increases costs, making it crucial to identify the optimal testing cycles that balance timely assessments with cost-effectiveness.

To achieve this, the study employs a stochastic deterioration prediction model known as the mixed Markov hazard (MMH) model. This model addresses the deterioration of road surfaces by using the International Roughness Index (IRI) as a key indicator. When the IRI reaches a failure condition, it triggers the need for immediate intervention, necessitating an FWD survey. Furthermore, the MMH model also accounts for the prediction of the remaining life of specific road sections. The remaining life may serve as an index to prioritize road sections for FWD testing across the network. However, to ensure a more comprehensive prioritization approach, it is necessary to consider additional criteria. Therefore, this study addresses the MCDM process

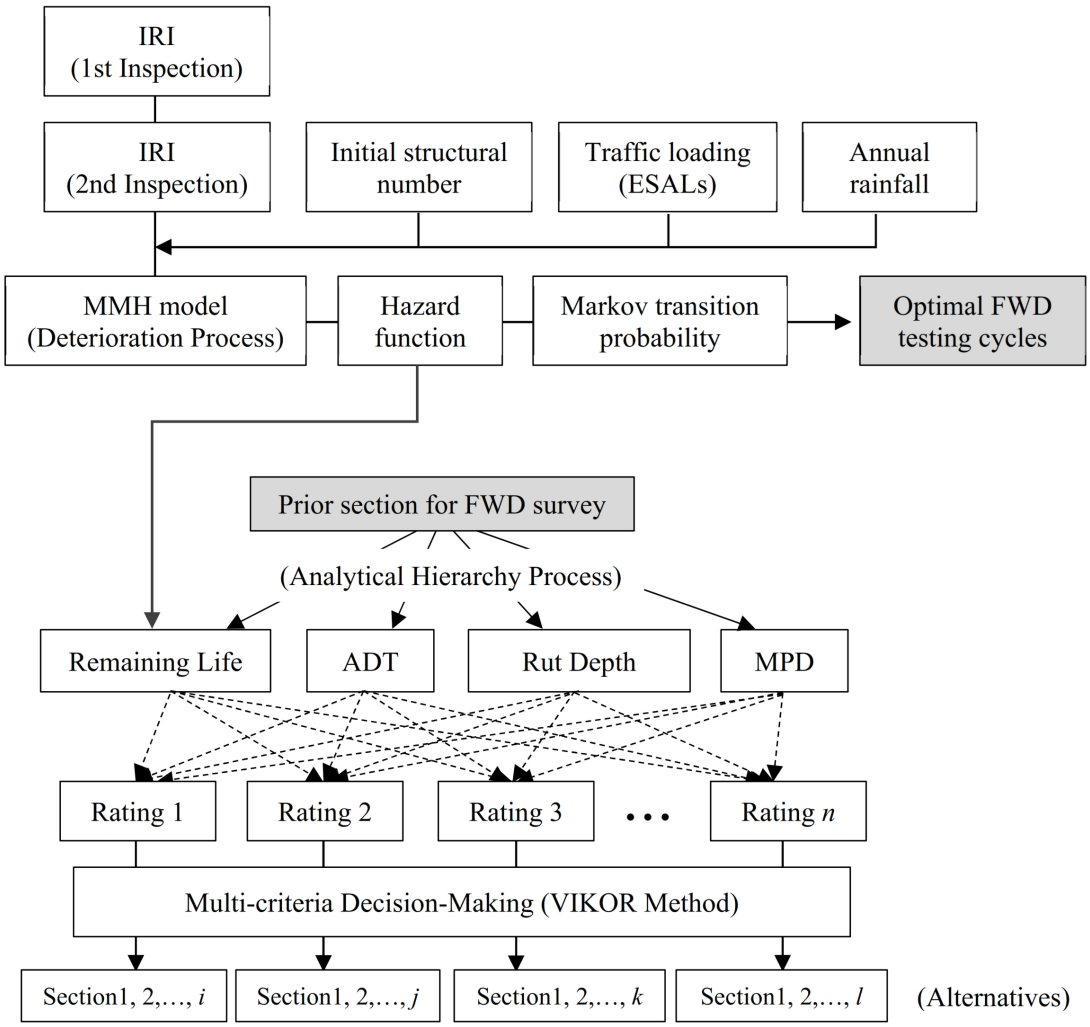


Figure 5.2: Proposed framework for FWD application.

involving the AHP for evaluating road sections and the VIKOR method for ranking them. The criteria used in this evaluation include the remaining life derived from the MMH model, average daily traffic (ADT), rut depth, and mean profile depth (MPD).

5.2.1 Mixed Markov hazard (MMH) model

The mixed Markov hazard (MMH) model, an extension of the Markov hazard model, accounts for distinct deterioration patterns across different groups of infrastructure [20]. Using a Bayesian estimation method, the model provides enhanced flexibility and robustness, facilitating more accurate and reliable predictions [21].

The MMH model, which utilizes the principles of Markov chain and survival analysis, represents pavement performance (e.g., IRI) with continuous values through discrete condition states $i(i = 1, ..., J)$, where $i = 1$ denotes the best condition and $i = J$ the worst. By assuming pavement' s health at first and second inspection as $h(\tau_A)$ and $h(\tau_B)$, respectively, the

probability of transitioning from a condition state i to j is given by:

$$\text{Prob}[h(\tau_B) = j \mid h(\tau_A) = i] = \pi_{ij} \tag{5.1}$$

$$\Pi = \begin{bmatrix} \pi_{11} & \cdots & \pi_{1J} \\ \vdots & \ddots & \vdots \\ 0 & \cdots & \pi_{JJ} \end{bmatrix}, \quad \pi_{ij} \geq 0, \quad \sum_{j=1}^{J} \pi_{ij} = 1 \tag{5.2}$$

The survival function $\tilde{F}_i(\zeta_i)$, given the hazard rate θ_i^k, is defined as:

$$\tilde{F}_i\left(y_i^k\right) = e^{-\theta_i^k y_i^k} \tag{5.3}$$

The hazard rate for road sections in group k is:

$$\theta_i^k = \bar{\varepsilon}^k \tilde{\theta}_i^k \tag{5.4}$$

where ε^k is the average heterogeneity factor for group k, and θ_i^k is the baseline hazard rate.

The heterogeneity factor ε^k is assumed to follow a gamma distribution. The survival function $F_i(y_i^k)$ in Equation 5.3 becomes:

$$\tilde{F}_i\left(y_i^k\right) = e^{-\bar{\varepsilon}^k \tilde{\theta}_i^k y_i^k} \tag{5.5}$$

The transition probabilities considering ε^k can be written as:

$$\pi_{ii} = e^{-\bar{\varepsilon}^k \tilde{\theta}_i^k Z^k} \tag{5.6}$$

$$\pi_{ij} = \sum_{p=i}^{j} \prod_{\substack{m=i \\ m \neq p}}^{j-1} \left(\frac{\tilde{\theta}_m^k}{\tilde{\theta}_m^k - \tilde{\theta}_p^k} \right) e^{-\bar{\varepsilon}^k \tilde{\theta}_p^s{}^k Z^k} = \sum_{p=i}^{j} \psi_{ij}^p\left(\tilde{\theta}^k\right) e^{-\bar{\varepsilon}^k \tilde{\theta}_p^k Z^k} \tag{5.7}$$

where $\psi_{ij}^p\left(\tilde{\theta}^k\right) = \prod_{\substack{m=i \\ m \neq p}}^{j-1} \frac{\tilde{\theta}_m^k}{\tilde{\theta}_m^k - \tilde{\theta}_p^k}$ and $\tilde{\theta}^k = \left(\tilde{\theta}_1^k, \ldots, \tilde{\theta}_{J-1}^k\right)$.

$$\pi_{iJ} = 1 - \sum_{j=i}^{J-1} \pi_{ij} \tag{5.8}$$

It is necessary to incorporate independent explanatory variables x^k to calculate $\tilde{\theta}_i^k$ by estimating the unknown parameters, $\boldsymbol{\beta}_i = (\beta_i, \beta_{i,1}, \ldots, \beta_{i,M})$ where $m = 1, \ldots, M$ denotes the number of explanatory variables.

$$\theta_i^k = f\left(\bar{\varepsilon}^k;\, x^k;\, \boldsymbol{\beta}_i\right) = \bar{\varepsilon}^k \tilde{\theta}_i^k = \bar{\varepsilon}^k e^{\beta_i + \beta_{i,1} x_1^k + \cdots + \beta_{i,M} x_M^k} \tag{5.9}$$

Consequently, the MTP matrix becomes $\pi_{ij}\left(\bar{\varepsilon}^k;\, \bar{z}^k;\, \bar{x}^k;\, \boldsymbol{\beta}_i\right)$ where z^k and x^k represent the measurable values during inspections and the bar "$^-$" indicates the average value. The life expectancy for state i and total life expectancy from state i to J are:

$$LE_i^k = \int_0^\infty \tilde{F}_i\left(y_i^k\right)\, dy_i^k = \int_0^\infty e^{-\theta_i^k y_i^k}\, dy_i^k = \frac{1}{\theta_i^k} \tag{5.10}$$

$$LE_{iJ}^k = \sum_{i=1}^{J-1} LE_i^k \tag{5.11}$$

The field survey data, represented as $\bar{\xi} = (\bar{\delta}_{ij}^k, \bar{z}^k, \bar{x}^k)$, includes a dummy variable $\bar{\delta}_{ij}^k$. This variable takes a value of 1 if $h(\tau_A^k) = i$ and $h(\tau_B^k) = j$, and 0 otherwise. In Bayesian inference, the posterior distribution is determined by combining the prior distribution with the likelihood function, followed by normalization. Following a multidimensional normal distribution, the posterior distribution can be written as follows:

$$\pi(\omega \mid \bar{\xi}) = \frac{L(\omega \mid \bar{\xi})\, \pi(\omega)}{\int L(\omega \mid \bar{\xi})\, \pi(\omega)\, d\omega} \quad \text{or} \quad \pi(\omega \mid \bar{\xi}) \propto L(\omega \mid \bar{\xi})\, \pi(\omega) \tag{5.12}$$

To sample the values of the parameter $\boldsymbol{\omega} = (\boldsymbol{\beta}_i, \phi, \varepsilon^k)$ directly from the posterior distribution described in above equation, the Markov Chain Monte Carlo (MCMC) method with the Metropolis-Hastings (M-H) algorithm is employed. With sufficient iterative process, the Markov chain that converges to the target distribution can be ensured.

5.2.2 Multi-criteria decision-making (MCDM)

The CRITIC method determines objective weights for criteria by analyzing both contrast intensity and the level of conflict between criteria using correlation analysis [22, 23]. It begins

by constructing a decision matrix containing the performance values of alternatives across different criteria, followed by normalizing the matrix using the ideal best and worst solutions to ensure comparability. The standard deviation of each criterion is then calculated to measure its variability, and a correlation matrix is constructed to assess the interdependence between criteria. Next, the criterion information is computed by combining the standard deviation and the level of conflict, and finally, the weights are determined by normalizing this information, reflecting the relative importance of each criterion based on its contrast intensity and conflict with others. The procedures for defining the relative importance and weight of each criterion are as follows:

- Step 1: Construct the decision matrix.

$$X = \begin{bmatrix} x_{11} & x_{12} & \cdots & x_{1m} \\ x_{21} & x_{22} & \cdots & x_{2m} \\ \vdots & \vdots & \ddots & \vdots \\ x_{m1} & x_{m2} & \cdots & x_{mm} \end{bmatrix} \tag{5.13}$$

- Step 2: Normalize the decision matrix. Using the ideal best solution (x_j^+) and the ideal worst solution (x_j^-), normalization is performed.

$$x_{ij}^T = \frac{x_{ij} - x_j^-}{x_j^+ - x_j^-}, \qquad \text{if } j \in B \text{ (Beneficial)} \tag{5.14}$$

$$x_{ij}^T = \frac{x_j^+ - x_{ij}}{x_j^+ - x_j^-}, \qquad \text{if } j \in NB \text{ (Non-beneficial)} \tag{5.15}$$

  where x_{ij}^T is the normalized value, and x_j^- and x_j^+ are the minimum and maximum values of the criteria, respectively.

- Step 3: Calculated the standard deviation (σ_j).

$$\sigma_j = \sqrt{\frac{1}{n-1}\sum_{i=1}^{n}(x_{ij} - \bar{x}_j)^2}, \qquad i = 1, \ldots, m \tag{5.16}$$

  where x_j display the mean of jth attributes and is computed as follows:

$$\bar{x}_j = \frac{1}{n}\sum_{i=1}^{n} x_{ij}, \qquad i = 1, \ldots, m$$

- Step 4: Construct the correlation matrix. The correlation coefficient r_{jk} between criteria j and k is computed as:

$$r_{jk} = \frac{\sum_{i=1}^{m}(x_{ij} - \bar{x}_j)(x_{ik} - \bar{x}_k)}{\sqrt{\left(\sum_{i=1}^{m}(x_{ij} - \bar{x}_j)^2\right)\left(\sum_{i=1}^{m}(x_{ik} - \bar{x}_k)^2\right)}} \tag{5.17}$$

- Step 5: Calculate the criterion information (C_j).

$$C_j = \sigma_j \cdot \sum_{k=1}^{m}(1 - r_{jk}) \tag{5.18}$$

- Step 6: Determine the final criteria weights (w_j).

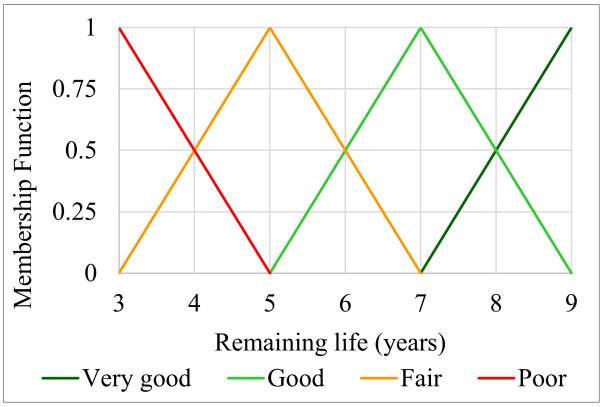
$$w_j = \frac{C_j}{\sum_{k=1}^{m} C_k} \tag{5.19}$$

  where w_j represents the weight of criterion j, considering its contrast intensity and conflict level relative to others.

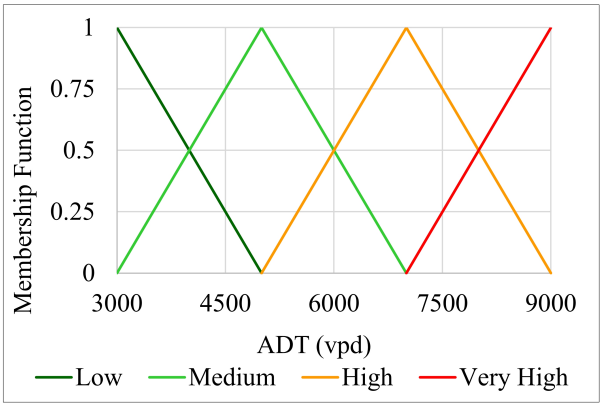
In this approach, the AHP is combined with CRITIC weights to enhance decision-making under uncertainty. The process begins by determining score comparisons using symmetric triangular fuzzy numbers. Next, a final fuzzy evaluation set is established by multiplying the CRITIC weight vector with the corresponding columns of a fuzzy judgment matrix. This matrix is derived by calculating the membership grades for each criterion relative to evaluation classes, resulting in a fuzzy comprehensive evaluation. The evaluation is then transformed into a crisp output using the Maximum Graded Principle (MGP), which assigns the highest membership grade as the final evaluation. This allows for the ranking and classification of road sections into rating groups such as Poor, Fair, Good, and Very Good, providing a clear and structured decision outcome. The complete procedure can be summarized in the following steps:

- Step 1: Construct the fuzzy pairwise comparison matrix using symmetric triangular fuzzy numbers, as shown in Figure 5.3.
- Step 2: Compute CRITIC weights, as presented in the previous section.
- Step 3: Construct the fuzzy relation matrix. Let $U = \{u_1, u_2, \ldots, u_n\}$ be the set of criteria and $V = \{v_1, v_2, \ldots, v_p\}$ the evaluation grades. The normalized fuzzy relation matrix is expressed as follows:

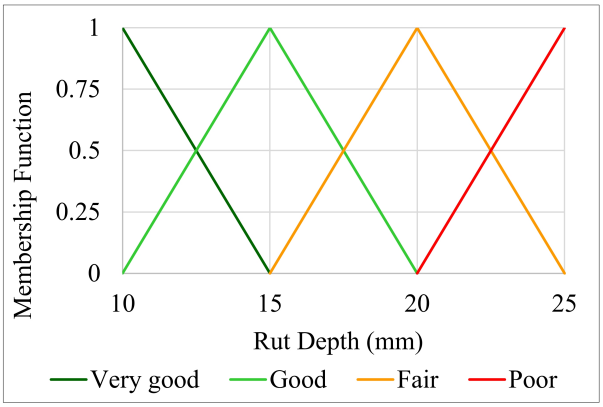
$$R' = [r'_{ij}]_{n \times p} \tag{5.20}$$



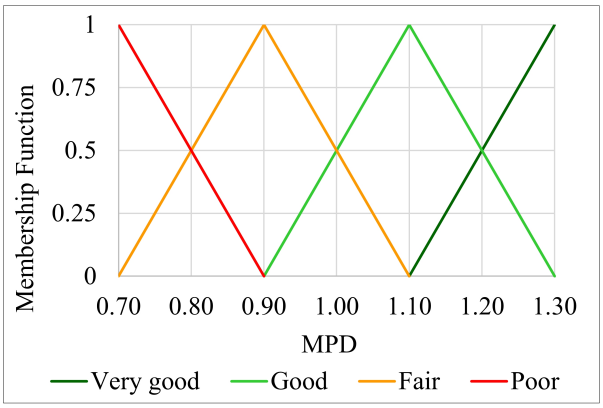
(a) Remaining Life.



(b) ADT.



(c) Rut Depth.



(d) MPD.

Figure 5.3: Membership functions of each criterion.

where the membership value for each criterion u_i and grade v_j, $r'_{ij} = \mu_{R'}(u_i, v_j)$.

- Step 4: Perform fuzzy comprehensive evaluation. Let $W = \{w_1, w_2, \ldots, w_n\}$ be the CRITIC weight vector. The fuzzy evaluation vector is obtained through:

$$Y = W \otimes R' \tag{5.21}$$

where $\otimes$ denotes the fuzzy weighted mapping. The membership of grade y_j is computed as:

$$\mu_Y(y_j) = \min\left(1, \sum_{i=1}^{n} w_i r'_{ij}\right) \tag{5.22}$$

- Step 5: Defuzzify using the Maximum Graded Principle (MGP).

The VIKOR (VlseKriterijumska Optimizacija I Kompromisno Resenje) is an MCDM approach that ranks alternatives based on conflicting criteria to identify the best compromise solution. The process involves evaluating alternatives against criteria, identifying the best

and worst values for each criterion, and normalizing the data to account for beneficial and non-beneficial factors. Next, ideal and worst-case scenarios are established, and two measures (group benefit and individual regret) are calculated to assess each alternative' s performance. These measures are combined into a single index, which ranks the alternatives, with lower scores indicating better performance. The final step ensures the top-ranked alternative is a stable and acceptable compromise by checking if it significantly outperforms the next best option or if further analysis is needed. The VIKOR method is implemented through the following steps:

- Construct the decision matrix $X = [x_{ij}]_{m\times n}$, where m alternatives are evaluated against n criteria:

$$X = \begin{bmatrix} x_{11} & x_{12} & \cdots & x_{1n} \\ x_{21} & x_{22} & \cdots & x_{2n} \\ \vdots & \vdots & \ddots & \vdots \\ x_{m1} & x_{m2} & \cdots & x_{mn} \end{bmatrix} \tag{31}$$

- Identify the best and worst criterion values for each criterion:

$$x_j^+ = \max_{1\le i\le m} x_{ij}, \tag{32}$$

$$x_j^- = \min_{1\le i\le m} x_{ij}. \tag{33}$$

- Normalize the decision matrix. For beneficial criteria:

$$r_{ij} = \frac{x_j^+ - x_{ij}}{x_j^+ - x_j^-} \tag{34}$$

  For non-beneficial criteria:

$$r_{ij} = \frac{x_{ij} - x_j^-}{x_j^+ - x_j^-} \tag{35}$$

- Determine the positive and negative ideal solutions:

$$r^+ = \{r_1^+, r_2^+, \ldots, r_m^+\} = \big(\max_{j\in B} r_{ij},\ \min_{j\in NB} r_{ij}\big), \tag{36}$$

$$r^- = \{r_1^-, r_2^-, \ldots, r_m^-\} = \big(\min_{j\in B} r_{ij},\ \max_{j\in NB} r_{ij}\big). \tag{37}$$

- Compute the benefit S_i and regret R_i measures:

$$S_i = \sum_{j=1}^{n} w_j \left(\frac{r^+ - r_{ij}}{r^+ - r^-}\right), \tag{38}$$

$$R_i = \max_{1 \le j \le n} \left\{ w_j \left(\frac{r^+ - r_{ij}}{r^+ - r^-} \right) \right\}, \tag{39}$$

where w_j are the criterion weights derived using the CRITIC method.

- Compute the VIKOR index Q_i:

$$Q_i = v \frac{S_i - S^*}{S^- - S^*} + (1 - v) \frac{R_i - R^*}{R^- - R^*}, \tag{40}$$

where

$$S^* = \min_i S_i, \quad S^- = \max_i S_i, \quad R^* = \min_i R_i, \quad R^- = \max_i R_i,$$

and v is the weight of maximum group utility (commonly $v = 0.5$).

- Rank the alternatives. A lower value of Q_i indicates a better compromise solution. If alternatives have similar Q_i values, both S_i and R_i must be examined to ensure a balanced decision.

- Determine the compromise solution. Let A_1 and A_2 be the first and second ranked alternatives:

$$Q(A_1) - Q(A_2) \ge D_Q, \qquad D_Q = \frac{1}{m-1}.$$

If this condition is satisfied, A_1 is the compromise solution. Otherwise, both S_i and R_i must be considered to verify the decision' s stability.

Traveling Salesman Problem (TSP) addresses the challenge of determining the shortest possible route that visits all selected road sections (nodes) and returns to the starting point. The ranked list of road sections generated by the AHP serves as the input nodes for the TSP. For large networks, exact solutions to the TSP are often computationally infeasible due to the exponential growth of possible routes. For instance, heuristic or approximate algorithms are typically employed to find near-optimal solutions within a reasonable timeframe. In this study, the TSP is solved using a tool called Route Solver, which is part of the Network Analyst extension in ArcGIS Pro. Route Solver leverages a combination of Dijkstra' s algorithm and heuristic search algorithms to identify the most efficient route.

5.3 Empirical Study

5.3.1 Data collection

The performance of 1-digit and 2-digit nationals roads, referring to primary and secondary arterial roads, was assessed using the International Roughness Index (IRI). The IRI in this study was measured with a road distress survey vehicle equipped with laser profilometers. A total of 6084 road sections combining AC and DBST pavements were selected, and data were gathered over two separate periods (2021-2022 and 2022-2023) to capture temporal variations in pavement deterioration.

The dataset used for the MMH model analysis included the following: (1) IRI from the first inspection $h(\tau_A)$, (2) IRI from the second inspection $h(\tau_B)$, (3) time interval between inspections $z = \tau_B - \tau_A$, and (4) explanatory variable $\bar{x}^k$ representing the factors influencing on deterioration process. These factors included the initial structure number (SN), which was back-calculated from the FWD measurements due to the unavailability of as-built records, traffic loading, expressed in Equivalent Single Axle Loads (ESALs), calculated from traffic count surveys and converted based on AASHTO guidelines [2]; and environmental conditions, represented by average annual rainfall. The rainfall data, sourced from the Asian Precipitation –Highly-Resolved Observational Data Integration Towards Evaluation (APHRODITE) dataset, were based on gauged observations across Cambodia, reflecting notable regional variations.

5.3.2 Data processing

To develop a meaningful deterioration model, we integrate all three influencing factors into a unified Markov deterioration process. The key explanatory variables driving changes in the IRI in this study include the initial SN, ESALs, and average annual rainfall data.

The application of Markov transition probabilities requires the use of discrete condition states. Accordingly, this study converts continuous IRI values into a condition rating scale ranging from the original state to a terminal condition that necessitates rehabilitation or reconstruction. The IRI values collected in the field are categorized into five discrete states, with condition state 5 representing the worst condition, as outlined in Table 5.1.

It is important to note that the model excludes any data reflecting improved condition states in the second inspection cycle due to repair or maintenance activities.

Table 5.1: Pavement performance rating.

Condition State	**IRI (m/km)**	**Rating Remark**
1	≤ 2	Excellent
2	$2-3$	Good
3	$3-4$	Fair
4	$4-5$	Poor
5	>5	Very Poor

5.4 Results

5.4.1 Estimation results based on MMH model

The MCMC sampling process involved a total of 40,000 iterations. The initial 20,000 iterations were treated as burn-in samples to ensure convergence, and the subsequent 20,000 iterations were used for parameter estimation. The final model parameters were calculated as the mean of these effective samples. Geweke' s Z-score, used to assess the convergence of β_i, was close to 0, indicating optimal convergence within the tolerance interval $[-1.96, 1.96]$. The life expectancy of each condition state is calculated based on hazard rate, reflecting the deterioration patterns of road sections. Finally, the predicted remaining life of each pavement section results from the summation of the life expectancy of each condition state from current condition state.

Table 5.2 shows the mean values of parameter distributions sampled in the MCMC method. Since the absolute value of Geweke' s Z-score is less than 1.96, the convergence to the posterior distribution was achieved. It is noted that there are inverse correlations between two explanatory variables (ESALs and Rainfall) with condition changes (1 to 2 and 4 to 5). On the other hand, the deterioration processes between AC and DBST pavements can be compared based on the heterogeneity factors ε^k with the benchmark process (i.e., $\varepsilon^k = 1$) of all samples. In brief, AC pavements having $\varepsilon^k < 1$ means slow deterioration speed, while DBST pavements having $\varepsilon^k > 1$ reflects fast deterioration speed. Taking into consideration of different levels of bearing capacities, ESALs, rainfall, and heterogeneity factors of each road section, the life expectancy LE^k can be calculated.

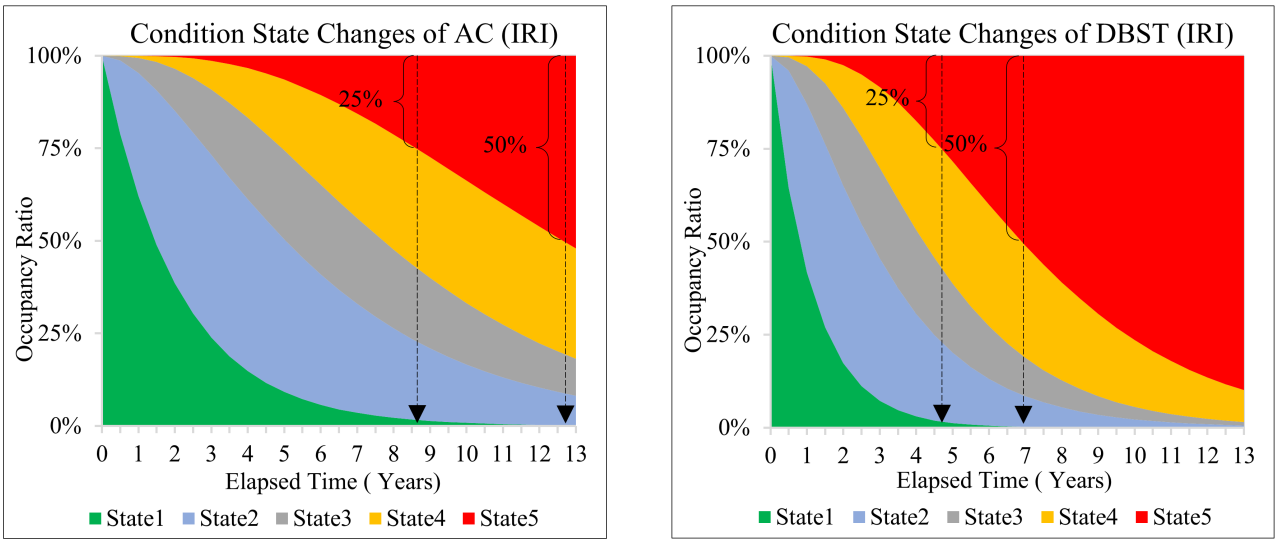
The matrices of Markov transition probability (MTP) of AC and DBST pavements, estimated by using the MMH model, are presented in Table 5.3. The values of transition properties are estimated based on the value of average hazard rates, which represents the deterioration transition pattern of each pavement type. The Bayesian mixed Markov hazard model satisfies the time adjustment condition $\Pi(nZ) = \{\Pi(Z)\}^n$ [24].

Table 5.2: Estimation results for model's parameters.

Condition State	ε^k		Hazard Rate θ_i	Parameter Estimates			
	AC	DBST		Constant β_i	SN β_{i1}	ESALs β_{i2}	Rainfall β_{i3}
$1 \rightarrow 2$	0.730	1.339	0.654	-1.02 (0.15)	2.23 (0.06)	–	–
$2 \rightarrow 3$			0.338	-1.93 (-0.04)	1.85 (-0.05)	0.89 (-0.38)	0.40 (-0.09)
$3 \rightarrow 4$			0.522	-2.62 (-0.00)	4.57 (-0.04)	1.63 (-0.32)	1.46 (0.01)
$4 \rightarrow 5$			0.261	-1.89 (0.74)	2.08 (-0.06)	–	–

Note:

- The [–] indicates insignificant variables due to inverted relationship.
- Geweke's Z-score in parentheses.



(a) AC pavement (b) DBST pavement

Figure 5.4: Condition state changes by elapsed year.

Figure 1 shows the distribution of condition states of IRI for the whole network by elapsed years n ($n = 1, \ldots, \infty$). In case of IRI, around 25% of AC pavements require FWD testing after 8.6 years, and the percentage reaches 50% after 12.6 years (as illustrated in Figure 5.4a). Whilst around 25% of DBST pavements require FWD testing after 4.7 years, and the percentage reaches 50% after 6.9 years (as illustrated in Figure 5.4b). This information is useful for establishing temporal policy of FWD testing within allowable probabilities of reaching worse conditions and can answer how frequently FWD should be conducted for AC and DBST pavements. In this study, we simply divide the elapsed time of probability reaching the worst condition at 25% and 50% by 2 to propose FWD testing frequency as shown in Table 5.4.

A hybrid decision-support system is developed in this section using the above discussed

Table 5.3: MTP matrix of AC and DBST pavement.

State	AC					DBST				
	1	**2**	**3**	**4**	**5**	**1**	**2**	**3**	**4**	**5**
1	0.621	0.333	0.041	0.005	0.000	0.417	0.454	0.101	0.026	0.003
2	–	0.781	0.181	0.036	0.002	–	0.636	0.255	0.096	0.013
3	–	–	0.683	0.287	0.030	–	–	0.497	0.416	0.087
4	–	–	–	0.826	0.174	–	–	–	0.705	0.295
5	–	–	–	–	1.000	–	–	–	–	1.000

Table 5.4: Proposed frequency of FWD testing.

Pavement Type	**Elapsed Time of Reaching Worst Condition (Years)**		**Proposed FWD Testing Frequency**
	At 25% probability	**At 50% probability**	
AC	8.6	12.6	Every 4 or 6 years
DBST	4.7	6.9	Every 2 or 3 years

AHP, CRITIC and VIKOR approaches. A total of 4 criteria were defined: remaining life, ADT, rut depth, and MPD. Remaining life and MPD are considered beneficial, meaning that higher values are preferred, whereas ADT and rut depth are considered non-beneficial, favoring lower values. The findings based on the CRITIC method reveal that remaining life (the duration for surface roughness to deteriorate from the current condition to the worst condition) carries the highest weight in this study (0.3), followed by rut depth (0.272), ADT (0.253), and MPD (0.174).

Final fuzzy evaluation set "V" for all road sections can be obtained by transforming fuzzy relation "R'" through a mapping operator as per relation. Along with final fuzzy evaluation set "V" the defuzzification results obtained using MGP approach is also presented in the column (3) of Table 5.5 meaning the conditions of whole road sections can be simply classified into four groups: Poor, Fair, Good, and Very Good. At this point, with linguistic assessments, the road networks can be evaluated and classified to macro level, however, the road agencies prefer determining the prioritized road sections corresponding to each rating to conduct FWD testing. After determining the weights for the criteria, the next step is to rank the alternatives for each MGP rating using the VIKOR technique. This method calculates a performance score for each alternative through the VIKOR index (Q_i). The road sections within each rating condition are then arranged in descending order of Q_i , placing the worst-condition road sections first and the best-condition road sections last. This process identifies the critical road sections in ascending order of priority for FWD testing, as shown in Figure 5.5.

Road conditions can be classified, and rankings can be determined for FWD testing across networks using the above methodologies. However, road agencies may prioritize conducting a

Table 5.5: Fuzzy relation and evaluation.

Road Section	Fuzzy Evaluation Set	MGP	S_i	R_i	Q_i	VIKOR Rank	FWD Priority
NR6_13800_13900	[1, 0, 0, 0]	P	0.90	0.30	1.00	1713	1
NR6_18900_19000	[0.89, 0.12, 0, 0]	P	0.86	0.30	0.95	1712	2
⋮	⋮	⋮	⋮	⋮	⋮	⋮	⋮
NR6_114400_114500	[0.34, 0.19, 0.17, 0.30]	P	0.41	0.13	0.01	1	1713
NR6_14500_14600	[0.38, 0.43, 0.19, 0]	F	0.80	0.25	0.86	628	1
NR62_7600_7700	[0.37, 0.39, 0.25, 0]	F	0.67	0.35	0.85	627	2
⋮	⋮	⋮	⋮	⋮	⋮	⋮	⋮
NR6_114300_114400	[0.22, 0.34, 0.14, 0.30]	F	0.43	0.14	0.08	1	628
NR73_26200_26300	[0.39, 0.20, 0.40, 0.01]	G	0.72	0.35	1.00	639	1
NR73_55000_55100	[0.34, 0.13, 0.35, 0.18]	G	0.68	0.35	0.93	638	2
⋮	⋮	⋮	⋮	⋮	⋮	⋮	⋮
NR7_162900_163000	[0.27, 0, 0.37, 0.35]	G	0.39	0.13	0.02	1	639
NR68_64000_64100	[0.47, 0, 0.04, 0.48]	VG	0.72	0.30	0.97	3104	1
NR62_31600_31700	[0.36, 0.19, 0.08, 0.37]	VG	0.71	0.30	0.95	3103	2
⋮	⋮	⋮	⋮	⋮	⋮	⋮	⋮
NR7_237500_237600	[0, 0, 0.005, 1]	VG	0.27	0.09	0.00	1	3104

Note: P = Poor, F = Fair, G = Good, and VG = Very Good.

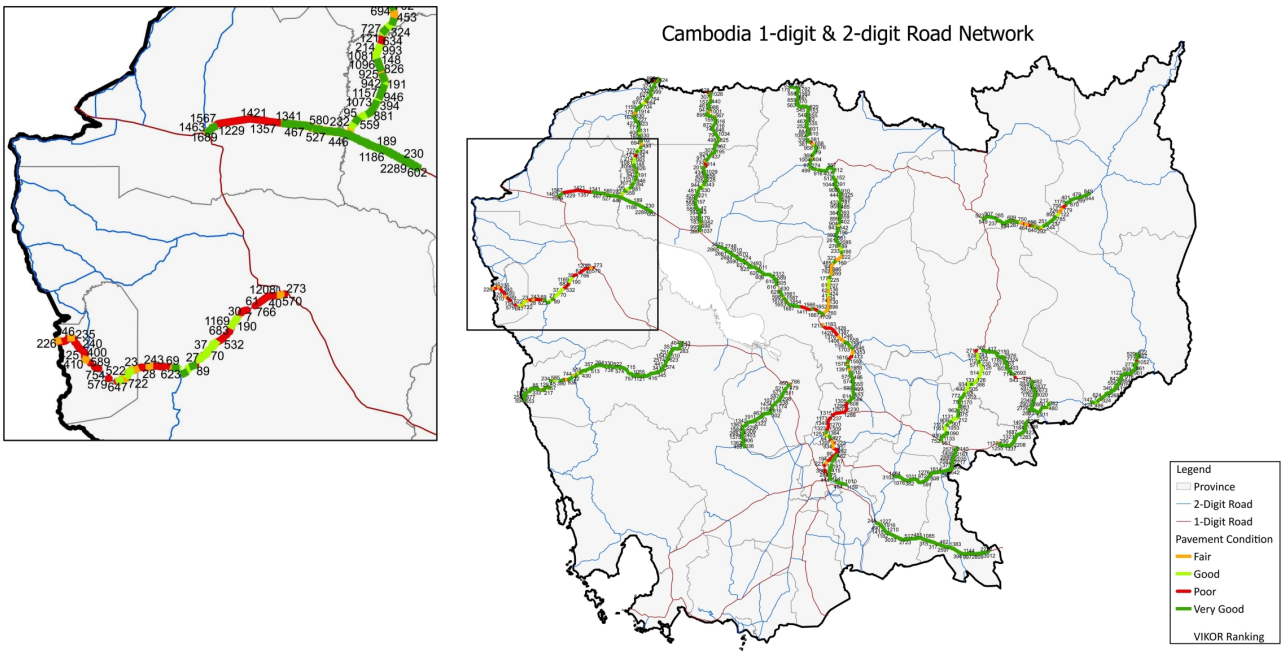
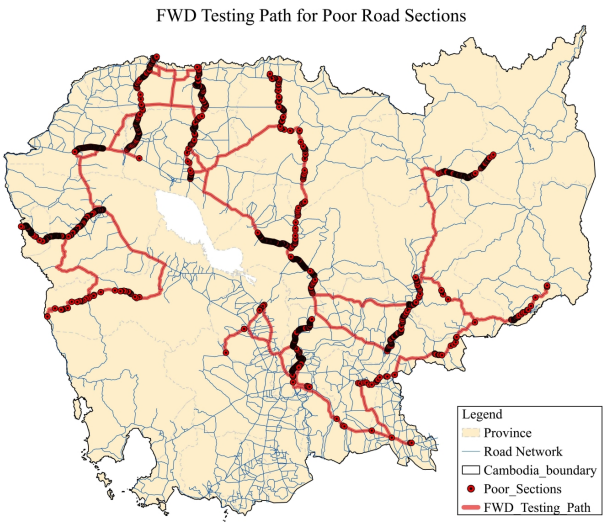


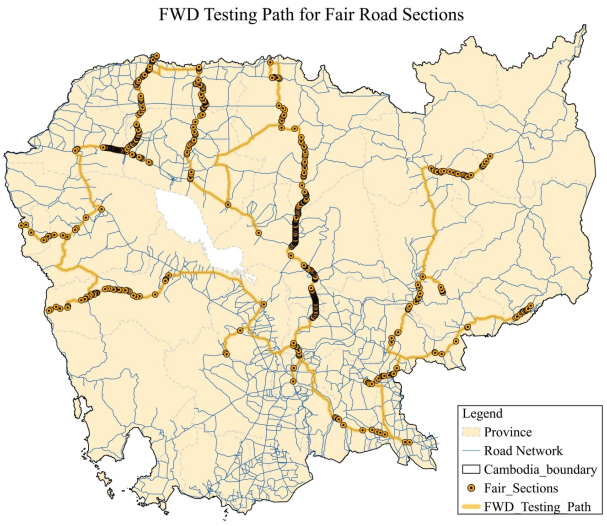
Figure 5.5: Prioritized road sections for FWD testing at network-level.

single round trip for data collection to minimize revisits and reduce travel distances between testing sections. To address this, the study employed the network analyst tool in ArcGIS Pro to calculate distances between road section points, as mapped within the application. The starting point for the route is the FWD warehouse, with distances to other road sections calculated along a defined network path.

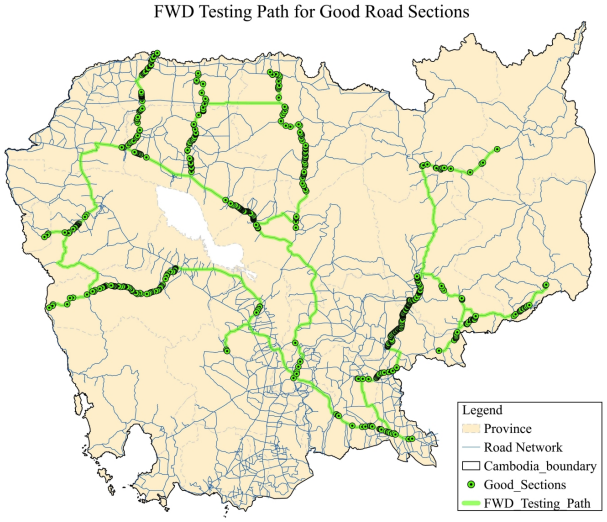
Using Dijkstra' s algorithm, integrated with hierarchical routing, ArcGIS Pro identifies the shortest path from the starting location to each destination. Through its Route Solver tool,



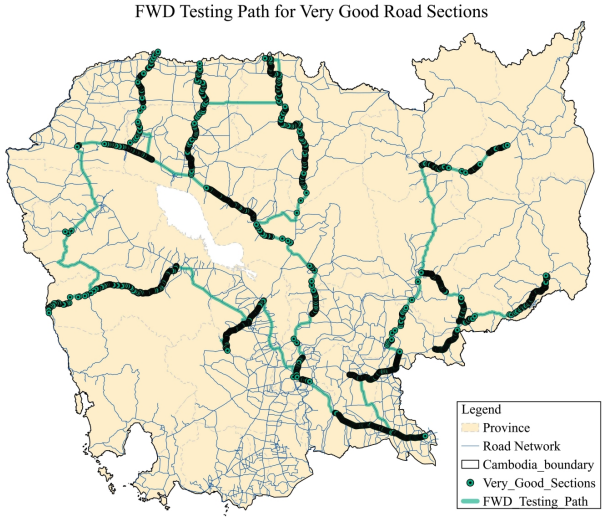
(a) Poor road sections



(b) Fair road sections



(c) Good road sections



(d) Very good road sections

Figure 5.6: Minimal FWD testing route.

ArcGIS Pro generates the optimal sequence for visiting stop locations, effectively solving the traveling salesman problem (TSP). The TSP is a combinatorial optimization problem, meaning there is no straightforward method to determine the best sequence. Instead, heuristics, such as a tabu search-based algorithm, are used to find effective solutions within a short time frame.

Figure 5.6 illustrates the optimal route paths for mobilizing FWD vehicles from the warehouse to testing sections and back, categorized by road conditions: (a) poor, (b) fair, (c) good, and (d) very good road sections.

5.5 Conclusions

This study developed a policy framework for the application of FWD testing at a network level, focusing on two primary objectives: determining optimal testing timing intervals and prioritizing road sections for FWD testing. Using advanced methodologies, including the Bayesian MMH model, CRITIC, and VIKOR approaches, the research provided a comprehensive decision-support system to enhance the planning and execution of FWD testing.

The findings highlighted significant differences in the deterioration rates of AC and DBST pavements, driven by key variables such as SN, ESALs, and average annual rainfall. The MMH model, validated using Geweke' s diagnostic, showed that AC pavements, with slower surface roughness deterioration, had a longer lifespan compared to DBST pavements. Consequently, FWD testing intervals for AC pavements can be extended relative to DBST pavements, aligning with their differing deterioration rates.

The transition probability matrices derived from the MMH model provided valuable insights into the time-series variation of pavement condition states. For AC pavements, 25% of sections reached critical IRI conditions after 8.6 years, with 50% reaching this state after 12.6 years. In contrast, DBST pavements reached the same thresholds at 4.7 years and 6.9 years, respectively. These results informed the development of a recommended FWD testing timing interval, ensuring prompt interventions to maintain road performance while optimizing resource allocation.

To prioritize road sections for FWD testing, the hybrid decision-support system combined the CRITIC approach for criteria weighting and the VIKOR technique for alternative ranking. Remaining life emerged as the most critical criterion, followed by rut depth, ADT, and MPD. The prioritization process ensured that road sections with higher index Q_i were addressed first, facilitating effective maintenance planning. In addition, the study addressed logistical challenges associated with FWD testing through the integration of ArcGIS Pro' s network analyst tool. By leveraging Dijkstra' s algorithm and hierarchical routing, optimal routes for FWD vehicle mobilization were determined, minimizing travel distances and operational costs. The route planning categorized road sections by condition (poor, fair, good, and very good), enabling a systematic and efficient approach to data collection. In conclusion, this research provides a robust framework for network-level FWD testing policy, balancing technical accuracy, cost-efficiency, and practical implementation. By determining optimal testing frequencies and prioritizing road sections for FWD testing, road agencies can enhance pavement management strategies, ensuring sustainable and well-maintained road networks.

References

[1] Alavi, S.; LeCates, J. F.; Tavares, M. P. *Falling Weight Deflectometer Usage*. Project 20-5 (Topic 38-15). 2008.

[2] AASHTO. *AASHTO Guide for Design of Pavement Structures*. Washington, DC: American Association of State Highway and Transportation Officials, 1993.

[3] European Cooperation in the Field of Scientific and Technical Research. *Use of Falling Weight Deflectometer in Pavement Evaluation*. 2nd. COST 336. Brussels, Belgium: European Commission, Directorate General Transport, 2005.

[4] Carvalho, R. L. et al. Procedure for Optimum Pavement Deflection Test Spacings for Network-Level Applications. *Transportation research record* 2012, **2304**(1), pp. 67–74. DOI: https://doi.org/10.3141/2304-08.

[5] Matini, N.; Tabatabaee, N.; Abbasghorbani, M. Protocol for FWD Data Collection at Network-Level Pavement Management in Iran. *Transportation Research Record* 2018, **2672**(40), pp. 68–77. DOI: https://doi.org/10.1177/0361198118758392.

[6] Alam, J.; Galal, K. A.; Diefenderfer, B. K. Network-Level Falling Weight Deflectometer Testing: Statistical Determination of Minimum Testing Intervals and Number of Drop Levels on Virginia's Interstate System. *Transportation research record* 2007, **1990**(1), pp. 111–118. DOI: https://doi.org/10.3141/1990-13.

[7] Diefenderfer, B. K. et al. *Network-Level Pavement Evaluation of Virginia's Interstate System Using the Falling Weight Deflectometer*. Tech. rep. Virginia Transportation Research Council (VTRC), 2008. URL: `https://rosap.ntl.bts.gov/view/dot/20107`.

[8] Damnjanovic, I.; Zhang, Z. Determination of Required Falling Weight Deflectometer Testing Frequency for Pavement Structural Evaluation at the Network Level. *Journal of transportation engineering* 2006, **132**(1), pp. 76–85. DOI: https://doi.org/10.1061/(ASCE)0733-947X(2006)132:1(76).

[9] Hossain, M. et al. Network-Level Pavement Deflection Testing and Structural Evaluation. *Journal of Testing and Evaluation* 2000, **28**(3), pp. 199–206. DOI: https://doi.org/10.1520/JTE12095J

[10] Noureldin, A. S. et al. Network Pavement Evaluation with Falling-Weight Deflectometer and Ground-Penetrating Radar. *Transportation research record* 2003, **1860**(1), pp. 90–99. DOI: https://doi.org/10.3141/1860-10.

[11] Angelo, A. A.; Sasai, K.; Kaito, K. Assessing Critical Road Sections: A Decision Matrix Approach Considering Safety and Pavement Condition. *Sustainability* 2023, **15**(9), p. 7244. DOI: https://doi.org/10.3390/su15097244.

[12] Angelo, A. A.; Sasai, K.; Kaito, K. Safety Integrated Network Level Pavement Maintenance Decision Support Framework as a Practical Solution in Developing Countries: The Case of Addis Ababa, Ethiopia. *Sustainability* 2023, **15**(11), p. 8884. DOI: https://doi.org/10.3390/su1

[13] Li, H. et al. Application of Analytic Hierarchy Process in Network Level Pavement Maintenance Decision-Making. *International Journal of Pavement Research and Technology* 2018, **11**(4), pp. 345–354. DOI: https://doi.org/10.1016/j.ijprt.2017.09.015.

[14] Liu, H.-C. et al. A Novel Approach for Failure Mode and Effects Analysis Using Combination Weighting and Fuzzy VIKOR Method. *Applied soft computing* 2015, **28**, pp. 579–588. DOI: https://doi.org/10.1016/j.asoc.2014.11.036.

[15] Quezon, E. T. Expert Choice-Based Approach on Analytical Hierarchy Process for Pavement Maintenance Priority Rating Using Super Decision Software in Addis Ababa City, Ethiopia. *American Journal of Civil Engineering and Architecture* 2020, **8**(3), pp. 105–118. DOI: https://doi.org/10.12691/ajcea-8-3-4.

[16] Shapiro, A. F.; Koissi, M.-C. Fuzzy Logic Modifications of the Analytic Hierarchy Process. *Insurance: Mathematics and Economics* 2017, **75**, pp. 189–202. DOI: https://doi.org/10.1016/j.insmat

[17] Ahmed, S.; Vedagiri, P.; Rao, K. K. Prioritization of Pavement Maintenance Sections Using Objective Based Analytic Hierarchy Process. *International Journal of Pavement Research and Technology* 2017, **10**(2), pp. 158–170. DOI: https://doi.org/10.1016/j.ijprt.2017.01.001.

[18] Babashamsi, P. et al. Integrated Fuzzy Analytic Hierarchy Process and VIKOR Method in the Prioritization of Pavement Maintenance Activities. 2016. DOI: https://doi.org/10.1016/j.ijprt.201

[19] Singh, A. P. et al. Pavement Condition Assessment Using Soft Computing Techniques. *International Journal of Pavement Research and Technology* 2018, **11**(6), pp. 564–581. DOI: https://doi.org/10.1016/j.ijprt.2017.12.006.

[20] Obama, K. et al. Disaggregated Hazard Rates Evaluation and Bench-marking. *J. Jpn. Soc. Civ. Eng* 2008, **64**, pp. 857–874.

[21] Kaito, K. et al. Hierarchical Bayesian Estimation of Mixed Hazard Models. *J. Jpn. Soc. Civ. Eng* 2012, **68**, pp. 255–271. DOI: https://doi.org/10.2208/jscejipm.68.255.

[22] Diakoulaki, D.; Mavrotas, G.; Papayannakis, L. Determining Objective Weights in Multiple Criteria Problems: The Critic Method. *Computers & operations research* 1995, **22**(7), pp. 763–770. DOI: https://doi.org/10.1016/0305-0548(94)00059-H.

[23] Mukhametzyanov, I. Specific Character of Objective Methods for Determining Weights of Criteria in MCDM Problems: Entropy, CRITIC and SD. *Decision Making: Applications in Management and Engineering* 2021, **4**(2), pp. 76–105. DOI: https://doi.org/10.31181/dmame21040207

[24] Tsuda, Y. et al. Estimating Markovian Transition Probabilities for Bridge Deterioration Forecasting. *Structural Engineering/Earthquake Engineering* 2006, **23**(2), 241s–256s. DOI: https://doi.org/10.2208/jsceseee.23.241s.

Chapter 6

Optimization of Pavement Maintenance Planning in Cambodia Using a Probabilistic Model and Genetic Algorithm

6.1 Introduction

Effective pavement maintenance plans require a proactive approach to ensure long-term functionality, performance, and cost-efficiency of road infrastructure. Recent advancements in transportation infrastructure management emphasize systematic and optimized maintenance strategies [1]. Consequently, road agencies are increasingly adopting advanced methodologies to prioritize preservation and maintenance strategies, ensuring the longevity and performance of existing pavement networks [2]. For example, optimization models can be used to determine multi-year maintenance and rehabilitation (M&R) strategies by incorporating predictions of future pavement condition [3, 4]. However, pavement deterioration is influenced by traffic loads, environmental conditions, material aging, and construction variability, making accurate long-term plans challenging [5]. Since uncertainties around pavement performance impact the reliability of maintenance, these uncertainties must be considered when making decisions [6].

Traditional pavement management systems (PMSs) at the network level often rely on deterministic deterioration models, assuming fixed inputs and outcomes [7]. Agencies with access to historical and extensive pavement condition data use statistical analysis to identify significant pavement deterioration trends [8]. While deterministic models provide a simplified decision-making framework, they fail to account for inherent uncertainties in pavement performance, resulting in suboptimal maintenance strategies [9]. Hence, a multi-year flexible pavement optimization approach must incorporate deterioration prediction models that explicitly consider uncertainty.

Unlike deterministic models, probabilistic models consider input variability, modeling pave-

ment performance as a range of possible outcomes [10, 11]. The Markov model, a common probabilistic approach, simplifies the assessment of infrastructure deterioration with minimal data requirements [12]. Integrating Bayesian methods into the Markov model enhances parameter estimation, resulting in more robust predictions even with limited data [13]. Building on these predictions, road agencies can employ optimization models to develop proactive and cost-effective maintenance strategies. Compared to traditional rule-based methods, optimization provides a systematic, data-driven framework aimed at maximizing pavement performance while minimizing life cycle costs.

A key challenge in long-term maintenance planning is aligning network-level strategies with project-level maintenance activities [14]. Broad network recommendations based on visible wear may not always align with the requirements of specific pavement sections, causing discrepancies in cost estimation and resource allocation. This is primarily because network-level strategies are generally derived from functional evaluations, which focus on surface conditions such as roughness [15–17]. In addition to functional assessments, recent structural assessments at the network level have been introduced using fast-moving measurement systems such as the Traffic Speed Deflectometer (TSD). However, while TSD provides valuable continuous deflection measurements at traffic speed, it has limitations in reliably evaluating subsurface structural properties, such as the resilient modulus of subgrade, when compared to the Falling Weight Deflectometer (FWD) [18–20]. Therefore, FWD testing remains essential for accurately capturing the underlying structural integrity of the pavement and bridging the gap between network-level strategies and project-level maintenance needs. The comprehensive structural information derived from FWD can then be integrated with an optimization approach that can accommodate various constraints, including budget limitations, resource availability, and project-specific requirements.

The genetic algorithm (GA) is one of the most robust optimization techniques widely used in pavement maintenance programming, as it can handle highly constrained problems and is even capable of addressing multi-objective optimization with relatively low computational effort [21, 22]. Inspired by natural selection and genetics, the GA iteratively refines solutions to achieve optimal or near-optimal outcomes. This method effectively optimizes pavement repair policies within pavement management. Mathew and Isaac proposed a bi-objective optimization framework to maximize performance while minimizing maintenance cost [23]. However, their deterministic prediction model did not account for uncertainties in pavement deterioration. In contrast, Obunguta and Matsushima employed a probabilistic Markov hazard model for deterioration prediction and a greedy algorithm (GrA) for optimization [10]. While computationally efficient, the GrA may result in suboptimal resource allocation. For instance, due to its myopic nature, the algorithm may prioritize roads in the worst condition over those at the fastest rate, or vice versa, depending on immediate decision-making criteria.

In this study, the integration of uncertainty-aware deterioration models is investigated within a multi-year optimization framework for flexible pavements. Specifically, a mixed Markov hazard (MMH) model is employed for probabilistic predictive analytics alongside a genetic algorithm (GA) for optimization. Furthermore, a comparative analysis between the GA and the GrA is conducted to demonstrate the GA' s effectiveness in delivering optimal solutions that outperform those of the GrA. By leveraging this combined approach, the proposed framework enhances PMS by enabling data-driven decision-making that adapts to the dynamic and uncertain nature of road infrastructure, ensuring cost-effectiveness and consistency.

6.2 Pavement management system in Cambodia

As of 2022, Cambodia' s road network comprises a system of national and provincial roads, as illustrated in Figure 6.1. The national roads (NRs) span 7415.09 km, including 9 primary (one-digit) and 72 secondary (two-digit) routes [24]. The provincial roads (PR) cover 12,380.04 km across 750 routes, including tertiary and local roads. The surfaces of one-digit NRs are typically constructed using asphalt concrete (AC), a mixture of asphalt binder and aggregates that provides a smooth and durable riding surface. In contrast, the surfaces of two-digit NRs and PRs, which are less costly and quicker to construct, are generally built using double bituminous surface treatment (DBST). This method involves spraying a bituminous binder over a prepared base layer, followed by the application of aggregates, typically 19 mm and 12 mm in size. Looking ahead, the Royal Government of Cambodia (RGC) has outlined plans to expand the national and provincial road network to 21,000 km by 2033 and 25,412 km by 2050 [25].

The RGC, through the Ministry of Public Works and Transport (MPWT), has been actively working to develop a more comprehensive and systematic approach to road asset management, aiming to optimize the use of its limited resources [26]. Currently, short-term maintenance planning, particularly the three-year rolling maintenance plan, follows a pavement condition policy that prioritizes the most severely damaged road sections.

Road condition data are primarily collected within sub-regions through visual inspections conducted routinely by the provincial Department of Public Works and Transport (DPWT), which assesses harmful surface defects and damage severity. In addition, the MPWT' s road data collection unit conducts functional evaluations of pavement conditions nationwide using the Dynamic Response Intelligent Monitoring System (DRIMS). This involves the use of a survey that mainly measures IRI and is typically carried out every one to two years. For structural evaluation, the FWD is used to assess pavement strength; however, due to high cost and time requirement, FWD testing is conducted less frequently, often on a one-off basis for specific projects. Despite these efforts, maintenance interventions are often determined through subjective decision-making by engineers, resulting in a reactive rather than proactive

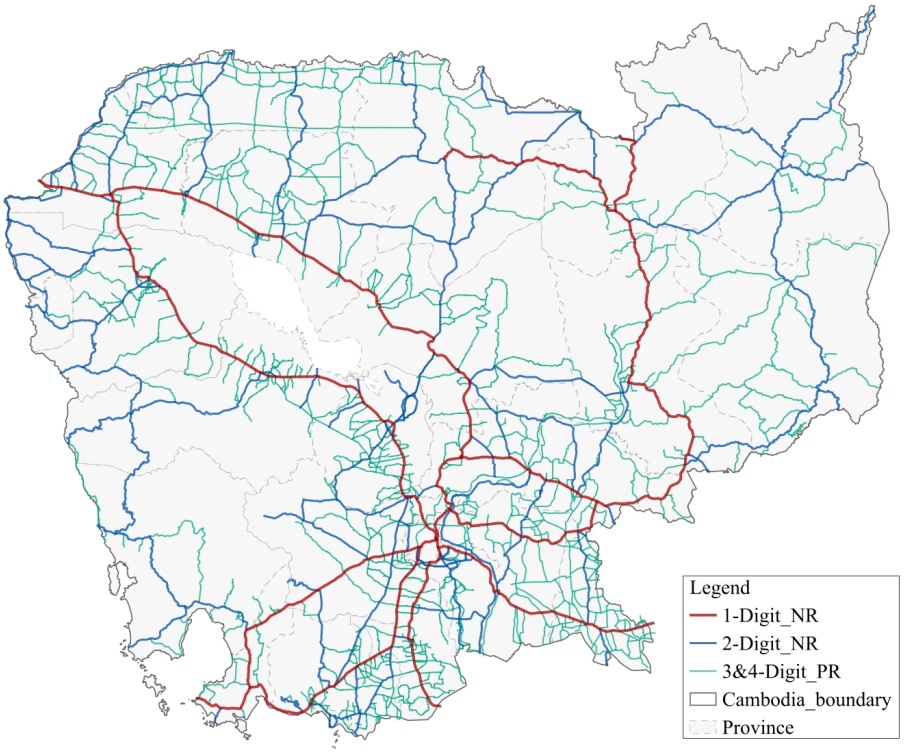


Figure 6.1: Road networks in Cambodia.

maintenance strategy.

The Road Asset Management Project II (RAMP II) was launched to strengthen asset management practices and improve planning through simplified models [27]. This project formulates short-term and medium-term maintenance programs by incorporating a Road Management Decision Support (RMDS) system, such as HDM-4, to evaluate road investment and maintenance needs. However, the application of HDM-4 poses challenges due to its high operation costs. Furthermore, it requires a broad variety of input data and can become data-intensive when detailed calibration is needed to align the model with a country' s specific conditions [28]. This process is not only time-consuming but also costly, particularly due to the need for comprehensive data collection and analysis.

6.3 Methodology

6.3.1 Decision process for repair action selection

Implementing multi-year maintenance planning involves accounting for various maintenance types aligned with specific pavement performance states [29]. The International Roughness Index (IRI) is a widely used metric for ride quality evaluation and is promoted under Sustainable Development Goal (SDG) 9 [30]. Predicting this indicator over time is crucial for effective

implementation of maintenance planning [31–33]. To minimize discrepancies between planned budget allocations at the network level and cost estimates at the project level, this study integrates two evaluation approaches: the assessment of surface condition based on the IRI state rating and the evaluation of sublayer bearing capacity using deflection bowl parameters (DBPs) derived from the FWD. This combined approach ensures a cost-effective and well-informed maintenance strategy, addressing both surface functional deficiencies and underlying structural issues.

The DBPs, comprising the Base Layer Index (BLI) (also known as the Surface Curvature Index, SCI), the Middle Layer Index (MLI) (also called the Base Curvature Index, BCI), and the Lower Layer Index (LLI) (sometimes referred to as the Base Damage Index, BDI), offer insight into the structural health of different pavement layers. Specifically, BLI indicates the strength of the combined surface and base course layers, MLI reflects the strength of the sub-base course layer, and LLI represents the strength of the combined selected and subgrade layer [34]. These indices, expressed in micron (µm), are calculated using the deflections measured at radial distances of 0, 300, 600, and 900 mm from the FWD load center, denoted as D_0, D_{300}, D_{600}, and D_{900}, respectively:

$$BLI = D_0 - D_{300} \tag{6.1}$$

$$MLI = D_{300} - D_{600} \tag{6.2}$$

$$LLI = D_{600} - D_{900} \tag{6.3}$$

FWD testing was conducted with a 50 kN impulse load and a 300 mm diameter loading plate. For AC pavements, since the surface course is highly sensitive to temperature, deflection values were corrected to a standard reference temperature of 20 °C to account for the influence of temperature on the stiffness of the asphalt layer [35, 36]. The empirical temperature correction model proposed by Březina et al. was applied in this study for practical implementation [37]. In contrast, for pavements with a thin bituminous surfacing layer over a granular base, such as DBST pavements, the bituminous layer has minimal influence on the overall structural response measured by the FWD [38, 39]. Because the pavement' s bearing capacity is primarily governed by the underlying granular layers and subgrade, deflections on DBST pavement in this study were assumed to be temperature-insensitive, and no temperature correction was applied.

The maintenance decision is primarily determined by the IRI state rating, and the IRI state is updated following the application of a specific maintenance type, as shown in Table 6.1. To

Table 6.1: IRI condition rating, maintenance requirement, and IRI state updates.

IRI (m/km)	State Rating	Maintenance Type	Maintenance Index	State Update
≤ 2	1	No Maintenance	1	1
2 – 3	2	Preventive Maintenance	2	1
3 – 4	3	Corrective Maintenance	3	2
4 – 5	4	Restorative Maintenance	4	2
5 – 6	5	Rehabilitation	5	1
> 6	6	Reconstruction	6	1

Table 6.2: Structural benchmark criteria. Adapted from [40], with permission from CRC Press, Talyor & Francis Group, 2025.

Structural Condition	**AC Pavement**			**DBST Pavement**		
	BLI **(μm)**	MLI **(μm)**	LLI **(μm)**	BLI **(μm)**	MLI **(μm)**	LLI **(μm)**
Sound	<140	<105	<45	<320	<150	<50
Warning	140–280	105–175	45–80	320–480	150–240	50–100
Severe	>280	>175	>80	>480	>240	>100

provide an optimal maintenance strategy, sublayer structural conditions were also implemented, represented by the DBPs: BLI, MLI, and LLI (see Table 6.2). These structural conditions were then classified into different groups based on combinations of these DBPs' ratings (see Table 6.3) and were updated after maintenance based on the treatment applied. Each rating system provides a corresponding maintenance type and index, ranging from 1 (No Maintenance) to 6 (Reconstruction). The final maintenance action is guided by the higher maintenance index derived from the two evaluation systems. For instance, if the IRI state rating suggests Preventive Maintenance (Index 2) but the DBP rating indicates Corrective Maintenance (Index 3), the latter decision is prioritized due to its higher index. This ensures that the most critical issues, whether functional or structural, are addressed promptly and effectively.

6.3.2 Model framework

The framework of this study enables strategic budget allocation, prioritization of critical maintenance projects, and proactive road management to mitigate costly emergency repairs, as illustrated in Figure 6.2. It integrates a probabilistic deterioration prediction model with GA optimization, enabling data-driven and cost-effective maintenance. The Markov model, a widely used probabilistic approach, predicts pavement degradation over time by capturing the uncer-

Table 6.3: Structural classification, maintenance requirement, and structural state updates.

Deflection Bowl Parameters			Structural Group		**Maintenance Action**		Structural Group Update	
BLI	**MLI**	**LLI**	**AC**	**DBST**	**Type**	**Index**	**AC**	**DBST**
Sound	Sound	Sound	1	28	No Maintenance	1	1	28
Sound	Sound	Warning	2	29	Preventive Maintenance	2	2	29
Sound	Sound	Severe	3	30	Preventive Maintenance	2	3	30
Sound	Warning	Sound	4	31	Preventive Maintenance	2	4	31
Sound	Warning	Warning	5	32	Preventive Maintenance	2	5	32
Sound	Warning	Severe	6	33	Corrective Maintenance	3	6	33
Sound	Severe	Sound	7	34	Preventive Maintenance	2	7	34
Sound	Severe	Warning	8	35	Corrective Maintenance	3	8	35
Sound	Severe	Severe	9	36	Reconstruction	6	1	28
Warning	Sound	Sound	10	37	Preventive Maintenance	2	10	37
Warning	Sound	Warning	11	38	Corrective Maintenance	3	11	38
Warning	Sound	Severe	12	39	Restorative Maintenance	4	3	30
Warning	Warning	Sound	13	40	Corrective Maintenance	3	13	40
Warning	Warning	Warning	14	41	Rehabilitation	5	2	29
Warning	Warning	Severe	15	42	Reconstruction	6	1	28
Warning	Severe	Sound	16	43	Rehabilitation	5	1	28
Warning	Severe	Warning	17	44	Rehabilitation	5	2	29
Warning	Severe	Severe	18	45	Reconstruction	6	1	28
Severe	Sound	Sound	19	46	Restorative Maintenance	4	1	28
Severe	Sound	Warning	20	47	Restorative Maintenance	4	2	29
Severe	Sound	Severe	21	48	Reconstruction	6	1	28
Severe	Warning	Sound	22	49	Rehabilitation	5	1	28
Severe	Warning	Warning	23	50	Rehabilitation	5	2	29
Severe	Warning	Severe	24	51	Reconstruction	6	1	28
Severe	Severe	Sound	25	52	Rehabilitation	5	1	28
Severe	Severe	Warning	26	53	Rehabilitation	5	2	29
Severe	Severe	Severe	27	54	Reconstruction	6	1	28

tainty and variability caused by various influencing factors. Meanwhile, GA is well-suited for exploring large solution spaces, making it effective for optimizing multi-year maintenance planning by maximizing cost-effectiveness within annual budget constraints.

As shown in Figure 6.2, pavement deterioration is primarily governed by the structural condition of the pavement, traffic loading, and annual rainfall. Higher traffic loading and greater rainfall intensity accelerate the growth of the IRI, leading to faster pavement deterioration and a shorter service life. In contrast, pavements with high structural stiffness (e.g., lower DBPs) exhibit slower deterioration. The relative influence of each factor is quantified through the estimated unknown parameters derived from the MMH model, presented in the Results Section. Specifically, the structural condition reflects the pavement' s bearing capacity between the first

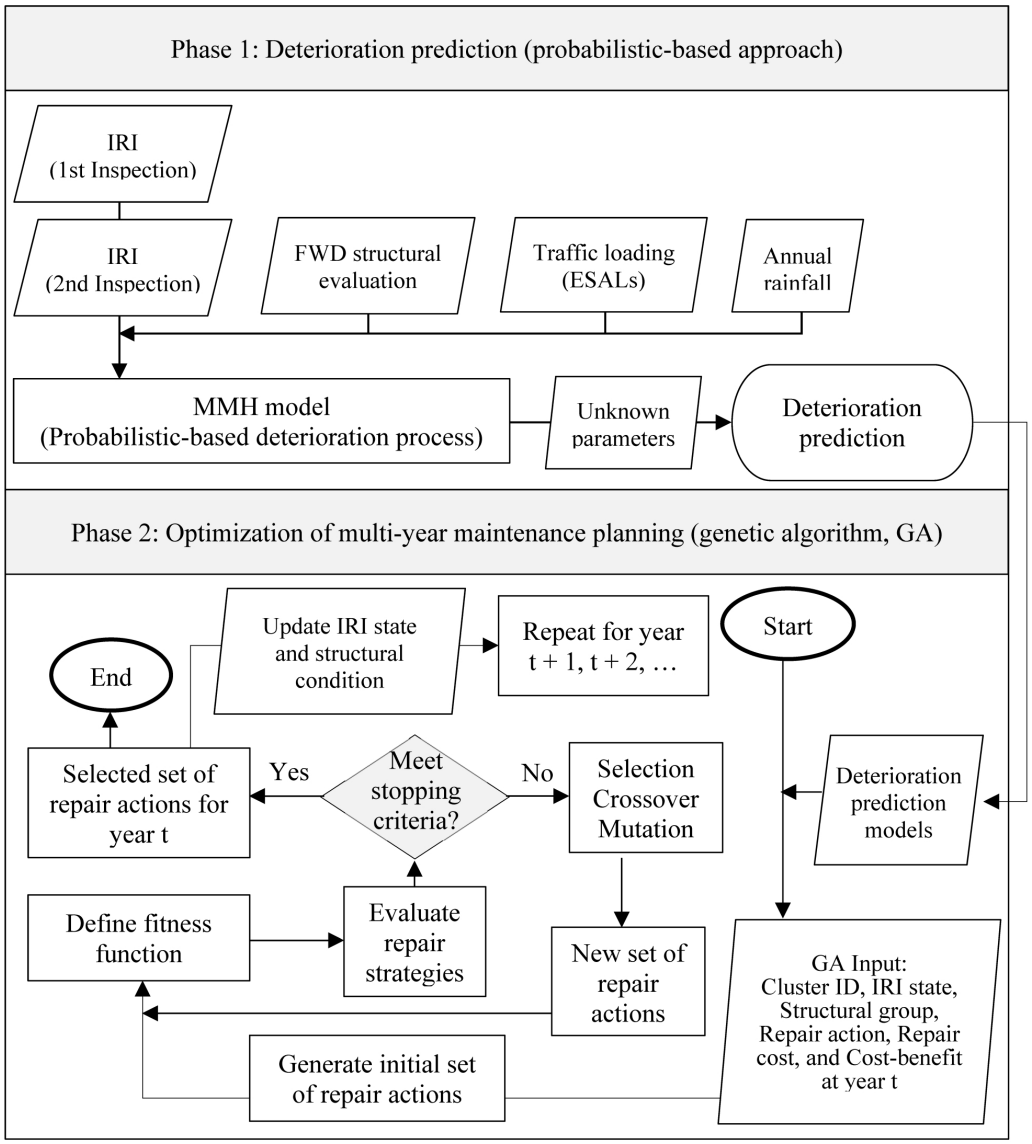


Figure 6.2: Flowchart of the model framework.

and second IRI inspections; traffic loading represents the cumulative ESALs; and annual rainfall indicates the average rainfall intensity over the same inspection period.

For the empirical study, IRI measurements were collected twice, in 2022 and 2023, across 6085 road sections, covering both AC and DBST pavements, along with FWD testing on the same sections. The cumulative ESALs for 2022–2023 were calculated by converting daily vehicle counts into a standard axle load of 80 kN [41]. The average annual rainfall for each road section was derived from the mean annual rainfall recorded between 2000 and 2015, based on gauged observations obtained from the Asian Precipitation—Highly-Resolved Observational Data Integration Towards Evaluation (APHRODITE) dataset.

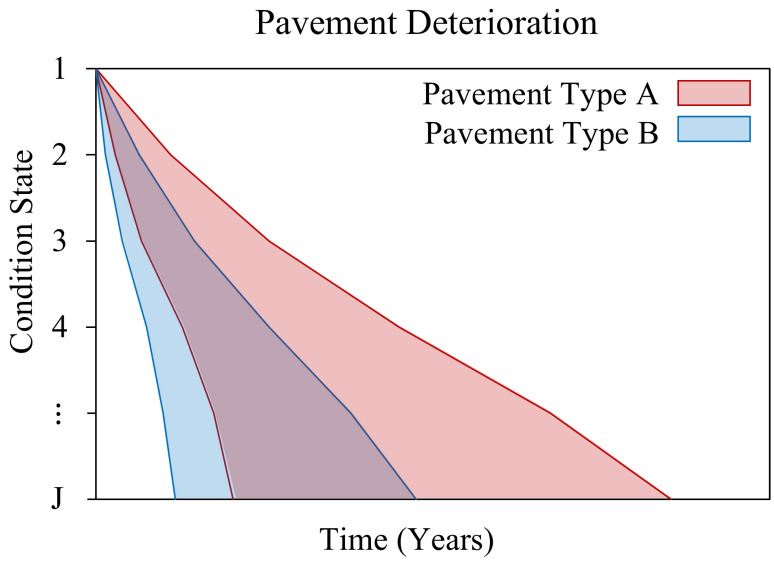


Figure 6.3: Illustration of pavement deterioration.

6.3.3 Deterioration prediction based on mixed Markov hazard (MMH) model

The mixed Markov hazard (MMH) model addresses the Markov deterioration process by incorporating a multi-stage exponential hazard framework with a heterogeneity factor [42]. The model follows survival analysis principles and captures heterogeneous deterioration patterns across different infrastructure groups (see Figure 6.3), with hazard rates evolving according to an underlying Markov process.

In this context, IRI is discretized into distinct condition states, denoted as $i = 1, 2, \cdots, J$, with $i = 1$ as the best, and $i = J$ ($J = 6$, as shown in Table 6.1, as the worst, requiring reconstruction. Condition state changes between two consecutive inspections are represented by Markov transition probabilities (MTPs), denoted as π_{ij}. The model considers no repair works between inspections, resulting in zero probabilities for transitions to better states. All procedures and derivations of the estimated hazard rates and transition probabilities follow the methodology described in [42]. The transition probability between inspections at τ_A and τ_B can be expressed as follows:

$$\Pr[h(\tau_B) = j \mid h(\tau_A) = i] = \pi_{ij} \tag{6.4}$$

$$\Pi = \begin{bmatrix} \pi_{11} & \cdots & \pi_{1J} \\ \vdots & \ddots & \vdots \\ 0 & \cdots & \pi_{JJ} \end{bmatrix} \tag{6.5}$$

Survival analysis principles, in association with Markov processes, were incorporated and further developed in the following steps to model the deterioration process of infrastructure [12]. This process is characterized by a hazard function, $\lambda_i(y_i^k)$, which represents the instantaneous risk of transitioning from state i to $i+1$. The hazard function is defined as:

$$\lambda_i(y_i^k) = \frac{f_i(y_i^k)}{\tilde{F}_i(y_i^k)} \tag{6.6}$$

Where $f_i(y_i^k)$ is the probability density function, and $\tilde{F}_i(y_i^k)$ is the survival function, representing the probability of remaining in the current state beyond time y_i^k. The survival function is given by:

$$\tilde{F}_i(y_i^k) = \text{Prob}\left[\zeta_i \in (y_i^k,\, y_i^k + dy_i^k) \,\middle|\, \zeta_i \geq y_i^k\right] = 1 - F_i(y_i^k) \tag{6.7}$$

Where $F_i(y_i^k)$ is the cumulative distribution function, given by:

$$F_i(y_i^k) = \int_0^{y_i^k} f_i(\zeta_i)\, d\zeta_i \tag{6.8}$$

Assuming the hazard function follows an exponential distribution, the hazard rate becomes constant due to the memoryless property. Given $\lambda_i(y_i^k) = \theta_i^k$, the survival function can be written as:

$$\tilde{F}_i(y_i^k) = e^{-\theta_i^k y_i^k} \tag{6.9}$$

To capture the variability in deterioration across different infrastructure groups, a heterogeneity factor ϵ^k, assumed to follow a gamma distribution, is incorporated. The survival function then becomes:

$$\tilde{F}_i(y_i^k) = e^{-\bar{\varepsilon}^k \tilde{\theta}_i^k y_i^k} \tag{6.10}$$

Where ϵ^k represents the mean value of the heterogeneity factor. Therefore, the probability of condition state changes can be determined as follows:

$$\pi_{ii} = e^{-\bar{\varepsilon}^k \tilde{\theta}_i^k z^k} \tag{6.11}$$

For π_{ij}, where $j > i$, the transition probability is:

$$\pi_{ij} = \sum_{l=i}^{j} \left[\prod_{\substack{m=i \\ m \neq l}}^{l-1} \frac{\tilde{\theta}_m^k}{\tilde{\theta}_m^k - \tilde{\theta}_l^k} \right] e^{-\bar{\varepsilon}^k \tilde{\theta}_l^k z^k} = \sum_{l=i}^{j} \psi_{ij}^l(\tilde{\theta}^k) e^{-\bar{\varepsilon}^k \tilde{\theta}_l^k z^k} \tag{6.12}$$

Where $\psi_{ij}^l(\tilde{\theta}^k) = \prod_{\substack{m=i \\ m \neq l}}^{j-1} \frac{\tilde{\theta}_m^k}{\tilde{\theta}_m^k - \tilde{\theta}_l^k}$, and $\tilde{\theta}^k = (\tilde{\theta}_1^k, \ldots, \tilde{\theta}_{J-1}^k)$.

Finally, the transition probability π_{iJ} (transitioning to the worst condition state J) is given by:

$$\pi_{iJ} = 1 - \sum_{j=i}^{J-1} \pi_{ij} \tag{6.13}$$

The hazard rate θ_i^k is modeled as a joint probability of factors influencing deterioration. It can then be written as a function of explanatory variables that address these factors. Hence, it can be expressed as:

$$\theta_i^k = f(\bar{\varepsilon}^k; x^k; \beta_i) = \bar{\varepsilon}^k \tilde{\theta}_i^k = \bar{\varepsilon}^k e^{\beta_{i,0} + \sum_{m=1}^{M} \beta_{i,m} x_m^k} \tag{6.14}$$

Where β_i is the baseline coefficient, and $\beta_{i,m}$ represents the coefficients of the explanatory variables contributing to the deterioration rate from state i to $i+1$. These coefficients are the unknown parameters that need to be estimated.

The life expectancy (LE) for state i remaining in state i until reaching state $i+1$ can be determined as follows:

$$LE_i^k = \int_0^\infty \tilde{F}_i(y_i^k)\, dy_i^k = \int_0^\infty e^{-\theta_i^k y_i^k}\, dy_i^k = \frac{1}{\theta_i^k} \tag{6.15}$$

The predicted lifespan of a road section is the summation of the life expectancy of each condition state. Using Bayes' theorem, the posterior distribution of the model parameters can be derived by combining the assumed prior distribution and the likelihood function. The posterior distribution for the transition probability matrix can be expressed as:

$$\pi(\omega \mid \bar{\xi}) = \frac{L(\omega \mid \bar{\xi})\, \pi(\omega)}{\int L(\omega \mid \bar{\xi})\, \pi(\omega)\, d\omega} \quad \text{or} \quad \pi(\omega \mid \bar{\xi}) \propto L(\omega \mid \bar{\xi})\, \pi(\omega) \tag{6.16}$$

Where $\bar{\xi} = (\bar{\delta}_{ij}^k, \bar{z}^k, \bar{x}^k)$ represents the field survey data ($\bar{z}^k$ and $\bar{x}^k$) and a dummy variable $\bar{\delta}_{ij}^k$, while $\omega = (\beta_i, \phi, \varepsilon^k)$ represents the estimated parameters. ϕ is an unknown parameter associated with ε^k in the Gamma distribution.

To avoid explicit mathematical derivations, the Metropolis–Hastings (M-H) algorithm is used in this study, a popular Markov Chain Monte Carlo (MCMC) method, to sample the values of the parameter directly from the posterior distribution under sufficient iterative processes, ensuring convergence [43].

It is important to note that, in this study, only the IRI state is predicted over time using the MMH model that incorporates influencing factors. However, the condition of DBPs is not modeled dynamically over time. Instead, DBPs are only updated following maintenance activities, where the applied repair action results in a revised structural condition. This limitation arises because repeated FWD testing is often impractical due to high operational costs. As a result, it is generally not possible to predict changes in the condition of DBPs via the MMH model, similar to IRI, which requires at least two time-series inspections.

6.3.4 GA optimization

The optimization technique used in this study to implement the maintenance strategy is a metaheuristic approach, specifically the GA. The GA is a type of evolutionary algorithm (EA) that simulates natural selection and genetic processes to efficiently search for optimal solutions [44]. The GA uses rules to find solutions efficiently rather than exhaustively searching every possibility. Since it relies on probability and approximation, the GA is not guaranteed to always find the global optimum solution. However, with proper tuning of its operations, it can find solutions that are very close to optimal and suitable for practical use [45]. Moreover, potential limitations may occur, such as high computation demand for very large networks (e.g., tens of thousands of segments); in such cases, alternative GA configurations or hybrid approaches may be required to maintain computational feasibility.

In this study, because the application involves a large road network with numerous sections, the GA begins by deterministically generating an initial population of 1000 genomes to ensure convergence toward a high-quality solution. A larger population size generally increases the likelihood of obtaining a more optimal solution, but also leads to higher computational demand. Different population sizes may be tested to identify the most efficient balance between computational effort and solution quality. Each genome encodes a maintenance decision using a chromosome representation, where individual genes indicate whether a set of road segments is selected for maintenance, as shown in Figure 6.4. The fitness of each genome is then evaluated based on the total cost-effectiveness, incorporating a penalty if the budget constraint is exceeded. Offspring are produced through three primary mechanisms: selection, crossover, and mutation. Tournament selection is employed to choose the fitness individuals for reproduction, while crossover is performed using a two-point method with a crossover rate (CR) of 0.8. Mutation is applied using a bit-flip function with a mutation rate (MR) of 0.05, introducing genetic

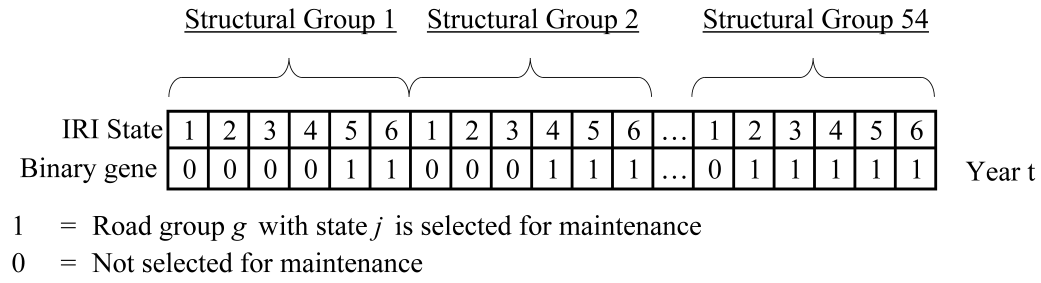


Figure 6.4: GA chromosome encoding.

diversity. If an offspring solution demonstrates higher fitness than the parent population, it replaces the weaker individuals. This iterative process continues for 500 generations until an optimal selection of projects is identified, at which point the stopping criteria prevent further evolution. The convergence of the algorithm is tracked and visualized, ensuring that the best solution meets the budgetary constraints while maximizing total effectiveness.

6.4 Benefit optimization

While some studies focus on minimizing life cycle cost (LCC) for maintenance planning, others adopt a cost–benefit analysis approach aimed at maximizing the effectiveness of repair actions under budget constraints [29, 46]. In this study, an optimized maintenance decision-making process is developed by evaluating all road sections based on their structural classification and current IRI condition state to determine the most beneficial repair strategy.

The effectiveness of maintenance is represented by the maintenance benefit area, defined as the shaded region between the pavement deterioration curves before and after repair (see Figure 6.5). In this study, the deterioration curves are modeled using third-order polynomial regression based on MMH model predictions. Within this framework, applying a repair action restores the IRI condition state to state 2 for repair actions 3 and 4, and to state 1 for all other repair actions (as indicated in Table 6.1). Details of repair strategies are summarized in Table 6.4. The depth of pavement removal and replacement determines the extent of structural restoration. For example, restorative maintenance upgrades the BLI to Sound condition, while rehabilitation improves both the BLI and MLI. The layers not targeted by the repair retain their existing condition. The combined improvement in BLI, MLI, and LLI elevates the overall structural classification to a stiffer group (as shown in Table 6.3).

The proposed optimization model in this study aims to achieve two primary objectives: maximizing the improvement in pavement conditions and minimizing maintenance costs. Maintenance costs are determined by multiplying the unit cost of each repair strategy by the area of the segments in each structural group to which it is applied. These two objectives are combined into a single metric, the cost–benefit (CB) value, which quantifies the benefit achieved

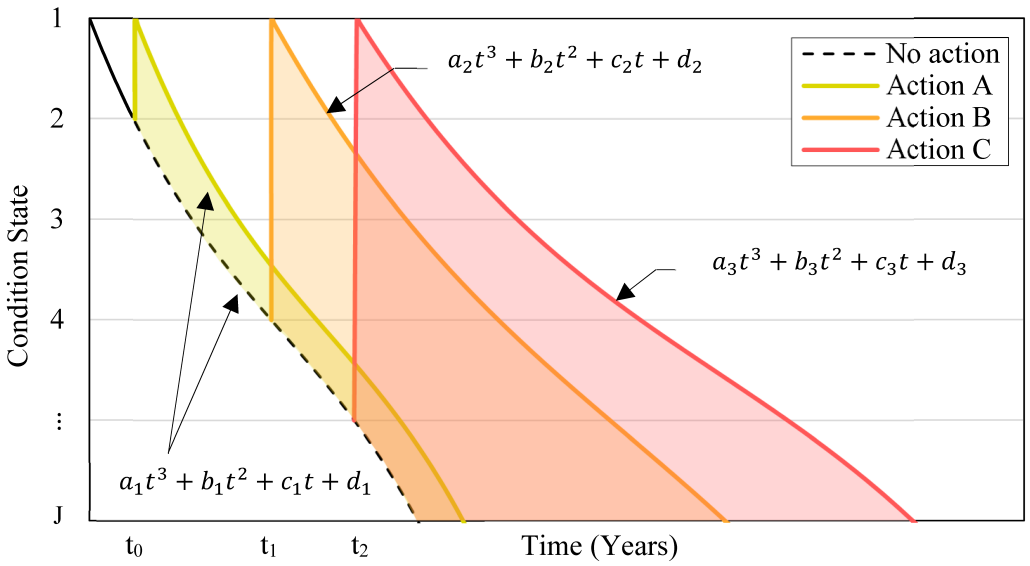


Figure 6.5: Effectiveness of maintenance activities.

per dollar spent.

The CB is calculated by dividing the benefit area by the total cost of the repair action, serving as the final measure of maintenance efficiency. The CB calculation for pavement sections in group g under repair action a at year t is computed as follows:

$$CB_{a,g,t} = \frac{\int_{t_0}^{t_f} [S_{a,g^*}(t) - S_{0,g}(t)]\, dt}{UnitCost_a \times Area_g} \tag{6.17}$$

Here, the $UnitCost_a$ represents the unit cost of repair action a (see Table 6.5), while $Area_g$ denotes the total area of road sections in group g. The function $S_{a,g^*}(t)$ describes the deterioration curve after applying action a, which restores the IRI condition state and updates the structural group to g^*. In contrast, $S_{0,g}(t)$ represents the deterioration curve of group g before maintenance.

The optimal cost–benefit allocation of repair treatments for a road network in year t is determined by maximizing the cumulative cost–benefit of selected maintenance strategies. Instead of directly selecting specific repair actions, the optimization model identifies pavement sections for maintenance, represented by the binary variable $x_{s,t}$. Although the repair action a is not explicitly treated as a decision variable, it evolves dynamically over time. The choice of repair action for a given section in year t depends on the pavement' s condition, specifically the structural condition of the sublayer, which is influenced by past maintenance decisions, and the IRI condition state, which deteriorates over time as predicted by the MMH model. For instance, if a section was maintained in year $t-1$, it may require a different (or no) intervention in year t. The objective function for year t is formulated as follows:

Table 6.4: Repair details by maintenance type.

Pavement Type	**Maintenance Type**	**Repair Detail**	**Action**
DBST	No Maintenance	Do nothing	1
	Preventive Maintenance	Crack sealing, patching, or DBST resurfacing	2
	Corrective Maintenance	5 cm milling, and DBST surfacing	3
	Restorative Maintenance	Remove 20 cm, place new 20 cm granular base, and DBST surfacing	4
	Rehabilitation	Remove 45 cm, place 25 cm granular sub-base + 20 cm granular base, and DBST surfacing	5
	Reconstruction	Remove 90 cm, place 45 cm subgrade + 25 cm granular sub-base + 20 cm granular base, and DBST surfacing	6
AC	No Maintenance	Do nothing	1
	Preventive Maintenance	Crack sealing, patching, or 2.5 cm AC overlay	2
	Corrective Maintenance	Leveling/patching, and 5 cm AC overlay	3
	Restorative Maintenance	Mill 20 cm by adding cement and asphalt emulsion, and 7 cm AC surfacing	4
	Rehabilitation	Remove 60 cm, place 25 cm granular sub-base + 25 cm granular base, and 10 cm AC surfacing	5
	Reconstruction	Remove 100 cm, place 40 cm subgrade + 25 cm granular sub-base + 25 cm granular base, and 10 cm AC surfacing	6

$$\text{Maximize: } \sum_{s=1}^{S} (CB_{s,t} \times x_{s,t}) \tag{6.18}$$

subject to budget constraint:

$$\sum_{s=1}^{S} (UnitCost_{s,t} \times Area_{s,t} \times x_{s,t}) \leq Budget_t, \quad x_{s,t} \in \{0, 1\} \tag{6.19}$$

Where $x_{s,t}$ is the decision that equals 1 if a given section s is selected for maintenance and 0 otherwise. Equation 6.19 ensures that the total expenditure on selected maintenance projects does not exceed the allocated budget for year t.

Table 6.5: Maintenance unit cost.

Maintenance Type	Action	Unit Cost (USD/m^2)	
		AC	**DBST**
No Maintenance	1	0.0	0.0
Preventive Maintenance	2	10.0	7.0
Corrective Maintenance	3	23.5	8.5
Restorative Maintenance	4	35.0	15.0
Rehabilitation	5	45.0	23.5
Reconstruction	6	50.0	30.0

6.5 Results

6.5.1 MMH model estimation result

Table 6.6 presents the results of parameter estimation that involved a total of 40,000 iterations, with the first 20,000 iterations discarded as burn-in samples to ensure convergence, and the remaining 20,000 iterations used for estimation. The heterogeneity factor ε^k captures the deterioration characteristics of different pavement types, AC and DBST. AC pavement ($\varepsilon^k = 0.732 < 1$) deteriorates at a slower rate, whereas DBST pavement ($\varepsilon^k = 1.206 > 1$) exhibits a faster deterioration rate. Furthermore, all factors, including pavement bearing capacities, traffic loading, and rainfall, demonstrate significant contributions to pavement deterioration. Among these, structural parameters show the most substantial impact, particularly the BLI, which reflects the strength of the top layers subject to high vehicle tire pressure. The convergence of the estimated parameters, β_i, is assessed using Geweke' s z-score in parentheses, with values within $[-1.96, 1.96]$ indicating convergence.

Using ε^k and β_i along with the average values of bearing capacities (BLI, MLI, and LLI), ESAL, and rainfall, the benchmark hazard rate can be computed using Equation 6.14. This allows for the estimation of the life expectancy of each condition state, enabling the visualization of the deterioration trend, as illustrated in Figure 6.6.

To account for the diverse deterioration characteristic of pavement and enhance the assessment of maintenance and repair effectiveness through benefit area calculations, pavement is categorized into distinct structural groups in this study. These groups are defined based on the ratings of BLI, MLI, and LLI, which are classified into three condition levels: Sound, Warning, and Severe, as indicated in Table 6.2. Given this classification, pavements consisting of AC and DBST can be divided into 54 structural groups: 27 for AC and 27 for DBST (see Table 6.3). By incorporating the average values of ESAL and rainfall, the deterioration

Table 6.6: Parameter estimation through Bayesian MMH model.

Condition State	ε^k		Hazard Rate θ_i	Parameter Estimates					
	AC	DBST		Constant $\beta_{i,0}$	BLI $\beta_{i,1}$	MLI $\beta_{i,2}$	LLI $\beta_{i,3}$	ESAL $\beta_{i,4}$	Rainfall $\beta_{i,5}$
$1 \rightarrow 2$	0.732	1.206	0.837	-0.75 (3.18)	1.31 (-2.87)	–	0.72 (-3.62)	–	–
$2 \rightarrow 3$			0.371	-1.56 (-1.14)	0.18 (0.85)	0.44 (0.00)	0.30 (-0.12)	0.79 (0.86)	0.42 (1.46)
$3 \rightarrow 4$			0.559	-2.05 (1.09)	1.15 (-0.88)	0.87 (0.10)	0.47 (-1.03)	1.65 (-0.84)	1.54 (0.57)
$4 \rightarrow 5$			0.283	-1.59 (-0.36)	0.46 (-0.15)	0.38 (-0.88)	0.35 (0.19)	–	0.06 (1.75)
$5 \rightarrow 6$			0.454	-1.40 (-2.38)	1.34 (1.57)	0.31 (0.91)	0.12 (0.64)	0.33 (1.20)	–

Note:

- Geweke' s Z-score in parentheses.
- [–] indicates inverted relationship variables.

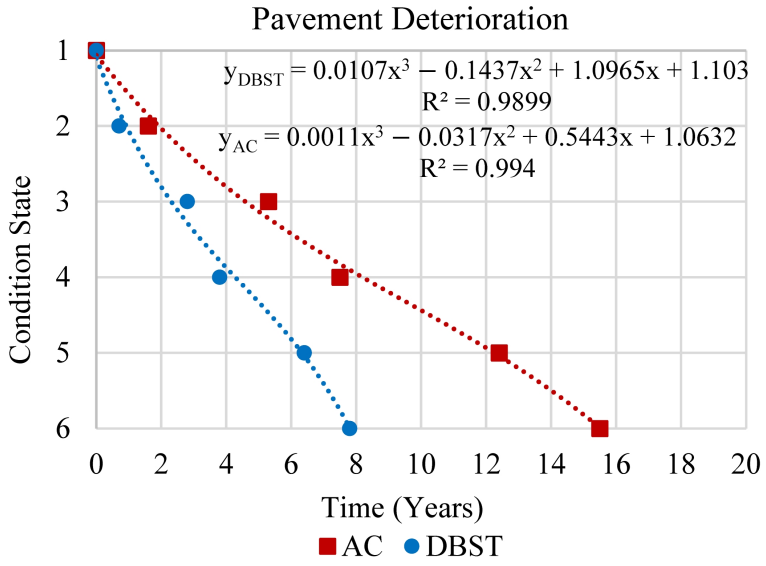


Figure 6.6: Pavement deterioration curves.

curves for these structural groups can be systematically determined and visualized, as shown in Figure 6.7. AC pavements with Sound ratings for *BLI*, *MLI*, and *LLI*, representing the stiffest structures, have an expected service life of 23.8 years. In contrast, DBST pavements rated Severe in all three indices, representing the weakest structural category, have a projected service life of only 3.2 years. These outcomes demonstrate that even when survey data are limited, as is often the case in developing countries, the Markov model can generate reliable deterioration predictions. By explicitly incorporating uncertainty in the deterioration process, the model avoids the need for decades of historical records, while still providing robust and practical estimates of pavement service life.

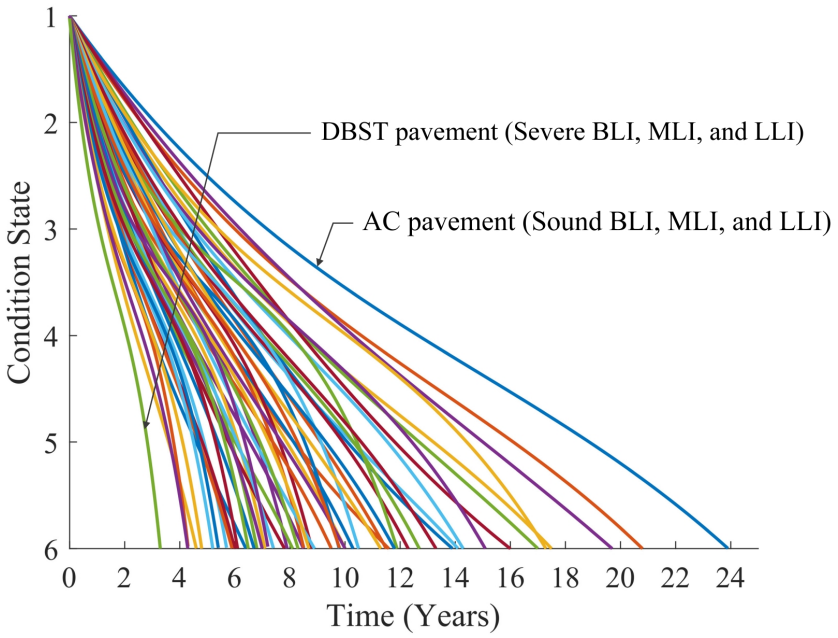


Figure 6.7: Deterioration curves through various structural groups (1–54).

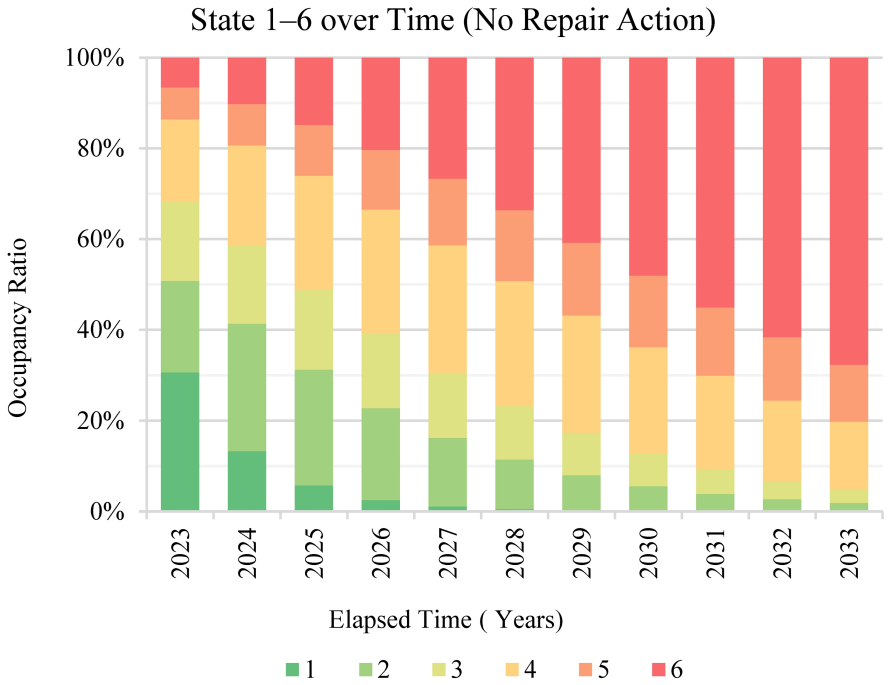


Figure 6.8: Condition state evolution of the network with no repairs.

The evolution of pavement performance over time can be expressed as $S(t_n) = S(t_0)[\Pi(Z)]^n$, where $S(t_0)$ represents the initial condition state of the road network and n denotes the number of time intervals. In this study, the initial condition states are derived from the most recent IRI inspection results. Figure 6.8 illustrates the condition state distribution based on the estimated transition probability matrix, highlighting the natural degradation over a 10-year period in the absence of maintenance interventions.

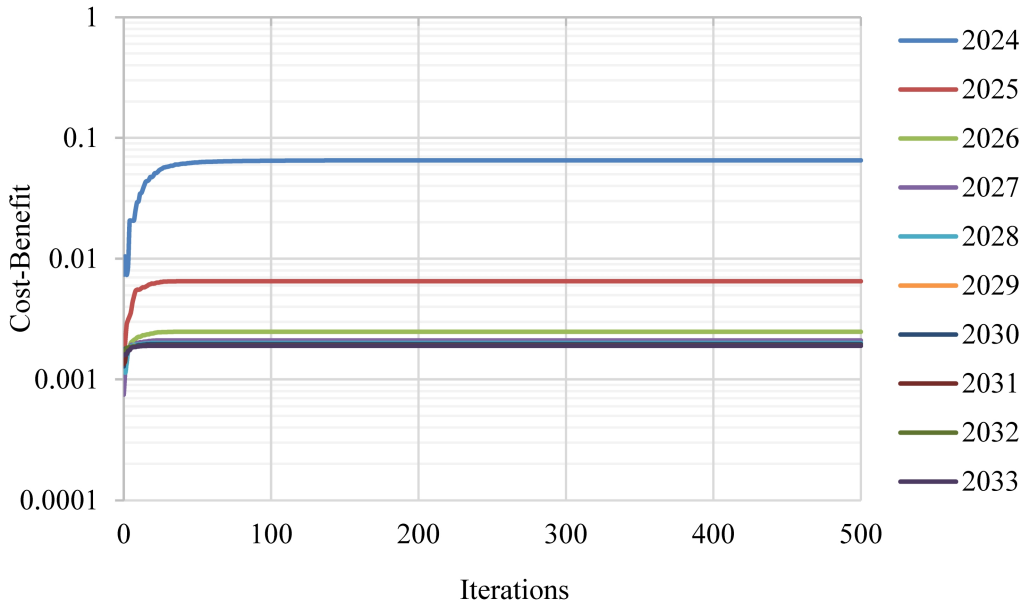


Figure 6.9: GA iteration process ($18M/Year Scenario).

6.5.2 GA optimization result

This study optimizes the selection of pavement sections for maintenance while adhering to annual budget constraints. Multiple budget scenarios were examined over a 10-year period (2024–2033) to assess their impact on network pavement conditions. The analyzed budget allocation included USD 12 million, USD 15 million, USD 18 million, USD 21 million, USD 24 million, and USD 27 million per year. This case study focuses on Cambodia' s road network, which comprises approximately 275.7 km of AC pavements and 332.7 km of DBST pavements. The GA identifies the optimal allocation of maintenance treatments that maximizes the network-wide cost–benefit ratio under each of these budget scenarios. To evaluate the efficiency of the optimization process, it is essential to use a diagram that visualizes the convergence of the solution. The performance plots in Figure 6.9 illustrate the USD 18 million-per-year scenario, demonstrating that the GA model successfully converged to optimal solutions within 500 iterations.

Figure 6.10 presents the impact of six budget scenarios examined over a 10-year period (2024–2033) on the progress of network performance. The analysis indicates that as the annual budget allocation increases, the overall condition of the road network improves. When the annual budget reaches USD 18 million, the percentage of roads in condition state 6 stabilizes below 10%.

To effectively assess the impact of different budget levels on the network performance, the overall or average IRI condition state can be calculated over time for each budget scenario in relation to a predefined performance threshold. In this study, condition state 3 (IRI $\leq$ 4 m/km) is set as an acceptable criterion that the road network should maintain throughout

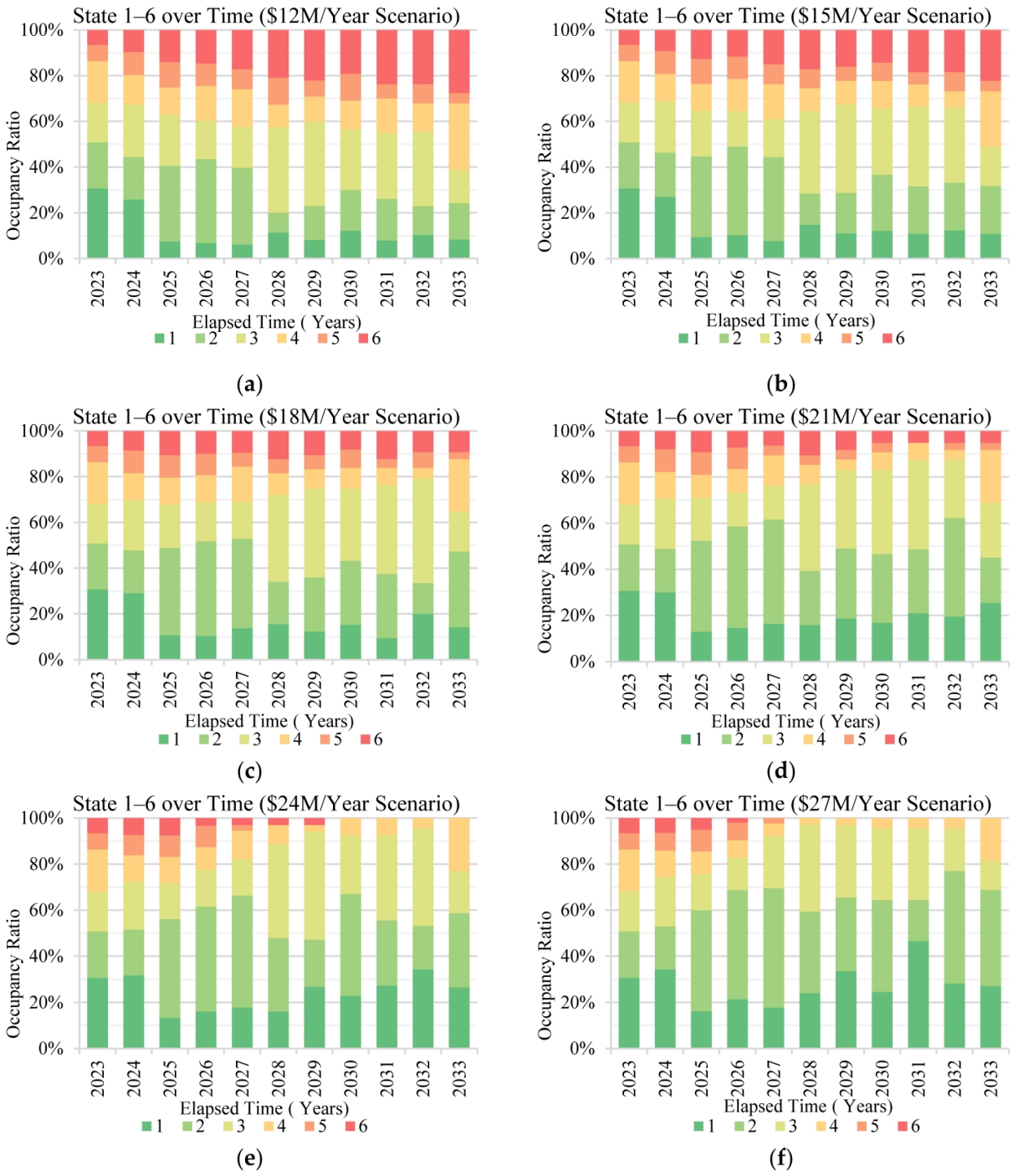


Figure 6.10: Condition state evolution of network under various annual budget scenarios: (a) USD 12 M, (b) USD 15 M, (c) USD 18 M, (d) USD 21 M, (e) USD 24 M, and (f) USD 27 M.

the maintenance planning period. The projected overall IRI condition state under various budget scenarios is illustrated in Figure 6.11.

The results suggest that a USD 18 million annual budget is the optimal budget level, ensuring functionality and serviceability while maintaining cost-effectiveness and maximizing benefits over the planned 10-year life cycle. Based on these findings, the analysis of the maintenance plan provides a detailed policy framework to assist road administrators in decision-making.

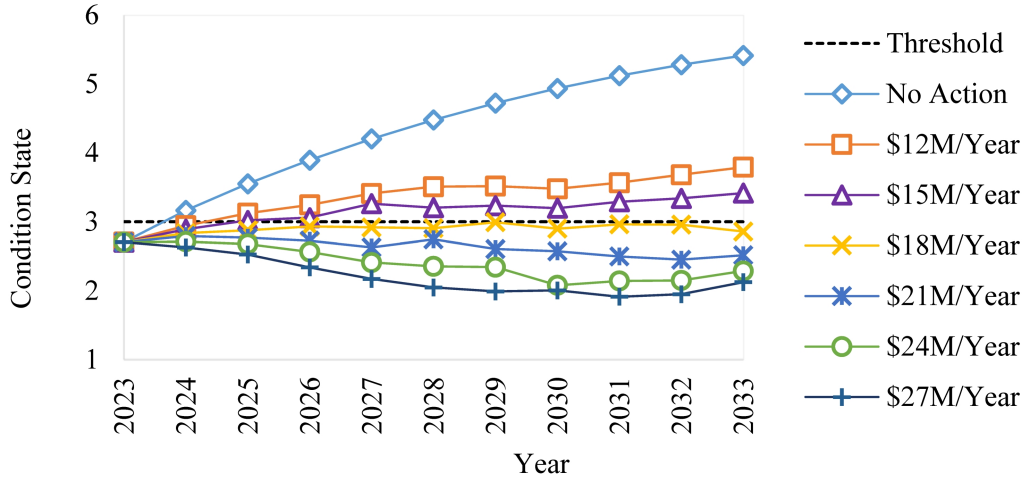


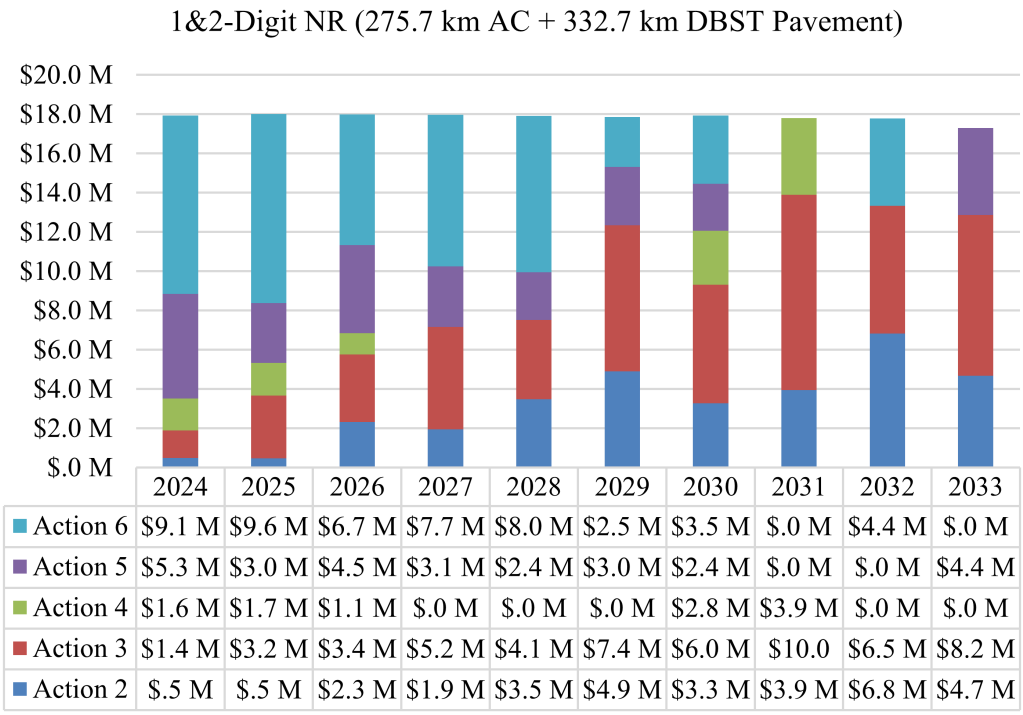
Figure 6.11: Predicted IRI condition state over the year under various budget scenarios.

This framework includes an assessment of maintenance costs associated with various repair strategies implemented annually for road networks, as depicted in Figure 6.12.

Notably, the highest cost–benefit ratio was achieved in the base year 2024 (Year 1), followed by a progressive decline in subsequent years. The trend of this scenario may result from improvements in the bearing capacities of road segments due to early maintenance interventions. As pavement conditions are enhanced in the initial years, their lifespan is extended, requiring only minor repair treatments in later years. For instance, major repair actions such as rehabilitation and reconstruction dominate in the early years, but their application decreases significantly in later years. This trend suggests a strategic shift from heavy repair works toward minor ones, such as preventive and corrective maintenance.

Furthermore, the performance trends of eight representative road sections under the USD 18 M annual scenario are shown in Figure 6.13. The analysis highlights the need for segment-specific maintenance scheduling based on surface condition and structural condition. For instance, NR78_32000_32100, initially in condition state 6, receives priority treatment in 2024, with no further intervention required until 2030. This indicates that timely maintenance can restore surface and structural conditions and sustain performance over several years. Conversely, NR1_63500_63600, despite initially being in good surface condition, exhibits a faster rate of deterioration and, therefore, warrants early maintenance intervention by 2026 to avoid performance decline. In contrast, maintenance work for segments with slower deterioration rates because of their strong structural conditions, such as NR55_15800_15900 and NR67_37600_37700, can be deferred until 2030 and 2033, respectively.

Moreover, the cumulative cost–benefit outcomes calculated over a 10-year planning period (2024 2033) in this study are compared against those of a GrA, under a fixed annual budget of USD 18 million. Figure 6.14 presents a comparative analysis of the cumulative cost–benefit achieved by both algorithms. Over the decade, both algorithms exhibit consistent year-over-



	2024	2025	2026	2027	2028	2029	2030	2031	2032	2033
Action 6	$9.1 M	$9.6 M	$6.7 M	$7.7 M	$8.0 M	$2.5 M	$3.5 M	$.0 M	$4.4 M	$.0 M
Action 5	$5.3 M	$3.0 M	$4.5 M	$3.1 M	$2.4 M	$3.0 M	$2.4 M	$.0 M	$.0 M	$4.4 M
Action 4	$1.6 M	$1.7 M	$1.1 M	$.0 M	$.0 M	$.0 M	$2.8 M	$3.9 M	$.0 M	$.0 M
Action 3	$1.4 M	$3.2 M	$3.4 M	$5.2 M	$4.1 M	$7.4 M	$6.0 M	$10.0	$6.5 M	$8.2 M
Action 2	$.5 M	$.5 M	$2.3 M	$1.9 M	$3.5 M	$4.9 M	$3.3 M	$3.9 M	$6.8 M	$4.7 M

Figure 6.12: Maintenance expenditure by repair action type ($18M/Year Scenario).

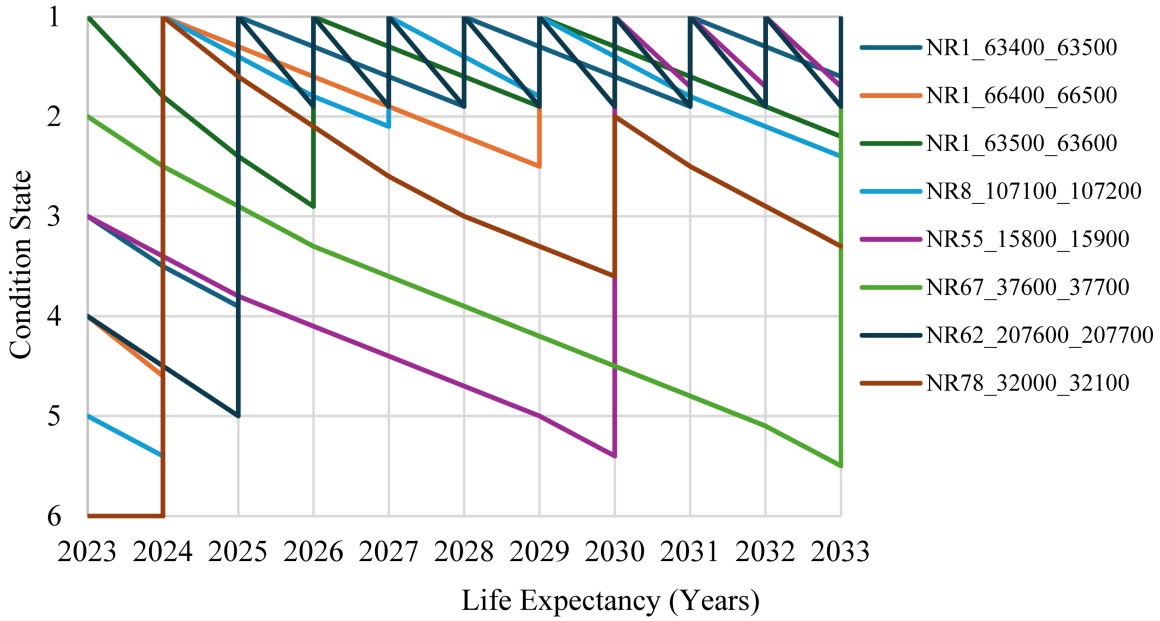


Figure 6.13: Performance of eight selected road segments ($18M/Year Scenario).

year growth in total cost–benefit, reflecting sustained improvements in maintenance outcomes. However, the GA achieves a slightly higher cumulative cost–benefit (0.4152) by the end of the planning period, outperforming the GrA (0.4088).

Furthermore, the GA indicates a more flexible and nuanced allocation strategy, effectively balancing immediate needs and long-term objectives, as illustrated in Figure 6.15 and Figure 6.16. In contrast, the GrA predominantly prioritizes major repair actions (e.g., Action 6:

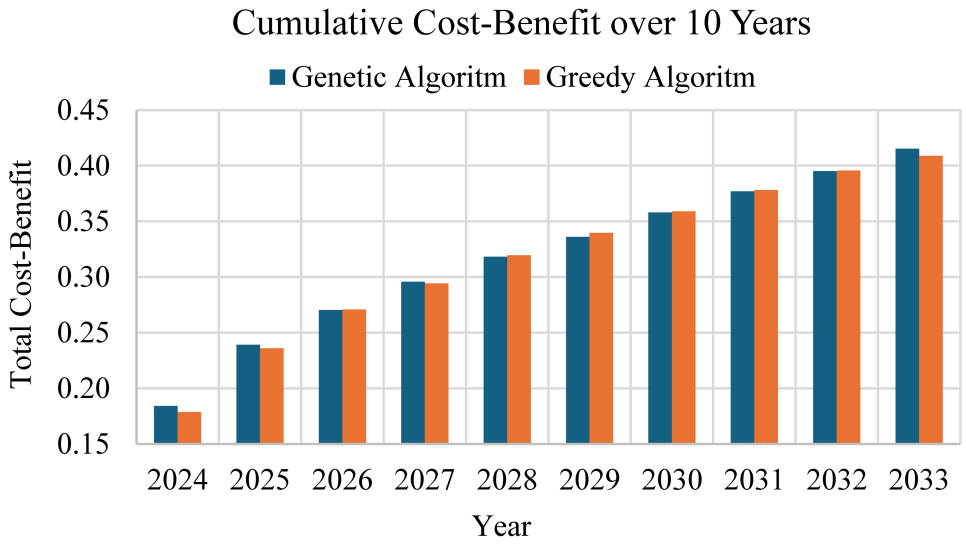


Figure 6.14: Cumulative cost–benefit: genetic vs. greedy algorithm.

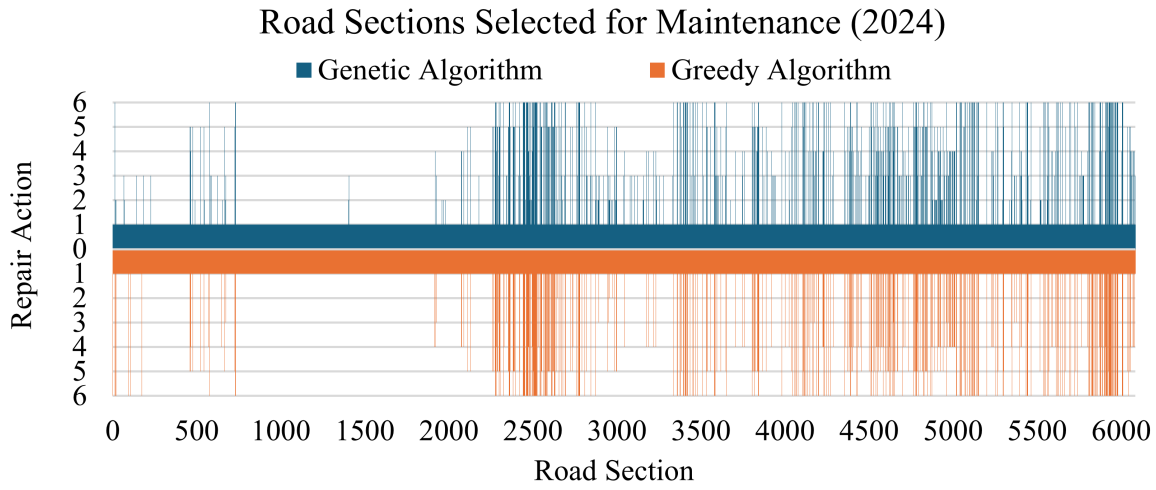


Figure 6.15: Road maintenance selection: genetic vs. greedy algorithm.

reconstruction), adhering to a step-by-step, locally optimal solution that may neglect broader systematic benefits. These findings suggest that the GA' s global optimization approach yields better long-term results compared to the GrA' s localized decision-making, reinforcing its suitability for large-scale multi-year maintenance planning.

6.6 Discussion

The proposed framework consists of two core components: deterioration forecasting and maintenance planning optimization. While the prediction of deterioration plays a pivotal role, the model specifically focuses on estimating the relative influence of various factors contributing to the deterioration process. Meanwhile, the optimization component aligns with Cambodia' s current multi-year rolling maintenance policy, shifting decision-making from subjective, human-

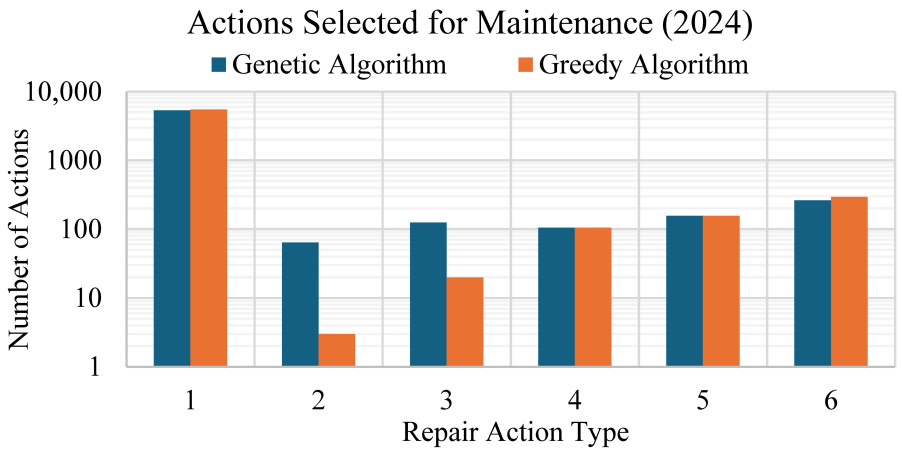


Figure 6.16: Repair action selected for maintenance: genetic vs. greedy algorithm.

based approaches toward objective, data-driven strategies. The framework allows maintenance planning to be dynamically updated based on annual government budget allocations and applied maintenance strategies without requiring a full restart of the planning process.

A notable observation from the parameter estimation results is the occurrence of inverted relationships for certain parameters across specific condition transitions (e.g., ESAL during the transitions from state $1 \rightarrow 2$ and $4 \rightarrow 5$). These counterintuitive results may stem from data reliability issues and an insufficient sample size, which can affect the stability of the estimated parameters. In this study, ESAL values were determined using conventional traffic count methods that assume fixed vehicle classifications and axle configurations, potentially misrepresenting actual field conditions.

To enhance input reliability, automated traffic load measurement systems, such as Weigh-In-Motion (WIM), are recommended. These systems provide continuous, reliable axle load data, which can significantly improve deterioration predictions [47]. Additionally, a richer and more frequent pavement monitoring dataset is essential to ensure a consistent and realistic relationship between influencing factors and all deterioration states. Regular inspections and expanded datasets would enable more robust calibration, better capturing deterioration dynamics and variability across the network.

Additionally, as the transition probability matrix in the MMH model is derived from the joint probability distribution of multiple influencing factors, introducing numerous variables can also complicate model convergence. This is evidenced by Geweke' s z-scores falling outside the acceptable range of [-1.96,1.96] for some parameters. This highlights the need for careful and accurate data collection using modern technology to ensure reliable input.

6.7 Conclusions

In this study, an optimal pavement maintenance framework at the network level is presented by integrating a MMH model to predict the deterioration curves of road segments. Key factors influencing deterioration include pavement bearing capacities, specifically the BLI, MLI, and LLI, traffic load (ESAL), and environmental conditions such as rainfall. Road sections were classified into 54 groups based on structural condition ratings of BLI, MLI, and LLI (Sound, Warning, and Severe) to account for varied deterioration patterns. This clustering enabled a more accurate analysis of deterioration within the network.

The GA was employed under six annual budget scenarios (USD 12, USD 15, USD 18, USD 21, USD 24, and USD 27 million) over a 10-year planning horizon to optimize maintenance planning. The findings indicate that an annual budget of $18 million provides the most effective maintenance policy, providing the best balance between maximizing benefits and budget allocation while meeting performance criteria. In this scenario, the IRI condition state 6 is kept below 10% by the end of the design period and sustains overall performance within IRI condition state 3 (IRI $\leq$ 4 m/km) throughout the planning period. Additionally, the study offers a comprehensive breakdown of annual maintenance costs and repair strategies for road networks, providing a tailored approach to each road section' s needs.

The comparison between GA and GrA highlights the core contribution of this study: GA achieves a more cost-effective and optimal solution over the planning horizon, outperforming GrA in terms of benefit maximization and budget allocation efficiency. The comparison shows that GA provides a cost−benefit of 0.4152, up to 1.6% higher than GrA (0.4088) under the same budget allocation, without exceeding the available budget. While the performance gap is moderate for smaller networks, the advantage of GA may become increasingly significant for larger and more complex networks, demonstrating the scalability and effectiveness of the proposed framework. This quantifiable advantage highlights that the additional computational complexity of GA translates into tangible improvements in effectiveness, making it a superior algorithm for efficient road asset management.

The findings of this study contribute significantly to data-driven decision-making for road asset management, aiding transportation authorities in prioritizing maintenance strategies within budget constraints while ensuring optimal road performance over time. Importantly, because the model predicts the IRI condition state based on structural parameters that can change over time, routine FWD data collection is recommended to update input parameters and support dynamic maintenance planning.

Nevertheless, several limitations should be acknowledged. First, the deterioration model would benefit from calibration using long-term inspection and maintenance history, improving

its predictive validity. Second, the current GA optimization approach simplifies input variability by using average values for traffic load and rainfall across structural categories. While this reduces complexity, it may overlook the impact of regional and temporal variability.

Future research should consider advanced GA techniques, such as parallel GA, hybrid GA, or adaptive GA, capable of efficiently navigating larger and more complex search spaces. This would enhance scalability and solution quality, particularly in large-scale network optimization under diverse operational conditions.

References

[1] Peraka, N. S. P.; Biligiri, K. P. Pavement Asset Management Systems and Technologies: A Review. *Automation in Construction* 2020, **119**, p. 103336. DOI: https://doi.org/10.1016/j.autcon.202

[2] Yamany, M. S. et al. Network-Level Pavement Maintenance and Rehabilitation Planning Using Genetic Algorithm. *Innovative Infrastructure Solutions* 2024, **9**(6), p. 208. DOI: https://doi.org/10.1007/s41062-024-01534-1.

[3] Chootinan, P. et al. A Multi-Year Pavement Maintenance Program Using a Stochastic Simulation-Based Genetic Algorithm Approach. *Transportation Research Part A: Policy and Practice* 2006, **40**(9), pp. 725–743. DOI: https://doi.org/10.1016/j.tra.2005.12.003.

[4] Chen, W.; Zheng, M. Multi-Objective Optimization for Pavement Maintenance and Rehabilitation Decision-Making: A Critical Review and Future Directions. *Automation in construction* 2021, **130**, p. 103840. DOI: https://doi.org/10.1016/j.autcon.2021.103840.

[5] Bhandari, S.; Luo, X.; Wang, F. Understanding the Effects of Structural Factors and Traffic Loading on Flexible Pavement Performance. *International Journal of Transportation Science and Technology* 2023, **12**(1), pp. 258–272. DOI: https://doi.org/10.1016/j.ijtst.2022.02.004.

[6] Ben-Akiva, M. et al. Infrastructure Management under Uncertainty: Latent Performance Approach. *Journal of Transportation Engineering* 1993, **119**(1), pp. 43–58. DOI: https://doi.org/10.10 947X(1993)119:1(43).

[7] Chang, C. M.; Salas, R.; Smith, R. E. Advancing Pavement Management Systems Using a Two-Tier Probabilistic Performance Modeling Approach for Improved Condition Forecasting and Budgeting Analysis. *International Journal of Transportation Science and Technology* 2025. DOI: https://doi.org/10.1016/j.ijtst.2025.06.003.

[8] AASHTO. *Pavement Management Guide*. 2nd. Washington, DC: American Association of State Highway and Transportation Officials, 2012.

[9] Xiao, F. et al. Enhanced Probabilistic Prediction of Pavement Deterioration Using Bayesian Neural Networks and Cuckoo Search Optimization. *Scientific Reports* 2025, **15**(1), p. 8665. DOI: https://doi.org/10.1038/s41598-025-92469-9.

[10] Obunguta, F.; Matsushima, K. Optimal Pavement Management Strategy Development with a Stochastic Model and Its Practical Application to Ugandan National Roads. *International Journal of Pavement Engineering* 2022, **23**(7), pp. 2405–2419. DOI: https://doi.org/10.1080/1

[11] Han, D. Heterogeneous Deterioration Process and Risk of Deficiencies of Aging Bridges for Transportation Asset Management. *Sustainability* 2021, **13**(13), p. 7094. DOI: https://doi.org/10.3390

[12] Tsuda, Y. et al. Estimating Markovian Transition Probabilities for Bridge Deterioration Forecasting. *Structural Engineering/Earthquake Engineering* 2006, **23**(2), 241s–256s. DOI: https://doi.org/10.2208/jsceseee.23.241s.

[13] Kobayashi, K.; Kaito, K.; Lethanh, N. A Bayesian Estimation Method to Improve Deterioration Prediction for Infrastructure System with Markov Chain Model. *International Journal of Architecture, Engineering and Construction* 2012, **1**(1), pp. 1–13. DOI: https://doi.org/10.7492/IJAEC.2012.001.

[14] Mbwana, J. R.; Turnquist, M. A. Optimization Modeling for Enhanced Network-Level Pavement Management System. *Transportation Research Record* 1996, **1524**(1), pp. 76–85. DOI: https://doi.org/10.1177/0361198196152400109.

[15] Pierce, L. M.; McGovern, G.; Zimmerman, K. A. Practical Guide for Quality Management of Pavement Condition Data Collection. 2013. URL: `https://rosap.ntl.bts.gov/view/dot/41482`.

[16] Wang, J. et al. A Comparison of Network Level Pavement Condition Assessment in Road Asset Management. *International Journal of Transportation Engineering and Technology* 2020, **6**(3), p. 95.

[17] Kargah-Ostadi, N.; Stoffels, S. M.; Tabatabaee, N. Network-Level Pavement Roughness Prediction Model for Rehabilitation Recommendations. *Transportation Research Record* 2010, **2155**(1), pp. 124–133. DOI: https://doi.org/10.3141/2155-14.

[18] Katicha, S. W. et al. *Network Level Pavement Structural Testing with the Traffic Speed Deflectometer*. Tech. rep. Virginia Transportation Research Council (VTRC), 2020. URL: `https://rosap.ntl.bts.gov/view/dot/54888`.

[19] Zhang, M. et al. Numerical Investigation of Pavement Responses under TSD and FWD Loading. *Construction and Building Materials* 2022, **318**, p. 126014. DOI: https://doi.org/10.1016/j.co

[20] Hamidi, A. et al. Comparative Evaluation of Falling Weight Deflectometer, Traffic Speed Deflectometer and Rapid Pavement Tester in Deflection Measurement. *Transportation Research Record* 2025, **2679**(2), pp. 1475–1494. DOI: https://doi.org/10.1177/03611981241270159.

[21] Fwa, T.; Chan, W.; Hoque, K. Analysis of Pavement Management Activities Programming by Genetic Algorithms. *Transportation Research Record* 1998, **1643**(1), pp. 1–6. DOI: https://doi.org/10.3141/1643-01.

[22] Slowik, A.; Kwasnicka, H. Evolutionary Algorithms and Their Applications to Engineering Problems. *Neural Computing and Applications* 2020, **32**(16), pp. 12363–12379. DOI: https://doi.org/10.1007/s00521-020-04832-8.

[23] Mathew, B. S.; Isaac, K. P. Optimisation of Maintenance Strategy for Rural Road Network Using Genetic Algorithm. *International Journal of Pavement Engineering* 2014, **15**(4), pp. 352–360. DOI: https://doi.org/10.1080/10298436.2013.806807.

[24] Infrastructure; Group, R. I. T. W., et al. *Overview of the Transport Infrastructure Sector in the Kingdom of Cambodia*. 2015.

[25] Royal Government. *Comprehensive Master Plan on Cambodia Intermodal Transport and Logistics System 2023–2033*. Phnom Penh, Cambodia: Royal Government, 2023.

[26] Bun, V. *Project Information Document–Integrated Safeguards Data Sheet—KH-Road Asset Management Project II Additional Financing—P165249*. English. Tech. rep. Washington, DC, USA: World Bank Group, 2018.

[27] World Bank. *Cambodia—Road Asset Management Project: Additional Financing—Environmental Assessment: Site Specific Environmental Management Plan for National Road 4*. English. Tech. rep. Phnom Penh, Cambodia: World Bank, 2018.

[28] Thao, N. D. et al. A Practical Process to Introduce a Customized Pavement Management System in Vietnam. *Journal of JSCE* 2015, **3**(1), pp. 246–258. DOI: https://doi.org/10.2208/journalof

[29] Han, C. et al. Long-Term Maintenance Planning Method of Rural Roads under Limited Budget: A Case Study of Road Network. *Applied Sciences* 2023, **13**(23), p. 12661. DOI: https://doi.org/10.3390/app132312661.

[30] Thegeya, A. et al. *Application of Machine Learning Algorithms on Satellite Imagery for Road Quality Monitoring: An Alternative Approach to Road Quality Surveys*. Tech. rep. ADB Economics Working Paper Series, 2022. DOI: https://doi.org/10.22617/WPS220587-2.

[31] Albuquerque, F. S.; Núñez, W. P. Development of Roughness Prediction Models for Low-Volume Road Networks in Northeast Brazil. *Transportation Research Record* 2011, **2205**(1), pp. 198–205. DOI: https://doi.org/10.3141/2205-25.

[32] Tamagusko, T.; Ferreira, A. Machine Learning for Prediction of the International Roughness Index on Flexible Pavements: A Review, Challenges, and Future Directions. *Infrastructures* 2023, **8**(12), p. 170. DOI: https://doi.org/10.3390/infrastructures8120170.

[33] Ghodratabadi, M.; Golroo, A.; Entezari, M. S. Machine Learning for Predicting Pavement Roughness and Optimising Maintenance. *Road Materials and Pavement Design* 2025, pp. 1–20. DOI: https://doi.org/10.1080/14680629.2025.2454376.

[34] Horak, E. Benchmarking the Structural Condition of Flexible Pavements with Deflection Bowl Parameters. *Journal of the South African Institution of Civil Engineering* 2008, **50**, pp. 2–9.

[35] Kim, Y. R.; Hibbs, B. O.; Lee, Y.-C. Temperature Correction of Deflections and Backcalculated Asphalt Concrete Moduli. *Transportation Research Record* 1995, (1473). URL: `http://onlinepubs.trb.org/Onlinepubs/trr/1995/1473/1473-007.pdf`.

[36] Lukanen, E.; Stubstad, R.; Briggs, R. *LTPP Guide to Asphalt Temperature Prediction and Correction*. Tech. rep. FHWA-RD-98-085, 71, 2002.

[37] Březina, I.; Machel, O.; Zavřel, T. Temperature Correction of Deflections and Backcalculated Elasticity Moduli Determined from Falling Weight Deflectometer Measurements on Asphalt Pavements. *Communications-Scientific letters of the University of Zilina* 2022, **24**(1), pp. D1–D8. DOI: https://doi.org/10.26552/com.C.2022.1.D1-D8.

[38] Garasia, K.; Juremalani, J. Modification of Temperature Correction Factor in Fwd Based On Field Experience in Indian Context. 2019.

[39] Smith, K. D. et al. *Using Falling Weight Deflectometer Data with Mechanistic-Empirical Design and Analysis, Volume I*. Tech. rep. United States. Federal Highway Administration, 2017. URL: https://rosap.ntl.bts.gov/view/dot/37574.

[40] Sovanneth, N. et al. "Defining Structural Thresholds for Cambodian Pavements Using Stochastic Approach". *Life-Cycle Performance of Structures and Infrastructure Systems in Diverse Environments*. CRC Press, 2025, pp. 1318–1335. DOI: https://doi.org/https://doi.org/10.1
160.

[41] AASHTO. *AASHTO Guide for Design of Pavement Structures*. Washington, DC: American Association of State Highway and Transportation Officials, 1993.

[42] Obama, K. et al. Disaggregated Hazard Rates Evaluation and Bench-marking. *J. Jpn. Soc. Civ. Eng* 2008, **64**, pp. 857–874.

[43] Han, D.; Kaito, K.; Kobayashi, K. Application of Bayesian Estimation Method with Markov Hazard Model to Improve Deterioration Forecasts for Infrastructure Asset Management. *KSCE Journal of Civil Engineering* 2014, **18**(7), pp. 2107–2119. DOI: https://doi.org/10.100
012-0070-6.

[44] Goldberg, D. E. *Genetic Algorithms in Search, Optimization, and Machine Learning*. Vol. 1. Reading, MA, USA: Addison-Wesley Publishing Company, 1989. URL: https://cir.nii.ac.jp/crid/1370576118699539492.

[45] Santos, J.; Ferreira, A.; Flintsch, G. An Adaptive Hybrid Genetic Algorithm for Pavement Management. *International Journal of Pavement Engineering* 2019, **20**(3), pp. 266–286. DOI: https://doi.org/10.1080/10298436.2017.1293260.

[46] Bo, W. et al. MILP-Based Approach for High-Altitude Region Pavement Maintenance Decision Optimization. *Applied Sciences* 2024, **14**(17), p. 7670. DOI: https://doi.org/10.3390/app141776

[47] Sujon, M. A. "Weigh-in-Motion Data-Driven Pavement Performance Prediction Models". PhD thesis. West Virginia University, 2023. DOI: https://doi.org/10.33915/etd.11901.

Chapter 7

Conclusions

7.1 Summary of presented research

This dissertation addressed several critical challenges in road asset management in developing countries, with a particular focus on the Cambodian national road networks. Cambodia, like many low- and middle-income countries, faces chronic constraints including insufficient inspection capacity, limited structural evaluation criteria, uncalibrated deterioration models, and subjective maintenance planning practices. These constraints impede the development of systematic, transparent, and cost-effective road management strategies needed to improve long-term asset performance and support socio-economic development.

Across four technical chapters, this dissertation developed and validated an integrated, data-driven framework that bridges automated condition data acquisition, structural condition benchmarking, strategic planning of FWD testing, and multi-year maintenance optimization. Together, these contributions form a cohesive foundation for modernizing road asset management and advancing Cambodia toward proactive, evidence-based maintenance strategies.

The first strand of the dissertation examined automated pavement condition evaluation to overcome the limitations of manual crack inspection. Chapter 3 presented an end-to-end framework that integrates YOLOv8 for crack detection with a fine-tuned Segmentation Anything Model (SAM) for pixel-level segmentation, using detection outputs as prompts without requiring large labeled datasets. The method achieved high accuracy on real-world images and competitive results on benchmark datasets. By incorporating OCR to extract geospatial metadata, the framework also enables automated GIS-compatible distress mapping, reducing annotation effort, improving survey consistency, and supporting more efficient maintenance planning.

The second strand of the dissertation focused on the structural condition of flexible pavements, which is often poorly assessed in developing countries due to limited testing resources and reference standards. Chapter 4 introduced a stochastic, deterioration-based method to

derive structural benchmarks from observed surface deterioration using a Bayesian Markov hazard model. By combining FWD and IRI data, critical thresholds were identified for key structural indices (D0, SNeff, MR, BLI, MLI, and LLI) for AC and DBST pavements, enabling classification into Sound, Warning, and Severe conditions. This approach avoids the need for detailed layer data and provides a practical, low-cost decision tool, while also showing the strong influence of upper pavement layers on roughness development and the importance of structural assessment alongside functional surveys.

The third research direction developed a policy framework for network-level FWD deployment. Because full-network testing is costly, Chapter 5 introduced an integrated approach combining a Bayesian mixed Markov hazard model with CRITIC–VIKOR decision analysis to optimize testing intervals and prioritize sections. The analysis showed that AC pavements deteriorate more slowly than DBST and therefore require less frequent testing. By considering remaining life, rut depth, average daily traffic (ADT), and mean profile depth (MPD), the framework enables objective segment selection, while route optimization improves field efficiency. Overall, the method supports efficient use of limited resources and timely detection of structural issues.

Finally, the dissertation combined deterioration forecasting with optimization for long-term maintenance planning. Chapter 6 developed a mixed Markov hazard model with a genetic algorithm to optimize multi-year maintenance strategies under budget constraints. Grouping road sections by structural condition improved deterioration modeling, and the GA outperformed a greedy algorithm with higher cost–benefit outcomes. An optimal annual budget was identified as the most effective for meeting service targets, keeping poor-condition segments below 10% by the end of the analysis period. Overall, the framework provides a scalable, data-driven planning tool that supports transparent and cost-effective decision-making.

In combination, these four research strands address key gaps in Cambodia' s road asset management system, including automated distress detection, structural benchmarking, testing prioritization, and multi-year maintenance programming. Collectively, they demonstrate that modern data-driven techniques can be effectively adapted to resource-constrained contexts, enabling more consistent inspections, enhanced understanding of underlying structural needs, and improved long-term investment planning.

7.2 Conclusions and recommendations

This dissertation provides several major insights and contributions that advance road asset management practices with limited resources. The overarching conclusions are summarized as follows:

- Automated condition data collection is achievable with lightweight, high-performing models. The proposed framework demonstrates that accurate detection and segmentation of pavement cracks can be performed without relying on expansive hardware, enabling cost-effective network-level monitoring and integration into existing GIS platforms.
- Structural benchmarking can be derived directly from deterioration processes. The structural threshold values for AC and DBST pavements bypass the need for detailed layer characterization, a crucial advantage for data-scarce countries, while ensuring the effective maintenance strategy recommendation.
- Strategic deployment of FWD testing maximizes the value of scarce structural data while avoiding excessive testing. By combining deterioration modeling, multi-criteria prioritization, and routing optimization, the framework identifies optimal testing frequency and ensures that limited FWD resources target sections where structural failure risk is highest.
- Integrated comprehensive deterioration forecasting and optimization significantly improve maintenance planning, specifically complying with Cambodian policy. The GA-based optimization method produces more cost-effective maintenance policies than conventional heuristics, offering a scalable alternative for budget-constrained agencies and enabling the transition from reactive to proactive asset management.

To further advance the field and improve the applicability of the developed frameworks, the following extensions are recommended:

- Refine and expand automated image analysis frameworks to address environmental challenges, such as shadows and motion blur, potentially through attention-based architectures or domain adaptation techniques.
- Validate structural thresholds through field sampling and laboratory testing, including DCP, coring, and material characterization to confirm mechanistic consistency.
- Incorporate multiple performance indicators such as rut depth, cracking severity, and structural strain to capture multi-dimensional deterioration processes.
- Integrate richer time-series data, including long-term IRI, FWD, rainfall, and maintenance history to improve calibration and predictive accuracy.
- Develop advanced metaheuristic optimization algorithms (e.g., hybrid GA, adaptive GA, parallel GA) to improve computation speed and scalability for nationwide networks.